СТРОИТЕЛЬНАЯ МЕХАНИКА ИНЖЕНЕРНЫХ КОНСТРУКЦИЙ И СООРУЖЕНИЙ

2025 Том 21 № 6

DOI: 10.22363/1815-5235-2025-21-6

http://journals.rudn.ru/structural-mechanics

Издается с 2005 г.

Свидетельство о регистрации СМИ ПИ № ФС 77-19706 от 13 апреля 2005 г.
выдано Федеральной службой по надзору в сфере связи, информационных технологий и массовых коммуникаций (Роскомнадзор)
Учредитель: Федеральное государственное автономное образовательное учреждение высшего образования
«Российский университет дружбы народов имени Патриса Лумумбы»

ISSN 1815-5235 (Print), 2587-8700 (Online)
Периодичность: 6 выпусков в год.
Языки: русский, английский.
Журнал индексируют: РИНЦ, RSCI, Cyberleninka, DOAJ, Google Scholar, Ulrich's Periodicals Directory, WorldCat, Dimensions.
Включен в Перечень ведущих научных журналов и изданий ВАК при Минобрнауки России по группе научных специальностей 2.1.1. Строительные конструкции, здания и сооружения (технические науки), 2.1.2. Основания и фундаменты, подземные сооружения (технические науки), 2.1.9. Строительная механика (технические науки).

Международный научно-технический журнал *«Строительная механика инженерных конструкций и сооружений»* знакомит читателей с достижениями отечественных и зарубежных ученых в области геометрии пространственных конструкций, сопротивления материалов, строительной механики, теории упругости и расчета строительных и машиностроительных конструкций, освещает вопросы научно-технического прогресса в строительстве и машиностроении, публикует аналитические обзоры по теме журнала.

Сайт журнала содержит полную информацию о журнале, его редакционной политике и этических принципах, требования к подготовке и условия публикации статей, а также полные выпуски журнала с 2008 г. (в рамках политики свободного доступа).

СОДЕРЖАНИЕ

АНАЛИТИЧЕСКИЕ И ЧИСЛЕННЫЕ МЕТОДЫ РАСЧЕТА КОНСТРУКЦИЙ

Alekseytsev A.V., Yurusov K.V. Analytical Modeling of Reinforced Concrete Columns Under Lateral Impact with Shear Failure (Аналитическая модель динамического расчета железобетонных колонн при горизонтальном ударе с разрушением по наклонному сечению) 497

Chepurnenko A.S., Al-Zgul S.H., Yazyev B.M. Rectangular Concrete-Filled Steel Tube Rational Dimensions under Uniaxial Eccentric Compression (Рациональные размеры прямоугольной трубобетонной колонны при внецентренном сжатии) 509

РАСЧЕТ И ПРОЕКТИРОВАНИЕ СТРОИТЕЛЬНЫХ КОНСТРУКЦИЙ

Лебедь Е.В. Напряженно-деформированное состояние ребристо-кольцевого купола при несимметричной и симметричной нагрузках с учетом разных узловых сопряжений и редко установленных колонн 524

Сунь Г., Миронова Л.И. Влияние изгибной жесткости соединения на работоспособность стального каркаса 537

Yakupov S.N., Giniyatullin R.R., Yakupov N.M., Nizameyev V.G., Rynkovskaya M.I. Diagnostics of Structures Under Vibration Loads and Elevated Temperatures (Диагностика состояния конструкций в условиях вибрационных нагрузок и повышенных температур) 551

РАСЧЕТ ТОНКИХ УПРУГИХ ОБОЛОЧЕК

Krivoshapko S.N., Chiadighikaobi P.Ch. Strength, Stability and Dynamics of Rigid Shells: Analysis of Recent Research (Прочность, устойчивость и динамика жестких оболочек: анализ современных исследований) ... 565

СТРОИТЕЛЬНЫЕ МАТЕРИАЛЫ И ИЗДЕЛИЯ

Ehsani A., Nasimi Sh., Shambina S.L., Yazyev S.B., Kireev O.L. Self-Healing Mechanisms in Nano-Modified Concrete: A Comprehensive Review of Synergy Between Microbial Biomineralization and Nano-Additives (Механизмы самовосстановления в наномодифицированном бетоне: комплексный обзор взаимодействия биоминерализации и нанодобавок) ... 585

ЭКСПЕРИМЕНТАЛЬНЫЕ ИССЛЕДОВАНИЯ

Корнев О.А., Шувалов А.Н., Корнилова А.В., Ермаков В.А. Интегральный критерий выбора алюминиевого сплава для строительства резервуаров в условиях Арктики 605

Редактор И.Л. Панкратова
Редактор англоязычных текстов С.Л. Шамбина
Дизайн обложки Ю.Н. Ефремовой
Компьютерная верстка Н.В. Маркеловой

Адрес редакции:
Российский университет дружбы народов имени Патриса Лумумбы
Российская Федерация, 117198, Москва, ул. Миклухо-Маклая, д. 6; тел./факс: +7 (495) 955-08-28; e-mail: stmj@rudn.ru, i_mamieva@mail.ru

Подписано в печать 24.12.2025. Выход в свет 30.12.2025. Формат 60×84/8.
Бумага офсетная. Печать офсетная. Гарнитура «Times New Roman». Усл. печ. л. 14,9. Тираж 250 экз. Заказ № 1686. Цена свободная.

Федеральное государственное автономное образовательное учреждение высшего образования «Российский университет дружбы народов имени Патриса Лумумбы»
Российская Федерация, 117198, Москва, ул. Миклухо-Маклая, д. 6

Отпечатано в типографии ИПК РУДН
Российская Федерация, 115419, Москва, ул. Орджоникидзе, д. 3

STRUCTURAL MECHANICS OF ENGINEERING CONSTRUCTIONS AND BUILDINGS

2025 VOLUME 21 NO. 6

DOI: 10.22363/1815-5235-2025-21-6

http://journals.rudn.ru/structural-mechanics

Founded in 2005

by Peoples' Friendship University of Russia named after Patrice Lumumba

ISSN 1815-5235 (Print), 2587-8700 (Online)
Published 6 times a year.
Languages: Russian, English.
Indexed by RSCI, Russian Index of Science Citation, Cyberleninka, DOAJ, Google Scholar, Ulrich's Periodicals Directory, WorldCat, Dimensions.
The journal has been included in the list of the leading review journals and editions of the Highest Certification Committee of Ministry of Education and Science of Russian Federation in which the basic results of PhD and Doctoral Theses are to be published.

International scientific-and-technical peer-reviewed journal *"Structural Mechanics of Engineering Constructions and Buildings"* shows the readers round the achievements of Russian and foreign scientists in the area of geometry of spatial structures, strength of materials, structural mechanics, theory of elasticity and analysis of building and machine-building structures, illumines the problems of scientific-and-technic progress in building and machine-building, publishes analytic reviews on the aims and scope of the journal.

OPEN ACCESS The journal website contains full information about the journal, editorial policy and ethics, requirements for the preparation and publication of the articles, etc., as well as full-text issues of the journal since 2008 (Open Access).

CONTENTS

ANALYTICAL AND NUMERICAL METHODS OF STRUCTURAL ANALYSIS

Alekseytsev A.V., Yurusov K.V. Analytical Modeling of Reinforced Concrete Columns Under Lateral Impact with Shear Failure 497

Chepurnenko A.S., Al-Zgul S.H., Yazyev B.M. Rectangular Concrete-Filled Steel Tube Rational Dimensions under Uniaxial Eccentric Compression 509

ANALYSIS AND DESIGN OF BUILDING STRUCTURES

Lebed E.V. Stress-Strain State of the Ribbed-Ring Dome Under Asymmetric and Symmetric Loads Taking Into Account Different Nodal Connections and Rarely-Spaced Columns..... 524

Sun G., Mironova L.I. Influence of Rotational Stiffness of Beam-to-Column Connection on Steel Frame Performance 537

Yakupov S.N., Giniyatullin R.R., Yakupov N.M., Nizameyev V.G., Rynkovskaya M.I. Diagnostics of Structures under Vibration Loads and Elevated Temperatures 551

ANALYSIS OF THIN ELASTIC SHELLS

Krivoshapko S.N., ***Chiadighikaobi P.Ch.*** Strength, Stability and Dynamics of Rigid Shells: Analysis of Recent Research 565

CONSTRUCTION MATERIALS AND PRODUCTS

Ehsani A., Nasimi Sh., Shambina S.L., Yazyev S.B., Kireev O.L. Self-Healing Mechanisms in Nano-Modified Concrete: A Comprehensive Review of Synergy Between Microbial Biomineralization and Nano-Additives 585

EXPERIMENTAL RESEARCH

Kornev O.A., Shuvalov A.N., Kornilova A.V., Ermakov V.A. Integral Criterion for the Selection of Aluminum Alloy for the Construction of Reservoirs in the Arctic 605

Copy Editor I.L. Pankratova
English Texts' Editor S.L. Shambina
Graphic Designer Iu.N. Efremova
Layout Designer N.V. Markelova

Address of the Editorial Board:
Peoples' Friendship University of Russia named after Patrice Lumumba
6 Miklukho-Maklaya St, Moscow, 117198, Russian Federation; tel./fax: +7 (495) 955-08-28; e-mail: stmj@rudn.ru, i_mamieva@mail.ru

Printing run 250 copies. Open price

Peoples' Friendship University of Russia named after Patrice Lumumba
6 Miklukho-Maklaya St, Moscow, 117198, Russian Federation

Printed at Publishing House of RUDN University
3 Ordzhonikidze St, Moscow, 115419, Russian Federation

СТРОИТЕЛЬНАЯ МЕХАНИКА ИНЖЕНЕРНЫХ КОНСТРУКЦИЙ И СООРУЖЕНИЙ
STRUCTURAL MECHANICS OF ENGINEERING CONSTRUCTIONS AND BUILDINGS

2025. 21(6). 497–508

ISSN 1815-5235 (Print), 2587-8700 (Online)
HTTP://JOURNALS.RUDN.RU/STRUCTURAL-MECHANICS

АНАЛИТИЧЕСКИЕ И ЧИСЛЕННЫЕ МЕТОДЫ РАСЧЕТА КОНСТРУКЦИЙ
ANALYTICAL AND NUMERICAL METHODS OF STRUCTURAL ANALYSIS

DOI: 10.22363/1815-5235-2025-21-6-497-508
EDN: EBFSNK

Research article / Научная статья

Analytical Modeling of Reinforced Concrete Columns Under Lateral Impact with Shear Failure

Anatoly V. Alekseytsev✉, **Konstantin V. Yurusov**

Moscow State University of Civil Engineering (National Research University), *Moscow, Russian Federation*
✉ aalexw@mail.ru

Received: September 26, 2025
Revised: November 20, 2025
Accepted: November 30, 2025

Abstract. The issue of ensuring the mechanical safety of load-bearing structures in buildings and facilities is currently of particular relevance. One critical aspect of this problem is the strength of compressed and compressed-bent elements under transverse impact loading. Several failure mechanisms can occur in reinforced concrete (RC) columns. This paper develops an analytical methodology for determining the ultimate load capacity of square cross-section elements under horizontal impact, specifically for the failure mode associated with diagonal shear. Such scenarios are possible in cases of vehicle collision with a column or impacts near the support zone of the structure. The analytical model is based on static equilibrium equations, which incorporate the ultimate mechanical characteristics of the materials, accounting for dynamic strengthening effects. The concrete deformation model considers the confining effect in the direction perpendicular to compression, which enhances the concrete's calculated resistance but induces additional stresses in the transverse reinforcement. A numerical example of the calculation for a building's RC column is provided, yielding specific numerical results. A comparison is made between the outcomes of the proposed methodology and those obtained from a detailed numerical simulation performed using a verified solid finite element model. The limitations of the proposed analytical method are identified, and its sufficiently high accuracy and efficiency are demonstrated. Finally, prospects for further development are outlined, and recommendations for the practical application of the method to ensure the mechanical safety of reinforced concrete columns are provided.

Keywords: lateral impact, reinforced concrete structures, dynamic loading, structural safety, shear strength

Conflicts of interest. The authors declare that there is no conflict of interest.

Authors' contribution: *Alekseytsev A.V.* — research concept, development of analytical model dependencies, preparation of figures, preparation of finite element model, scientific editing; *Yurysov K.V.* — development of analytical model dependencies, verification of finite element model, execution of numerical calculation examples, preparation of text, analysis of calculation results. Both of the authors read and approved the final version of the article.

For citation: Alekseytsev A.V., Yurusov K.V. Analytical modeling of reinforced concrete columns under lateral impact with shear failure. *Structural Mechanics of Engineering Constructions and Buildings.* 2025;21(6):497–508. http://doi.org/10.22363/1815-5235-2025-21-6-497-508 EDN: EBFSNK

Anatoly V. Alekseytsev, Doctor of Technical Sciences, Professor of the Department of Reinforced Concrete and Masonry Structures, Moscow State University of Civil Engineering (National Research University), 26 Yaroslavskoye Shosse, Moscow, Russian Federation; eLIBRARY SPIN-code: 3035-5571, ORCID: 0000-0002-4765-5819; e-mail: aalexw@mail.ru

Konstantin V. Yurusov, Postgraduate student of the Department of Reinforced Concrete and Masonry Structures, Moscow State University of Civil Engineering (National Research University), 26 Yaroslavskoye Shosse, Moscow, Russian Federation; eLIBRARY SPIN-code: 8084-3827, ORCID: 0009-0004-1970-3491; e-mail: walrk@mail.ru

Аналитическая модель динамического расчета железобетонных колонн при горизонтальном ударе с разрушением по наклонному сечению

А.В. Алексейцев✉, **К.В. Юрусов**

[1] Национальный исследовательский Московский государственный строительный университет, *Москва, Российская Федерация*

✉ aalexw@mail.ru

Поступила в редакцию: 26 сентября 2025 г.
Доработана: 20 ноября 2025 г.
Принята к публикации: 30 ноября 2025 г.

Аннотация. Проблема обеспечения механической безопасности несущих конструкций зданий и сооружений представляется особенно актуальной. Одним из важных аспектов этой проблемы является прочность сжатых и сжато-изогнутых элементов при действии поперечной ударной нагрузки. При этом для железобетонных колонн может реализовываться несколько схем разрушения. Разработана методика аналитического определения предельной нагрузки от горизонтального удара для элементов квадратного поперечного сечения при реализации схемы разрушения по наклонному сечению. Характерными аварийными ситуациями, соответствующими этой схеме разрушения, являются столкновения с колонной автомобиля или удары вблизи зоны опорного закрепления конструкции. Основой аналитического расчета являются уравнения статического равновесия, в которых используются предельные механические характеристики материалов с учетом динамического упрочнения. При деформировании бетона учитывается эффект от стеснения в направлении, перпендикулярном сжатию, что повышает расчетное сопротивление бетона, но вызывает дополнительные напряжения в поперечной арматуре. Выполнен пример расчета железобетонной колонны здания, доведенный до числовых значений, и приведено сопоставление результатов предлагаемой методики с численным расчетом. В качестве инструмента численного расчета использовалась верифицированная объемная конечно-элементная модель. Выявлены ограничения предлагаемого аналитического метода и установлена его достаточно высокая точность и эффективность. Сформулированы перспективы дальнейших разработок и даны рекомендации по конкретному использованию метода для обеспечения механической безопасности железобетонных колонн.

Ключевые слова: поперечный удар, железобетонные конструкции, динамическое нагружение, механическая безопасность, сдвиговая прочность

Заявление о конфликте интересов. Авторы заявляют об отсутствии конфликта интересов.

Вклад авторов: *Алексейцев А.В.* — концепция исследования, разработка зависимостей аналитической модели, подготовка рисунков, подготовка конечноэлементной модели, научное редактирование; *Юрусов К.В.* — разработка зависимостей аналитической модели, верификация конечноэлементной модели, выполнение числовых примеров расчета, подготовка текста, анализ результатов расчета. Оба автора ознакомлены с окончательной версией статьи и одобрили ее.

Для цитирования: *Алексейцев А.В., Юрусов К.В.* Аналитическая модель динамического расчета железобетонных колонн при горизонтальном ударе с разрушением по наклонному сечению // Строительная механика инженерных конструкций и сооружений. 2025. Т. 21. № 6. С. 497–508. http://doi.org/10.22363/1815-5235-2025-21-6-497-508 EDN: EBFSNK

1. Introduction

An important aspect of ensuring the safety of buildings and structures with reinforced concrete frames is checking the strength of columns and beam-columns against lateral impact. This issue has received considerable attention, which indicates the relevance of this research area. Factors such as the load-bearing capacity of reinforced concrete columns, taking into account the effect of confinement of concrete (confined concrete) [1], the deformability of composite reinforced concrete columns in carbon fiber reinforced plastic (CFRP) tubes [2], and the dynamic response and energy absorption capacity of structures with modified concrete, for example, with the addition of rubber crumb [3]. A large amount of experimental research, analytical and numerical modeling has been carried out, which shows interest in a comprehensive study of the behavior of compressed columns under impact loads. This includes corrosion damage [4], considering the longitudinal (vertical) coupler splicing of rebar along the length [5], and considering combinations of bending and compressive actions [6]. One of the most important aspects of research in column dynamics is its response and damage assessment due to horizontal impact [7]. The point of application of the impact load is important. For example, in [8], impact on a part of a column near its support node is considered. The authors of this study prove the effect of the type of supports on the load-bearing capacity of columns.

A number of papers are devoted to the study of compressed structures under low-velocity impact, for example [9]. For such an impact, the damping properties of the column and its ability to absorb energy can be increased by strengthening it with CFRP [10]. Low-velocity impact can be modeled in calculations as both quasi-static [11] and impulse load [12], where it is noted that the limit state of columns can be reached either by fracture or buckling. Buckling usually prevails for slender reinforced concrete columns with a slenderness ratio of more than 50. The complexity of describing the deformation and modeling of columns under horizontal impact has necessitated the development of simplified analytical approaches to calculations and engineering methods. Various features of these methods are presented in the following papers. Article [13] compares simplified approaches to assessing the load-bearing capacity of conventional and CFRP-strengthened reinforced concrete columns, paper [14] describes the probabilistic nature of the loading effect and assesses the reliability of structures, and study [15] reveals the influence of the percentage of longitudinal reinforcement on the load-bearing capacity. Analytical models for determining the load-bearing capacity under dynamic impact are based on quasi-static equilibrium equations [16], which have been refined for cases of random corrosion damage [17] and various compressive and impact force ratios [18]. There are significant differences in calculation methods depending on the impact velocity, the stiffness of the impactor body, the stiffness of the column itself, and the penetration of the impactor tip into it. In [19], a significant reduction in the stiffness and load-bearing capacity of a compressed column as a result of corrosion is noted, but stiffness can also decrease due to cracking under combined loads, including static moments and shear forces [20]. A number of studies focus on the stiffness of the impactor. If the stiffness of the impactor body is high, then all the kinetic energy is transferred to the impacted structure (“hard” impact), and if the impactor itself can absorb energy during impact, such an impact is considered soft [21]. In addition to the stiffness of the impact, the shape of the cross-section has a significant effect on the dynamics of columns. Thus, when comparing the results of studies [22] (square cross-section) and [23] (round cross-section), it can be seen that round columns are more vulnerable to brittle shear failure than square ones.

A number of considered studies [7; 8; 18; 22] involve the use of intensive computational procedures and require highly qualified researchers, which significantly hinders the practical application of the proposed developments.

Therefore, the purpose of this article is to develop an engineering method for calculating compressed columns under impact causing shear failure. To achieve this goal, it is necessary to solve the problem of constructing a simplified method for evaluating the load-bearing capacity and to verify it on the basis of experiments and numerical modeling. The object of the study is a compressed reinforced concrete column subjected to horizontal impact at the support, and the subject of the study is the ultimate shear bearing capacity.

2. Methods

When a horizontal force is dynamically applied to the column, most researchers, including [24], identified the following failure patterns: local crushing, which may be accompanied by chipping or punching (local failure), bending failure (along normal sections), and shear failure (along inclined sections) (Figure 1).

Considering experimental and theoretical studies of column shear failure, as well as qualitative results of numerical modeling, it is noted that the load-bearing capacity is significantly affected by the level of compressive loading, as well as the magnitude and direction of the static shear force present in the frame structure. As a result of dynamic impact, the column is loaded by both shear force and bending moment. Therefore, similar to normal operation, two strength conditions must be formed: strength along the inclined section under shear force taking into account added stress from dynamic loading; strength along the inclined section under bending moment taking into account its change under dynamic loading:

$$\begin{cases} k_{d1} Q_{\max} \le Q_{cd,ult}, \\ k_{d2} M_{\max} \le M_{cd,ult}, \end{cases} \tag{1}$$

where k_{d1}, k_{d2} are the dynamic load coefficients of the system; $Q_{\max}$, $M_{\max}$ are the internal forces due to load for the considered inclined section; $Q_{cd,ult}$, $M_{cd,ult}$ are the ultimate force values determined by the resistance of concrete and reinforcement in case of shear failure.

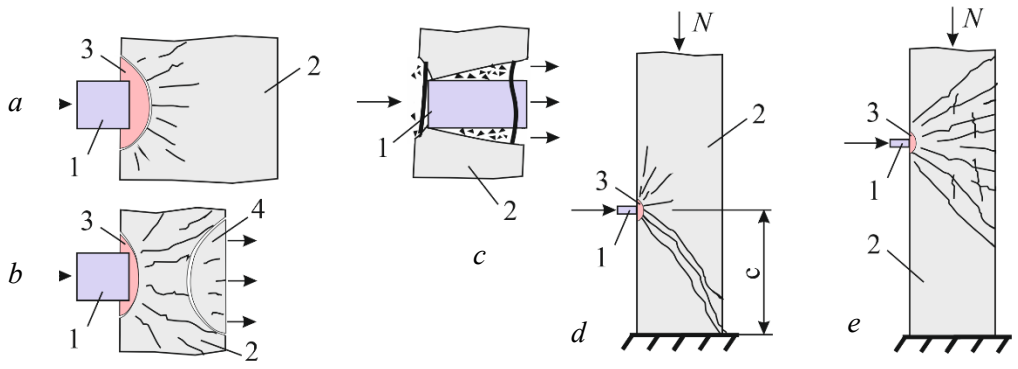

Figure 1. Failure modes under horizontal impact:
a, b, c — local crushing at various impact velocities; *d* — diagonal shear failure of a compressed column;
e — flexural failure: *1* — impactor; *2* — column; *3* — local crushing zone;
4 — concrete spall on the side opposite to the contact area between the impactor and the column
S o u r c e: made by A.V. Alekseytsev.

The method chosen for solving the system of inequalities (1) consists of compiling static equilibrium equations with respect to the lateral axis of the column and with respect to the point passing through the beginning of the inclined section. Cases of local failure (Figure 1, *a–c*) are not considered in this study. For numerical verification, the method of direct integration using the implicit scheme of differential equations of motion of the system, discretized using the finite element method (FEM), was adopted. For a reinforced concrete frame, this equation can be represented in the form of (2).

$$M\,\ddot{\vec{y}} + C\,\dot{\vec{y}} + K_\tau \vec{y} = \vec{F}, \tag{2}$$

where $\ddot{\vec{y}}, \dot{\vec{y}}, \vec{y}$ are the acceleration, velocity and displacement vectors respectively, $\vec{F}$ is the vector of nodal forces, M is the mass matrix. Damping matrix C and global shear stiffness matrix K_τ in formula (2) are determined using formula (3):

$$C = \beta K_\tau;\; K_\tau = K_{co} + K_{ro} + K_{so}, \tag{3}$$

where β is the structural damping constant; K_{co}, K_{ro}, K_{so} are the shear coefficient matrices for concrete, reinforcement and supports (in case when the column rests on a deformable base).

3. Results and Discussion

3.1. Calculation Procedure

The *first strength condition* is obtained from expression (1). If there is static load present in the system before the dynamic impact, the following formula is proposed:

$$\left(\frac{\Delta Q_d}{k_N^d Q_d^{ult}} \pm \frac{Q_{st}}{Q_{bN} + Q_{swN}} \right) \le 1, \tag{4}$$

where ΔQ_d is the added shear force caused by the horizontal impact; k_N^d is the coefficient accounting for the restraints and the column stress state under service load; Q_d^{ult} is the ultimate shear force in the section taking into account dynamic strengthening of concrete and reinforcement and the confinement effect; Q_{st}, Q_{bN}, Q_{swN} are respectively: the shear force from the design static load, the shear force resisted by concrete, and the shear force resisted by transverse reinforcement during normal operation, taking into account the presence of longitudinal force N_e.

Coefficient k_N^d is determined according to formula (5):

$$k_N^d = \begin{cases} \dfrac{1}{\sqrt{1.5-\mu}}\left(k_e + \left(\dfrac{N_e}{N_{ult}}\sqrt{\dfrac{P_{Ne}^{ult}}{P_{ult}}}\right)\right)^{-1}, & \dfrac{N_e}{N_{ult}} < 0.6, \\ \left(\dfrac{P_{Ne}^{ult}}{P_{ult}} + k_e\right)^{-1}, & \dfrac{N_e}{N_{ult}} \geq 0.6, \end{cases} \tag{5}$$

where P_{Ne}^{ult} is the static equivalent of the lateral impact load, at the value of the service longitudinal force equal to Ne and when bending failure of the column occurs; P_{ult} is the same for longitudinal force $Ne = 0$; μ is the coefficient for converting the design column length to the geometric length. When one end of the column is fixed and the other is pinned, $\mu = 0.7$; when both ends are fixed, but compression remains possible, $\mu = 0.5$. Evaluation of P_{Ne}^{ult}, P_{ult} is performed taking into account the influence of bending moments and deflections caused by these forces. The value of N_{ult} is determined for the case of small eccentricity (virtually axially compressed bar) using the formula from SP 63.13330[1]:

$$N_{ult} = \varphi(R_b A_b + R_{sc} A_{sc}), \tag{6}$$

where φ is the buckling coefficient; R_b, R_{sc} are the design compressive strengths of concrete and reinforcement respectively; A_b, A_{sc} are the areas of concrete and reinforcement.

The value of k_e refers to the level of the confinement effect. For a square cross-section based on the basic recommendations of J. Mander's model [25], it is determined based on the percentage of longitudinal reinforcement and the geometry of transverse reinforcement:

$$k_e = \frac{1}{1-\mu_{sc}}\left(1 - \frac{S_w - d_w}{2d}\right)^2, \tag{7}$$

where μ_{sc}, d_w are the percentage of longitudinal reinforcement taking into account the area of the confinement contour (рис. 2) and the transverse rebar diameter respectively; d is the transverse rebar length along the side, which is parallel to the plane of impact P within the bounds of the centers of gravity of the transverse rebars perpendicular to P.

Ultimate force Q_d^{ult} can be determined based on the expression that is valid for shear failure with a projection length of the inclined section $c = 2h_0$:

$$Q_d^{ult} = \sqrt{3k_b R_{bt}(1+k_e)^{\left(1+\sqrt{N_e/N_{ult}}\right)} b h_0^2 q_{sw}^d}, \tag{8}$$

[1] SP 63.13330. Concrete and reinforced concrete structures. General provisions. JSC Research Center of Construction — A.A. Gvozdev Research Institute of Concrete and Reinforced Concrete (NIIZHB). 2019.

where R_{bt} is the design tensile strength of concrete; k_b is the coefficient of dynamic strengthening of concrete; b, h_0 are the width and the design height of the cross-section; q_{sw}^d is the intensity of the load resisted by the transverse reinforcement, taking into account dynamic strengthening of steel and the stress from confined concrete core (Figure 2).

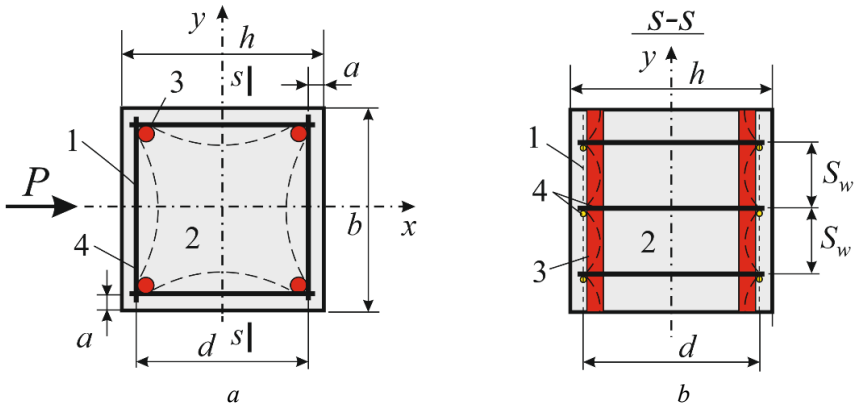

Figure 2. Determination of the confinement level:
a — column cross-section; *b* — section *s*–*s*: *1* — confinement boundary;
2 — core zone of the confinement; *3* — longitudinal rebars; *4* — transverse rebars
S o u r c e: made by A.V. Alekseytsev.

The value of q_{sw}^d is determined as

$$q_{sw}^d = k_s \frac{R_{sw} A_{sw}}{S_w} \left(1 - (0.2 + k_e) \frac{N_e}{N_{ult}}\right), \tag{9}$$

where R_{sw}, A_{sw} are the design strength and the area of transverse reinforcement; k_s is its coefficient of dynamic strengthening.

The value of the shear force resisted by concrete, taking into account compression by the longitudinal force, is calculated as follows, based on the methodology described in SP 63.13330 for the design of prestressed reinforced concrete structures:

$$Q_{bN} = \frac{1.5 \varphi_n R_{bt} b h_0^2}{c}, \; 0.5 \varphi_n R_{bt} b h_0 \le Q_{bN} \le 2.5 R_{bt} b h_0, \tag{10}$$

where c is the projection of the inclined section onto the vertical axis, and the value of φ_n accounts for the presence of normal stress caused by the compressive force. It is determined as follows:

$$\varphi_n = \begin{cases} 1.25, & 0.25 R_b \le \sigma_b < 0.5 R_b \\ 2.5 - \left(1 - \dfrac{\sigma_b}{R_b}\right), & 0.5 R_b \le \sigma_b \le R_b \end{cases}, \; \sigma_b = \frac{N_e}{A_b + \dfrac{\alpha E_b \varepsilon_{b0}}{R_b} A_{sc}}, \tag{11}$$

where in the case of small eccentricity (all of the section is non-uniformly compressed) A_{sc} is the area of the longitudinal reinforcement; A_b is the area of concrete; $\alpha = E_s / E_b$ is the ratio of the elastic moduli of concrete and reinforcement, determined taking into account the stress state of the column; R_b is the design compressive strength of concrete; $\varepsilon_{b0} = 0.002$ is the concrete strain for short-term load.

The value of c can be determined as:

$$c = \sqrt{\frac{1.5\varphi_n R_{bt} b h_0^2}{0.75 q_{sw}^c}}, c \le 2h_0, \tag{12}$$

where the intensity q_{sw}^c of the load resisted by the transverse reinforcement is determined according to (5) at $k_s = 1$.

The second strength condition from expression (1) has the form given in SP 63.13330 and, in general, if the required development length of longitudinal reinforcement is achieved, it is satisfied

$$k_{d2} M_{\max} \le M_{cd,ult} = M_s + M_{sw}, \tag{13}$$

where M_s, M_{sw} are the bending moments resisted by the longitudinal and transverse reinforcement of the column, respectively.

3.2. Analytical Calculation

A column with the following parameters is considered: cross-section of 400×400 mm, length of 4.0 m, B25 grade concrete ($R_b = 11.5$ MPa, $R_{bt} = 0.9$ MPa), A500 grade longitudinal reinforcement with $R_s = 435$ MPa, transverse reinforcement of the same grade, but with $R_{sw} = 300$ MPa, coefficients of dynamic strengthening taking into account [26] $k_1 = 1.1$ for concrete, and $k_2 = 1.2$ for reinforcement, fixed at the base, pinned connection to the upper floor slab, $\mu = 0.7$, the distance from the exterior face of concrete (horizontal and vertical) to the center of gravity of the longitudinal reinforcement $a = 5$ cm (Figure 3).

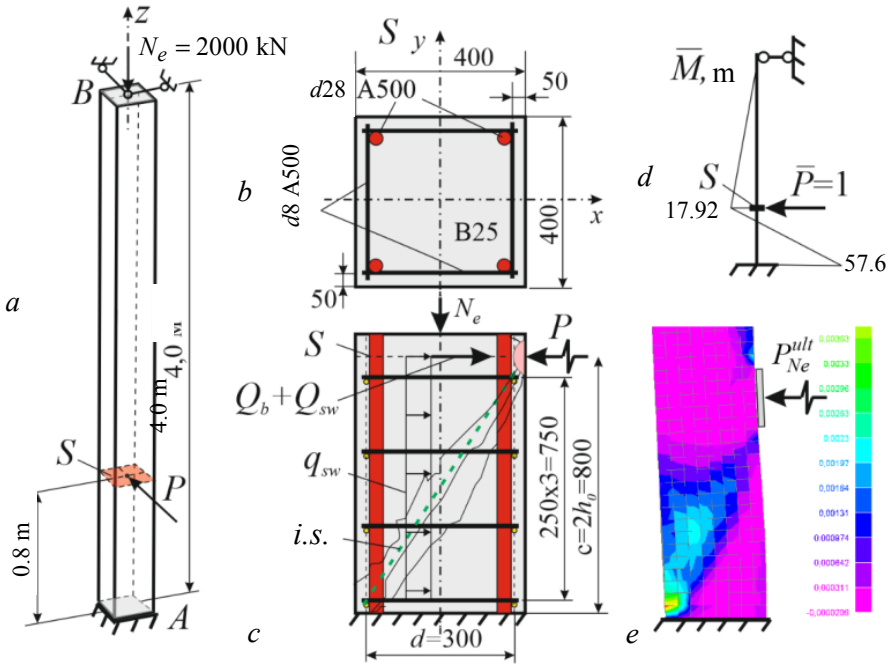

Figure 3. Calculation example for a column under horizontal impact:
a — initial structure; *b* — cross–section *S*; *c* — design model with an inclined section (i.s.);
d — bending moment diagram from a unit impact load; *e* — principal tensile strains in concrete at the peak dynamic force under service load Ne

S o u r c e: made by A.V. Alekseytsev.

The column is reinforced with 4*d*28 longitudinal bars, $A_{sc0}^{4d28} = 24.63$ cm^2, symmetrically at the corners. The transverse reinforcement represents a closed frame made of 4*d*8, and this frame is arranged at a constant spacing of 250 mm along the height of the column, rebar area $A_{sw}^{d8} = 0.503$ cm^2. The column is assumed to be virtually axially compressed under service load $N_e = 2000$ kN, shear force $Q_{st} = 0$ kN.

The column is subjected to dynamic action in the form of a horizontal impact from car collision. This impact is simulated by a mechanical force applied at a distance of 0.8 m from the base support. It is necessary to determine the maximum value of this dynamic force, assuming that the shape of the impact impulse is rectangular.

In the calculation, it is assumed that the failure occurs along an inclined section with a projection length of $c = 2h_0$, and the strength condition for the inclined section under the action of bending moment is satisfied (the value of the moment is small compared to the beam elements).

Condition (4) takes the form $\Delta Q_d \le k_N^d Q_d^{ult}$. For determining k_N^d, the following values are calculated: $\mu_{sc} = 24.63/30\cdot 30 = 2.73\%$, where *d* = 30 cm is the size of the square confinement region (Figure 3, *b, c*).

Then the confinement level

$$k_e = \frac{1}{1-\mu_{sc}}\left(1-\frac{S_w - d_w}{2d}\right)^2 = \frac{1}{1-0.0273}\left(1-\frac{25-2.8}{2\cdot 30}\right)^2 = 0.408,$$

and

$$N_{ult} = \varphi(R_b A_b + R_{sc} A_{sc0}) = 0.9(1.15\cdot 40\cdot 40 + 43.5\cdot 24.64) = 2620 \text{ kN}.$$

Ratio $N_e / N_{ult} = 2000/2620 = 0.763 \ge 0.6$, the equilibrium equation at the beginning of the inclined section passing through section *S* (Figure 3, *c*), is used, and the conditional ultimate horizontal forces at $N_e = 0$ kN, $N_e = 2000$ kN, which would cause bending failure, are calculated. The maximum moment from the action of these forces will be at the fixed support (Figure 3, *d*), an equilibrium equation is formed for this section. The deflection from the horizontal force at the fixed support is zero, so the equation will take the form:

$M_{\max} + N_e e_f = k_1 R_b \cdot b \cdot h_0^2 \cdot \alpha_R + k_2 R_{sc} \cdot A_{sc}^{2d28} \cdot (h_0 - a)$, the maximum moment is determined using the displacement method under the condition that it is caused by force P_{Ne}^{ult}, eccentricity $e_f = ((35-5)/2) = 15$ cm. Constant α_R, associated with ensuring plastic failure mode, is determined, for which the boundary value of the relative height of compressed concrete under impact is calculated: $\xi_R = 0.8 \div \left(1 + \left(435 \div 2\cdot 10^5\right) \div 0.0035\right) = 0.493$, then $\alpha_R = 0.493(1 - 0.493/2) = 0.37$. Substituting all the obtained values into the equilibrium equation yields:

$$0.144\cdot 400 P_{Ne}^{ult} + 2000\cdot 15 = 1.1\cdot 1.15\cdot 40\cdot 35^2\cdot 0.37 + 1.2\cdot 43.5\cdot 12.32\cdot (35-5),$$

$$57.6 P_{Ne}^{ult} = 22934 + 19293 - 30000,\ P_{Ne}^{ult} = 212.74 \text{ kN}.$$ When $N_e = 0$ kN, $P_{ult} = 733.1$ kN.

Then $k_N^d = (0.403 + 212.74/733.1)^{-1} = 1.4427$. The intensity of the impact load resisted by two *d*8 transverse reinforcement bars taking into account the confinement effect level and the presence of service compressive force (5) is calculated:

$$q_{sw}^d = 1.2\cdot \frac{30\cdot 1.01}{25}\left(1-(0.2+0.403)\left(\frac{2000}{2620}\right)\right) = 1.4544(1-0.422) = 0.78493 \text{ kN/cm}.$$

The adopted diameter of the transverse reinforcement, taking into account the presence of longitudinal force and the adopted reinforcement spacing, must be checked for developing its full strength in concrete. Elasticity coefficient:

$$\nu_b = R_b \div E_{b0}\varepsilon_b = 11.5 \div \left(27.5 \cdot 0.002 \cdot 10^3\right) = 0.209 .$$

Average stress is calculated as

$$\sigma = N / A_{red} = 2000 / \left(40 \cdot 40 + 0.209^{-1} \cdot (2 / 2.75) \cdot 10 \cdot 24.64\right) = 1.017 \text{ kN/cm}^2,$$

coefficient

$$\varphi_n = 2.5\left(1 - \frac{\sigma}{R_в}\right) = 2.5\left(1 - \frac{1.017}{1.15}\right) = 0.289 ,$$

$$q_{sw}^d \geq q_{sw,\min} = 0.25\varphi_n R_{bt} b = 0.25 \cdot 0.289 \cdot 0.09 \cdot 40 = 0.2601 .$$

The condition is satisfied. Then, according to (4):

$$Q_d^{ult} = \sqrt{3 \cdot 1.1 \cdot 0.09 \cdot (1 + 0.403)^{\left(1+\sqrt{2/2.62}\right)} \cdot 40 \cdot 35^2 \cdot 0.7849} = 146.8 \text{ kN}.$$

The value of $\Delta Q_d = Q_d^{ult} \cdot k_N^d = 146.8 \cdot 1.4427 = 211.8 \text{ kN}.$

That is, with an impact time of 1 second, the column can withstand a mechanical force of 211.8 kN.

3.3. Numerical Verification of Calculation Results

Due to the complexity of setting up and conducting a full-scale experiment that reproduces the calculated situation, the problem is verified using a three-dimensional finite element model. The Drucker — Prager plasticity model [27] was used for concrete, with the possibility of material softening under shear stress, which simulates shear failure. The reinforcement was modeled using a bilinear diagram with a limit on the rupture strain. The parameters of the concrete and reinforcement deformation models, as well as the hyperparameters of the calculation algorithm, are given in Table 1.

Verification of the finite element method (FEM) model with respect to bending strain with concrete deformation model parameters was carried out in [28]. For compressive strain, a design comparison at the ultimate force $N_{ult} = 2620$ kN is performed. Numerical simulation of this process, taking into account slow (close to static) loading, yielded a value of 2778 kN. Numerical and analytical calculations with other material parameters also yielded similar results for the ultimate compressive force. However, there are the following differences in the strength parameters obtained on the basis of the numerical and analytical models. The compressive stress in concrete obtained in the finite element model corresponds to the value of R_b, but the stress in the longitudinal reinforcement at the limit state is at the level of $\sigma = (0.4 \div 0.7) R_{sc}$, and the main criterion for stopping the load growth is the stress in the transverse reinforcement reaching its limit $\sigma = R_{sw}$. It has been established that the growth of strain in the transverse reinforcement leads to concrete failure. It is evident that analytical models need to take into account the concrete confinement effect and the formation of strength criteria in terms of strain in the presence of transverse reinforcement, as well as the need to consider the aspects of concrete deformation in the area surrounding the reinforcement, which has been done in [29].

Using the verified finite element model, calculations of the considered column were made at various values of N_e, and these were compared with the results obtained using the proposed analytical method (Table 2).

Table 1. **FEM-analysis constants**

Material / Hyperparameters	Parameters				
	Cohesion stress	**Internal friction angle**	**Dilation angle**	**Yield strength**	**Ultimate strain**
B25 concrete	3.3 MPa	38 deg.	28 deg.	0.9 MPa (tension) 11.5 MPa (compression)	0.0001 (tension) 0.0035 (compression)
A500 longitudinal rebars	–	–	–	435	0.025
A500 transverse rebars	–	–	–	300	0.025
General damping ratio	5%				
Convergence criterion	Load convergence tolerance 0.1%				
Nonlinear iteration	25 Newton — Raphson iterations per step, stiffness matrix updates each 5 iterations				
Integration step and time	$\Delta t = 0.05$ s , $t = 1.5$ s				

S o u r c e: made by A.V. Alekseytsev.

Table 2. **Comparison of the ΔQ_d values**

Method	ΔQ_d , with axial compression force Ne equal to				
	2500 kN	**2000 kN**	**1500 kN**	**1000 kN**	**500 kN**
FEA	109	195	256	287	309
Proposed method (M)	**257.28**	211.8	272.4	275.3	298.2
Tolerance $\delta = $(FEA-M)/M	**–91 %**	–0.07	–0.048	0.026	0.022

S o u r c e: made by A.V. Alekseytsev.

The FEA results in this problem agree well with the analytical ones. As the table shows, the applicability of the proposed methodology should be limited by the level $N_e / N_{ult} < 0.8$, since the error of the method as $N_e \to N_{ult}$ becomes very large. Calculations have shown that in the presence of service transverse force Q_{st} condition (1) yields results, which correspond with numerical modeling quite satisfactorily.

3.4. Discussion and Perspectives

The presented method is based on one of the possible scenarios of column failure, when the dynamic force increases at a relatively low rate, so that the stress in the concrete does not exceed the crushing stress, and its strain rate does not exceed the critical values leading to the formation of crack fans. If the load application rate is high, then during contact interaction, a failure pattern in the form of punching or chipping may occur. The calculation models for compressed elements given in a number of regulatory documents do not currently take into account the effects of concrete dilation, confinement effect, and the emergence of stress in the transverse reinforcement due to this confinement, but numerical models and experiments confirm these effects. Numerical models show that the load-bearing capacity of a compressed column along an inclined cross-section, taking into account lateral impact, significantly depends on the stress state of the concrete. The proposed model indirectly takes into account the effects of the emergence of stress in the transverse reinforcement when calculating parameter q_{sw} (5), however, microcracking and, as a result, concrete dilation are not taken into account, nor is the resistance of concrete on the descending branch. Therefore, it is assumed that a significant error arises as $N_e \to N_{ult}$.

The developed method can be used as an additional tool for solving problems related to assessing the survivability of buildings and structures [30; 31] in the event of man-induced accidents of mechanical nature. Prospects for improving this method include refining it for calculating elongated rectangular cross-sections (pylons) and slender reinforced concrete columns ($\lambda \geq 50$). It is also interesting to introduce various types of initial or acquired damage into the model, as well as to adapt the method to the calculation of reinforced concrete columns strengthened with steel or carbon fiber.

4. Conclusion

1. A method for analytical calculation of the lateral impact load capacity for reinforced concrete beam-columns causing shear failure has been developed. Verification showed satisfactory agreement with the obtained results based on the calculation of the solid FEM model in the range of compressive force values corresponding to characteristic loading of columns in civil buildings. The difference in results at $N_e < 0.8N_{ult}$ is no more than 5%.

2. The analytical model takes into account the confinement effect of concrete under compression, considering different spacing, diameter, and grade of transverse reinforcement. Limitations in the application of the method have been identified in terms of the compressive force, which must be less than 80% of the ultimate value.

3. A possibility has been established to quickly, compared to a solid FEM model, assess the safety of reinforced concrete columns in accidental situations such as collisions of technological or other transport with columns, man-induced mechanical impacts on columns in support areas, when failure occurs due to the action of a lateral force with a projection length of the inclined section $2h_0 \leq c \leq 3h_0$.

4. The proposed relationships are recommended for use in the design of preventive measures aimed at improving the mechanical safety of buildings and structures, including their protection against progressive collapse.

References

1. Jaiswal D.K., Murty C.V.R. Lateral deformation capacity of cantilever RC hollow columns using physics-based concrete confinement model. *Structures.* 2025;75:108662. https://doi.org/10.1016/j.istruc.2025.108662

2. Bai H., Zhang M., Wang D. Ultimate lateral load capacity of FRP tube-confined concrete-encased cross-shaped steel column: Experimental and numerical investigation. *Constr Build Mater.* 2025;492:142856.

3. Azunna S.U., Aziz F.N.A.A., Rashid R.S.M. Dynamic response of rubberized geopolymer concrete column subjected to lateral impact. *Progress in Engineering Science*. 2025;2:100130. https://doi.org/10.1016/j.pes.2025.100130

4. Ma C., Sun H., Ning C., Wu S., Niu X. Experimental evidence of failure mode transition for reinforced concrete rectangular columns with corroded stirrup. *Eng Fail Anal*. 2026;183:110193.

5. Chen Q.-J., Lei J., Wang Y.-T., Liu X., Gao W., Yao M.-J., Cai J. Dynamic performance of precast concrete columns with pressed sleeve connections under horizontal impact loads. *Engineering Structures.* 2026;346:121707.

6. Bao X., Li D., Zhao D., Shen J., Che, X., Cui H. Lateral impact responses of inclined steel-reinforced concrete column: experimental and numerical investigations. *Structures.* 2025;74:108601. https://doi.org/10.1016/j.istruc.2025.108601

7. Wei J., Xue J., Hu Z., Qi L., Xu J. Dynamic response and post-impact damage assessment of steel reinforced concrete columns under lateral impact loads. *Engineering Structures.* 2025;328:119735. https://doi.org/10.1016/j.engstruct.2025.119735 EDN: TIVYRD

8. Tamrazyan A.G. Horizontal dynamic impact at the bottom of the column with regard to the joint operation with the structural element. *Reinforced Concrete Structures.* 2025;10(2):3–16. (In Russ.) https://doi.org/10.22227/2949-1622.2025.2.3-16 EDN: IFYDUF

9. Lai D., Demartino C., Xu J., Xu J., Xiao Y. GFRP bar RC columns under lateral low-velocity impact: an experimental investigation. *International Journal of Impact Engineering.* 2022;170:104365. https://doi.org/10.1016/j.ijimpeng.2022.104365 EDN: WLJUZK

10. Swesi A.O., Cotsovos D.M., Val D.V. Effect of CFRP strengthening on response of RC columns to lateral static and impact loads. *Composite Structures*. 2022;287:115356. https://doi.org/10.1016/j.compstruct.2022.115356 EDN: RKLKFR

11. Anil O., Cem Yilmaz M., Barmaki W. Experimental and numerical study of RC columns under lateral low-velocity impact load. *Proceedings of the Institution of Civil Engineers: Structures and Buildings.* 2020;173(8):549–567. https://doi.org/10.1680/jstbu.18.00041 EDN: FXKMYL

12. Alekseytsev A.V. Stability of the RC column under horizontal impacts. *Reinforced Concrete Structures.* 2023;2(2): 3–12. (In Russ.) https://doi.org/10.22227/2949-1622.2023.2.3-12 EDN: VCYHKK

13. Li X., Yin Y., Li T., Zhu X., Wang R. Analytical study on reinforced concrete columns and composite columns under lateral impact. *Coatings.* 2023;13(1):152. https://doi.org/10.3390/coatings13010152 EDN: RWPKLQ

14. Zhao W., Qian J. Resistance mechanism and reliability analysis of reinforced concrete columns subjected to lateral impact. *International Journal of Impact Engineering.* 2020;136:103413. https://doi.org/10.1016/j.ijimpeng.2019.103413 EDN: QVIKKB

15. Wang X., Zhang Y., Su Y., Feng Y. Experimental investigation on the effect of reinforcement ratio to capacity of RC column to resist lateral impact loading. *Systems Engineering Procedia*. 2011;33(2):2725–2733. https://doi.org/10.1016/j.sepro.2011.08.007 EDN: OBCWIH

16. Puzankov Yu.I. *Strength and deformability of compressed reinforced concrete elements under lateral dynamic load.* Dissertation for the degree of Candidate of Technical Sciences. Moscow, 1979. (In Russ.) EDN: WLDCER

17. Daneshvar K., Moradi M.J., Ahmadi K., Mahdavi G., Hariri-Ardebili M.A. Dynamic behavior of corroded RC slabs with macro-level stochastic finite element simulations. *Engineering Structures*. 2021;239:112056. https://doi.org/10.1016/j.engstruct.2021.112056 EDN: XNGSLW

18. Sun J.-M., Yi W.-J., Chen H., Peng F., Zhou Y., Zhang W.-X. Dynamic responses of RC columns under axial load and lateral impact. *Journal of Structural Engineering*. 2023;149(1). https://doi.org/10.1061/jsendh/steng-11612 EDN: BRWXNG

19. Alekseytsev A.V., Yurusov K.V. A study on the bearing capacity of compressed corrosion-affected reinforced concrete elements subjected to transverse impulse loading. *Bulletin of Moscow State University of Civil Engineering.* 2025;20(5):667–682. (In Russ.) https://doi.org/10.22227/1997-0935.2025.5.667-682 EDN: ZKVQJE

20. Kolchunov V.I., Al-Hashimi O.I., Protchenko M.V. Stiffness of reinforced concrete structures under bending with transverse and longitudinal forces. *Construction and Reconstruction*. 2021;6(98):5–19. (In Russ.) https://doi.org/10.33979/2073-7416-2021-98-6-5-19 EDN: HOBBKE

21. Yilmaz T., Kiraç N., Anil Ö. Experimental investigation of axially loaded reinforced concrete square column subjected to lateral low-velocity impact loading. *Structural Concrete*. 2019;20(4):1358–1378. https://doi.org/10.1002/suco.201800276

22. Zhao W., Ye J. Dynamic behavior and damage assessment of RC columns subjected to lateral soft impact. *Engineering Structures.* 2022;251:113476. https://doi.org/10.1016/j.engstruct.2021.113476 EDN: YULMOI

23. Demartino C., Wu J.G., Xiao Y. Response of shear-deficient reinforced circular RC columns under lateral impact loading. *International Journal of Impact Engineering*. 2017;109:196–213. https://doi.org/10.1016/j.ijimpeng.2017.06.011

24. Zabegaev A.V. *Strength and deformability of reinforced concrete structures under accidental impact loading*. Dissertation for the degree of Doctor of Engineering Sciences. Moscow; 1992. (In Russ.) EDN: NPQPEB

25. Mander J.B., Priestley M.J.N., Park R. Theoretical Stress-Strain Model for Confined Concrete. *Journal of Structural Engineering.* 1988;114(8). https://doi.org/10.1061/(ASCE)0733-9445(1988)114:8(1804)

26. Kolchunov V.I., Fedorova N.V., Savin S.Yu. Dynamic effects in statically indeterminate physically and structurally nonlinear structural systems. *Industrial and Civil Engineering.* 2022;(9):42–51. https://doi.org/10.33622/0869-7019. (In Russ.) EDN: OTJLOQ

27. Arslan G. Sensitivity study of the drucker–prager modeling parameters in the prediction of the nonlinear response of reinforced concrete structures. *Materials and Design.* 2007;28:2596–2603. https://doi.org/10.1016/J.MATDES.2006.10.021 EDN: KUKOHN

28. Tamrazyan A., Alekseytsev A.V. Optimization of reinforced concrete beams under local mechanical and corrosive damage. *Engineering Optimization.* 2023;55(11):1905–1922. https://doi.org/10.1080/0305215x.2022.2134356 EDN: VKGOVU

29. Kolchunov Vl.I., Fedorova N.V., Ilyushchenko T.A. Strength model for concrete in near-reinforcement region. *Structural Mechanics of Engineering Constructions and Buildings*. 2024;20(5):391–403. (In Russ.) https://doi.org/10.22363/1815-5235-2024-20-5-391-403 EDN: ZRBRFL

30. Tamrazyan A.G. Methodology of theoretical bases of robustness of building systems. *Reinforced Concrete Structures*. 2025;9(1):3–17. (In Russ.) https://doi.org/10.22227/2949-1622.2025.1.3-17 EDN: SJBCSO

31. Tamrazyan A.G., Alekseytsev A.V., Mishina E.S. Probabilistic criterion for assessing the robustness of reinforced concrete frames during fracture localization. *Bulletin of MGSU.* 2025;20(7):1061–1071. (In Russ.) https://doi.org/10.22227/1997-0935.2025.7.1061-1071 EDN: UCPSKZ

СТРОИТЕЛЬНАЯ МЕХАНИКА ИНЖЕНЕРНЫХ КОНСТРУКЦИЙ И СООРУЖЕНИЙ
STRUCTURAL MECHANICS OF ENGINEERING CONSTRUCTIONS AND BUILDINGS

2025. 21(6). 509–523

ISSN 1815-5235 (Print), 2587-8700 (Online)

HTTP://JOURNALS.RUDN.RU/STRUCTURAL-MECHANICS

DOI: 10.22363/1815-5235-2025-21-6-509-523
EDN: ECJWUG

Research article / Научная статья

Rectangular Concrete-Filled Steel Tube Rational Dimensions under Uniaxial Eccentric Compression

Anton S. Chepurnenko✉, **Samir H. Al-Zgul**, **Batyr M. Yazyev**

Don State Technical University, *Rostov-on-Don, Russian Federation*

✉ anton_chepurnenk@mail.ru

Received: July 20, 2025
Revised: August 27, 2025
Accepted: September 5, 2025

Abstract. An algorithm for generating the training dataset and the machine learning model for selecting the cross-sectional dimensions of eccentrically compressed concrete filled steel tubular (CFST) columns have been developed. The paper presents a predictive model based on the CatBoost algorithm for determining the optimal geometric parameters (width b and height h) of the cross-section of rectangular CFST columns in compliance with regulatory strength requirements. The input parameters used were the concrete compressive strength class B according to Russian standards, the magnitude of the longitudinal force F, the wall thickness of the steel section t and the eccentricity of load application e. The model was trained on a synthetic sample formed taking into account the conditions of limit equilibrium under the combined action of the axial force and bending moment, restrictions on the cross-sectional dimensions in the range from 100 to 500 mm, strength conditions, as well as the requirements for minimizing the cost of the structure. The application of the CatBoost algorithm allowed achieving high forecasting accuracy with an average of two target variable metrics: the determination coefficient $R^2 = 0.999122$ and the average error in determining the section dimensions of 2.485 mm. The obtained results demonstrate the significant potential for using the developed model in the practical activities of design organizations, ensuring the accuracy of calculations while simultaneously optimizing material costs and reducing the time for implementing design solutions.

Keywords: bearing capacity, limit equilibrium, cross-section optimization, machine learning, Catboost

Conflicts of interest. The authors declare that there is no conflict of interest.

Authors' contribution: *Chepurnenko A.S.* — software, writing, review and editing; *Al-Zgul S.H.* — conducting research, software, data processing, graphic design, text writing; *Yazyev B.M.* — supervision, conceptualization. All of the authors read and approved the final version of the article.

Data Availability Statement. The training dataset is available for download at: https://doi.org/10.13140/RG.2.2.10073.99683

For citation: Chepurnenko A.S., Al-Zgul S.H., Yazyev B.M. Rectangular concrete-filled steel tube rational dimensions under uniaxial eccentric compression. *Structural Mechanics of Engineering Constructions and Buildings.* 2025;21(6):509–523. http://doi.org/10.22363/1815-5235-2025-21-6-509-523 EDN: ECJWUG

Anton S. Chepurnenko, Doctor of Technical Sciences, Professor of the Department of Structural Mechanics and Theory of Structures, Don State Technical University, 1 Gagarin Sq., Rostov-on-Don, 344003, Russian Federation; eLIBRARY SPIN-code: 7149-7981, ORCID: 0000-0002-9133-8546; e-mail: anton_chepurnenk@mail.ru

Samir H. Al-Zgul, Postgraduate student of the Department of Structural Mechanics and Theory of Structures, Don State Technical University, 1 Gagarin Sq., Rostov-on-Don, 344003, Russian Federation; eLIBRARY SPIN-code: 4483-8340, ORCID: 0000-0001-6182-786X; e-mail: samiralzgulfx@gmail.com

Batyr M. Yazyev, Doctor of Technical Sciences, Professor of the Department of Structural Mechanics and Theory of Structures, Don State Technical University, 1 Gagarin Sq., Rostov-on-Don, 344003, Russian Federation; eLIBRARY SPIN-code: 5970-5350, ORCID: 0000-0002-5205-1446; e-mail: ps62@yandex.ru

Рациональные размеры прямоугольной трубобетонной колонны при внецентренном сжатии

А.С. Чепурненко ✉, С.Х. Аль-Згуль, Б.М. Язьев

Донской государственный технический университет, *Ростов-на-Дону, Российская Федерация*
✉ anton_chepurnenk@mail.ru

Поступила в редакцию: 20 июля 2025 г.
Доработана: 27 августа 2025 г.
Принята к публикации: 5 сентября 2025 г.

Аннотация. Разработан алгоритм формирования обучающего датасета, а также модель машинного обучения для подбора размеров поперечного сечения внецентренно сжатых трубобетонных колонн. Представлена прогнозная модель на основе алгоритма CatBoost для определения оптимальных геометрических параметров (ширины b и высоты h) поперечного сечения прямоугольных трубобетонных колонн с соблюдением нормативных требований по прочности. В качестве входных параметров использованы класс бетона по прочности на сжатие B согласно российским стандартам, величина продольной силы F, толщина стенки стального профиля t и эксцентриситет приложения нагрузки e. Обучение модели проводилось на синтетической выборке, сформированной с учетом условий предельного равновесия при комбинированном действии продольной силы и изгибающего момента, ограничений на габариты сечения в диапазоне от 100 до 500 мм, условия прочности, а также требования минимизации стоимости конструкции. Применение алгоритма CatBoost позволило достичь высокой точности прогнозирования с усредненным по двум целевым переменным метрикам: коэффициентом детерминации $R^2 = 0{,}999122$ и средней ошибкой определения размеров сечения 2,485 мм. Полученные результаты демонстрируют значительный потенциал использования разработанной модели в практической деятельности проектных организаций, обеспечивая точность расчетов при одновременной оптимизации материальных затрат и сокращении времени выполнения проектных решений.

Ключевые слова: внецентренное сжатие, трубобетонная колонна, несущая способность, предельное равновесие, оптимизация размеров поперечного сечения, машинное обучение, Catboost

Заявление о конфликте интересов. Авторы заявляют об отсутствии конфликта интересов.

Заявление о доступности данных. Обучающий датасет доступен для скачивания по ссылке: https://doi.org/10.13140/RG.2.2.10073.99683

Вклад авторов: *Чепурненко А.С.* — программное обеспечение, подготовка текста статьи, рецензирование и редактирование; *Аль-Згуль С.Х.* — проведение исследования, программное обеспечение, обработка данных, графическое оформление, написание текста статьи; *Язьев Б.М.* — общее научное руководство, формулировка концепции исследования. Все авторы ознакомлены с окончательной версией статьи и одобрили ее.

Для цитирования: *Чепурненко А.С., Аль-Згуль С.Х., Язьев Б.М.* Рациональные размеры прямоугольной трубобетонной колонны при внецентренном сжатии // Строительная механика инженерных конструкций и сооружений. 2025. Т. 21. № 6. С. 509–523. http://doi.org/10.22363/1815-5235-2025-21-6-509-523 EDN: ECJWUG

1. Introduction

The paper investigates rectangular concrete filled steel tube (CFST) columns under uniaxial eccentric compression. The widespread use of such structures in modern construction is explained by a number of key advantages: the synergistic effect of the combined resistance of the steel tube and concrete filling [1], increased fire resistance [2], high energy capacity under dynamic loads and economic efficiency at all stages of construction and operation of the structure. Due to their high spatial rigidity and ability to resist combined loads, these structures are widely used in construction as load-bearing elements both in Russia [3] and abroad [4]. However, their widespread implementation faces serious difficulties due to the lack of reliable calculation methods that adequately take into account the complex nature of the interaction between the steel shell and concrete filling under various types of loading.

The foundation of modern research in the field of CFST column analysis is experimental data obtained during field and laboratory tests [5; 6]. This data serves as the basis for the development of more accurate analytical methods that take into account the nonlinear behavior of materials [7]. For a detailed stress analysis, researchers widely use numerical modeling, such as the finite element method. To work effectively with growing amounts of information, specialized databases are created to systematize experimental results [8–10]. Since the start of the 21st century, the use of artificial intelligence and machine learning has been

actively developing. These technologies are applied to predict the load-bearing capacity of structures and optimize their parameters. Taken together, all these areas allow to comprehensively study the behavior of composite structures and develop improved calculation methods.

The development of machine learning methods for designing CFST columns is largely driven by fundamental limitations of both normative and numerical calculation methods. On one hand, traditional normative approaches (Eurocode 4[1], AISC 360-16[2], SP 266.1325800.2016[3]), despite their widespread use in design practice, have significant drawbacks: they are only applicable to a narrow range of material characteristics, do not allow for reverse design tasks, are limited to certain types of cross-sections, and do not take into account complex loading cases.

On the other hand, numerical methods implemented in existing finite element software (ABAQUS, ANSYS, SCAD, LIRA, etc.), although they provide more accurate modeling of nonlinear behavior of structures [11], require significant computing resources, labor-intensive model calibration, and are insufficiently effective for practical use in design work [12; 13].

These limitations of the traditional approaches have created the conditions for the introduction of innovative analysis technologies, in particular artificial neural networks and other artificial intelligence methods capable of adequately accounting for complex nonlinear interactions in structures.

An artificial neural network for calculating the load-bearing capacity of square CFST columns under axial compression was first used in a study by H. Gao [14], where a three-layer feedforward network trained on experimental data showed high prediction accuracy when validated on an independent sample. This study confirmed the fundamental possibility of using neural network models as an effective auxiliary tool for engineering calculations.

Subsequent studies [15–19] significantly expanded the scope of application of artificial neural networks for CFST column analysis. These papers present improved neural network architectures trained on both experimental data and numerical simulation results.

Alongside the development of neural network approaches, significant progress has been made in the field of gradient boosting algorithms, which demonstrate comparable accuracy with greater computational efficiency and interpretability of results.

In [20], a comparative study was conducted on the accuracy of predicting the load-bearing capacity of reinforced concrete columns using five machine learning algorithms: AdaBoost, GBR, XGBoost, LightGBM, and CatBoost. The analysis used a database of experimental data, including, in particular, 401 tests of rectangular eccentrically compressed columns, containing the following parameters: geometric characteristics (cross-sectional dimensions, wall thickness, element length), physical and mechanical properties of materials, eccentricity values, and ultimate load-bearing capacity values. Statistical analysis confirmed the representativeness of the data for a wide range of parameters. This database was previously validated by Thai et al. [21] for the evaluation of normative methods (AISC 360, Eurocode 4, AS/NZS 2327[4]), which attests to its reliability.

A comparative analysis showed that CatBoost provides the highest prediction accuracy for eccentrically loaded rectangular columns, while LightGBM demonstrates slightly lower accuracy, but outperforms it in training speed by 1.5–2 times. Although the LightGBM algorithm is characterized by high training speed when working with large amounts of data due to the optimization of the tree construction process and supports distributed computing, CatBoost was preferred in this study. The key factor in the choice was the

[1] EN 1994-1-1 (2004) (English): Eurocode 4: Design of composite steel and concrete structures. Available from: https://www.phd.eng.br/wp-content/uploads/2015/12/en.1994.1.1.2004.pdf (accessed: 13.06.2025).

[2] ANSI/AISC 360-22. An American National Standard Specification for Structural Steel Buildings. Chicago: American Institute of Steel Construction; 2022. Available from: https://www.aisc.org/publications/steel-standards/aisc-360/ (accessed: 13.06.2025).

[3] SP 266.1325800.2016 Composite steel and concrete structures. Design rules. Moscow: Stroitel'stvo Publ.; 2017.

[4] AS/NZS 2327:2017. Composite structures — Composite steel-concrete construction in buildings. AS/NZS 2327:2017. Composite structures — Composite steel-concrete construction in buildings. Available from: https://www.standards.org.au/standards-catalogue/standard-details?designation=as-nzs-2327-2017 (accessed: 13.06.2025).

need to simultaneously predict two interrelated geometric parameters: the height and width of the cross-section of CFST columns. Unlike LightGBM, CatBoost has built-in mechanisms for multidimensional regression, which eliminates the need to create complex user-defined loss functions. An important advantage of CatBoost is its resistance to overfitting, provided by a combination of ordered boosting and automatic L2 regularization, which is especially important when working with synthetic data. Thus, despite the absence of categorical features in the analyzed data and the potential advantages of LightGBM in processing speed, the choice of CatBoost proved to be methodologically reasonable, as it best suits the specifics of the problem at hand, given that for the dataset under consideration, the gain in processing speed is not a determining factor, while the advantages of CatBoost in terms of accuracy and prediction stability become of primary importance.

It is also worth noting that despite the significant number of studies devoted to CFST columns, most of them focus on verification calculations in determining the load-bearing capacity [22; 23], while issues related to determining the required cross-sectional dimensions remain insufficiently studied. Moreover, while a few studies do address design tasks, they are mainly limited to cases of central compression of round columns, while the issues of optimal design of rectangular CFST columns under eccentric loading are practically not considered, despite the importance of such calculations.

In this regard, it seems particularly relevant to develop new approaches to solving these problems for rectangular cross-sections under eccentric compression. This article is a continuation of the research [24–28] aimed at obtaining the most convenient and reliable tools for performing verification and design calculations for CFST columns.

The model proposed in this article can be used for automated design of CFST columns, reducing calculation time and increasing the economic efficiency of structural solutions. The results of the study are of interest to structural designers involved in the development and implementation of CFST columns, as well as for further scientific research in the field of optimization design of these structures.

2. Methods

Short columns are considered, for which deformations are small and do not lead to a significant change in the eccentricity of the longitudinal force. The following values were taken as input parameters for the machine learning model:

1) Concrete compressive strength class B, MPa according to the Interstate Standard in force in Russia GOST 18105-2018[5];

2) Compressive force magnitude F, kN;

3) Tube wall thickness t, mm;

4) Compressive force eccentricity e, mm;

The output parameters of the model are width b, mm and height h, mm of the cross-section.

Synthetic data was generated to train the model. The concrete class ranged from B15 to B80. The compressive load varied from 500 to 10000 kN in increments of 100 kN, the wall thickness varied from 3 mm to 22 mm in increments of 1 mm, and the eccentricity of the longitudinal force varied from 10 to 250 mm in increments of 10 mm. The selection of these concrete class ranges was determined by the possibility of purchasing concrete mixes with the declared strength from mass producers (ultra-high-strength concrete and low-grade concrete were not considered). The selected wall thickness range is determined by the rolled steel sections available in the Russian Federation. The minimum eccentricity value of 10 mm in the training set corresponds to the minimum value of random eccentricity according to SP 63.13330.2018[6]. The upper eccentricity limit of 250 mm is justified by the fact that at large eccentricities of

[5] GOST 18105-2018. Concrete. Rules for control and strength assessment. A.A. Gvozdev Concrete and Reinforced Concrete Research Institute. Moscow: Standardinform Publ.; 2019.

[6] SP 63.13330.2018. Concrete and reinforced concrete structures. General provisions. Available from: https://docs.cntd.ru/document/554403082 (accessed: 13.06.2025).

the longitudinal force, when the structure resists mainly bending rather than compression, the use of CFST structures becomes irrational. For each set of values $[B, F, t, e]$ the problem of determining the optimal values of dimensions b and h was solved under minimum cost of the structure taking into account the requirement to satisfy the strength condition.

Since most rectangular tube sections manufactured for the Russian market are made from grade 09G2S steel, yield strength R_y of the tube material is assumed to be constant. For this grade of steel, it averages 345 MPa.

The cost of 1 linear meter of the structure S is determined by the formula:

$$S = S_b bh + S_s \rho_s 2(b+h)t \to \min, \quad (1)$$

where S_b is the cost of 1 m^3 of concrete; S_s is the cost of 1 tonne of steel; $\rho_s = 7.85\text{t/m}^3$ is the density of steel.

The value of S_s was assumed to be 86800 rubles per tonne as an average value for tube sections of grade 09G2S steel according to the data of Metallotorg JSC[7] as on 27.03.2025 for the city of Rostov-on-Don, Russian Federation. The value of S_b depends on the concrete class. Table 1 contains the values of S_b for the considered concrete classes in this study according to the data of Astragal company[8]. This table also shows the values of the design strength of concrete depending on its class based on the Russian code SP 63.13330.2018[9].

Table 1. **The cost of 1 m^3 of concrete depending on its compressive strength class, as well as the design compressive strength**

Concrete class B	The cost of 1 m^3 of concrete, S_b, rub	Design compressive strength R_b, MPa
B15	5300	8.5
B20	5700	11.5
B25	6250	14.5
B30	6650	17
B35	6900	19.5
B40	7700	22
B45	8700	25
B50	9200	27.5
B55	10200	30
B60	10800	33
B70	12700	37
B80	13400	41

S o u r c e: made by S.H. Al-Zgul.

For designing the cross-section, it is necessary to write the strength condition of the CFST element under eccentric compression. This article considers the case when bending moment acts only in one plane. The effect of strength increase due to the resistance of concrete in confined conditions is not taken into account. The wall thickness of the tube is assumed to be small compared to the cross-sectional dimensions *b* and *h*. The external dimensions of the column are considered approximately equal to the dimensions of the concrete core.

[7] Metallotorg. Available from: https://www.metallotorg.ru/ (accessed: 13.06.2025).
[8] Astragal. Available from: https://www.astragal.su/ (accessed: 13.06.2025).
[9] SP 63.13330.2018. Concrete and reinforced concrete structures. General provisions. Available from: https://docs.cntd.ru/document/554403082 (accessed: 13.06.2025).

The limit equilibrium method is used to determine the ultimate load under eccentric compression. Previously, this method for CFST columns was validated using experimental data in [29]. The stress in the compressed zone of the concrete core is assumed to be equal to R_b. The stress in the tension zone of the concrete core is not taken into account. The stresses in the compression and tension zones of the steel tube are assumed to be equal to R_y with the corresponding signs (Figure 1).

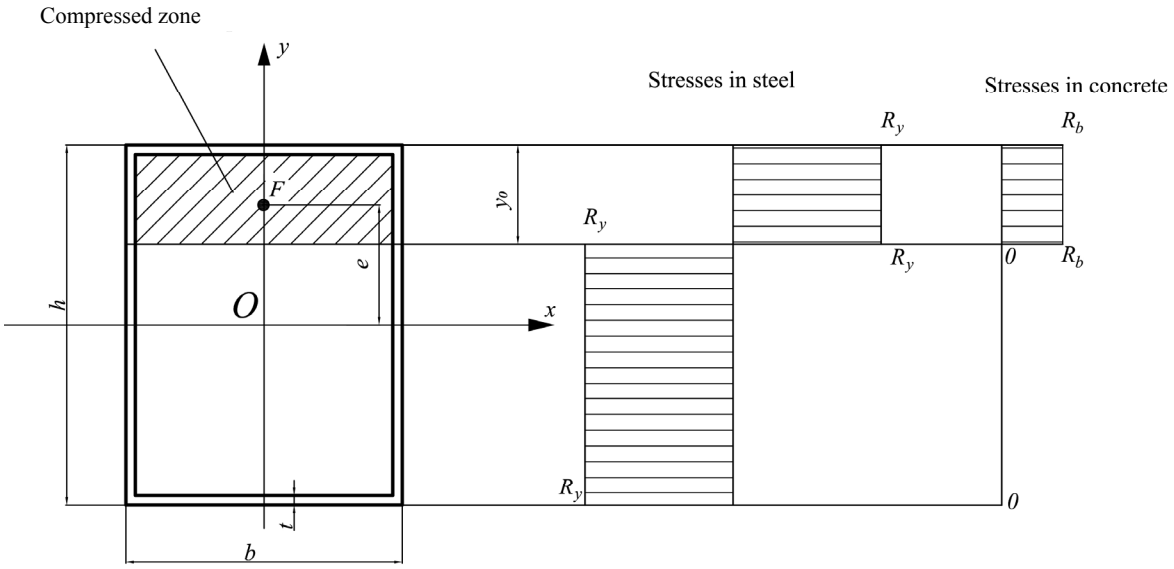

Figure 1. Diagram for determining the maximum load
S o u r c e: made by S.H. Al-Zgul.

The equation of equilibrium between internal and external forces projected onto the longitudinal axis of the column is as follows:

$$F = R_b b y_0 + 2R_y t y_0 + R_y t b - R_y t b - 2R_y t\left(h - y_0\right). \tag{2}$$

From (2), parameter y_0 is expressed as:

$$y_0 = \frac{F + 2R_y t h}{R_b b + 4R_y t}. \tag{3}$$

The equation of equilibrium between internal and external moments with respect to the *x*-axis in the limit state is written as:

$$\begin{aligned} Fe = {} & R_b b y_0\left(\frac{y_0}{2} - \left(y_0 - \frac{h}{2}\right)\right) + 2R_y t b\frac{h}{2} + 2R_y t y_0\left(\frac{y_0}{2} - \left(y_0 - \frac{h}{2}\right)\right) + \\ & + 2R_y t\left(h - y_0\right)\left(y_0 - \frac{h}{2} + \frac{h - y_0}{2}\right). \end{aligned} \tag{4}$$

Or, after simplification:

$$Fe = \frac{1}{2}R_b b y_0\left(h - y_0\right) + R_y t\left(bh + 2y_0\left(h - y_0\right)\right). \tag{5}$$

Substituting (3) into (5) yields a quadratic equation with respect to F, from which ultimate load F_{ult} is determined as the minimum positive root of this equation satisfying the condition:

$$y_0 = \frac{F_{ult} + 2R_y th}{R_b b + 4R_y t} \le h. \tag{6}$$

If none of the positive roots of the quadratic equation satisfy condition (6), this indicates that the compressed zone covers the entire concrete core and the neutral line runs either at the boundary between the concrete core and the lower side of the tube (Figure 2) or directly at the lower side of the tube. These cases are possible when the longitudinal force has a small eccentricity.

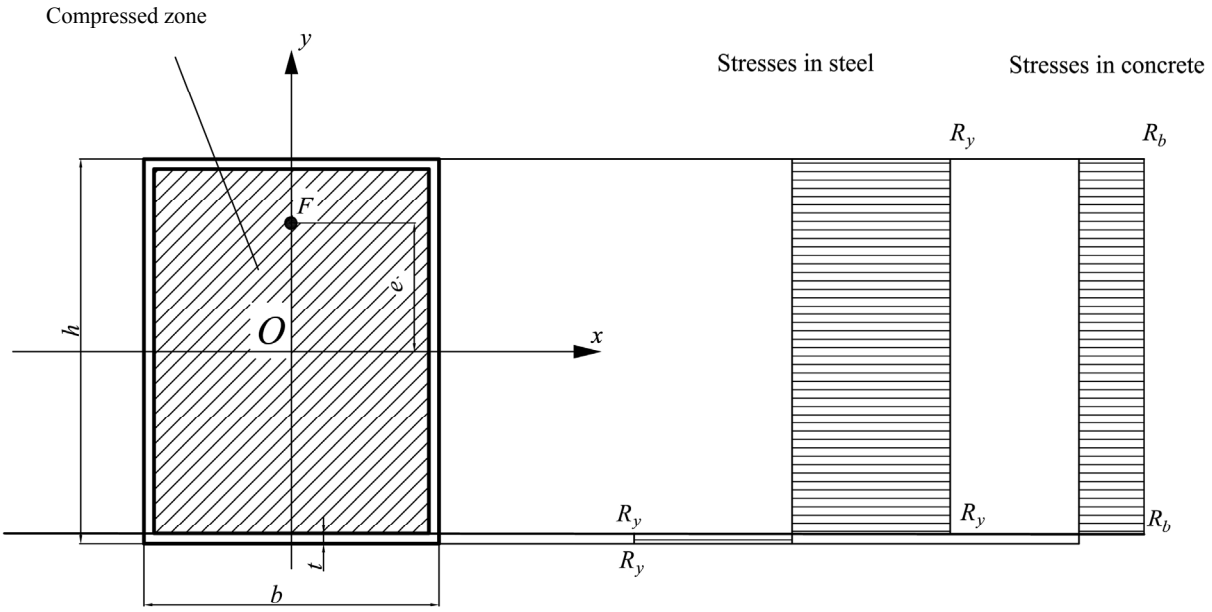

Figure 2. The case when the compressed zone covers the entire concrete core
S o u r c e: made by S.H. Al-Zgul.

For the case shown in Figure 2, the ultimate load is determined by the formula:

$$F_{ult2} = R_b bh + 2R_y ht. \tag{7}$$

If the neutral line is inside the lower side of the pipe, then F_{ult} will take an intermediate value between F_{ult2} and F_{ult0}, corresponding to the case of central compression:

$$F_{ult0} = R_b bh + 2R_y (h+b)t. \tag{8}$$

If when calculating y_0 it was obtained that $y_0 > h$, the ultimate load was determined using formula (7), which was included in the factor of safety.

The problem of finding the values of b and h from the minimum condition of cost function S limited by $F \le F_{ult}$ was solved as a nonlinear optimization problem using the interior point method [30] in the MATLAB R2024b environment (Optimization Toolbox package, fmincon function). Besides the limitation of $F \le F_{ult}$, the minimum and maximum values of dimensions b and h were also constrained. These

constraints are dictated by the possibility of laying concrete inside the tube (limit on minimum dimensions) and the current range of rectangular tube sections (limit on maximum dimensions):

$$\begin{aligned} &100\ \text{mm} \le b \le 500\ \text{mm}; \\ &100\ \text{mm} \le h \le 500\,\text{mm}. \end{aligned} \tag{9}$$

Only the data for which a solution to the optimization problem could be found under the specified constraints were included in the training dataset. The total volume of the training data set ultimately amounted to 504841 rows. A fragment of the training dataset is shown in Table 2.

Table 2. **A fragment of the training dataset**

No.	*B*, MPa	*F*, kN	*t*, mm	*e*, mm	*b*, mm	*h*, mm
1	15	500	3	10	100	171
2	15	500	3	20	100	171
3	15	500	3	30	100	171
4	15	500	3	40	100	178
5	15	500	3	50	100	191
6	15	500	3	60	100	204
7	15	500	3	70	100	217
8	15	500	3	80	100	229
9	15	500	3	90	100	240
10	15	500	3	100	100	252
…	…	…	…	…	…	…
504832	80	10000	22	160	259	500
504833	80	10000	22	170	272	500
504834	80	10000	22	180	285	500
504835	80	10000	22	190	299	500
504836	80	10000	22	200	312	500
504837	80	10000	22	210	326	500
504838	80	10000	22	220	341	500
504839	80	10000	22	230	355	500
504840	80	10000	22	240	369	500
504841	80	10000	22	250	384	500

S o u r c e: made by S.H. Al-Zgul.

In this study, a program was developed in Python language with support of version 3.11+, implementing the gradient boosting algorithm (Catboost) for predicting two physically interrelated geometric characteristics (width and height) of CFST column cross-sections based on four initial characteristics (design compressive strength of concrete, magnitude of compressive force, tube wall thickness, eccentricity of compressive force). Since the presented model has a small number of parameters, it can be trained and used on most modern (as of 2025) consumer GPUs or even in cloud environments with free quotas (e.g., Google Colab, Kaggle). When setting the regression problem, the MultiRMSE (Composite RMSE) metric was used — a generalized case of the standard RMSE for simultaneous optimization of the loss function for two target variables — the width (b) and height (h) of the cross-section (10):

$$\text{MultiRMSE} = \sqrt{\frac{1}{2N}\sum_{i=1}^{N}\left[\left(b_i - \hat{b}_i\right)^2 + \left(h_i - \hat{h}_i\right)^2\right]}, \tag{10}$$

where N is the number of records (columns) in the sample; 2 is the number of target variables; b_i is the true width of the i-th column section, mm; h_i is the true height of the i-th column section, mm; $\hat{b}_i$ is the predicted width of the i-th column section, mm; $\hat{h}_i$ is the predicted height of the i-th column section, mm.

As part of the study, the initial dataset was divided into three independent subsamples. The initial split was carried out in a 80% to 20% ratio, with 20% of the data being set aside as an isolated test sample for the final evaluation of the model quality. The remaining 80% of the data, constituting the training pool, was further divided: 25% was allocated for the validation sample (corresponding to 20% of the total data volume), and the remaining 75% (60% of the total volume) formed the final training sample.

The following control metrics were selected: the composite MultiRMSE metric on the validation dataset to evaluate the overall predictive power of the model, as well as individual metrics for each variable: MAE to evaluate the average accuracy of the model (in understandable, interpretable units), RMSE — allows detecting the influence of outliers when selecting the final model, and the coefficient of determination — R^2 demonstrates the advantage of the current model compared to the average prediction.

The split was performed by fixing the random seed parameter using the train_test_split function from the scikit-learn library. This makes the procedure completely deterministic and reproducible.

To verify the quality of the split, a statistical test for the homogeneity of distributions (Kruskal — Wallis for categorical/continuous features) between samples was performed based on key features. The test results (p_value > 0.05) did not reveal any statistically significant differences, which confirms the correctness of the random split.

3. Results and Discussion

The model training graph (Figure 3) demonstrates virtually identical behavior of the training and validation curves. At the initial stage (before ~500 iterations), there is a sharp decrease in RMSE from ~1.2 to ~0.1, after which the process enters a phase of smooth optimization, reaching a stable plateau after ~2000 iterations.

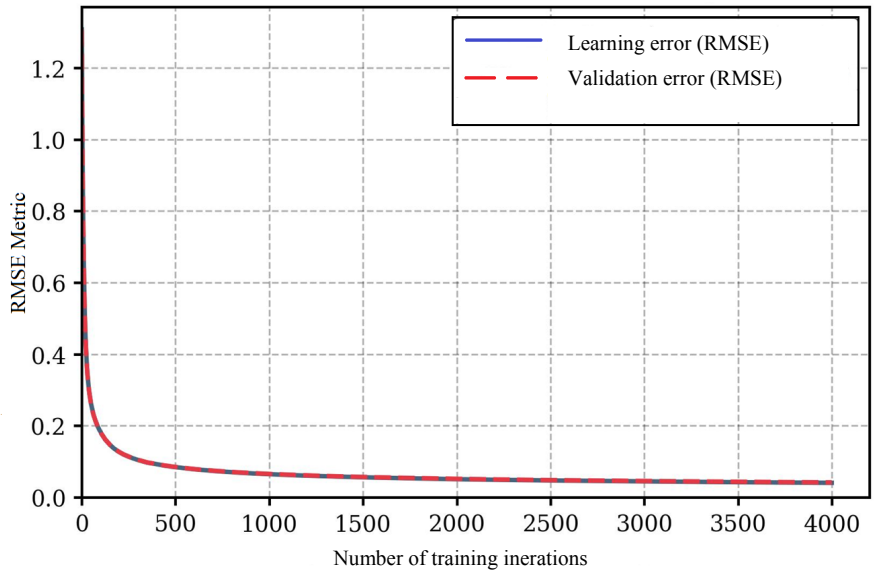

Figure 3. Graph of the learning curve for training and validation samples

S o u r c e: made by S.H. Al-Zgul.

The analysis of the model accuracy (Figures 4, 5) showed that the coefficient of determination reaches R^2 = 0.999033 for the cross-section width (b) and R^2 = 0.999211 the cross-section height (h), which indicates that the predicted values correspond almost perfectly to the target values. It is worth to note the uniform distribution of errors across the entire range of the studied dimensions (100–500 mm). This fact, along with the small dispersion, confirms the high reliability of the algorithm. It should be emphasized that the difference in prediction accuracy between the parameters does not exceed 2%, which indicates the

balance of the predictive power of the model for the two target variables. Since the application of the Catboost algorithm is essentially a solution to the problem of multidimensional nonlinear interpolation, the limits of the model application are determined by the range of input parameters in the training dataset.

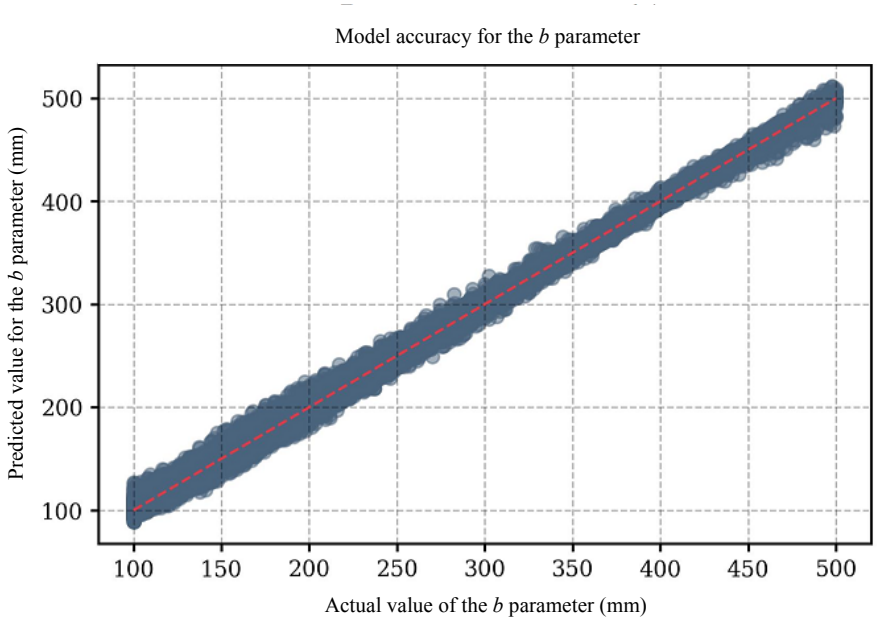

Figure 4. Accuracy of prediction of section width (*b*)
S o u r c e: made by A.S. Chepurnenko, S.H. Al-Zgul.

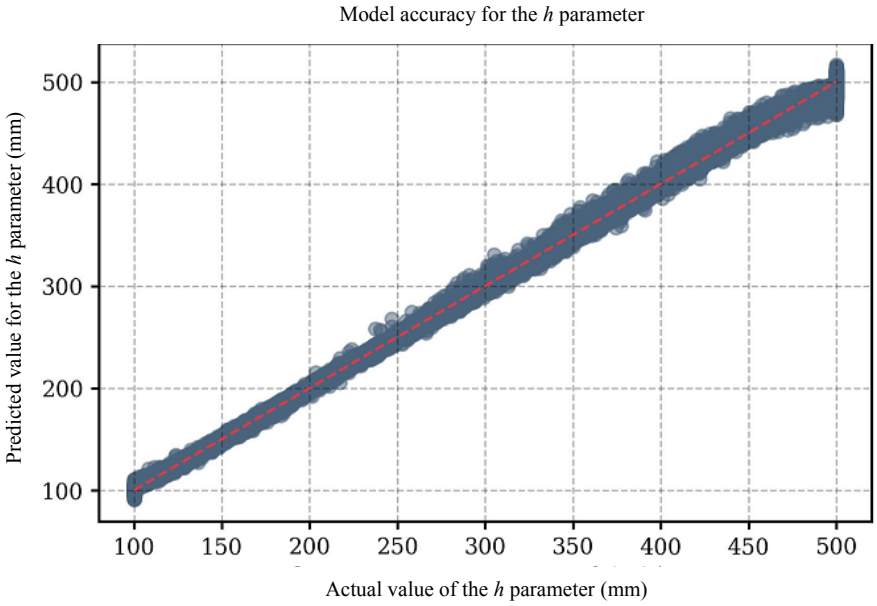

Figure 5. Accuracy of prediction of section height (*h*)
S o u r c e: made by A.S. Chepurnenko, S.H. Al-Zgul.

To evaluate the contribution of individual features to the final result, it was decided to use SHAP analysis. This method, based on the principles of game theory, allows to accurately determine the independent contribution of each feature, unlike the standard feature importances, which can give distorted results due to the possible uneven distribution of Gain when splitting initially balanced subsamples.

SHAP-value calculation requires a trained model and a test dataset. SHAP values were calculated for the entire test sample. TreeExplainer was used, which employs the TreeSHAP algorithm for efficient and accurate calculation. As the background distribution, which is required to determine the basic mathematical expected value E[f(x)] of the model, 100 randomly selected objects from the training sample were used (100 objects is the optimal compromise between accuracy and computational efficiency). Feature importance was estimated as the mean absolute SHAP-value (mean |SHAP|) across all objects in the test sample.

The results of the feature importance analysis using SHAP-values demonstrate a clear, physically justified hierarchy of the influence of input parameters (or, more accurately, features) on the geometric characteristics of the cross-section (Figures 6, 7). At the same time, the SHAP dependence graphs demonstrate the nature of the influence of individual variables on the target value (Figures 8, 9).

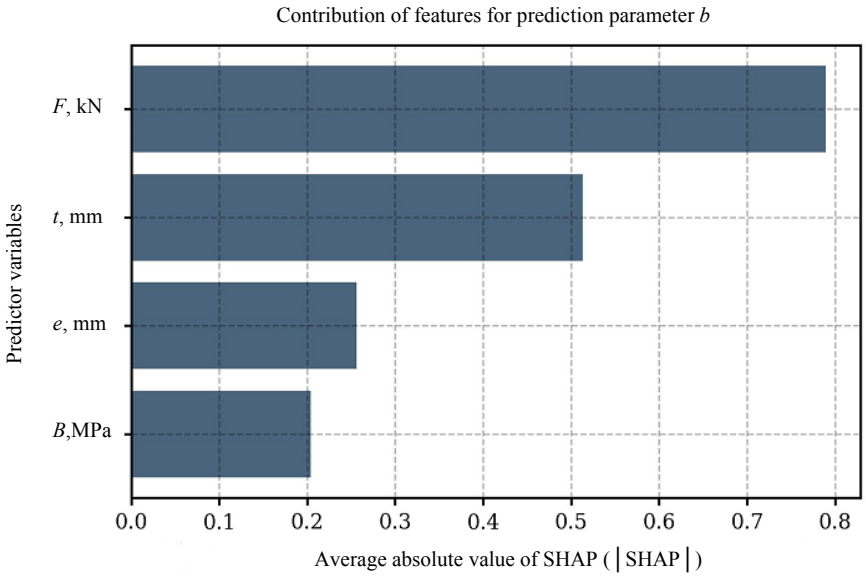

Figure 6. Analysis of the importance of features for predicting the section width (*b*)
S o u r c e: made by A.S. Chepurnenko, S.H. Al-Zgul.

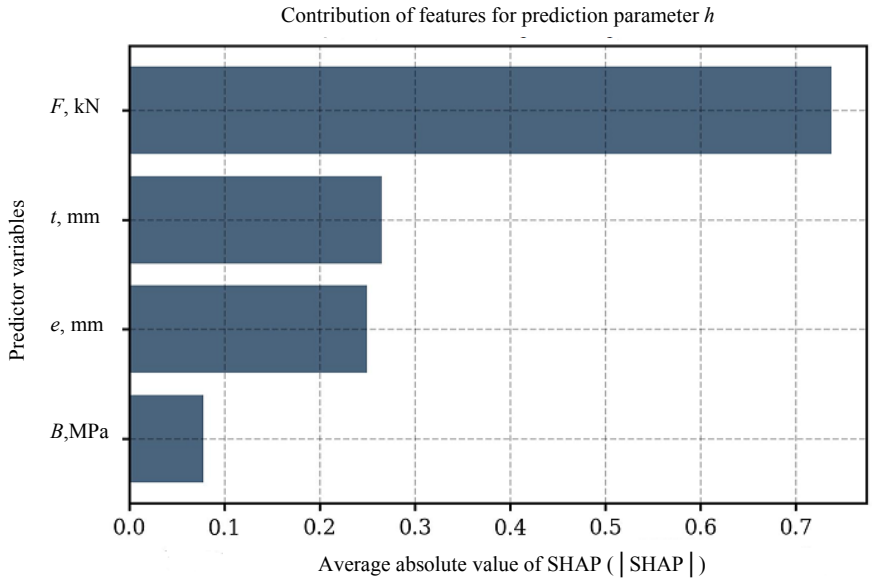

Figure 7. Analysis of the importance of features for predicting the section height (*h*)
S o u r c e: made by A.S. Chepurnenko, S.H. Al-Zgul.

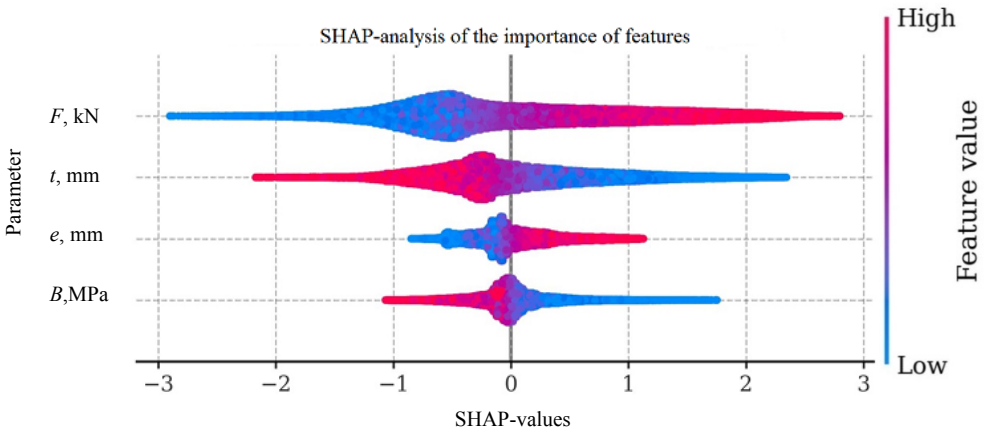

Figure 8. SHAP-analysis of the influence of factors on the width of the section
S o u r c e: made by A.S. Chepurnenko, S.H. Al-Zgul.

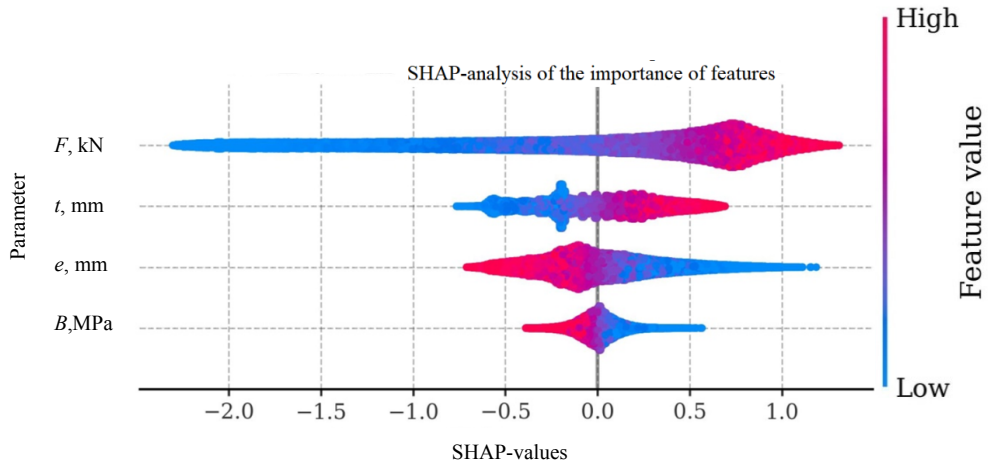

Figure 9. SHAP-analysis of the influence of factors on the height of the section
S o u r c e: made by A.S. Chepurnenko, S.H. Al-Zgul.

Data analysis revealed the dominant influence of the longitudinal force (F) on the geometric parameters of the cross-section, which is confirmed by the maximum values of SHAP indicators (0.79 for the width and 0.75 for the height). This pattern is fully consistent with the fundamental principles of calculating the load-bearing capacity of compressed elements. It is worth noting that the character of the influence of the load differs for the parameters under consideration: the section width demonstrates a more pronounced dependence with the SHAP-value in the range ≈ ±3 compared to the height in the range ≈ ±2, which is explained by the aspects of stress distribution in a rectangular section under eccentric compression. The results show a positive dependence between the increase in load and the increase in the geometric parameters of the cross-section (width b and height h), which is confirmed by the data in Figures 8 and 9.

The analysis reveals a significant difference in the degree of influence of the eccentricity (e) on the section parameters. Although eccentricity is significant for both dimensions, its effect on height is more pronounced (2nd in importance) than on width (3rd in importance). This is explained by the quadratic dependence of the moment resistance on the height of the cross-section, which makes an increase in h more effective in counteracting eccentric loads (Figures 6, 7). Graphical visualization confirms the need for |a proportional increase of both dimensions as eccentricity increases, which corresponds to the mechanics of the structure resistance to the combined action of bending moments and longitudinal forces.

The study using SHAP-value revealed a greater influence of wall thickness (t) on the cross-sectional width (SHAP~0.51) compared to the height (SHAP~0.25) (Figures 6, 7). According to the results, an increase in wall thickness leads to a decrease in both geometric parameters (b and h), which is expected, since an increase in the wall thickness increases the proportion of forces absorbed by the steel shell.

Concrete class (B) demonstrates a statistically significant but relatively weak influence on the geometric parameters of the cross-section, which is particularly pronounced for the height (Figures 6, 7). This behavior is fully consistent with the mechanics of composite CFST structures, where the concrete core is mainly involved in the resistance at the ultimate stages of loading. The analysis revealed a clear inverse relationship between the concrete class and the cross-sectional dimensions: as the strength characteristics of the concrete increased, there was a regular decrease in both the width and height of the cross-section (Figures 8, 9).

The results of the analysis reveal significant dependencies between the structural parameters (wall thickness), mechanical properties of materials (concrete class, steel strength), and loading conditions (longitudinal force, eccentricity) on one hand, and the geometric characteristics of CFST columns on the other.

4. Conclusion

The following scientific results were obtained based on the findings of the study:

1. A regression model based on the CatBoost algorithm has been developed and validated for predicting the optimal geometric parameters (width b and height h) of rectangular concrete filled steel tube columns under eccentric compression. The model demonstrates high prediction accuracy with a total composite metric MultiRMSE ≈ 3.6 mm (on the validation dataset), as well as MAE = 2.503 mm for width b, MAE = 2.467 mm for height h (on the test dataset) with a coefficient of determination $R^2 > 0.999$ for both target parameters. The design values of the height and width of the cross-section obtained using the algorithm are for reference only. The final selection of the geometric parameters must comply with the requirements of GOST, SP, or other regulatory documents and is agreed upon by the structural designer based on detailed calculations and a technical and economic justification.

2. A multi-criteria optimization method has been developed that takes into account strength conditions, design constraints, and economic efficiency by minimizing the cost function S.

3. The interior point method has proven its effectiveness in solving this nonlinear problem, providing an optimal balance between load-bearing capacity, overall dimensions, and economic parameters of the structure, as well as allowing design requirements and technological constraints to be taken into account at the stage of forming the training sample.

4. SHAP-analysis allowed to establish a clear hierarchy of importance of the input parameters, where the longitudinal force demonstrates dominant influence (SHAP-values in the range of 0.75-0.79), which quantitatively confirms its key role in determining the dimensions of the structure. At the same time, a differentiated influence of eccentricity on the geometric parameters was revealed — its influence on section height h was more pronounced compared to width b. The obtained distribution of feature importance fully corresponds to the fundamental theoretical principles of structural mechanics, which confirms the physical validity of the developed model.

The developed approach ensures optimal design of rectangular concrete filled steel tube structures under eccentric compression while meeting reliability and cost-effectiveness requirements within the range of input parameters on which the model was trained.

The obtained results form the scientific and methodological basis for the automation of concrete filled steel tube structure design processes, opening up promising areas for further research, including: expanding the model to account for long-term loads and complex loading conditions, integration with BIM technologies, and the development of regulatory recommendations for the implementation of machine learning methods in design practice. These areas will significantly improve the efficiency of structural design while ensuring the required reliability and cost-effectiveness.

References

1. Rimshin V.I., Semenova M.N., Shubin I.L., Krishan A.L., Astafieva M.A. Studies of the bearing capacity of non-centrally compressed steel-tube concrete columns. *Construction Materials*. 2022;(6):8–14. (In Russ.) https://doi.org/10.31659/0585-430X-2022-803-6-8-14 EDN: YHDXCL

2. Pan Y.C., Wang G.H., Xiang K. Overview of research progress for concrete-filled steel tubular columns after exposure to fire. *Applied Mechanics and Materials*. 2014;638–640:197–201. https://doi.org/10.4028/www.scientific.net/AMM.638-640.197

3. Krishan A.L., Krishan M.A., Sabirov R.R. Perspectives to apply concrete filled steel tube columns in construction projects of Russia. *Vestnik of Nosov Magnitogorsk State Technical University*. 2014;1(45):137–140. (In Russ.) EDN: RZPTUD

4. Hirakawa K. Saburi K., Kushima S., Kojima K. Performance-based design of 300 m vertical city "Abeno Harukas." *International Journal of High-Rise Buildings*. 2014;3(1):35–48. Available from: https://civil808.com/sites/default/files/performance_based_design_of_300.pdf (accessed: 10.03.2025).

5. Knowles R.B., Park R. Strength of concrete filled steel tubular columns. *Journal of the Structural Division*. 1969;95:2565–2588. Available from: https://trid.trb.org/view.aspx?id=105608 (accessed: 12.06.2025).

6. Sakino K., Nakahara H., Morino S., & Nishiyama I. Behavior of centrally loaded concrete-filled steel-tube short columns. *Journal of Structural Engineering*. 2004;130(2):180–188. https://doi.org/10.1061/(ASCE)0733-9445(2004)130:2(180

7. Tran V.-L., Thai D.K. A new empirical formula for prediction of the axial compression capacity of CCFT columns. *Steel and Composite Structures*. 2019;33(2):181–194. https://doi.org/10.12989/scs.2019.33.2.181

8. Tao Z., Uy B., Han L.-H., He S.-H. Design of Concrete-Filled Steel Tubular Members According to the Australian Standard AS 5100 Model and Calibration. *Australian Journal of Structural Engineering*. 2008;8(3):197–214. https://doi.org/10.1080/13287982.2008.11464998

9. Goode C.D. Composite columns-1819 tests on concrete-filled steel tube columns compared with Eurocode 4. *The Structural Engineer*. 2008; 86(16):33–38.

10. Gao P., Zhou X., Liu J., Lin X., Wang X., Chen Y.F. Experimental Assessment on the Size Effects of Square Concrete-Filled Steel Tubular Columns under Axial Compression. Engineering Structures. 2023;281:115706. https://doi.org/10.1016/j.engstruct.2023.115706

11. Chepurnenko A., Yazyev B., Khashkhozhev K., Chepurnenko V., Meskhi B., Beskopylny A. Simplified 2D finite element model for calculation of the bearing capacity of eccentrically compressed concrete-filled steel tubular columns. *Applied Sciences (Switzerland)*. 2021;11(24):11645. https://doi.org/10.3390/app112411645 EDN: AKSSMM

12. Lu D., Chen Zh., Ding F., Chen Zh., Sun P. Prediction of mechanical properties of the stirrup-confined rectangular cfst stub columns using fem and machine learning. *Mathematics*. 2021;9(14):1643. https://doi.org/10.3390/math9141643 EDN: MXXJFT

13. Mustafa R., Ahmad M.T. Appraisal of numerous machine learning techniques for the prediction of axial load carrying capacity of rectangular concrete column. *Asian J Civ Eng*. 2024;25:4471–4486. https://doi.org/10.1007/s42107-024-01060-6

14. Gao H. Calculation of load-carrying capacity of square concrete filled tube columns based on neural network. *Applied Mechanics and Materials*. 2011;71-78:847–850. https://doi.org/10.4028/www.scientific.net/AMM.71-78.847

15. Ahmadi M., Naderpour H., Kheyroddin A. Utilization of artificial neural networks to prediction of the capacity of CCFT short columns subject to short term axial load. *Archives of Civil and Mechanical Engineering*. 2014;14(3):510–517. https://doi.org/10.1016/j.acme.2014.01.006 EDN: IUXPQY

16. Wang H.J., Zhu H.B., Wei H. Bearing capacity of concrete filled square steel tubular columns based on neural network. *Advanced Materials Research*. 2012;502:193–197. https://doi.org/10.4028/www.scientific.net/AMR.502.193

17. Du Y., Chen., Wang Y.-B., Liew J.Y.R. Ultimate resistance behavior of rectangular concrete-filled tubular beam-columns made of high-strength steel. *Journal of Constructional Steel Research*. 2017;133:418–433. https://doi.org/10.1016/j.jcsr.2017.02.024

18. Le T.T., Asteris P.G., Lemonis M.E. Prediction of axial load capacity of rectangular concrete-filled steel tube columns using machine learning techniques. *Engineering with Computers*. 2022;38:3283–3316. https://doi.org/10.1007/s00366-021-01461-0

19. Zarringol M., Patel V.I., Liang Q.Q. Artificial neural network model for strength predictions of CFST columns strengthened with CFRP. *Engineering Structures*. 2023;281:115784. https://doi.org/10.1016/j.engstruct.2023.115784 EDN: AEKDAT

20. Degtyarev V.V., Thai H.T. Design of concrete-filled steel tubular columns using data-driven methods. *Journal of Constructional Steel Research*. 2023;200:107653. https://doi.org/10.1016/j.jcsr.2022.107653 EDN: AUPVMJ

21. Thai H.T., Thai S., Ngo T., Uy B., Kang W.H., Hicks S.J. Reliability considerations of modern design codes for CFST columns. *Journal of Constructional Steel Research*. 2021;177:106482. https://doi.org/10.1016/j.jcsr.2020.106482 EDN: FYAXTF

22. Megahed K. Strength prediction of ECC-CES columns under eccentric compression using adaptive sampling and ML techniques. *Scientific Reports*. 2025;15:1202. https://doi.org/10.1038/s41598-024-83666-z

23. Zarringol M., Naser M.Z. Explainable machine learning model for prediction of axial capacity of strengthened CFST columns. In Book: *Interpretable Machine Learning for the Analysis, Design, Assessment, and Informed Decision Making for Civil Infrastructure.* Elsevie Publ.; 2024. P. 229–253. https://doi.org/10.1016/B978-0-12-824073-1.00016-2

24. Chepurnenko A., Yazyev B., Khashkhozhev K., Chepurnenko V., Meskhi B., Beskopylny A. Simplified 2D finite element model for calculation of the bearing capacity of eccentrically compressed concrete-filled steel tubular columns. *Applied Sciences (Switzerland)*. 2021;11(24):11645. https://doi.org/10.3390/app112411645 EDN: AKSSMM

25. Chepurnenko A., Turina V., Akopyan V. Simplified method for calculating the bearing capacity of slender concrete-filled steel tubular columns. *Civil Eng*. 2023;4(3):1000–1015. https://doi.org/10.3390/civileng4030054 EDN: TDQHJD

26. Chepurnenko A., Al-Zgul S., Tyurina V. Machine learning for predicting required cross-sectional dimensions of circular concrete-filled steel tubular columns. *Buildings.* 2025;15(9):1438. https://doi.org/10.3390/buildings15091438

27. Al-Zgul S., Tyurina T., Chepurnenko A., Chepurnenko A., Akopyan V. Artificial neural network models for predicting required cross-section dimensions of concrete filled steel tubular columns. *The Open Civil Engineering Journal.* 2025;19(1). https://doi.org/10.2174/0118741495387193250411105201

28. Chepurnenko A.,Yazyev B., Al-Zgul S., Tyurina V. Simplified finite element model for rectangular CFST columns strength calculation under eccentric compression. *Magazine of Civil Engineering*. 2025;18(2):13406. https://doi.org/10.34910/MCE.134.6

29. Al-Zgul S., Tyurina V., Chepurnenko A. A simplified method for determining the bearing capacity of eccentrically compressed rectangular CFST columns with eccentricities in two planes. *The Open Construction & Building Technology Journal*. 2025;19:e18748368402845. https://doi.org/10.2174/0118748368402845250709060829

30. Chepurnenko A., Turina V., Akopyan V.F. Optimization rectangular and box sections in oblique bending and eccentric compression. *Construction Materials and Products.* 2023;6(5):1–14. https://doi.org/10.58224/2618-7183-2023-6-5-2

СТРОИТЕЛЬНАЯ МЕХАНИКА ИНЖЕНЕРНЫХ КОНСТРУКЦИЙ И СООРУЖЕНИЙ
STRUCTURAL MECHANICS OF ENGINEERING CONSTRUCTIONS AND BUILDINGS

2025. 21(6). 524–536

ISSN 1815-5235 (Print), 2587-8700 (Online)
HTTP://JOURNALS.RUDN.RU/STRUCTURAL-MECHANICS

РАСЧЕТ И ПРОЕКТИРОВАНИЕ СТРОИТЕЛЬНЫХ КОНСТРУКЦИЙ
ANALYSIS AND DESIGN OF BUILDING STRUCTURES

DOI: 10.22363/1815-5235-2025-21-6-524-536
EDN: FOEWDB

Научная статья / Research article

Напряженно-деформированное состояние ребристо-кольцевого купола при несимметричной и симметричной нагрузках с учетом разных узловых сопряжений и редко установленных колонн

Е.В. Лебедь

Национальный исследовательский Московский государственный строительный университет, *Москва, Российская Федерация*
✉ evglebed@mail.ru

Поступила в редакцию: 30 сентября 2025 г.
Доработана: 23 ноября 2025 г.
Принята к публикации: 30 ноября 2025 г.

Аннотация. Исследовано влияние несимметричной нагрузки на деформацию каркаса и на напряженное состояние основных элементов ребристо-кольцевого купола. Выявлена особенность работы купольного каркаса на несимметричную нагрузку по сравнению с симметричной при увеличении расстояния между поддерживающими купол колоннами. Одновременно с этим также установлена зависимость напряженно-деформированного состояния купольного каркаса от вида узловых сопряжений его элементов. В качестве объекта исследования рассматривался металлический ребристо-кольцевой купол из стальных труб. Купол имел четыре разные схемы опирания, характеризующиеся тем, что колонны располагались не под каждым ребром, но циклически симметрично по контуру. Для каждой схемы опирания в куполе изменялись виды узловых сопряжений элементов каркаса между собой. Разных схем по комбинациям видов сопряжений было пять. Исследования проводились посредством расчетов разных схем каркасов на компьютерных моделях. Всего исследованных расчетных компьютерных моделей насчитывалось двадцать. В процессе расчетов определялись деформации и напряжения в основных элементах купола каждой модели. Получены сведения о напряженно-деформированном состоянии всех моделей для несимметричной и симметричной нагрузок, которые сравнивались друг с другом. Составлены сравнительные диаграммы зависимостей деформаций купола и напряжений в его основных элементах от несимметричной и симметричной нагрузок для всех рассмотренных моделей. Диаграммы показали существенное влияние несимметричной нагрузки на деформацию купола и напряженное состояние элементов ребристо-кольцевого купола для всех схем опирания и видов узловых сопряжений. Отмечено, что при несимметричной нагрузке наибольшее увеличение напряжений по сравнению с симметричной происходит в меридиональных ребрах и значительное в верхнем кольце купола. В наибольшей степени увеличение деформаций и напряжений наблюдается при шарнирных узловых сопряжениях и зависит от схемы опирания купольного каркаса.

Ключевые слова: ребристо-кольцевой купол, компьютерная модель, меридиональные ребра, верхнее кольцо, нижнее кольцо, колонны, шарнирные и жесткие узлы, статический расчет

Заявление о конфликте интересов. Автор заявляет об отсутствии конфликта интересов.

Для цитирования: *Лебедь Е.В.* Напряженно-деформированное состояние ребристо-кольцевого купола при несимметричной и симметричной нагрузках с учетом разных узловых сопряжений и редко установленных колонн // Строительная механика инженерных конструкций и сооружений. 2025. Т. 21. № 6. С. 524–536. http://doi.org/10.22363/1815-5235-2025-21-6-524-536 EDN: FOEWDB

Лебедь Евгений Васильевич, кандидат технических наук, доцент кафедры металлических и деревянных конструкций, Национальный исследовательский Московский государственный строительный университет (НИУ МГСУ), Российская Федерация, 129337, г. Москва, Ярославское шоссе, д. 26; eLIBRARY SPIN-код: 5297-2700, ORCID: 0000-0003-3926-8701; e-mail: evglebed@mail.ru

Stress-Strain State of the Ribbed-Ring Dome Under asymmetric and Symmetric Loads Taking Into Account Different Nodal Connections and Rarely-Spaced Columns

Evgeny V. Lebed

[1] Moscow State University of Civil Engineering, *Moscow, Russian Federation*
✉ evglebed@mail.ru

Received: September 30, 2025
Revised: November 23, 2025
Accepted: November 30, 2025

Abstract. The effect of asymmetric load on the deformation of the frame and on the stress state of the main elements of the ribbed-ring dome was studied. The aspects of the dome frame resistance under asymmetric load compared with a symmetrical one with increase in the distance between the columns supporting the dome were investigated. At the same time, the relationship between the stress-strain state of the dome frame and the type of nodal connections of its elements was also established. A metal ribbed-ring dome made of steel pipes was considered as the object of the study. The dome had four different support arrangements, characterized by the fact that the columns were not located under each rib, but cyclically symmetrical along the contour. For each support scheme in the dome, the types of nodal connections of the frame elements to each other varied. There were five different connection type combinations. The research was carried out by calculating different frame systems as computer models. There were twenty computer models studied in total. During the calculations, strain and stress in the main elements of each dome model were determined. Data on the stress-strain state of all models under asymmetric and symmetrical loads were obtained, which were compared with each other. Comparative diagrams of the relationships the dome deformations and stress in its main elements and asymmetric and symmetrical loads for all the considered models have been compiled. The diagrams showed a significant influence of the asymmetric load on the deformation of the dome and the stress state of the elements of the ribbed-ring dome for all support arrangements and types of nodal connections. It is noted that with an asymmetric load, the greatest increase in stresses compared to a symmetrical one occurs in the meridional ribs and a significant increase — in the upper ring of the dome. The greatest increase in deformations and stress occurs with hinged nodal connections and depends on the support arrangement of the dome frame.

Keywords: computer model, meridional ribs, upper ring, lower ring, columns, hinged and rigid nodes, static calculation

Conflicts of interest. The author declares that there is no conflict of interest.

For citation: Lebed E.V. Stress-strain state of the ribbed-ring dome under asymmetric and symmetric loads taking into account different nodal connections and rarely-spaced columns. *Structural Mechanics of Engineering Constructions and Buildings.* 2025; 21(6):524–536. (In Russ.) http://doi.org/10.22363/1815-5235-2025-21-6-524-536 EDN: FOEWDB

1. Введение

Металлические купола являются пространственными конструктивными системами, применяются в качестве покрытий уникальных зданий во всем мире из-за выразительной формы и высокой надежности. Благодаря пространственной жесткости купольных каркасов и экономичности расхода металла по сравнению с другими конструкциями они занимают ведущее место среди большепролетных покрытий [1–3].

Геометрические схемы каркасов металлических куполов зависят от перекрываемых пролетов и назначения здания[1] [4]. Наиболее простыми по геометрическому строению считаются ребристо-кольцевые купола, в которых, однако, возможны различные схемы как по числу секторов по окружности, так и количеству ярусов по высоте. Кроме того, важным фактором в работе купольного каркаса является количество поддерживающих его колонн. От этого зависит статическая схема каркаса всего сооружения и напряженное состояние элементов купола. Отсутствуют в печати сравнительные характеристики работы купольных каркасов на симметричные и несимметричные нагрузки.

[1] Металлические конструкции: справочник проектировщика : в 3 т. / под общ. ред. В.В. Кузнецова (ЦНИИпроектстальконструкция им. Н.П. Мельникова). Т. 2. Стальные конструкции зданий и сооружений. Москва : АСВ, 1998. 512 с. ISBN 5-87829-081-2

Evgeny V. Lebed, Candidate of Technical Sciences, Associate Professor of the Department of Metal and Timber Structures, Moscow State University of Civil Engineering (National Research University), 26 Yaroslavskoye Shosse, Moscow, 129337, Russian Federation; eLIBRARY SPIN-code: 5297-2700, ORCID: 0000-0003-3926-8701; e-mail: evglebed@mail.ru

Обычно колонны в ребристо-кольцевых куполах размещают под каждым меридиональным ребром. Однако при большом числе ребер в купольном каркасе такое конструктивное решение может оказаться неприемлемым для архитектурного замысла. В этом случае используют меньшее количество колонн по сравнению с числом меридиональных ребер, что приводит, как подтвердило предыдущее исследование автора [5], к изменению работы купола и, как следствие, изменению внутренних усилий в элементах купольного каркаса. Это исследование показало также, что, несмотря на похожесть характера деформаций купола, с уменьшением количества колонн происходит существенное увеличение его прогибов.

Исследования стержневых систем купольного типа в различных компьютерных программах выполнялись многими учеными. Так, например, напряженное состояние купольного каркаса анализировалось при изменении его геометрических параметров [6], при разных отношениях высоты купола к диаметру для разных пролетов [7], при включении в работу ограждения в ячейках каркаса между ребрами и кольцами [8], при разных соотношениях высоты и диаметра и разных сечениях элементов [9], при разной высоте по сравнению с пролетом купольного каркаса со связями [10]. Автором выполнялось также сравнительное исследование ребристо-кольцевых куполов при различных количествах связей [11] и разных размерах верхнего кольца [12].

Отсутствуют публикации, кроме упомянутой ранее авторской [5], по исследованию зависимости напряженного состояния от редко установленных поддерживающих купол колонн. Кроме того, могут использоваться различные виды сопряжений элементов купольных каркасов, что также влияет на их работу. Влияние жесткости узловых сопряжений на напряженное состояние купола затронуто в публикации [13], где представлен сравнительный анализ работы ребристо-кольцевого стального купола диаметром 41 м и высотой 7 м. Купол насчитывал 20 ребер и 10 колец, опирался меридиональными ребрами непосредственно на фундаменты, а на кольцах-прогонах была устроена стеклянная обшивка. В этой публикации рассмотрены модели купольного каркаса, различающиеся линейным и нелинейным расчетами, а также двумя видами соединения: с креплением колец к ребрам и без крепления. Однако пояснений к интерпретации соединений в компьютерной модели нет. В некоторых моделях в работу включена обшивка, а в некоторых диагональные связи во всех секторах. В публикации анализировались деформации купола, внутренние усилия и напряжения в элементах.

Автор ранее уже исследовал работу каркаса ребристо-кольцевого купола с учетом разных узловых сопряжений и редко установленных колонн [14], целью которого было выявление закономерности изменения усилий в основных элементах купольного каркаса. Это исследование показало, что с уменьшением количества колонн внутренние усилия N существенно возрастают в колоннах и умеренно в меридиональных ребрах, а изгибающие моменты M значительно возрастают в нижнем кольце и немного в колоннах и верхнем кольце. Отмечено, что степень изменения усилий N и M зависит также и от вида узловых сопряжений элементов между собой.

Цель представленного материала — проведение сравнительного исследования напряженно-деформированного состояния каркаса ребристо-кольцевого купола при работе на несимметричную нагрузку по отношению к симметричной. Исследование проводилось на ранее созданных расчетных компьютерных моделях [14] и выполнено в полном соответствии с принципами анализа различных состояний стержневых пространственных систем.

2. Методы

В процессе исследования рассматривались двадцать разных расчетных компьютерных моделей каркаса круглого в плане сооружения с куполом. Они разделялись на четыре группы по схемам опирания купола на колонны, и каждая группа включала в себя пять разных комбинаций видов узловых сопряжений элементов каркаса между собой.

Исходным каркасом для исследования служил ребристо-кольцевой купол сферической формы с радиусом кривизны 23 м, разделенный меридиональными ребрами на 36 секторов и насчитывающий

7 колец вместе с верхним и нижним, который опирается на 36 колонн [14] (рис. 1). Диаметр нижнего кольца 39,3 м, диаметр верхнего кольца 5,0 м, высота купола 11 м, высота колонн 7,0 м.

Все элементы каркаса приняты из стальных труб по результатам предварительного расчета на нагрузки от веса ограждающих конструкций (1,0 кН/м^2), от веса снега (2,1 кН/м^2) и от собственного веса: меридиональные ребра из О 530×9, верхнее кольцо из О 530×9, нижнее кольцо из О 630×20, промежуточные кольца из О 273×7, колонны из О 402×10.

Исходный каркас соответствует первой схеме опирания, при которой колонны расположены под каждым сопряжением меридионального ребра с опорным кольцом. Вторая, третья и четвертая схемы опирания образуются путем циклически симметричного уменьшения количества поддерживающих купол колонн, т.е. их регулярного удаления из компьютерной модели. Отличительным признаком всех схем опирания являлось число секторов между колоннами. Поэтому исходная схема опирания каркаса, в которой колонны устанавливались через один сектор, обозначалась как *1*. Если же колонны устанавливались через два, четыре и шесть секторов, то и схемы обозначались как схемы опирания *2*, *4* и *6* соответственно (рис. 2).

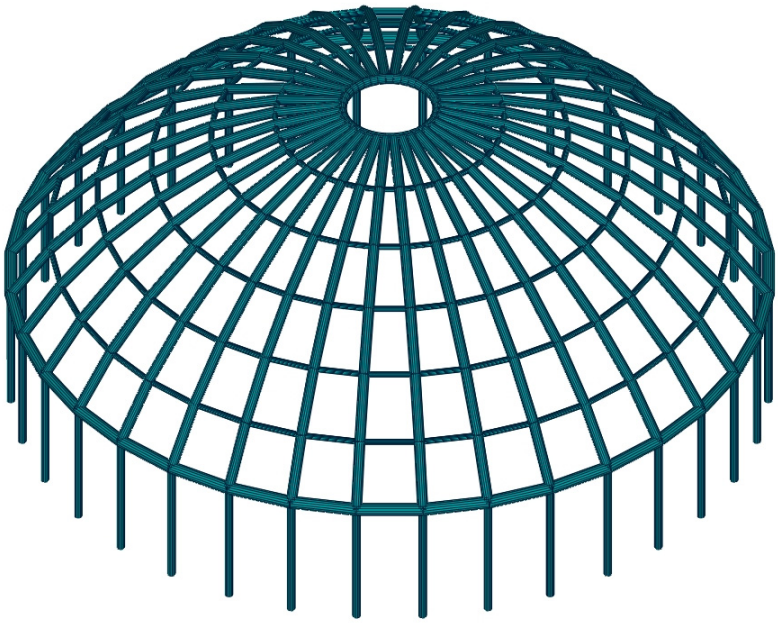

Рис. 1. Исходная схема каркаса исследуемого купола с колоннами под каждым ребром
И с т о ч н и к: выполнено Е.В. Лебедем.

Figure 1. The initial model of the dome under study with columns under each rib
S o u r c e: made by E.V. Lebed.

Собственный вес ограждающих и несущих конструкций представляет собой симметричную нагрузку, а нагрузка от веса снега представлена двумя вариантами[2]: симметричным и несимметричным. В симметричном варианте *1* снег лежит равномерно по поверхности в верхней части купола с углом ската $\alpha \le 30^\circ$, а с увеличением этого угла его толщина уменьшается до нулевого значения при $\alpha \ge 60^\circ$ (рис. 3, *а*). В несимметричном варианте *2* снег лежит только с одной стороны купола, который проецируется на полукруг, с наибольшими значениями в его середине, внутри которого его толщина сначала увеличивается по скату до максимума при $\alpha = 30^\circ$, потом уменьшается до фиксированного

[2] СП 20.13330.2016. Нагрузки и воздействия. Актуализированная редакция СНиП 2.01.07-85*. Москва : Минстрой России, 2016. 80 с.

значения при $\alpha = 45^{\circ}$, а затем до нулевого значения при $\alpha \geq 60^{\circ}$, а в кольцевых направлениях толщина уменьшается до нулевого значения на границе полукруга (рис. 3, *б*). При этом наибольшая сила от снеговой нагрузки на узел самого загруженного промежуточного кольца в варианте *2* по величине в 2,42 раза больше, чем в варианте *1*. Таким образом, в комбинации с весом ограждающих и несущих конструкций купола вес снега на нем по варианту *2* создает несимметричную нагрузку, а по варианту *1* симметричную нагрузку.

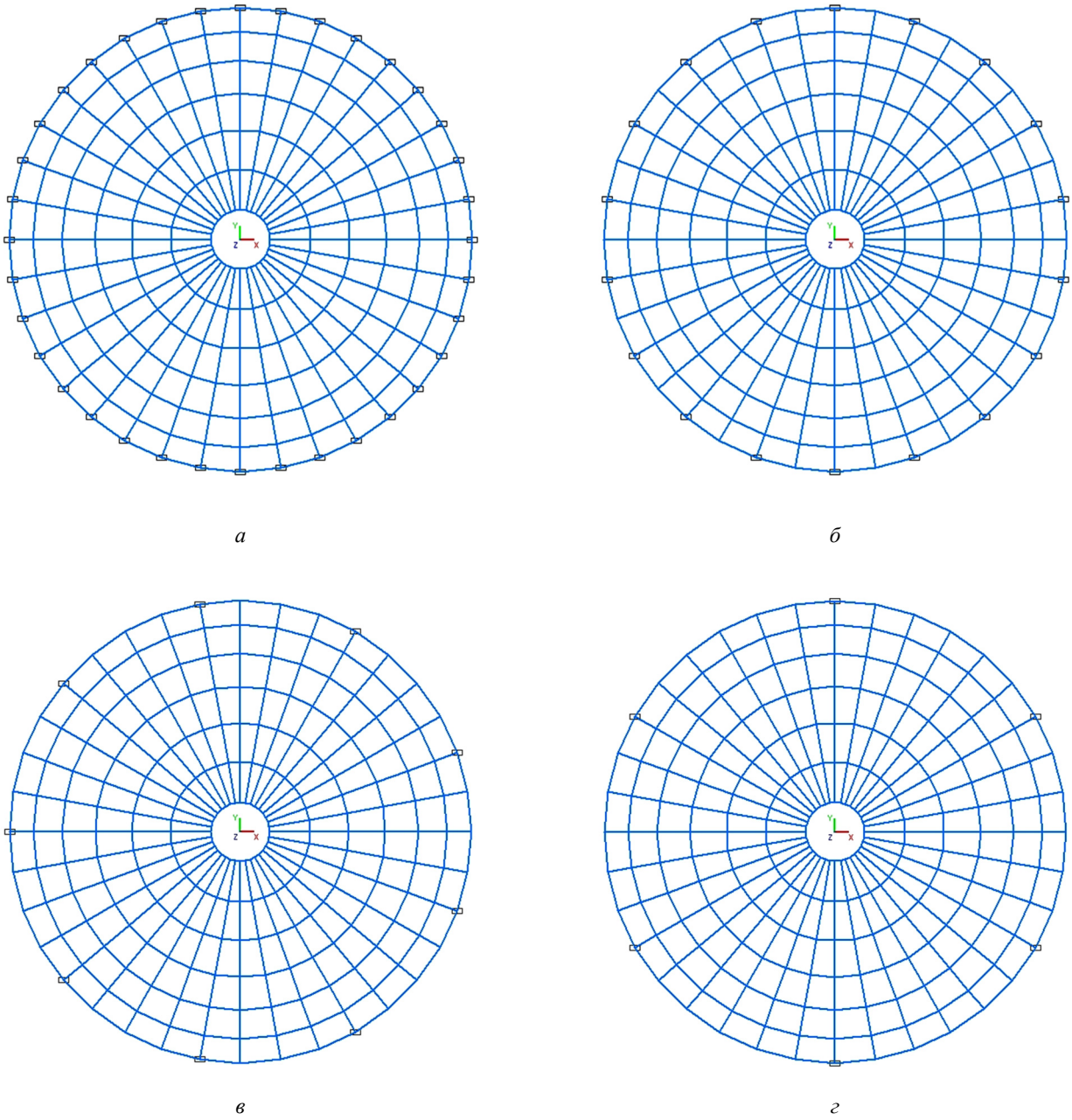

а *б* *в* *г*

Рис. 2. Схемы каркасов с разным числом секторов между колоннами под куполом:
а — 1 сектор; *б* — 2 сектора; *в* — 4 сектора; *г* — 6 секторов
И с т о ч н и к: выполнено Е.В. Лебедем.

Figure 2. Models of frames with different numbers of sectors between the columns under the dome:
а — 1 sector; *б* — 2 sectors; *в* — 4 sectors; *г* — 6 sectors
S o u r c e: made by E.V. Lebed.

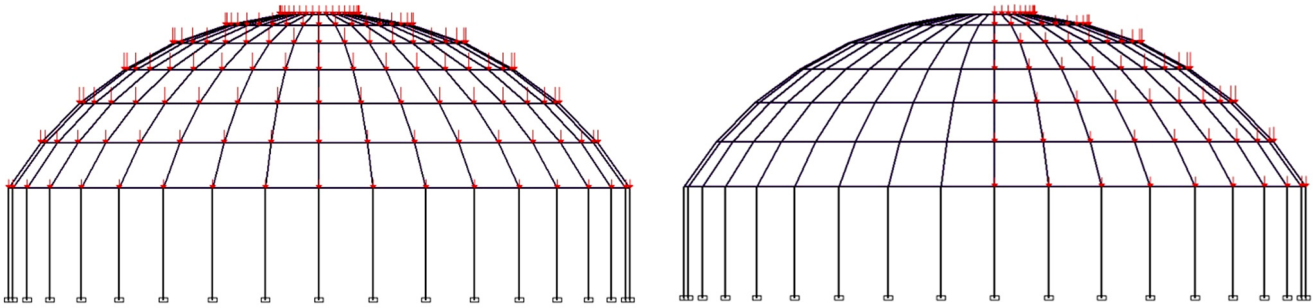

а *б*

Рис. 3. Схемы загружений купольных каркасов от веса снега:
а — вариант *1* (симметричный); *б* — вариант *2* (несимметричный)
И с т о ч н и к: выполнено Е.В. Лебедем.

Figure 3. Loading schemes of dome frames from the weight of snow:
а — option *1* (symmetrical); *б* — option *2* (asymmetrical)
S o u r c e: made by E.V. Lebed.

Исследования выполнялись на компьютерных расчетных моделях каркасов с ребристо-кольцевым куполом в программе SCAD как пространственных стержневых систем [15; 16].

Во всех схемах опирания стержни верхнего кольца, нижнего кольца и меридиональных ребер соединены друг с другом жестко. Соединение ребер с верхним и нижним кольцами, соединения колонн с нижним кольцом и соединения промежуточных колец с ребрами в каждой схеме опирания были различными: от шарниров в двух плоскостях (рис. 4) до жестких в двух плоскостях. В процессе исследования рассматривалось пять видов узловых сопряжений, обозначение и описание которых приведено в таблице.

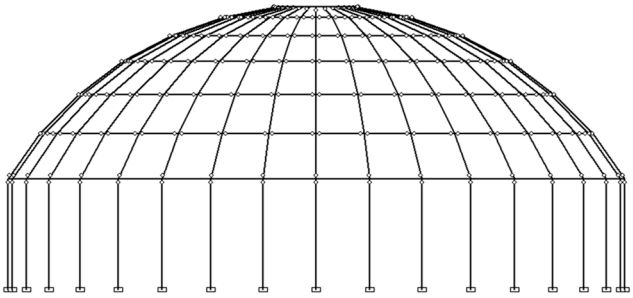

Рис. 4. Схема исходного каркаса
с шарнирными узловыми сопряжениями
И с т о ч н и к: выполнено Е.В. Лебедем.

Figure 4. Model of the initial frame
with hinged node connections
S o u r c e: made by E.V. Lebed.

Разрешения поворотов вокруг собственных осей в узловых сопряжениях
Rotational degrees of freedom around proper axes in nodal connections

Вид сопряжения / Joint type	**Наименование сопряжений элементов / Element joint name**							
	Ребер с верхним кольцом / Ribs to upper ring		**Ребер с нижним кольцом / Ribs to lower ring**		**Колонн с нижним кольцом / Columns to lower ring**		**Промежуточных колец с ребрами / Intermediate rings to ribs**	
	UX	UY	UX	UY	UX	UY	UX	UY
Ш3	v	v	v	v	v	v	v	v
Ш2	–	v	v	v	v	v	v	v
Ш1	–	v	v	v	v	v	–	v
Ж1	–	v	–	v	–	v	–	v
Ж2	–	–	–	–	–	–	–	–

Примечание: Знак «v» означает разрешение поворота вокруг оси, а знак «–» означает запрет /
Note: The “v” sign means that rotation around the axis is allowed, and the “–” sign means that it is prohibited.
И с т о ч н и к: выполнено Е.В. Лебедем / S o u r c e: made by E.V. Lebed.

Напряженно-деформированное состояние купольного каркаса во всех схемах опирания оценивалось по его прогибам f и по напряжениям σ^* в основных элементах, которые вычислялись по внутренним усилиям N, M_x, M_y, M_t. При этом эти внутренние усилия выбирались в наиболее нагруженных стержнях меридиональных ребер, верхнего кольца и нижнего кольца купола.

Оценка напряженного состояния каркаса выполнялась по приведенным напряжениям в его элементах

$$\sigma^* = \sqrt{\sigma^2 + 3\tau^2} \ . \tag{1}$$

Нормальные напряжения σ для трубчатого сечения

$$\sigma = \frac{N}{\mathrm{A}} \pm \frac{M}{\mathrm{W}_x}, \tag{2}$$

где для труб $M = \sqrt{M_x^2 + M_y^2}$ — это равнодействующая величина моментов M_x, M_y.

Касательные напряжения τ при наличии крутящего момента M_t

$$\tau = \frac{M_t}{\mathrm{W}_t} \ . \tag{3}$$

Следует отметить, что выполненные автором ранее исследования кручения [17] показали, что касательные напряжения τ значительное влияние оказывают на верхнее кольцо, кроме сопряжений Ш3, и заметное на нижнее кольцо для сопряжений Ж1. В меридиональных ребрах касательные напряжения τ также оказывают существенное влияние. Там же приведены и диаграммы приведенных напряжений σ^* в меридиональных ребрах, верхнем и нижнем кольцах купола.

3. Результаты

При симметричной нагрузке деформации купольного каркаса также проявляют симметрию смещения узлов и, как правило, вниз. При несимметричной нагрузке деформации не только становятся асимметричными, но и характеризуются смещениями узлов со стороны большего нагружения вниз, а со стороны меньшего нагружения вверх. Причем смещения вниз (прогиб) по абсолютной величине гораздо больше, чем смещение вверх (выгиб).

В исходной схеме каркаса (схема опирания *1*), а также в схеме опирания *2* при симметричной нагрузке изменение видов узловых сопряжения от Ш3 до Ж2 практически не влияет на прогибы купола (рис. 5). В каркасах со схемами опирания *4* и *6* при симметричной нагрузке прогибы увеличиваются по отношению к исходной схеме и на их величины влияют виды узловых сопряжений.

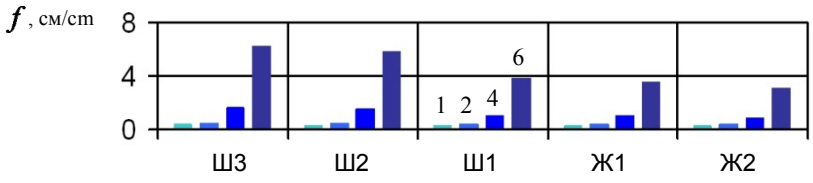

Рис. 5. Максимальные прогибы купольных каркасов при симметричной нагрузке:
1, *2*, *4*, *6* — число секторов между колоннами
И с т о ч н и к: выполнено Е.В. Лебедем.

Figure 5. Maximum deflections of dome frames under symmetrical load:
1, *2*, *4*, *6* — number of sectors between columns
S o u r c e: made by E.V. Lebed.

Несимметричная нагрузка приводит к значительному увеличению прогибов во всех схемах опирания, и вместе с тем изменение видов узловых сопряжения от Ш3 до Ж2 существенно влияет на прогибы купола (рис. 6). В каркасах со схемой опирания *6* при несимметричной нагрузке прогибы характеризуются наибольшими величинами для всех видов узловых сопряжений.

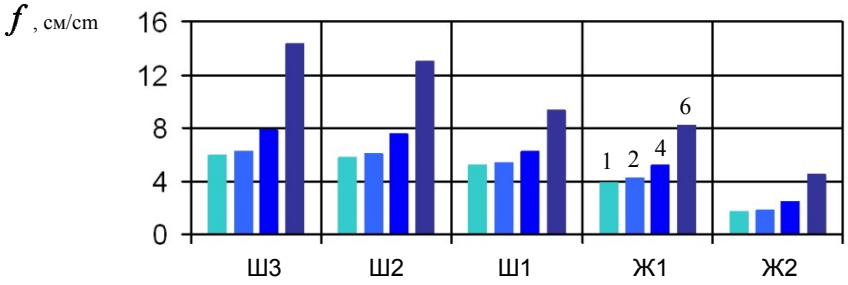

Рис. 6. Максимальные прогибы купольных каркасов при несимметричной нагрузке:
1, *2*, *4*, *6* — число секторов между колоннами
И с т о ч н и к: выполнено Е.В. Лебедем.

Figure 6. Maximum deflections of dome frames under asymmetrical load:
1, *2*, *4*, *6* — number of sectors between columns
S o u r c e: made by E.V. Lebed.

Прогибы купольных каркасов многократно увеличиваются при несимметричной нагрузке по сравнению с аналогичными прогибами при симметричной нагрузке, и это увеличение зависит как от схемы опирания купола, так и от вида узловых сопряжений его элементов. Отношения прогибов f_2/f_1 при несимметричной нагрузке f_2 к прогибам при симметричной нагрузке f_1 демонстрируют значения для узловых сопряжений с Ш3 до Ж2 в следующих диапазонах (рис. 7): в исходной схеме опирания *1* от 17,7 до 5,1, в схеме опирания *2* — от 14,2 до 4,5, в схеме опирания *4* от — 4,9 до 2,7, в схеме опирания *6* — от 2,3 до 1,5.

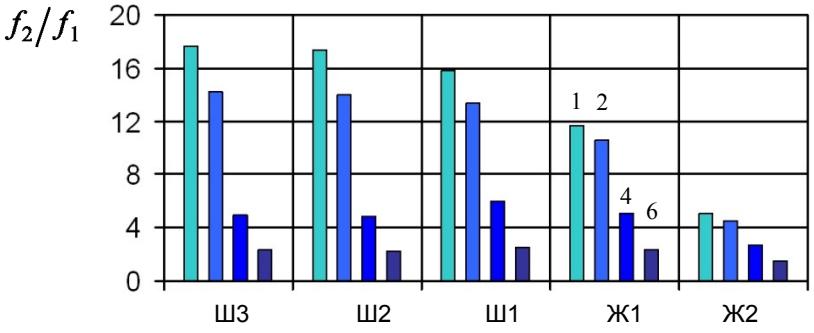

Рис. 7. Отношение прогиба при несимметричной f_2 к прогибу при симметричной f_1 нагрузках:
1, *2*, *4*, *6* — число секторов между колоннами.
И с т о ч н и к: выполнено Е.В. Лебедем.

Figure 7. The ratio of deflection under asymmetrical load f_2 to deflection under symmetrical load f_1:
1, *2*, *4*, *6* — number of sectors between columns
S o u r c e: made by E.V. Lebed.

Вычисленные по формуле (1) приведенные напряжения σ^* имеют некоторый условный характер, поскольку максимальные вычисленные по формуле (2) нормальные напряжения σ и вычисленные по формуле (3) максимальные касательные напряжения τ могли возникать в разных сечениях однотипных элементов. Такой подход объясняется тем, что в действительности эти напряжения сочетаются по величинам в широком диапазоне значений σ с широким диапазоном значений τ и их максимальные значения могли не совпадать. Однако принятые в данном исследовании сочетания в полной мере отражают влияние кручения на несущую способность элементов с максимальными значениями нормальных напряжений σ.

Согласно предыдущему авторскому исследованию [17], в меридиональных ребрах купола приведенные напряжения σ^* зависят от видов узловых сопряжений элементов и почти не изменяются при изменении схем опирания от *1* до *6*, за исключением узловых сопряжений Ж1 и Ж2 схемы опирания *6*. В верхнем кольце купола приведенные напряжения σ^* зависят от видов сопряжений и также остаются стабильными в схемах опирания *1–4*, а в схеме опирания *6* существенно возрастают. В нижнем кольце купола в наибольшей степени отражается зависимость приведенных напряжений σ^* от схемы опирания купола. Величины σ^* возрастают в несколько раз при переходе к схемам опирания с уменьшенным количеством колонн (в схемах *2*, *4* и *6*) и в то же время влияние на них видов узловых сопряжений усиливается.

В меридиональных ребрах отношения σ_2^*/σ_1^* приведенных напряжений при несимметричной нагрузке σ_2^* к приведенным напряжениям при симметричной нагрузке σ_1^* для узловых сопряжений от Ш3 до Ж2 показали очень большие значения. Но значения отношений σ_2^*/σ_1^* проявились поразному в следующих диапазонах (рис. 8): в схеме опирания *1* — от 7,4 до 2,9; в схеме опирания *2* — от 7,4 до 2,6; в схеме опирания *4* — от 4,9 до 2,1, а в схеме опирания *6* отношение σ_2^*/σ_1^* колеблется в диапазоне от 1,7 до 2,4.

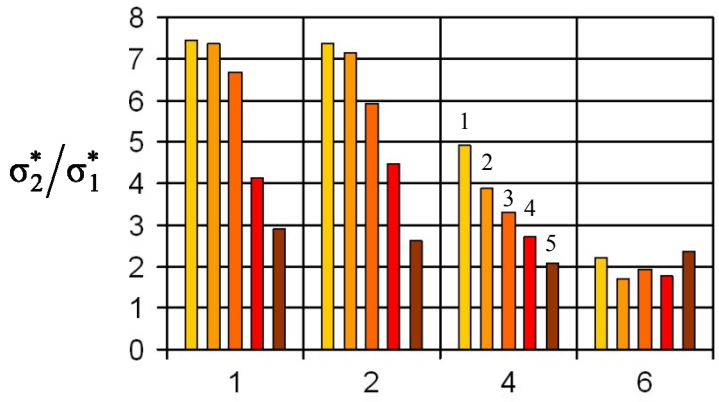

Рис. 8. Отношение напряжения при несимметричной σ_2^* к напряжению при симметричной σ_1^* нагрузках в меридиональных ребрах.
Виды сопряжений: *1* — Ш3, *2* — Ш2, *3* — Ш1, *4* — Ж1, *5* — Ж2
И с т о ч н и к: выполнено Е.В. Лебедем.

Figure 8. The ratio of stress under asymmetrical load σ_2^* to stress under symmetrical load σ_1^* in the meridional ribs.
Types of connections: *1* — Ш3, *2* — Ш2, *3* — Ш1, *4* — Ж1, *5* — Ж2
S o u r c e: made by E.V. Lebed.

В верхнем кольце отношения σ_2^*/σ_1^* приведенных напряжений при несимметричной нагрузке σ_2^* к приведенным напряжениям при симметричной нагрузке σ_1^* для узловых сопряжений от Ш3 до Ж2 показали существенные значения. Но отношения σ_2^*/σ_1^* имеют наибольшие значения для узловых сопряжений Ш1 и не намного отличаются в разных схемах опирания купола в следующих диапазонах (рис. 9): в исходной схеме опирания *1* — от 2,4 до 1,4; в схеме опирания *2* — от 2,5 до 1,4; в схеме опирания *4* — от 2,0 до 1,4, а в схеме опирания *6* — от 1,6 до 1,1.

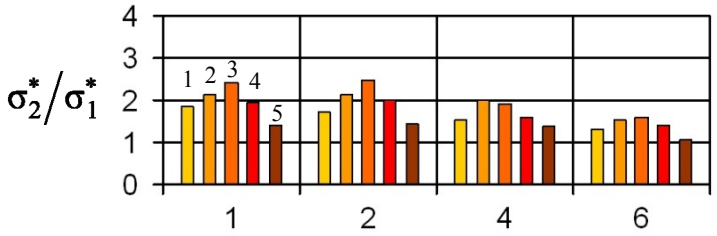

Рис. 9. Отношение напряжения при несимметричной σ_2^* к напряжению при симметричной σ_1^* нагрузках в верхнем кольце.

Виды сопряжений: *1* — Ш3, *2* — Ш2, *3* — Ш1, *4* — Ж1, *5* — Ж2

И с т о ч н и к: выполнено Е.В. Лебедем.

Figure 9. The ratio of stress under asymmetrical load σ_2^* to stress under symmetrical load σ_1^* in the upper ring:

Types of connections: *1* — Ш3, *2* — Ш2, *3* — Ш1, *4* — Ж1, *5* — Ж2

S o u r c e: made by E.V. Lebed.

В нижнем кольце отношения σ_2^*/σ_1^* приведенных напряжений при несимметричной нагрузке σ_2^* к приведенным напряжениям при симметричной нагрузке σ_1^* характеризуются незначительными значениями в схемах опирания *4* и *6* для узловых сопряжений от Ш3 до Ж2 в диапазонах от 1,0 до 1,2 и от 1,1 до 1,2 соответственно (рис. 10). А в схеме опирания *1* и в схеме опирания *2* это отношение проявилось существенными значениями в диапазонах от 1,3 до 2,0 и от 1,2 до 1,7 соответственно с наибольшими значениями для узловых сопряжений Ж1 и Ж2.

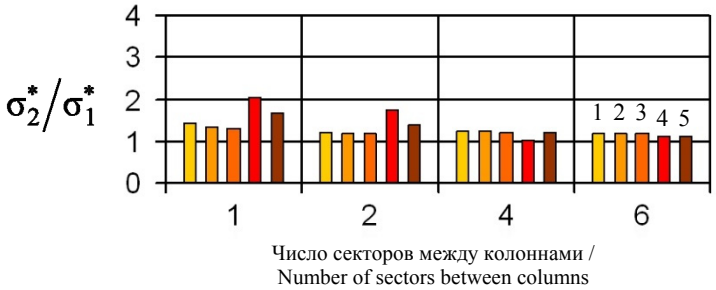

Рис. 10. Отношение напряжения при несимметричной σ_2^* к напряжению при симметричной σ_1^* нагрузках в нижнем кольце.

Виды сопряжений: 1 — Ш3, 2 — Ш2, 3 — Ш1, 4 — Ж1, 5 — Ж2

И с т о ч н и к: выполнено Е.В. Лебедем.

Figure 10. The ratio of stress under asymmetrical load σ_2^* to stress under symmetrical load σ_1^* in the lower ring:

Types of connections: 1 — Ш3, 2 — Ш2, 3 — Ш1, 4 — Ж1, 5 — Ж2

S o u r c e: made by E.V. Lebed.

В процессе исследования отдельно выявлялось влияние части напряжений только от продольных сил N, т.е. $\sigma_N = N/\mathrm{A}$. Исследование показало, что влияние долей напряжений σ_N на итоговые напряжения σ^* неодинаково для разных элементов купольного каркаса. Величины этих долей, представленные отношением напряжений $\Delta_N = \sigma_N / \sigma^*$, зависят как от схем опирания, так и от видов узловых сопряжений. Для несимметричной нагрузки значения Δ_N изменяются так: в меридиональных ребрах в диапазоне — от 0,14 до 0,46; в верхнем кольце в диапазоне — от 0,12 до 0,41; в нижнем кольце в диапазоне — от 0,05 до 0,73.

Отношения напряжений от продольных сил N при несимметричной нагрузке σ_{N2} к аналогичным напряжениям при симметричной нагрузке σ_{N1}, т. е. σ_{N2}/σ_{N1}, в разных элементах показали незначительные отличия друг от друга. Для разных видов узловых сопряжений значения σ_{N2}/σ_{N1} составили: менее 4 % от средних значений в меридиональных ребрах, менее 2 % от средних значений в верхнем кольце, менее 7 % от средних значений в нижнем кольце. Поэтому была установлена зависимость от схем опирания отношений средних значений σ_{N2}/σ_{N1} для всех узловых сопряжений (Ш3, Ш2, Ш1, Ж1, Ж2) в основных элементах купола (рис. 11). Эта зависимость показывает, что продольные силы N в каждом из основных элементов купола изменяются одинаково и при симметричной, и при несимметричной нагрузках в разных схемах опирания. Однако в меридиональных ребрах напряжения при несимметричной нагрузке σ_{N2} становятся на 20 % больше напряжений при симметричной нагрузке σ_{N1}, в верхнем кольце напряжения при несимметричной нагрузке σ_{N2} становятся на 33 % меньше напряжений при симметричной нагрузке σ_{N1}, а в нижнем кольце напряжения при несимметричной нагрузке σ_{N2} практически не отличаются от напряжений при симметричной нагрузке σ_{N1}.

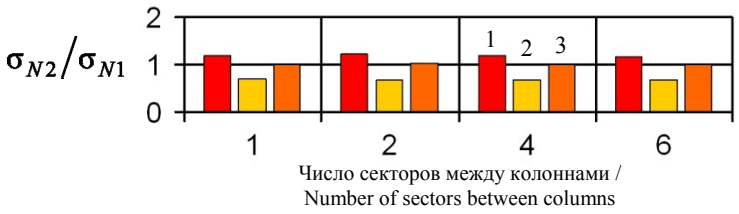

Рис. 11. Отношение средних напряжений от разных узловых сопряжений при несимметричной нагрузке σ_{N2} к аналогичным напряжениям при симметричной σ_{N1}:
1 — меридиональное ребро; *2* — верхнее кольцо; *3* — нижнее кольцо
И с т о ч н и к: выполнено Е.В. Лебедем.

Figure 11. The ratio of the average stresses from different node connections under asymmetrical load σ_{N2} to corresponding stresses under symmetrical load σ_{N1}:
1 — the meridional rib; *2* — the upper ring; *3* — the lower ring
S o u r c e: made by E.V. Lebed.

4. Заключение

На основании изложенного материала можно сделать следующие *выводы:*

1. При несимметричной нагрузке купольный каркас не только деформируется асимметрично, но и его прогибы во много раз превосходят прогибы при симметричной.

2. Прогибы ребристо-кольцевого купола при несимметричной нагрузке характеризуются ростом значений при увеличении количества шарнирных узловых сопряжений, а с уменьшением количества поддерживающих колонн возрастают в 1,8–2,7 раза.

3. При несимметричной нагрузке напряженное состояние элементов купольного каркаса по сравнению с симметричной изменяется по-разному. В наибольшей степени увеличиваются напряжения в меридиональных ребрах (от 1,7 до 7,4 раза), и этот рост зависит как от схемы опирания, так и от вида узловых сопряжений. Наименьший рост напряжений при этом наблюдается в схеме опирания *б*, а наибольший в схеме опирания *1*.

4. Меньшее, но существенное увеличение напряжений при несимметричной нагрузке по сравнению с симметричной наблюдается в верхнем кольце, где в зависимости от вида узловых сопряжений они возрастают в интервале от 1,1 до 2,5 раза с наибольшим ростом в схеме опирания *1*.

5. Незначительное увеличение напряжений при сравнении несимметричной нагрузки с симметричной наблюдается в нижнем кольце, где они возрастают в интервале от 1,0 до 1,4, за исключением жестких узловых сопряжений в схемах опирания *1* и *2* (рост до 2 раз).

6. Независимо от вида узловых сопряжений и схем опирания увеличение напряжений в основных элементах купола при несимметричной нагрузке в сравнении с симметричной происходит в основном из-за роста изгибающих моментов M_x, M_y, а также кручения M_t.

7. Среди всех рассмотренных видов узловых сопряжений элементов меньшей чувствительностью к несимметричной нагрузке во всех схемах опирания характеризуется купольный каркас с жесткими узлами.

Список литературы

1. *Тур В.И.* Купольные конструкции: формообразование, расчет, конструирование, повышение эффективности. Москва : Изд-во АСВ, 2004. 96 с. ISBN 5-93093-249-2

2. *Кривошапко С.Н.* Металлические ребристо-кольцевые и сетчато-стержневые оболочки XIX — первой половины XX-го веков // Строительная механика инженерных конструкций и сооружений. 2014. № 6. С. 4–15. EDN: SYZJFN

3. *Кривошапко С.Н.* К вопросу о применении параболических оболочек вращения в строительстве в 2000–2017 годах // Строительная механика инженерных конструкций и сооружений. 2017. № 4. С. 4–14. https://doi.org/10.22363/1815-5235-2017-4-4-14 EDN: ZHAIXB

4. *Лебедь Е.В., Алукаев А.Ю.* Большепролетные металлические купольные покрытия и их возведение // Строительная механика инженерных конструкций и сооружений. 2018. Т. 14. № 1. С. 4–16. https://doi.org/10.22363/1815-5235-2018-14-1-4-16 EDN: YOJITL

5. *Лебедь Е.В.* Работа металлического каркаса ребристо-кольцевого купола при уменьшении количества поддерживающих его колонн // Строительная механика инженерных конструкций и сооружений. 2024. Т. 20. № 1. С. 14–26. https://doi.org/10.22363/1815-5235-2024-20-1-14-26 EDN: YPWZQU

6. *Anuj C.* Analysis and design of steel dome using software // International Journal of Research in Engineering and Technology (IJRET). 2014. Vol. 03. Issue 03. P. 35–39. https://doi.org/10.15623/ijret.2014.0303006

7. *Chacko P., Dipu V.S., Manju P.M.* Finite Element Analysis of Ribbed Dome // International Journal of Engineering Research and Applications (IJERA). 2014. P. 25–32. ISSN: 2248-9622

8. *Jasim N.A., Saleh I.S., Faleh S.K.* Structural Analysis of ribbed domes using finite element Method // International Journal of Civil Engineering Research. 2017. Vol. 8. No. 2. P. 113–130. URL: https://faculty.uobasrah.edu.iq/uploads/publications/1644004697.pdf (accessed: 15.08.2024).

9. *Anu J.S., Preethi M.* Parametric Analysis of Single layer Ribbed dome with Diagonal members // International Research Journal of Engineering and Technology (IRJET). 2017. Vol. 04. Issue 08. P. 870–877.

10. *Eldhose M., Rajesh A.K., Ramadass S.* Finite Element Analysis and Parametric Study of Schwedler Dome Using ABAQUS Software // International Journal of Engineering Trends and Technology (IJETT). 2015. Vol. 28. No. 7. P. 333–338. URL: http://www.ijettjournal.org (accessed: 15.08.2024).

11. *Лебедь Е.В.* Влияние связей на напряженное состояние каркаса ребристо-кольцевого купола // Строительная механика инженерных конструкций и сооружений. 2022. Т. 18. № 5. С. 417–427. http://doi.org/10.22363/1815-5235-2022-18-5-417-427 EDN: MVUUGT

12. *Lebed E.V.* Influence of the size of the upper ring on the stressed state of the ribbed-ring metal dome // Строительная механика инженерных конструкций и сооружений. 2023. Т. 19. № 5. С. 450–458. http://doi.org/10.22363/1815-5235-2023-19-5-450–458 EDN: DTILTG

13. *Jeleniewicz K., Jaworski J., Żółtowski M., Izabela Uziębło I., Stefańska A., Dixit S.* Steel ribbed dome structural performance with different node connections and bracing system // Scientific Reports. 2024. Vol. 14. Article no. 14013. https://doi.org/10.1038/s41598-024-64811-0 EDN: DXKSNY

14. *Лебедь Е.В.* Влияние узловых сопряжений на усилия в элементах металлического каркаса ребристо-кольцевого купола с учетом разного количества поддерживающих его колонн // Строительная механика инженерных конструкций и сооружений. 2025. Т. 21. № 1. С. 3–17. http://doi.org/10.22363/1815-5235-2025-21-1-3-17

15. *Карпиловский В.С., Криксунов Э.З., Маляренко А.А., Перельмутер А.В., Перельмутер М.А.* SCAD Office. Вычислительный комплекс SCAD. Москва : АСВ. 2006. 592 с. ISBN 5-93093-289-1 EDN: QNMHYR

16. *Городецкий А.С., Евзеров И.Д.* Компьютерные модели конструкций. Киев : Факт, 2005. 344 с. URL: https://dwg.ru/dnl/1952 (дата обращения: 15.08.2024)

17. *Lebed E.V.* Torsion in the Elements of the Metal Dome Frame, Supported by Sparsely Installed Columns // International Journal for Computational Civil and Structural Engineering. 2025. Vol. 21 No. 1. P. 136–145. https://doi.org/10.22337/2587-9618-2025-21-1-136-145

References

1. Tur V.I. *Dome Structures: Morphogenesis, Analysis, Design, Increase in Effectiveness*. Moscow: ASV Publ.; 2004. (In Russ.) ISBN 5-93093-249-2

2. Krivoshapko S.N. Metal ribbed-and-circular and lattice shells from the XIXth until the first half of the XXth centurie. *Structural Mechanics of Engineering Constructions and Buildings*. 2014;(6):4–15. (In Russ.) EDN: SYZJFN

3. Krivoshapko S.N. On application of parabolic shells of revolution in civil engineering in 2000-2017. *Structural Mechanics of Engineering Constructions and Buildings*. 2017;(4):4–14. (In Russ.) https://doi.org/10.22363/1815-5235-2017-4-4-14 EDN: ZHAIXB

4. Lebed E.V., Alukaev A.U. Large-span metal dome roofs and their construction. *Structural Mechanics of Engineering Constructions and Buildings.* 2018;14(1):4–16. (In Russ.) https://doi.org/10.22363/1815-5235-2018-14-1-4-16 EDN: YOJITL

5. Lebed E.V. Behavior of metal frame of ribbed-ring dome with decrease in number of supporting columns. *Structural Mechanics of Engineering Constructions and Buildings.* 2024;20(1):14–26. (In Russ.) https://doi.org/10.22363/1815-5235-2024-20-1-14-26 EDN: YPWZQU

6. Anuj Ch. Analysis and design of steel dome using software. *International Journal of Research in Engineering and Technology (IJRET)*. 2014;03(03):35–39. https://doi.org/10.15623/ijret.2014.0303006

7. Chacko P., Dipu V.S., Manju P.M. Finite Element Analysis of Ribbed Dome. *International Journal of Engineering Research and Applications (IJERA)*. 2014;2248-9622:25–32.

8. Jasim N.A., Saleh I.S., Faleh S.K. Structural analysis of ribbed domes using finite element method. *International Journal of Civil Engineering Research*. 2017;8(2):113–130. Available from: https://faculty.uobasrah.edu.iq/uploads/publications/1644004697.pdf (accessed: 15.08.2024).

9. Anu J.S., Preethi M. Parametric Analysis of Single layer Ribbed dome with Diagonal members. *International Research Journal of Engineering and Technology (IRJET)*. 2017;04(08):870–877.

10. Eldhose M., Rajesh A.K., Ramadass S. Finite Element Analysis and Parametric Study of Schwedler Dome Using ABAQUS Software. *International Journal of Engineering Trends and Technology (IJETT)*. 2015;28(7):333–338. Available from: http://www.ijettjournal.org (accessed: 15.08.2024).

11. Lebed E.V. The influence of bracing on the stress state of the ribbed-ring dome framework. *Structural Mechanics of Engineering Constructions and Buildings*. 2022;18(5):417–427. (In Russ.) http://doi.org/10.22363/1815-5235-2022-18-5-417-427 EDN: MVUUGT

12. Lebed E.V. Influence of the size of the upper ring on the stressed state of the ribbed-ring metal dome. *Structural Mechanics of Engineering Constructions and Buildings*. 2023;19(5):450–458. http://doi.org/10.22363/1815-5235-2023-19-5-450–458 EDN: DTILTG

13. Jeleniewicz K., Jaworski J., Żółtowski M., Uziębło I., Stefańska A., Dixit S. Steel ribbed dome structural performance with different node connections and bracing system. *Scientific Reports*. 2024;14:14013. https://doi.org/10.1038/s41598-024-64811-0

14. Lebed E.V. Influence of joint type on member forces in metal ribbed-ring dome frame taking into account different number of supporting columns. *Structural Mechanics of Engineering Constructions and Buildings.* 2025;21(1):3–17. (In Russ.) http://doi.org/10.22363/1815-5235-2025-21-1-3-17

15. Karpilovskiy V.S., Kriksunov E.Z., Malyarenko A.A., Perel'muter A.V., Perel'muter M.A. *SCAD Office. Computer system SCAD.* Moscow: ASV Publ.; 2006. (In Russ.) ISBN 5-93093-289-1 EDN: QNMHYR

16. Gorodetskiy A.S., Evzerov I.D. *Computer models of structures*. Kiev: Fakt Publ.; 2005. (In Russ.) Available from: https://dwg.ru/dnl/1952 (accessed: 15.08.2024)

17. Lebed E.V. Torsion in the Elements of the Metal Dome Frame, Supported by Sparsely Installed Columns. *International Journal for Computational Civil and Structural Engineering.* 2025;1(1):136–145. https://doi.org/10.22337/2587-9618-2025-21-1-136-145

СТРОИТЕЛЬНАЯ МЕХАНИКА ИНЖЕНЕРНЫХ КОНСТРУКЦИЙ И СООРУЖЕНИЙ
STRUCTURAL MECHANICS OF ENGINEERING CONSTRUCTIONS AND BUILDINGS

2025. 21(6). 537–550

ISSN 1815-5235 (Print), 2587-8700 (Online)
HTTP://JOURNALS.RUDN.RU/STRUCTURAL-MECHANICS

DOI: 10.22363/1815-5235-2025-21-6-537-550
EDN: FOHZXB

Научная статья / Research article

Влияние изгибной жесткости соединения на работоспособность стального каркаса

Г. Сунь ✉, Л.И. Миронова

Уральский федеральный университет имени первого Президента России Б.Н. Ельцина, *Екатеринбург, Российская Федерация*
✉ guofeng.sun@mail.ru

Поступила в редакцию: 12 сентября 2025 г.
Доработана: 16 ноября 2025 г.
Принята к публикации: 28 ноября 2025 г.

Аннотация. Объектом исследования является стальной каркас с болтовыми фланцевыми соединения, которые рассматриваются как полужесткое соединение, основанное на понятии стальных соединений, соответствующем Еврокоду-3. Цель данной работы — разработка метода расчета стального каркаса с фланцевыми соединениями и выявление влияния перемещения узла на работу всего каркаса. Проведен анализ поведения стального каркаса с болтовыми фланцевыми соединениями, в котором соединение может частично поворачиваться. В этом случае матрица жесткости может быть использована для упругопластического анализа каркаса с полужесткими соединениями. Проведена оптимизация матрицы жесткости с учетом жесткости соединения балки с колонной. Разработан метод расчета угла поворота узла балки с колонной, учитывая линейную жесткость балки и поперечную жесткость колонны. Обобщены методы расчета изгибающей жесткости болтовых фланцевых соединений вращения, основанные на компонентном методе из Еврокода-3. Проведена верификация точности и эффективности разработанной методики, результаты которой свидетельствуют о достаточной высокой точности выполненных экспериментов. В качестве результатов выполненного исследования можно выделить собственно метод проектирования каркаса с учетом поворота узла и выявление влияния изгибной жесткости на работоспособность целого каркаса. На основании полученных результатов сделан вывод о том, что использование разработанной методики позволяет точно прогнозировать работу стальных каркасов с фланцевыми соединениями и оптимальным вариантом для проверенного стального каркаса является применение фланцевых соединений с толщиной фланца 16,4 мм.

Ключевые слова: стальная конструкция, матрица жесткости, отношение жесткости, угол поворота, механизм разрушения

Заявление о конфликте интересов. Авторы заявляют об отсутствии конфликта интересов.

Вклад авторов: *Сунь Г.* — разработка концепции статьи, методология, разработка модели, программное обеспечение, верификация результатов, подготовка рукописи статьи; *Миронова Л.И.* — руководство, редактирование, корректура, валидация. Оба автора ознакомлены с окончательной версией статьи и одобрили ее.

Для цитирования: *Сунь Г., Миронова Л.И.* Влияние изгибной жесткости соединения на работоспособность стального каркаса // Строительная механика инженерных конструкций и сооружений. 2025. Т. 21. № 6. С. 537–550. http://doi.org/10.22363/1815-5235-2025-21-6-537-550 EDN: FOHZXB

Сунь Гофэн, аспирант кафедры строительных конструкций и механики грунтов, Уральский федеральный университет имени первого Президента России Б.Н. Ельцина, Российская Федерация, 620062, г. Екатеринбург, ул. Мира, д. 19; eLIBRARY SPIN-код: 4032-1759, ORCID: 0000-0002-7535-1599; e-mail: guofeng.sun@mail.ru

Миронова Людмила Ивановна, доктор педагогических наук, кандидат технических наук, профессор кафедры строительных конструкций и механики грунтов, Уральский федеральный университет имени первого Президента России Б.Н. Ельцина, Российская Федерация, 620062, г. Екатеринбург, ул. Мира, д. 19; eLIBRARY SPIN-код: 1201-1155, ORCID: 0000-0002-3675-6008; e-mail: mironovali@urfu.ru

Influence of Rotational Stiffness of Beam-to-Column Connection on Steel Frame Performance

Guofeng Sun✉, **Lyudmila I. Mironova**

Ural Federal University named after the first President of Russia B.N.Yeltzin, *city Yekaterinburg, Russia*
✉ guofeng.sun@mail.ru

Received: September 12, 2025
Revised: November 16, 2025
Accepted: November 28, 2025

Abstract. The object of this study is a bolted end-plate connection, which is considered as a semi-rigid connection based on the concept of steel connections corresponding to Eurocode 3. The aim of this work is to develop a method for calculating a steel frame with bolted end-plate connection and to identify the effect of joint displacement on the behavior of the entire frame. Method. The behavior of a steel frame with bolted flange connections is analyzed, in which the connection can partially rotate. In this case, the stiffness matrix can be used for the elastic-plastic analysis of a frame with semi-rigid connections. Optimization of the stiffness matrix is carried out taking into account the stiffness of the beam-column connection. A method for calculating the rotation angle of the beam-column joint is developed, taking into account the linear stiffness of the beam and the transverse stiffness of the column. Methods for calculating the bending stiffness of bolted flange connections of rotation, based on the component method from Eurocode 3, are summarized. The accuracy and effectiveness of the developed methodology were verified, and the results demonstrate a sufficiently high level of accuracy in the experiments. The results of the study include a frame design method that takes into account joint rotation and the influence of bending stiffness on the overall frame performance. Based on the results, it can be concluded that the developed methodology enables accurate prediction of the performance of steel frames with flanged connections, and that the optimal option for the tested steel frame is the use of flanged connections with a flange thickness of 16.4 mm.

Keywords: steel structure, stiffness matrix, stiffness ratio, rotation, failure mechanism

Conflicts of interest. The authors declare that there is no conflict of interest.

Authors' contribution: *Sun G.* — conceptualization, methodology, modelling, software, verification of results, text writing; *Mironova L.I.* — guidance, editing, proofreading, validation. Both of the authors read and approved the final version of the article.

For citation: Sun G., Mironova L.I. Influence of rotational stiffness of beam-to-column connection on steel frame performance. *Structural Mechanics of Engineering Constructions and Buildings.* 2025;21(6):537–550. (In Russ.) http://doi.org/10.22363/1815-5235-2025-21-6-537-550 EDN: FOHZXB

1. Введение

Стальные конструкции стремительно развиваются. В Китае, по оценкам исследователей, к 2035 г. на стальные конструкции будет приходиться около 40 % нового строительства [1]. В России есть запрос на скорость, экологичность и качество строительства, которые не всегда может гарантировать монолит. Вместе с тем, согласно национальному проекту «Жилье и городская среда», к 2030 г. в сегменте массового жилищного строительства должно возводиться 80 млн м^2 ежегодно (сейчас возводится менее 50 млн м^2 в год) [2]. Применение стальных конструкций отвечает требованиям к скорости и качеству возведения. При этом для соединения балки с колонной часто используют болтовые фланцевые соединения (ФС) [3; 4].

Болтовые фланцевые соединения (ФС) обладают пятью основными преимуществами, к которым относятся замена высококвалифицированной сборочной сварки простым монтажом болтов, монтаж в различных климатических условиях (включая низкие температуры), высокая надежность при действии динамических нагрузок, удобство контролирования качества монтажа и производства, возможность демонтажа без повреждения конструкции. Согласно норме EN1993-1-8[1], кривую зависимость между моментом и углом поворота (M-θ) рекомендовано использовать в качестве основы про-

[1] EN 1993-1-8:2005: Eurocode 3: Design of steel structures - Part 1-8: Design of joints.

Guofeng Sun, Postgraduate student of the Department of Building Structures and Soil Mechanics, Ural Federal University named after the first President of Russia B.N. Yeltsin, 19 Mira St, Ekaterinburg, 620062, Russian Federation; eLIBRARY SPIN-code: 4032-1759, ORCID: 0000-0002-7535-1599; e-mail: guofeng.sun@mail.ru

Lyudmila I. Mironova, Doctor of Pedagogical Sciences, Candidate of Technical Sciences, Professor of the Department of Building Structures and Soil Mechanics, Ural Federal University named after the first President of Russia B.N. Yeltsin, 19 Mira St, Ekaterinburg, 620062, Russian Federation; eLIBRARY SPIN-code: 1201-1155, ORCID: 0000-0002-3675-6008; e-mail: mironovali@urfu.ru

ектирования. Изгибная жесткость и несущая способность ФС являются ключевыми параметрами, определяющими зависимость M-θ. В [5] авторы использовали компонентный метод для прогнозирования начальной изгибной жесткости и несущей способности ФС с разными ребрами жесткости, что позволило получить зависимость M-θ. В [6] проведено упрощение процедуры проектирования для ФС высокой несущей способности за счет объединения метода The yeild line theory с Т-образным элементом для проектирования ФС с более чем четырьмя болтами в зоне растяжения. Результаты работы [6] показали, что механические свойства высокопрочных ФС сложнее, чем у обычных. В [7] разработан метод расчета начальной жесткости ФС, основанный на трех механизмах разрушения Т-образных элементов. В [8] проведено экспериментальное исследование механических свойств Т-образных элементов в условиях циклических нагрузок. В [9] усовершенствована модель метода The yield line theory для расчета элементов на изгиб и разработана методика расчета несущей способности для Т-образных элементов, включающая пластическую деформацию. В [10; 11] предложен подход к проектированию пространственных стальных рам, основанный на изучении ФС, расположенных как вдоль сильной, так и вдоль слабой осей.

Однако в вышеописанных исследованиях не говорится об анализе работы целого стального каркаса. В ранее проведенных исследованиях [12–17] для стального каркаса также рассматривались характеристики узлов для оптимизации матрицы жесткости. В [12] представлен эффективный метод оптимизации для полужестких пространственных стальных конструкций, использующий передовой практический анализ в сочетании. В [13] сделана оптимизация проектирования полужестких пространственных стальных каркасов с использованием открытого интерфейса прикладного программирования MATLAB-SAP2000. Результаты работы [13] показали, что жесткость соединения играет важную роль в оптимизации стальных пространственных каркасов и влияет на вес конструкции. В [14–16] исследовано неупругое поведение пространственного стального каркаса второго порядка и проведен численный расчет для верификации. В [17] проведено компьютерное проектирование и анализ трехмерных стальных рам с полужесткими соединениями и выполнен нелинейный анализ, учитывающий влияние податливости соединений. Но в [12–17] отсутствует исследование влияния классификации соединения по жесткости на работоспособность стального каркаса.

Изучение зависимости между деформацией и распределением силы элементов соединения и торца балки позволяет разработать методику расчета поворота торца балки с учетом различных условий жесткости соединения, что позволит оптимизировать матрицу жесткости.

Объектом исследования является стальной каркас с болтовыми фланцевыми соединения. Предмет исследования — механическая модель полужесткого стального каркаса. *Цель исследования* — разработка метода расчета стального каркаса с фланцевыми соединениями и выявление влияния перемещения узла на работу всего каркаса.

В данной работе применен компонентный метод, соответствующий норме EN1993-1-8 для исследования изгибной жесткости соединения ФС и прогнозирования линейной жесткости балок. На основе этого оценивается влияние механизма разрушения и жесткости соединения на механические характеристики целого каркаса. Проведено численное исследование для верификации точности и эффективности разработанной методики.

2. Методы

На рис. 1 показан процесс разделения ФС на несколько Т-образных элементов. В [18–23] Т-образный элемент используется для исследования общей работоспособности ФС.

В [7] разработана методика расчета начальной изгибной жесткости. В [7; 8; 24] подчеркивается, что к механизмам разрушения ФС относятся следующие три типа разрушений, показанные на рис. 2, со следующими характеристиками:

- во фланце полностью разрушен пластический шарнир (Type-1);
- разрушены болты при частичном разрушении пластического шарнира во фланце (Type-2);
- разрушены болты (Type-3).

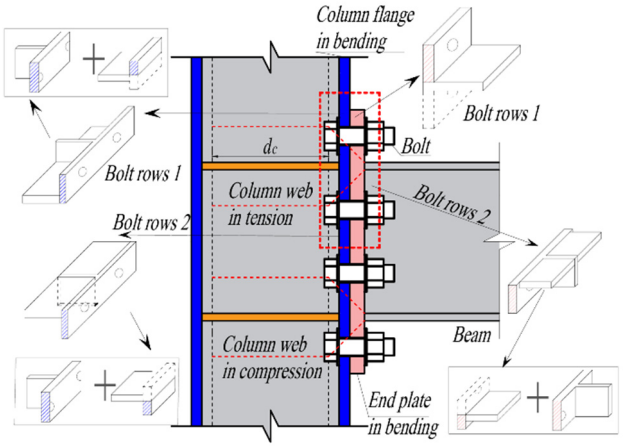

Рис. 1. Разделение ФС на несколько Т-образных элементов
И с т о ч н и к: выполнено Г. Сун.

Figure 1. Decomposition of bolted end-plate connections into T-stubs
S o u r c e: made by G. Sun.

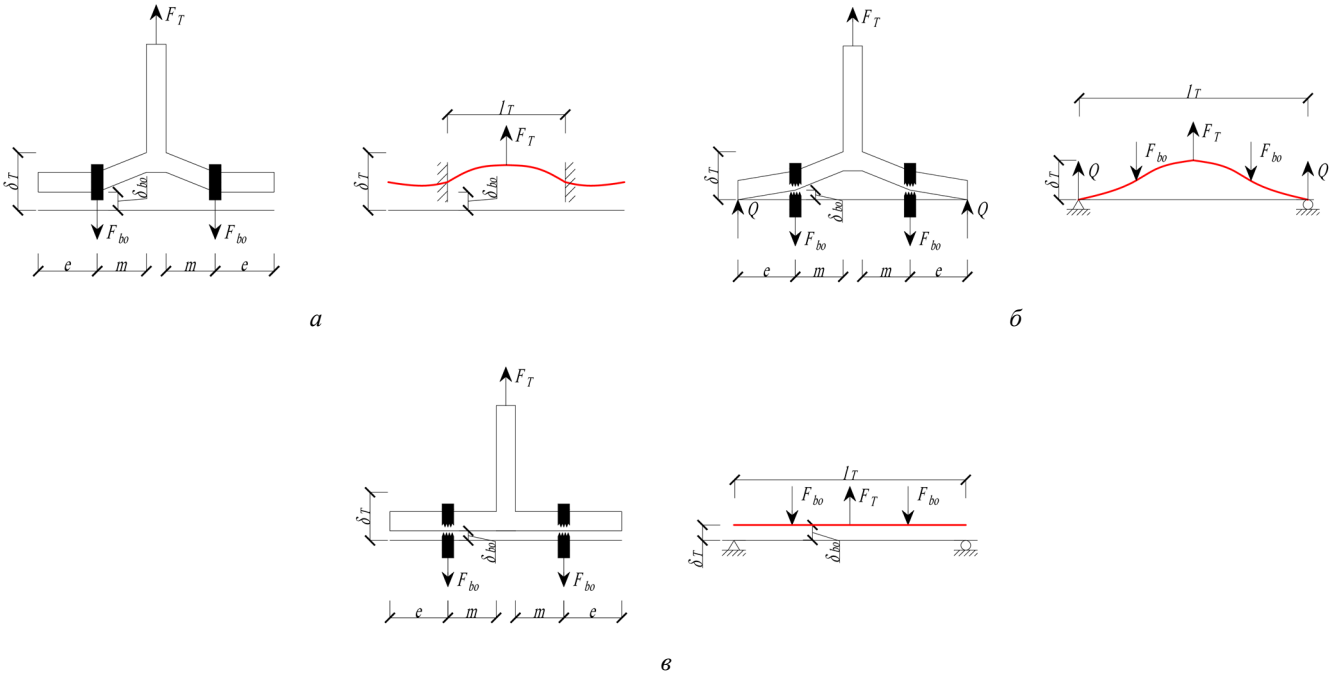

Рис. 2. Механическая модель Т-образного элемента [7]:
а — Type-1; *б* — Type-2; *в* — Type-3
И с т о ч н и к: выполнено Г. Сунь.

Figure 2. Failure modes of bolted T-stubs:
а — Type-1; *б* — Type-2; *в* — Type-3
S o u r c e: made by G. Sun.

В норме EN1993-1-8 начальная изгибная жесткость S_{ini} определена по формулам:

$$S_{ini} = E_y h_b^2 k_{eq} / \mu_s, \tag{1}$$

$$\mu_s = \begin{cases} 1 & , \ M \le M_y, \\ \left(M / M_y\right)^{2.7} & , \ M_y < M, \end{cases} \tag{2}$$

$$k_{eq} = \sum_i k_{eq,i} h_i \Big/ h_{eq}, \tag{3}$$

$$k_{eq,i} = 1 \Big/ \sum_i 1 / k_j, \tag{4}$$

$$h_{eq} = \sum_i k_{eq,i} h_i^2 \Big/ \sum_i k_{eq,i} h_i, \tag{5}$$

где M — момент, действующий на соединении; M_y *а* — Type-1; *б* — Type-2; *в* — Type-3 — момент при текучести; k_{eq} *а* — Type-1; *б* — Type-2; *в* — Type-3 — эквивалентный коэффициент жесткости целого соединения; $k_{eq,i}$ — эквивалентный коэффициент жесткости i-пары болтов; k_j *а* — Type-1; *б* — Type-2; *в* — Type-3 — эквивалентный коэффициент жесткости j-элемента; h_{eq} *а* — Type-1; *б* — Type-2; *в* — Type-3 — расчетное плечо; h_i *а* — Type-1; *б* — Type-2; *в* — Type-3 – расстояние от i-пары болтов до нейтральной оси; h_b *а* — Type-1; *б* — Type-2; *в* — Type-3 – высота балки; μ_s *а* — Type-1; *б* — Type-2; *в* — Type-3 — отношение пластической жесткости к начальной жесткости; E_y *а* — Type-1; *б* — Type-2; *в* — Type-3 — модуль упругости.

В таблице приведены формулы для расчета начальной жесткости ФС [7].

Расчет начальной жесткости ФС / Initial stiffness calculation of each component

Элемент / Component	**Формулы / Formula**
Начальная жесткость зоны на растяжение / Initial rotational stiffness of area in tension	$S_{ini,t} = E_y h_t^2 \Big/ \left(\frac{1}{k_{bo}} + \frac{1}{k_{cw,t}} + \frac{1}{k_f} + \frac{1}{k_{cf}} \right)$ (6)
Начальная жесткость зоны на сжатие / Initial rotational stiffness of area in compression	$S_{ini,c} = E_y h_c^2 \Big/ \left(\frac{1}{k_{cw,c}} + \frac{1}{k_p} + \frac{1}{k_{cf}} \right)$ (7)
Болт на растяжение / Bolt in tension	$k_{bo} = 8 A_{bo} / l_{bo}$ (8)
Стенка колонны на растяжение / Column web in tension	$k_{cw,t} = 4 A_{cw,t} / d_c$ (9)
Внешняя зона фланца на изгиб (Type-1) / External area of the end-plate in bending	$k_{p,1} = 1 \Big/ \left(\frac{m^3}{12 I_p} + \frac{l_{bo}}{22 A_{bo}} \right)$ (10)
Внешняя зона фланца на изгиб (Type-2) / External area of the end-plate in bending	$k_{p,2} = \frac{24 I_p (a+q)}{l_T^3 a}$ (11)
Внешняя зона фланца на изгиб (Type-3) / External area of the end-plate in bending	$k_{p,3} = k_{bo}$ (12)
Внутренняя зона фланца на изгиб / Internal area of the end-plate in bending	$k_{p,i} = 12 \left(I_{p,1} \Big/ m_1^3 + I_{p,2} \Big/ m_2^3 \right)$ (13)

Примечание. $S_{ini,t}$ — начальная жесткость зоны на растяжение; $S_{ini,c}$ — начальная жесткость зоны на сжатие, k_{bo} — коэффициент жесткости болта на растяжение; $k_{cw,t}$, $k_{cw,c}$ — коэффициент жесткости стенки колонны на растяжение и на сжатие, соответственно; k_p — коэффициент жесткости фланца на изгиб; k_{cf} — коэффициент жесткости полки колонны на изгиб; h_t — расстояние от полки колонны на растяжение до нейтральной оси; l_{bo} — удлинение болта; $A_{cw,t}$ — площадь поверхности растяжения стенки колонны при растяжении; I_p — момент инерции сечения фланца; m — расстояние от оси болта до поверхности полки балки; d_c — расчетная ширина стенки колонны, l_T — пролет Т-образного элемента; $I_{p,1}$, $I_{p,2}$ — момент инерции поперечного сечения двух Т-образных элементов в соответствии с m_1 и m_2 внутренней зоны фланца, показано на рис.3; m_1, m_2 — расстояние от оси болтов до стенки Т-образного элемента; $k_{p,1}$, $k_{p,2}$, $k_{p,3}$ — коэффициент жесткости внешней зоны фланца в соответствии с тремя механизмами разрушения (Type-1, Type-2, Type-3); a, q — расчетные коэффициенты, определенные по формулам (14) и (15).

Note. $S_{ini,t}$ is the initial tensile stiffness of the zone; $S_{ini,c}$ — the initial compressive stiffness of the zone, k_{bo} is the tensile stiffness coefficient of the bolt; $k_{cw,t}$, $k_{cw,c}$ — the tensile and compressive stiffness coefficients of the column web, respectively; k_p is the bending stiffness coefficient of the end plate; k_{cf} — the bending stiffness coefficient of the column flange; h_t — the distance from the tensile column flange to the neutral axis; l_{bo} — the bolt elongation; $A_{cw,t}$ — the tensile surface area of the column web under tension; I_p — the moment of inertia of the flange section; m is the distance from the bolt axis to the beam flange surface; d_c is the design width of the column web; l_T — the span of the T-stubs; $I_{p,1}$, $I_{p,2}$ — moment of inertia of the cross-section of two T-stubs in accordance with m_1 and m_2 of the inner zone of the end plate, shown in Figure 3; m_1, m_2 – distance from the axis of the bolts to the wall of the T-stubs; $k_{p,1}$, $k_{p,2}$, $k_{p,3}$ — stiffness coefficient of the outer zone of the flange in accordance with three destruction mechanisms (Type-1, Type-2, Type-3); a, q — design coefficients determined by formulas (14) and (15).

Источник: выполнено Г. Сунь / Source: made by G. Sun.

Формулы (14) и (15) используются для расчета коэффициентов a, q, приведенных в табл.:

$$q = l_T^3 \left(3\alpha_T - 4\alpha_T^3\right)/24, \tag{14}$$

$$a = \frac{l_{bo}}{\left(1/I_p + 1/I_{cf}\right) A_{bo}}, \tag{15}$$

где $\alpha_T = e / l_T$ — коэффициент расчета Т-образного элемента; e — расстояние от оси болта до кромки фланца.

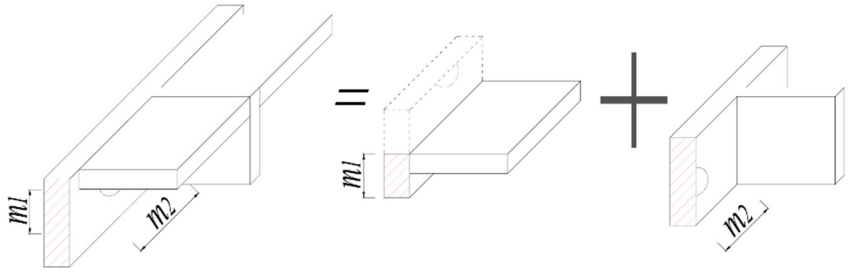

Рис. 3. Механическая модель внутренней зоны фланца
И с т о ч н и к: выполнено Г. Сунь.

Figure 3. Mechanical model of the inner end-plate zone
S o u r c e: made by G. Sun.

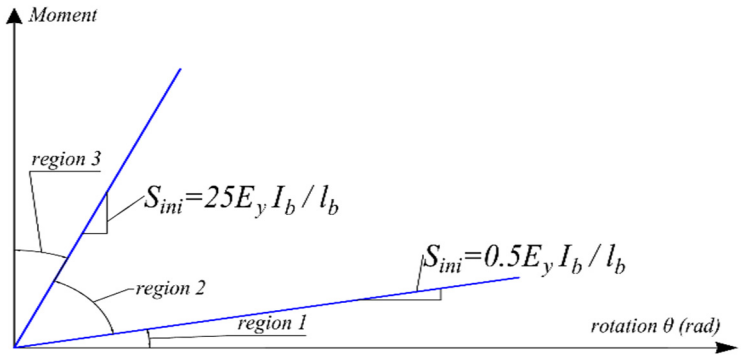

Рис. 4. Классификация соединения балки с колонной на основании нормы EN1993-1-8
И с т о ч н и к: выполнено Г. Сунь.

Figure 4. Node stiffness division of EN1993-1-8
S o u r c e: made by G. Sun.

Классификация соединения балки с колонной по жесткости, представленная в норме EN1993-1-8, показана на рис. 4, где выделены три отдельные области:

- область 1, жесткая;
- область 2, полужесткая, и все соединения в области 2 следует классифицировать как полужесткие;
- область 3, номинально шарнирное соединение.

На рис. 5 показаны перемещения торцов балки. Зависимость внутренней силы от смещения концов балки выражается формулой

$$[P] = [S_b][\Delta_b], \tag{16}$$

где $[P]$ — матрица сил; $[S_b]$ — матрица жесткости балки без учета поворота узла колонны с балкой; $[\Delta_b]$ — матрица перемещений двух торцов балки без учета поворота узла колонны с балкой.

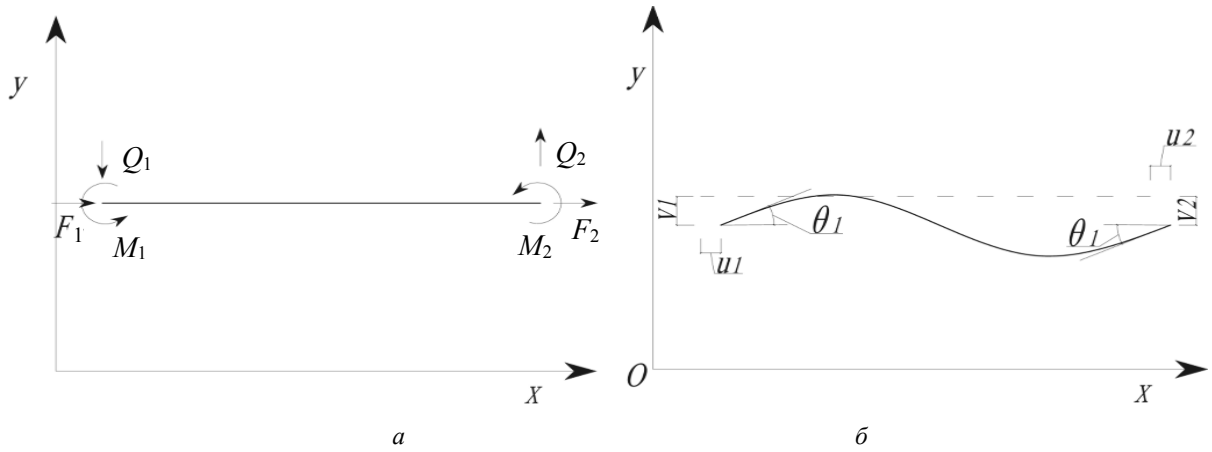

а *б*

Рис. 5. Перемещения балки:
а — нагрузка на торцах балки; *б* — перемещения на торцах балки
И с т о ч н и к: выполнено Г. Сунь.

Figure 5. Beam displacements:
а — load at beam ends; *б* — displacements at beam ends
S o u r c e: made by G. Sun.

Матрица угла поворота стального каркаса определена по формуле

$$[\theta]=[\theta_b]+[\theta_c], \tag{17}$$

где $[\theta]$ — матрица общего угла поворота торца балочной модели; $[\theta_b]$ — матрица общего угла поворота торца балки; $[\theta_c]$ — матрица общего угла поворота узла колонны с балкой.

Матрица вертикальных перемещений торца балки определена по формуле

$$[v]=[v_b]+[v_c], \tag{18}$$

где $[v]$ — матрица перемещений от сдвига торца балочной модели; $[v_b]$ — матрица перемещений от сдвига торца балки без учета поворота узла колонны с балкой; $[v_c]$ — матрица общего угла поворота узла колонны с балкой с учетом поворота узла колонны с балкой.

Зависимость между моментом и перемещением определена по формуле

$$[M]=\frac{3}{l_b}S_b\begin{pmatrix}1 & -1\\ 1 & -1\end{pmatrix}[v_b]+S_b\begin{pmatrix}1 & -1\\ 1 & -1\end{pmatrix}[\theta_b], \tag{19}$$

где $[M]$ — матрица изгибающих моментов; S_b — удвоенная линейная жесткость балки, которая определена по формуле

$$S_b=2E_yI_b/l_b, \tag{20}$$

где I_b — момент инерции балки; l_b — расчетный пролет балки.

Зависимость между моментом и поворотом узла балки с колонной определена по формуле

$$[M]=[S_c][\Delta_c]=\begin{pmatrix}S_{1c} & 0\\ 0 & S_{2c}\end{pmatrix}[\theta_c], \tag{21}$$

где $[S_c]$ — матрица начальной жесткости соединений при изгибе; $[\Delta_c]$ — матрица поворота соединения; S_{1c} — начальная жесткость соединения при изгибе на левом торце балки; S_{2c} — начальная жесткость соединения при изгибе на правом торце балки.

Объединяя уравнения (19) и (21), получаем формулы:

$$\begin{pmatrix} S_{1c} & 0 \\ 0 & S_{2c} \end{pmatrix}[\theta_c] = \frac{3}{l_b} S_b \begin{pmatrix} 1 & -1 \\ 1 & -1 \end{pmatrix}[v_b] + S_b \begin{pmatrix} 1 & -1 \\ 1 & -1 \end{pmatrix}[\theta_b], \tag{22}$$

$$[S_\alpha][\theta_c] = \frac{3}{l_b} \begin{pmatrix} 1 & -1 \\ 1 & -1 \end{pmatrix}[v] + \begin{pmatrix} 2 & 1 \\ 1 & 2 \end{pmatrix}[\theta], \tag{23}$$

где $[S_\alpha]$ — матрица, состоящая из коэффициентов α_i; α_i — коэффициент относительной жесткости, $\alpha_i = S_{ic}/(S_b)$.

В этом случае $[S_{\boldsymbol{\alpha}}]$ и $[S_{\boldsymbol{\alpha}}]^{-1}$ выражаются по формулам, подобным (24)–(25):

$$[S_\alpha] = \begin{pmatrix} \alpha_1 + 2 & 1 \\ 1 & \alpha_2 + 2 \end{pmatrix}, \tag{24}$$

$$[S_\alpha]^{-1} = \frac{1}{k} \begin{pmatrix} \alpha_2 + 2 & -1 \\ -1 & \alpha_1 + 2 \end{pmatrix}, \tag{25}$$

где k — коэффициент связан с α_i, $k = (\alpha_1 + 2)(\alpha_2 + 2) - 1$.

Угол поворота соединения балки с колонной определена по формуле

$$[\theta_c] = [S_\alpha]^{-1} \frac{3}{l_b} \begin{pmatrix} 1 & -1 \\ 1 & -1 \end{pmatrix}[v] + [S_\alpha]^{-1} \begin{pmatrix} 2 & 1 \\ 1 & 2 \end{pmatrix}[\theta]. \tag{26}$$

Объединим формулы (21) и (26) и получим формулу (27) для определения зависимости между $[M]$ и от $[\theta]$:

$$[M] = [S_c][\Delta_c] = \frac{3S_b}{l_b k} \begin{pmatrix} \alpha_1(\alpha_2 + 1) & -\alpha_1(\alpha_2 + 1) \\ \alpha_2(\alpha_1 + 1) & -\alpha_2(\alpha_1 + 1) \end{pmatrix}[v] + \frac{S_b}{k} \begin{pmatrix} 2\alpha_1(\alpha_2 + 1{,}5) & \alpha_1\alpha_2 \\ \alpha_1\alpha_2 & 2\alpha_2(\alpha_1 + 1{,}5) \end{pmatrix}[\theta]. \tag{27}$$

Кроме того, необходимо учитывать влияние θ на перемещение при сдвиге. Зависимость между вертикальной силой $[Q]$ и перемещением балки определена по формуле (28)

$$[Q] = \frac{6S_b}{l_b^2} \begin{pmatrix} 1 & -1 \\ -1 & 1 \end{pmatrix}[v_b] + \frac{3S_b}{l_b} \begin{pmatrix} 1 & 1 \\ -1 & -1 \end{pmatrix}[\theta_b]. \tag{28}$$

Объединим формулы (17) и (28) и получим формулы (29) и (30) для определения зависимости между $[Q]$ и $[\theta]$:

$$[Q] = \frac{6S_b}{l_b^2} \begin{pmatrix} 1 & -1 \\ -1 & 1 \end{pmatrix}[v_b] + \frac{3S_b}{l_b} \begin{pmatrix} 1 & 1 \\ -1 & -1 \end{pmatrix}([\theta] - [\theta_c]), \tag{29}$$

$$[Q] = \frac{6S_b}{l_b^2} \left(1 - \frac{1{,}5(\alpha_1 + \alpha_2 + 2)}{k}\right) \begin{pmatrix} 1 & -1 \\ -1 & 1 \end{pmatrix}[v] + \frac{3S_b}{kl_b} \begin{pmatrix} 1 - \dfrac{2\alpha_2 + \alpha_1 + 3}{k} & 1 - \dfrac{2\alpha_1 + \alpha_2 + 3}{k} \\ -\left(1 - \dfrac{2\alpha_2 + \alpha_1 + 3}{k}\right) & -\left(1 - \dfrac{2\alpha_1 + \alpha_2 + 3}{k}\right) \end{pmatrix}[\theta]. \tag{30}$$

На основании вышеприведенного анализа получена матрица жесткости элементов балки (31), учитывающая деформации полужестких соединений, представляемая следующим образом:

$$\begin{pmatrix} \overrightarrow{Q_1} \\ \overrightarrow{M_1} \\ \overrightarrow{Q_2} \\ \overrightarrow{M_2} \end{pmatrix} = S_b \begin{pmatrix} \frac{6}{l_b^2}a_{v,1} & \frac{3}{l_b}a_{\theta,1} & -\frac{6}{l_b^2}a_{v,2} & \frac{3}{l_b}a_{\theta,2} \\ \frac{3}{l_b}f_{v,1} & 2f_{\theta,1} & -\frac{3}{l_b}f_{v,2} & f_{\theta,2} \\ -\frac{6}{l_b^2}a_{v,1} & -\frac{3}{l_b}a_{\theta,1} & \frac{6}{l_b^2}a_{v,2} & -\frac{3}{l_b}a_{\theta,2} \\ \frac{3}{l_b}g_{v,1} & g_{\theta,1} & -\frac{3}{l_b}g_{v,2} & 2g_{\theta,2} \end{pmatrix} \begin{pmatrix} \overrightarrow{v_1} \\ \overrightarrow{\theta_1} \\ \overrightarrow{v_2} \\ \overrightarrow{\theta_2} \end{pmatrix}, \tag{31}$$

где $a_{v,1}$, $a_{v,2}$, $a_{\theta,1}$, $a_{\theta,2}$, $f_{v,1}$, $f_{v,2}$, $f_{\theta,1}$, $f_{\theta,2}$, $g_{v,1}$, $g_{v,2}$, $g_{\theta,1}$, $g_{\theta,2}$ — коэффициенты расчета, которые определены по формулам:

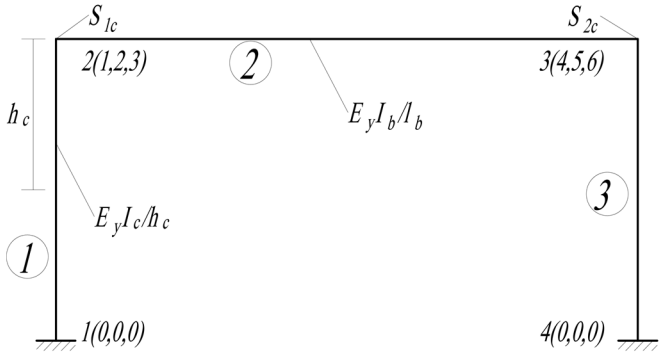

Рис. 6. Однопролетный стальной каркас
И с т о ч н и к: выполнено Г. Сунь.

Figure 6. Single- span steel frame
S o u r c e: made by G. Sun.

$$a_{v,1} = a_{v,2} = 1 - 1{,}5\left(\alpha_1 + \alpha_2 + 2\right)/k; \tag{32}$$

$$a_{\theta,1} = 1 - \left(2\alpha_2 + \alpha_1 + 3\right)/k; \tag{33}$$

$$a_{\theta,2} = 1 - \left(2\alpha_1 + \alpha_2 + 3\right)/k; \tag{34}$$

$$f_{v,1} = f_{v,2} = \alpha_1\left(\alpha_2 + 1\right)/k; \tag{35}$$

$$f_{\theta,1} = \alpha_1\left(\alpha_2 + 1{,}5\right)/k; \tag{36}$$

$$f_{\theta,2} = g_{\theta,1} = \alpha_1\alpha_2/k; \tag{37}$$

$$g_{v,1} = g_{v,2} = \alpha_2\left(\alpha_1 + 1\right)/k; \tag{38}$$

$$g_{\theta,2} = \alpha_2\left(\alpha_1 + 1{,}5\right)/k. \tag{39}$$

Для однопролетного стального каркаса, показанного на рис. 6, можно получить матрицу жесткости с учетом жесткости колонны

$$[S] = \begin{pmatrix} \frac{E_y A_b}{l_b} & \frac{E_y A_c}{h_c} & 0 & -\frac{E_y A_b}{l_b} & -\frac{E_y A_c}{h_c} & 0 \\ -\frac{6}{h_c^2}S_{co} & \frac{6}{l_b^2}a_{v,1}S_b & \frac{3}{l_b}a_{\theta,1}S_b + \frac{3}{h_c}S_{co} & \frac{6}{h_c^2}S_{co} & -\frac{6}{l_b^2}a_{v,2}S_b & \frac{3}{l_b}a_{\theta,2}S_b + \frac{3}{h_c}S_{co} \\ -\frac{3}{h_c}S_{co} & \frac{3}{l_b}f_{v,1}S_b & 2S_b f_{\theta,1} + 2S_{co} & \frac{3}{h_c}S_{co} & -\frac{3}{l_b}f_{v,2}S_b & f_{\theta,2}S_b + S_{co} \\ -\frac{E_y A_b}{l_b} & -\frac{E_y A_c}{h_c} & 0 & \frac{E_y A_b}{l_b} & \frac{E_y A_c}{h_c} & 0 \\ \frac{6}{h_c^2}S_{co} & -\frac{6}{l_b^2}a_{v,1}S_b & -\frac{3}{l_b}S_b a_{\theta,1} + \frac{3}{h_c}S_{co} & -\frac{6}{h_c^2}S_{co} & \frac{6}{l_b^2}a_{v,2}S_b & -\frac{3}{l_b}a_{\theta,2}S_b - \frac{3}{h_c}S_{co} \\ -\frac{3}{h_c}S_{co} & \frac{3}{l_b}g_{v,1}S_b & S_b g_{\theta,1} + S_{co} & \frac{3}{h_c}S_{co} & -\frac{3}{l_b}g_{v,2}S_b & 2g_{\theta,2}S_b + 2S_{co} \end{pmatrix}, \tag{40}$$

где A_b — расчетная площадь поперечного сечения балки; A_c — расчетная площадь поперечного сечения колонны; h_c — расчетная высота колонны, S_{co} определена по формуле

$$S_{co} = 2E_y I_{co} / h_{co}, \tag{41}$$

где I_{co} — момент инерции поперечного сечения колонны.

В случае $S_{1c} = S_{2c}$ начальная изгибная жесткость однопролетного каркаса с учетом жесткости соединения $S_{g,b}$ определена по формуле

$$S_{g,b} = S_b \left(f_{\theta,1} - f_{\theta,2} \right) + S_{co}. \tag{42}$$

3. Результаты и обсуждение

В [25] проведено экспериментальное исследование однопролетного пространственного стального каркаса с ФС. На рис. 7 показана схема образца SF-1 и расположение нагрузок. В данном образце конструирование является симметричным, поэтому формула (41) может использоваться для расчета изгибной жесткости данного каркаса. Пролет каркаса — 1,5 м, высота колонны — 0,8 м. Профиль балки — 150×75×5×7 мм и профиль колонны 150×150×7×10 мм. Размер фланца — 250×100×14 мм. Диаметр болтов — M16 и класс болтов 10,9. Изгибная жесткость узла образца SF-1 составляет 8851 kN·m/rad. Несущая способность стального каркаса при текучести составляет 21,96 kN·m.

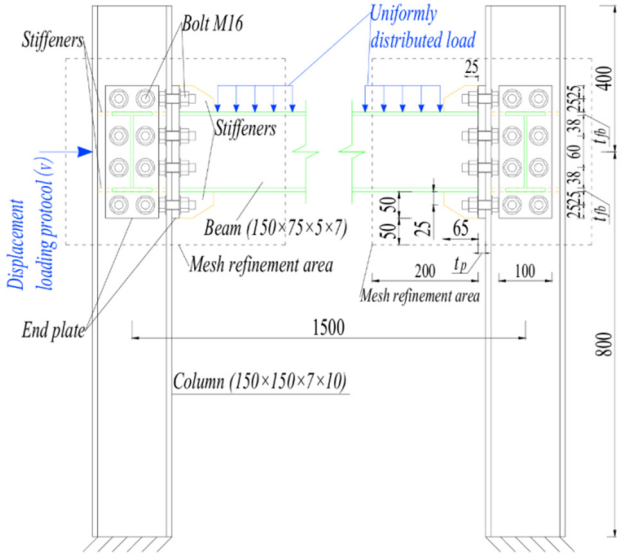

Рис. 7. Образец SF-1 из работы [15] и расположение нагрузок
И с т о ч н и к: выполнено Г. Сунь.

Figure 7. Specimen SF-1 from [15] and the location of the loads
S o u r c e: made by G. Sun.

Выполнен расчет вышеописанного стального каркаса. Расчетная начальная изгибная жесткость соединения S_c составляет 8749 kN·m/rad, и расчетная начальная изгибная жесткость торца балки стального каркаса с учетом жесткости соединения $S_{g,b}$ составляет 8991 kN·m/rad. Значение отношения изгибной жесткости, полученной в ходе эксперимента, к $S_{g,b}$ составляет 1,01, что позволяет утверждать, что использование разработанной методики обеспечивает точное прогнозирование изгибной жесткости стального каркаса с ФС.

На рис. 8, *а*, показана зависимость коэффициента жесткости фланца на изгиб k_p и толщиной фланца t_p, которая помогает определить механизм разрушения ФС. На рис. 8, *б*, показана зависимость α и t_p, которая указывает тип соединения. Из рис. 8, *б*, видно, что ФС является полужестким соединением в соответствии с критериями классификации, показанными на рис. 4.

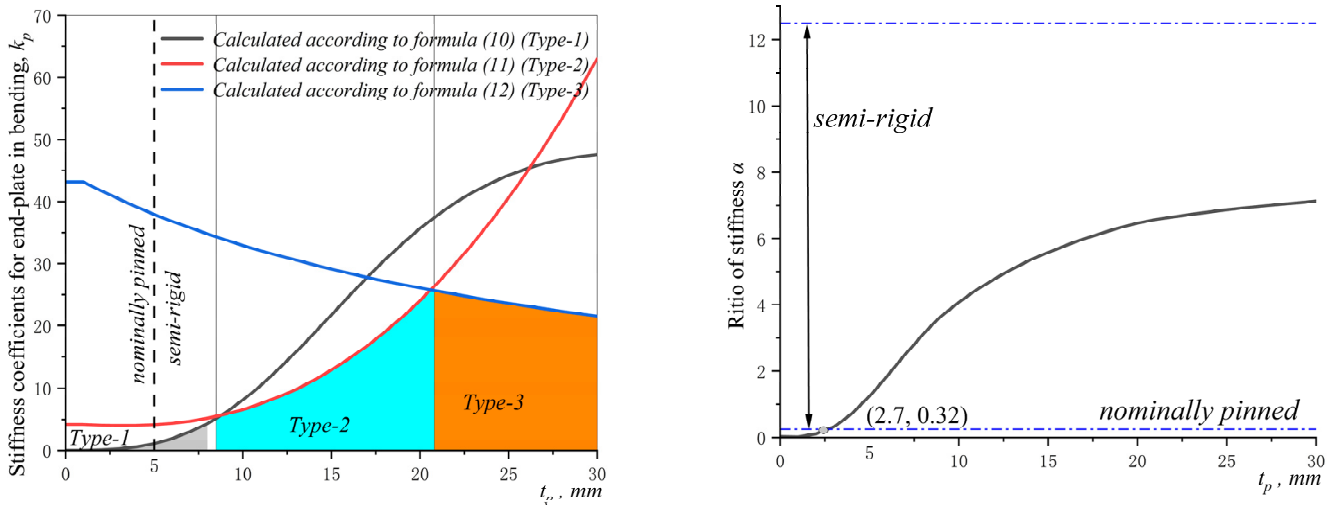

а *б*

Рис. 8. Результаты расчета:
а — зависимость k_p–t_p; *б* — зависимость α–t_p
И с т о ч н и к: выполнено Г. Сунь.

Figure 8. Calculated results:
а — curve k_p–t_p; *б* — curve α–t_p
S o u r c e: made by G. Sun.

Линейная жесткость образца балки составляет 818 kN·m/rad, жесткость колонны S_{co} — 7647 kN·m/rad. На рис. 9 показана зависимость изгибной жесткости и t_p. В формуле (рис. 9) видно, что увеличение изгибной жесткости соединения S_c влияет на возрастание изгибной жесткости целого каркаса $S_{g,b}$ в случае, когда толщина фланца t_p расположена в диапазоне (0, 8,8), который соответствует ФС с первым механизмом разрушения (Type-1). Для образца SF-1 изгибная жесткость $S_{g,b}$ почти постоянна в случае, когда толщина фланца t_p расположена в диапазоне (8,8, 30), который соответствует ФС со вторым и третьим механизмами разрушения (Type-2 и Type-3). Это значит, что без учета фактора несущей способности ФС с толщиной фланца t_p = 8,8 мм и α = 3,66 является самым эффективным решением с точки зрения изгибной жесткости. По результатам эксперимента несущая способность балки до развития пластической деформации составляет 21,96 kN·m. С учетом безопасности соединения самым эффективным вариантом с точки зрения изгибной жесткости является ФС с толщиной фланца t_p = 16,4 мм и α = 5,85, т.е. несущая способность соединения превышает несущую способность балки до развития пластической деформации при данном варианте. Из графиков (рис. 9) видно, что координаты в соответствии с ФС с t_p = 8,8 мм и t_p = 16,4 мм расположены в диапазоне второго механизма разрушения, поэтому рекомендуем применять соединения механизма разрушения Type-2 для стального каркаса.

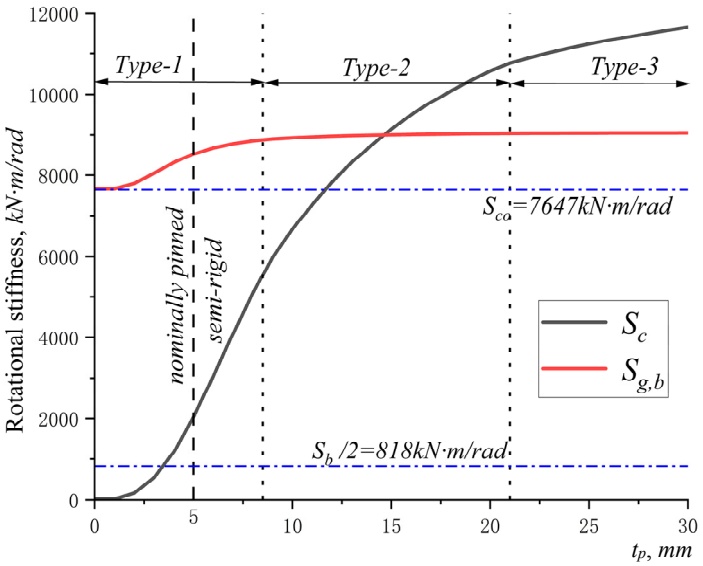

Рис. 9. Зависимость между толщиной фланца t_p и изгибной жесткости
И с т о ч н и к: выполнено Г. Сунь.

Figure 9. Rotational stiffness and end-plate thickness curve
S o u r c e: made by G. Sun.

4. Заключение

В исследовании представлено описание методики расчета жесткости стального каркаса с болтовыми фланцевыми соединениями с учетом поворота узла. Проанализировано влияние жесткости соединения на работоспособность целого каркаса. По результатам проведенного исследования можно сделать ряд выводов.

1. Использование разработанной методики позволяет точно прогнозировать изгибную жесткость стальных каркасов.

2. Разработанная методика может использоваться для определения механизма разрушения болтовых фланцевых соединений и типа соединения по жесткости.

3. Для стальных каркасов с болтовыми фланцевыми соединениями рекомендуется применять соединения механизма разрушения Type-2.

4. Для обеспечения работы целого каркаса и эффективного проектирования следует применять соединения с толщиной фланца t_p = 16,4 мм и α = 5,85.

Список литературы

1. *Li Q.*, *Yue Q.*, *Feng P.*, *Xie N.*, *Liu Y.* Development status and prospect of steel structure industry based on carbon peak and carbon neutrality target // Progress in Steel Building Structures. 2022. Vol. 24. No. 4. P. 1–7. https://doi.org/10.13969/j.cnki.cn31-1893.2022.04.001

2. *Данилов А.Н.* Развитие отрасли стального строительства // Промышленное и гражданское строительство. 2021. № 10. С. 4–8. https://doi.org/10.33622/0869-7019.2021.10.04-08 EDN: YEGQZK

3. *Sun G.F.*, *Mironova L.I.* Reinforcement of end-plate connections under low cyclic loading // Construction of Unique Buildings and Structures. 2025. No. 116. Article no. 11603. https://doi.org/10.4123/CUBS.116.3 EDN: XVUVHY

4. *Hüseyin K.*, *Gokhan S.* Semi-Rigid connections in steel structures State-of-the-Art report on modelling, analysis and design // Steel and Composite Structures. 2022. Vol. 45. No. 1. P. 1–21. https://doi.org/10.12989/scs.2022.45.1.001.

5. *Zhang Y.*, *Wang M.*, *Shi G.* Parametric analysis and design method of bolted extended end-plate beam-column connections in portal frames retrofitted with prefabricated cover plate com-ponents // Journal of Building Engineering. 2025. Vol. 111. Article no. 113399. https://doi.org/10.1016/j.jobe.2025.113399

6. *Liu X.*, *Sha X.*, *Guo C.*, *Wang Y.*, *Zhang Z.* Simplified design methods of large-capacity moment end-plate connections // Structures. 2025. Vol. 78. Article no. 109095. https://doi.org/10.1016/j.istruc.2025.109095

7. *Сунь Г.*, *Миронова Л.И.*, *Лю Ч.* Изгибная жесткость болтовых фланцевых соединений балки с колонной // Строительство и реконструкция. 2025. Т. 117. № 1. С. 26–39. https://doi.org/10.33979/2073-7416-2025-117-1-26-39 EDN: LNUUSN

8. *Piluso V.*, *Rizzano G.* Experimental analysis and modelling of bolted T-stubs under cyclic loads // Journal of Constructional Steel Research. 2008. Vol. 64. No. 6. P. 655–669. https://doi.org/10.1016/j.jcsr.2007.12.009

9. *Özkılıç Y.O.*, *Topkaya C.* The plastic and the ultimate resistance of four-bolt extended end-plate connections // Journal of Constructional Steel Research. 2021. Vol. 181. Article no. 106614. https://doi.org/10.1016/j.jcsr.2021.106614 EDN: MSKFMB

10. *Lu S.*, *Chen H.*, *Wang Z.*, *Wang M.* Exploration of the seismic behavior of full-scale steel frame with endplate connection based on component model // Structures. 2025. Vol. 81. Article no. 110245. https://doi.org/10.1016/j.istruc.2025.110245

11. *Chen X.*, *Liang Y.*, *Li A.*, *Dai Y.*, *Yuan H.* Structural performance of stainless steel frames with non-compact I-sections under monotonic loading // Thin-Walled Structures. 2025. Vol. 217. Article no. 113780. https://doi.org/10.1016/j.tws.2025.113780

12. *Truong V.H.*, *Nguyen P.C.*, *Kim S.E.* An efficient method for optimizing space steel frames with semi-rigid joints using practical advanced analysis and the micro-genetic algorithm // Journal of Constructional Steel Research. 2017. Vol. 128. P. 416–427. https://doi.org/10.1016/j.jcsr.2016.09.013

13. *Artar M.*, *Daloğlu A.T.* Optimum weight design of steel space frames with semi-rigid connections using harmony search and genetic algorithms // Neural Computing and Applications. 2018. Vol. 29. P. 1089–1100. https://doi.org/10.1007/s00521-016-2634-8 EDN: SOMRPE

14. *Ngo-Huu C.*, *Kim S.E.*, *Oh J.R.* Nonlinear analysis of space steel frames using fiber plastic hinge concept // Engineering Structures. 2007. Vol. 29. P. 649–657. https://doi.org/10.1016/j.engstruct.2006.06.008

15. *Ngo-Huu C.*, *Nguyen P.C.*, *Kim S.E.* Second-order plastic-hinge analysis of space semi-rigid steel frames // Thin-Walled Structures. 2012. Vol. 60. P. 98–104. https://doi.org/10.1016/j.tws.2012.06.019

16. *Kim S.E.*, *Lee D. H.* Second-order distributed plasticity analysis of space steel frames // Engineering Structures. 2002. Vol. 24. No. 6. P. 735–744. https://doi.org/10.1016/S0141-0296(01)00136-5

17. *Sagiroglu M.*, *Abdulkadir C.A.* Design and analysis of non-linear space frames with Semi-rigid connections // Steel and Composite Structures. 2015. Vol. 18. No. 6. P. 1405–1421. https://doi.org/10.12989/scs.2015.18.6.1405

18. *Шафрай С.Д.* Влияние конструктивно-технологической формы фланцевого соединения на его работоспособность // Известия вузов. Строительство. 2012. № 9. С. 92–100. EDN: PYYPXN

19. *Шафрай К.А.*, *Шафрай С.Д.* Особенности работы фланцевых соединений архитектурно-строительных конструкций. Внецентренное растяжение болтов // Известия вузов. Строительство. 2013. № 7. С. 84–92. EDN: PUMYSJ

20. *Шафрай К.А.*, *Шафрай С.Д.* Особенности работы фланцевых соединений архитектурно-строительных конструкций. Контактные напряжения и рычажные силы // Известия вузов. Строительство. 2013. № 11–12. С. 89–96. EDN: SAWVCV

21. *Шафрай К.А.*, *Шафрай С.Д.* Особенности архитектурного конструирования фланцевых соединений // Региональные архитектурно-художественные школы. 2014. № 1. С. 148–154. EDN: PUMYSJ

22. *Шафрай К.А.*, *Шафрай С.Д.* Прочность сварных швов фланцевых соединений стальных конструкций // Известия вузов. Строительство. 2018. № 8. С. 36–47. EDN: YSFVHN

23. *Shafray K.*, *Shafray S.* Work flange connections of structural elements of an open profile on high-strength bolts // Journal of Physics Conference Series. 2019. No. 1. Article no. 012072. https://doi.org/10.1088/1742-6596/1425/1/012072 EDN: VYACXC

24. *Перельмутер А.В.*, *Крискунов Э.З.*, *Юрченко В.В.* Проектирование болтовых фланцевых соединений согласно Eurocode и украинским нормам: согласованность и противоречия // Металлические конструкции. 2010. Т. 16. № 2. С. 93–104. EDN: MUVVGT

25. *Lu S.*, *Wang Z.*, *Pan J.*, *Wang P.* The seismic performance analysis of semi-rigid spatial steel frames based on moment-rotation curves of end-plate connection // Structures. 2022. Vol. 36. P. 1032–1049. https://doi.org/10.1016/j.istruc.2021.12.064 EDN: HYCLEP

References

1. Li Q., Yue Q., Feng P., Xie N., Liu Y. Development status and prospect of steel structure industry based on carbon peak and carbon neutrality target. *Progress in Steel Building Structures*. 2022;24(4):1–7. https://doi.org/10.13969/j.cnki.cn31-1893.2022.04.001

2. Danilov A.N. Steel construction development. *Industrial and Civil Engineering*. 2021;10:4–8. (In Russ.) https://doi.org/10.33622/0869-7019.2021.10.04-08

3. Sun G.F., Mironova L.I. Reinforcement of end-plate connections under low cyclic loading. *Construction of Unique Buildings and Structures*. 2025;116:11603. https://doi.org/10.4123/CUBS.116.3 EDN: XVUVHY

4. Hüseyin K., Gokhan S. Semi-Rigid connections in steel structures State-of-the-Art report on modelling, analysis and design. *Steel and Composite Structures*. 2022;45(1):1–21. https://doi.org/10.12989/scs.2022.45.1.001

5. Zhang Y., Wang M., Shi G. Parametric analysis and design method of bolted extended end-plate beam-column connections in portal frames retrofitted with prefabricated cover plate com-ponents. *Journal of Building Engineering*. 2025;111:113399. https://doi.org/10.1016/j.jobe.2025.113399

6. Liu X., Sha X., Guo C., Wang Y., Zhang Z. Simplified design methods of large-capacity moment end-plate connections. *Structures*. 2025;78:109095. https://doi.org/10.1016/j.istruc.2025.109095

7. Sun G., Mironova L.I., Liu C. Bending rigidity of bolt end-plate connections of joint beam to column. *Building and Reconstruction*. 2025;1:26–39. (In Russ.) https://doi.org/10.4123/CUBS.116.3 EDN: LNUUSN

8. Piluso V., Rizzano G. Experimental analysis and modelling of bolted T-stubs under cyclic loads. *Journal of Constructional Steel Research*. 2008;64(6): 655–669. https://doi.org/10.1016/j.jcsr.2007.12.009

9. Özkılıç Y.O., Topkaya C. The plastic and the ultimate resistance of four-bolt extended end-plate connections. *Journal of Constructional Steel Research*. 2021;181:106614. https://doi.org/10.1016/j.jcsr.2021.106614 EDN: MSKFMB

10. Lu S., Chen H., Wang Z., Wang M. Exploration of the seismic behavior of full-scale steel frame with endplate connection based on component model. *Structures*. 2025;81:110245. https://doi.org/10.1016/j.istruc.2025.110245

11. Chen X., Liang Y., Li A., Dai Y., Yuan H. Structural performance of stainless steel frames with non-compact I-sections under monotonic loading. *Thin-Walled Structures*. 2025;217:113780. https://doi.org/10.1016/j.tws.2025.113780

12. Truong V.H., Nguyen P.C., Kim S.E. An efficient method for optimizing space steel frames with semi-rigid joints using practical advanced analysis and the micro-genetic algorithm. *Journal of Constructional Steel Research*. 2017;128: 416–427. https://doi.org/10.1016/j.jcsr.2016.09.013

13. Artar M., Daloğlu A.T. Optimum weight design of steel space frames with semi-rigid connections using harmony search and genetic algorithms. *Neural Computing and Applications*. 2018;29:1089–1100. https://doi.org/10.1007/s00521-016-2634-8 EDN: SOMRPE

14. Ngo-Huu C., Kim S.E., Oh J.R. Nonlinear analysis of space steel frames using fiber plastic hinge concept. *Engineering Structures*. 2007;29:649–657. https://doi.org/10.1016/j.engstruct.2006.06.008

15. Ngo-Huu C., Nguyen P.C., Kim S.E., Kim S.E. Second-order plastic-hinge analysis of space semi-rigid steel frames. *Thin-Walled Structures*. 2012;60:98–104. https://doi.org/10.1016/j.tws.2012.06.019

16. Kim S.E., Lee D.H. Second-order distributed plasticity analysis of space steel frames. *Engineering Structures*. 2002;24(6):735–744. https://doi.org/10.1016/S0141-0296(01)00136-5

17. Sagiroglu M., Abdulkadir C.A. Design and analysis of non-linear space frames with Semi-rigid connections. *Steel and Composite Structures*. 2015;18(6):1405–1421. https://doi.org/10.12989/scs.2015.18.6.1405

18. Shafray S. The influence constructive-technological form of the flanged connection on his capacity to work. *News of higher educational institutions. Construction*. 2012;9:92–100. (In Russ.) EDN: PYYPXN

19. Shafray K., Shafray S. Features the work of flanged connections architectural and building structures. vnecentrennoe tensile bolts. *News of higher educational institutions*. 2013;7:84–92. (In Russ.) EDN: PUMYSJ

20. Shafray K., Shafray S. Features the work of flanged connections for building structures. Contact pressure and prying forces. *News of higher educational institutions*. 2013;11-12:89–96. (In Russ.) EDN: SAWVCV

21. Shafray K., Shafray S. Features of architectural design of flanged joints. *Regional architectural and art schools*. 2014;1:148–154. (In Russ.) EDN: PUMYSJ

22. Shafray K., Shafray S. Strength of welds flanges steel structures. *News of higher educational institutions*. 2018; 8:36–47. EDN: YSFVHN

23. Shafray K., Shafray S. Work flange connections of structural elements of an open profile on high-strength bolts. *Journal of Physics Conference Series*. 2019;1:012072. (In Russ.) https://doi.org/10.1088/1742-6596/1425/1/012072 EDN: VYACXC

24. Perelmuter A.V., Kriskunov E.Z., Yurchenko V.V. Design of flange bolt connections according to the Eurocode and Ukrainian codes: Coordination and contradictions. *Metal constructions*. 2010;16(2):93–104. (In Russ.) EDN: MUVVGT

25. Lu S., Wang Z., Pan J., Wang P. The seismic performance analysis of semi-rigid spatial steel frames based on moment-rotation curves of end-plate connection. *Structures*. 2022;36:1032–1049. https://doi.org/10.1016/j.istruc.2021.12.064

СТРОИТЕЛЬНАЯ МЕХАНИКА ИНЖЕНЕРНЫХ КОНСТРУКЦИЙ И СООРУЖЕНИЙ
STRUCTURAL MECHANICS OF ENGINEERING CONSTRUCTIONS AND BUILDINGS

2025. 21(6). 551–564

ISSN 1815-5235 (Print), 2587-8700 (Online)

HTTP://JOURNALS.RUDN.RU/STRUCTURAL-MECHANICS

DOI: 10.22363/1815-5235-2025-21-6-551-564
EDN: FPZIWY

Research article / Научная статья

Diagnostics of Structures under Vibration Loads and Elevated Temperatures

Samat N. Yakupov[1], Rishat R. Giniyatullin[1], Nukh M. Yakupov[1], Vasil G. Nizameyev[2], Marina I. Rynkovskaya[3]✉

[1] Federal research center "Kazan Scientific Center of Russian Academy of Sciences," *Kazan, Russian Federation*
[2] REMSTROYPROMPROEKT LLC, *Kazan, Russian Federation*
[3] RUDN University, *Moscow, Russian Federation*

✉ rynkovskaya-mi@rudn.ru

Received: September 11, 2025
Revised: November 22, 2025
Accepted: November 30, 2025

Abstract. Industrial building structures operate under severe conditions. An apt example of such structures are fan cooling towers, which resist significant vibration loads caused by a running fan; at the same time, the internal surfaces of the structures are exposed to relatively high temperatures from contact with cooled water, and the external surfaces are constantly exposed to the environment. The well-known approach to structural diagnostics does not take into account changes in the integral mechanical properties of thin-walled structural elements and the formation of local depressions and holes. Using the example of a large-sized fan cooling tower, an approach to diagnostics of structures affected by vibration from a running fan and the temperature of the cooled water, as well as the environment, is described. The effect of vibration and temperature on the process of corrosion wear of thin-walled structural elements has been studied experimentally and theoretically. Based on a new version of the finite element method developed for calculating structures in a cylindrical coordinate system, the initial and current state of the metal part of the fan cooling tower is investigated, taking into account plastic deformations. When analyzing the current state, corrosion defects and changes in the stiffness properties of thin-walled elements caused during operation as a result of the combined effects of vibration and relatively high temperatures were taken into account. It has been established that the presence of vibration and elevated ambient temperature contribute to accelerated corrosion; at the same time, the effect increases with increasing temperature and time of exposure to vibration. Corrosion wear leads to a significant increase in stresses and the formation of plastic deformations, which leads to a redistribution of stresses. It is noted that the discovered effects must be taken into account in the design and service of metal structures that experience significant vibration loads and operate at high temperatures.

Keywords: thin-walled structures, fan cooling tower, corrosion wear, experimental and theoretical method, mechanical properties, thin-walled elements, defects, high temperature, interpolation splines, finite element method variant, stress-strain state, elastic and plastic deformations

Samat N. Yakupov, Candidate of Technical Sciences, Senior Researcher, Kazan Scientific Center of Russian Academy of Science, Institute of Mechanics and Engineering, 2/32, Lobachevskogo St, Kazan, 420111, Russian Federation; eLIBRARY SPIN-code: 7382-4759, ORCID: 0000-0003-0047-3679; e-mail: tamas_86@mail.ru

Rishat R. Giniyatullin, Candidate of Technical Sciences, Researcher, Kazan Scientific Center of Russian Academy of Science, Institute of Mechanics and Engineering, 2/32, Lobachevskogo St, Kazan, 420111, Russian Federation; eLIBRARY SPIN-code: 7606-3211, ORCID: 0000-0003-2176-6913; e-mail: true_way@mail.ru.

Nukh M. Yakupov, Doctor of Technical Sciences, Leading Researcher, Kazan Scientific Center of Russian Academy of Science, Institute of Mechanics and Engineering, 2/32, Lobachevskogo St, Kazan, 420111, Russian Federation; eLIBRARY SPIN-code: 2933-5615, ORCID: 0000-0001-8248-1589; e-mail: yzsrr@mail.ru

Vasil G. Nizameyev, Candidate of Physical and Mathematical Sciences, Chief Project Engineer, REMSTROYPROMPROEKT LLC, office 16, Chistopolskaya St, Kazan, 421001, Russian Federation; eLIBRARY SPIN-code: 8079-8186, ORCID:0000-0001-8525-7611; e-mail: nizameev@kgasu.ru

Marina I. Rynkovskaya, Candidate of Technical Sciences, Associate Professor of the Department of Construction Technology and Structural Materials, Academy of Engineering, RUDN University, 6 Miklukho-Maklaya St, Moscow, 117198, Russian Federation; eLIBRARY SPIN-code: 9184-7432; ORCID: 0000-0003-2206-2563; e-mail: rynkovskaya-mi@rudn.ru

Conflicts of interest. The authors declare that there is no conflict of interest.

Authors' contribution: *Yakupov N.M.* — conceptualization, methodology, text writing — initial version; *Giniyatullin R.R., Yakupov S.N.* — validation, research (experimental method), visualization; *Nizameyev V.G.* — data processing, formal analysis; *Rynkovskaya M.I.* — review and editing. All of the authors read and approved the final version of the article.

Acknowledgments: The research was carried out within the framework of the state Assignment of mechanical Engineering of the FITC KazNC RAS, Kazan, Russian Federation.

For citation: Yakupov S.N., Giniyatullin R.R., Yakupov N.M., Nizameyev V.G., Rynkovskaya M.I. Diagnostics of structures under vibration loads and elevated temperatures. *Structural Mechanics of Engineering Constructions and Buildings*. 2025;21(6): 551–564. http://doi.org/10.22363/1815-5235-2025-21-6-551-564 EDN: FPZIWY

Диагностика состояния конструкций в условиях вибрационных нагрузок и повышенных температур

С.Н. Якупов[1], Р.Р. Гиниятуллин[1], Н.М. Якупов[1], В.Г. Низамеев[2], М.И. Рынковская[3]✉

[1] Институт механики и машиностроения ФИЦ Казанский научный центр РАН, *Казань, Российская Федерация*
[2] ООО «РЕМСТРОЙПРОМПРОЕКТ», *Казань, Российская Федерация*
[3] Российский университет дружбы народов, *Москва, Российская Федерация*

✉ rynkovskaya-mi@rudn.ru

Поступила в редакцию: 11 сентября 2025 г.
Доработана: 11 ноября 2025 г.
Принята к публикации: 30 ноября 2025 г.

Аннотация. Промышленные строительные конструкции работают в тяжелых эксплуатационных условиях. Ярким примером таких конструкций являются вентиляторные градирни, которые воспринимают существенные вибрационные нагрузки, вызываемые от работающего вентилятора; при этом внутренние поверхности конструкций испытывают воздействие относительно высоких температур от контакта с охлаждаемой водой, а наружные поверхности находятся постоянно под воздействием окружающей среды. Известный подход диагностики конструкции не учитывает изменение интегральных механических свойств тонкостенных элементов конструкций и образование локальных углублений и сквозных отверстий. На примере крупногабаритной вентиляторной градирни описан подход диагностики конструкций, подверженных воздействию вибрации от работающего вентилятора и температуры охлаждаемой воды, а также окружающей среды. Экспериментально-теоретическим методом исследовано влияние вибрации и температуры на процесс коррозионного износа тонкостенных элементов конструкций. На базе нового варианта метода конечных элементов, развитого для расчета конструкций в цилиндрической системе координат, исследовано исходное и актуальное состояние металлической части вентиляторной градирни с учетом пластических деформаций. При расчете актуального состояния были учтены коррозионные дефекты и изменения жесткостных свойств тонкостенных элементов, возникших в процессе эксплуатации в результате комплексного воздействия вибрации и относительно высоких температур. Установлено, что наличие вибрации и повышенная температура среды способствуют ускоренной коррозии; при этом с увеличением температуры и времени воздействия вибрации эффект усиливается. Коррозионный износ приводит к существенному росту напряжений и образованию пластических деформаций, что обусловливает перераспределение напряжений. Отмечено, что обнаруженные эффекты необходимо учитывать при проектировании и эксплуатации металлических конструкций, испытывающих существенные вибрационные нагрузки и работающих при высоких температурах.

Ключевые слова: тонкостенные конструкции, вентиляторная градирня, коррозионный износ, экспериментально-теоретический метод, механические свойства, тонкостенные элементы, дефекты, высокая температура, интерполяционные сплайны, вариант метода конечных элементов, напряженно-деформированное состояние, упругие и пластические деформации

Заявление о конфликте интересов. Авторы заявляют об отсутствии конфликта интересов.

Вклад авторов: *Якупов Н.М.* — концептуализация, методология, написание текста – первоначальный вариант; *Гиниятуллин Р.Р., Якупов С.Н.* — проверка достоверности, исследование (экспериментальный метод), визуализация; *Низамеев В.Г.* — обработка данных, формальный анализ; *Рынковская М.И.* — рецензирование и редактирование. Все авторы ознакомлены с окончательной версией статьи и одобрили ее.

Благодарности. Исследование выполнено в рамках государственного Задания машиностроения ФИЦ КазНЦ РАН, г. Казань, Рссийская Федерация.

Для цитирования: *Якупов С.Н., Гиниятуллин Р.Р., Якупов Н.М., Низамеев В.Г., Рынковская М.И.* Диагностика состояния конструкций в условиях вибрационных нагрузок и повышенных температур // Строительная механика инженерных конструкций и сооружений. 2025. Т. 21. № 6. С. 551–564. http://doi.org/10.22363/1815-5235-2025-21-6-551-564 EDN: FPZIWY

1. Introduction

The structure of a fan cooling tower (Figure 1, *a, b*) is a complex spatially curved system of reinforced concrete and steel elements. The inclined supports and cylindrical part of the cooling tower are made of reinforced concrete [1]. The metal part consists of a reducer — a converging truncated conical shell, a neck — fragments of toroidal and cylindrical shells, and a diffuser — a diverging truncated conical shell. The 4 mm thick shells are reinforced on the outside with a longitudinal and transverse set of channels, angles and plates. At the neck level and near the upper section of the diffuser, the structure is strengthened with ribs that are fixed to the cooling tower body with bars. The cooling tower design includes technological windows, as well as platforms and a stair system for maintenance.

a *b*

Figure 1. Large-sized cooling tower:
a — general view; *b* — metal part
S o u r c e: compiled by N.M. Yakupov

In addition to wind, vacuum, and weight loads, the cooling tower structure is subjected to vibration loads. Vacuum and vibration loads occur during the operational period when the fan is running. The internal surfaces of the structures are exposed to relatively high temperatures from contact with cooled water (up to 60°C and above), while the external surfaces and part of the internal surface are constantly exposed to the ambient temperature.

Severe service conditions contribute to intense corrosion wear. Field surveys of the condition of the structural elements of a number of cooling towers have shown that reinforced concrete supports and part of the metal shell are most susceptible to corrosion wear.

During more than 20 years of operation, the strength of concrete for some columns has significantly decreased. Concrete loosens, micro and macro cracks develop, and corrosion spots appear in the reinforcement. As a result, the strength properties of reinforced concrete structures are reduced. Figures 2 and 3 show fragments of the most worn areas ***1***, ***2***, and ***3*** (according to Figure 1) of the reinforced concrete structural elements.

In the metal part of the cooling tower, the neck area is experiences maximum corrosion wear, where the maximum air flow velocity, high vibration loads, and the greatest temperature impact take place. As a result of intense corrosion, the thickness of the shell has decreased significantly, in particular, in the neck

area; the thickness has decreased to 2 mm. There are a large number of holes and local depressions. A number of shell panels have turned into a "sieve". This pattern is observed in the neck area and in the lower parts of the reducer and diffuser. Active corrosion wear occurs at the panel joints, in the narrow gaps between the panel elements, and above the stiffening ribs. The supporting elements of the cooling tower, due to their external location, show less wear. Figure 3 shows some fragments of the most worn structural elements in the area where the reducer rests on the upper reinforced concrete ring (region ***4*** in Figure 1) and in the neck area (region ***5*** in Figure 1).

a *b* *c*

Figure 2. Defects (according to Figure 1):
a — in the area of inclined supports; *b* — in the area of the base; *c* — in the cylindrical part
S o u r c e: compiled by S.N. Yakupov.

a *b* *c*

Figure 3. Defects:
a — in the area of the upper reinforced concrete ring; *b* — in the reducer in the area of the reinforced concrete ring; *c* — in the area of the neck (inside view)
S o u r c e: compiled by S.N. Yakupov.

Metal corrosion is a physical and chemical interaction between metal and the environment — the oxidation of metal with the formation of corrosion products (rust), resulting in the reduction of the geometric parameters of structural elements. Upon that, the surface layers of structural elements are loosened to a certain depth or to the entire depth for thin-walled elements, which changes the mechanical properties of the element.

A thin protective passivating layer forms on the metal surface in water or other environments (Figure 4). When this layer is destroyed, corrosion damage begins [2].

It is evident that various factors influence the destruction of the protective passivating layer: physical and mechanical fields, environment and temperature, and others.

The influence of stress state on the kinetics of corrosion processes has been previously considered by the authors. Studies have shown that an increase in tensile stress contributes to the destruction of the protective layer and, thus, leads to accelerated corrosion wear. When analyzing the performance of structures, especially thin-walled structures exposed to corrosion, in addition to changes in geometric parameters, it is necessary to take into account changes in the reduced mechanical properties, as well as the level and nature of mechanical loads.

The influence of various physical fields on the state of the protective passivating layer has not been sufficiently studied. The influence of an active magnetic field on the corrosion process has been noted in [3–10].

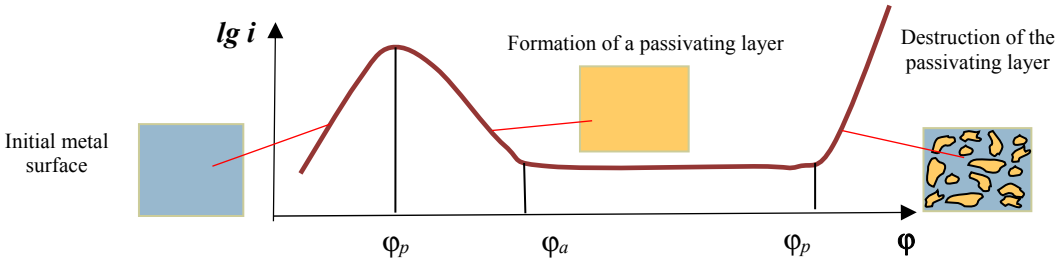

Figure 4. Relationship between the rate of anodic dissolution of metal *i* and the potential φ
S o u r c e: compiled by N.M. Yakupov

In structural design, the amount of material wear per unit of time (e.g., 0.1 mm per year) is generally specified. This approach does not take into account changes in the integral mechanical properties of thin-walled structural elements, as well as the formation of local depressions and holes. The results of a study of thin-walled beams with local defects are given in [13]. Some results of studying the influence of the environment on the creep and long-term strength of metals are given in [14–16]. The influence of vibration on the corrosion rate of protective anodes made of magnesium, aluminum, and zinc in fresh and sea water of the Persian Gulf is noted in [17]. The results of a study of the influence of vibration excitation during high-temperature processing on the mechanical properties and corrosion resistance of cast steel under stress are presented in [18].

The aim of this work is to develop an approach for diagnostics of thin-walled structures exposed to corrosion wear in the presence of vibration and elevated temperatures, using the example of a large-scale fan cooling tower. Research objectives: investigation of the effect of vibration and temperature on the corrosion wear process in thin-walled structural elements using a combined experimental and theoretical method; stress analysis of the initial and current condition of the metal part of the fan cooling tower, taking into account plastic deformations based on a version of the finite element method [11] developed for calculating stress-strain state of structures in cylindrical coordinate system.

2. Method

To evaluate the degree of corrosion wear of samples exposed to vibration and temperature field for a specific period of time in a given environment, a combined experimental-theoretical method [12] is used, based on the synthesis of experimental data and theoretical relationships obtained from nonlinear shell theory. This approach is an effective method for evaluating the integral stiffness properties of various thin-walled elements of complex structures. A diagram of the setup for flat samples is shown in Figure 5.

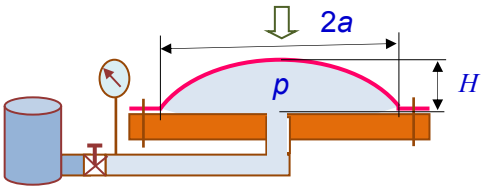

Figure 5. Diagram of the experimental setup
S o u r c e: compiled by N.M. Yakupov.

Round samples, aged for a specific period of time in the test environment under vibration and temperature exposure, are restrained along their contour and loaded with uniform pressure p. As pressure p increases, the shape of the dome is monitored, in particular, rise H of the dome is measured, and a pressure p — deflection H graph is constructed. At the theoretical stage, using the ratios obtained from nonlinear shell theory for the case of moderate bending and the experimental pressure p — deflection H relationship for metal samples, the reduced tangential stiffness for tension-compression B and the reduced bending stiffness D are calculated [12]:

$$B = 0.3037 pa\left(\frac{a}{H}\right)^3, \quad D = 0.0253 p\frac{a^4 h^2}{H^3}, \tag{1}$$

and also the modulus of elasticity, according to formula:

$$E = \frac{0.303 pa^4(1-\nu^2)}{hH^3}, \tag{2}$$

where h and a — the thickness and radius of the test part; ν — the Poisson's ratio.

3. Results

3.1. Influence of Vibration on Corrosion Wear

A study of the influence of vibration on the corrosion wear process of St3 steel samples with an initial thickness h = 0.6 mm in an aqueous medium has been conducted.

Thin round samples are placed separately in containers with the medium. The containers are placed on a vibrating platform. Specifically, on a platform attached to a compressor (rotation frequency n = 2800 rev / min).

Cases of horizontal and vertical sample placement are considered (Figure 6, *a, b*).

The samples were kept in the aqueous medium for a specified period of time. The control group of containers was located in an area free from vibration. The degree of corrosion of the samples was evaluated using a combined experimental-theoretical method [12].

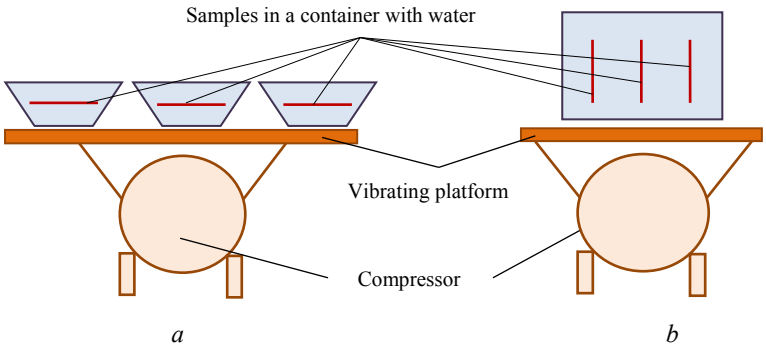

Figure 6. Schemes for placing samples on a vibrating platform:
a — horizontal placement of samples; *b* — vertical placement of samples
S o u r c e: compiled by N.M. Yakupov.

In the first series of tests, samples were placed horizontally on a special compressor platform (Figure 6, *a*). The compressor turned on automatically for two months (except Sundays) from 9:00 a.m. to 6:00 p.m.: during the day, the compressor periodically turned on (vibration — 20 seconds) and off (no vibration — 3 minutes 40 seconds).

In the second series of tests, samples were placed vertically on a special compressor platform (Figure 6, *b*). The compressor operated for four months in automatic mode: it turned on (vibration) for 30 seconds and turned off (no vibration) for 6 minutes and 10 seconds. In each series of tests, the control group of samples, that were not subjected to vibration, was examined.

Using the combined experimental-theoretical method mentioned above, the relationship between the maximum deflection H and pressure p was determined for each sample. Pressure p — deflection H curves were constructed based on the average values of the maximum deflections of the samples, which are presented for the first series of tests in Figure 7, *a*, and for the second series — in Figure 7, *b*.

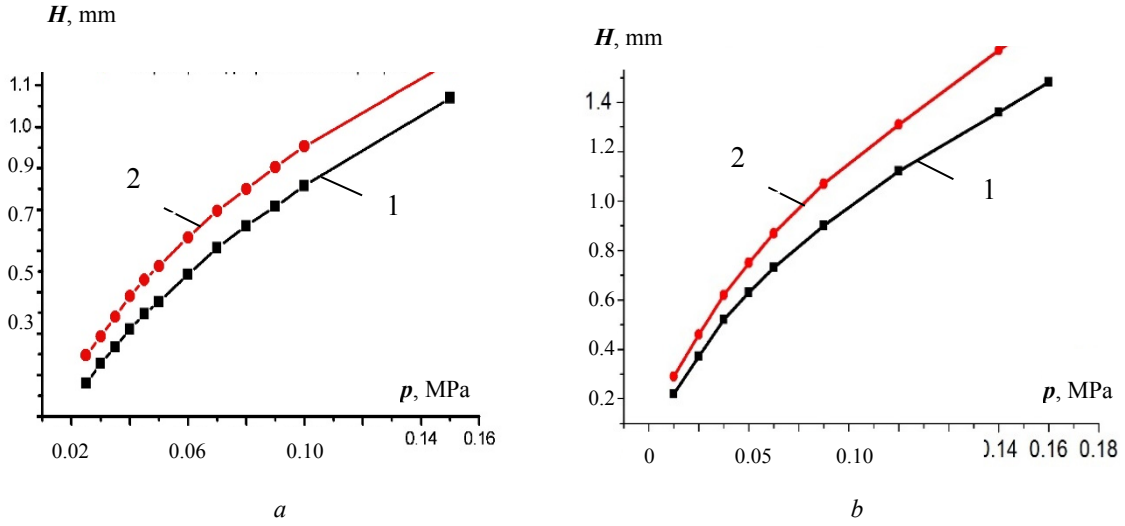

Figure 7. $p - H$ relationships when samples are placed:
a — horizontally, *b* — vertically; *1* — at rest; *2* — under vibration
S o u r c e: compiled by N.M. Yakupov.

As can be seen, in both series of tests, samples from the group exposed to vibration (2) deflect more than samples from the control group (1) at the same pressure, i.e., samples under vibration experience greater corrosion wear than samples from the control group. This conclusion is consistent with the measurements of the thickness of the samples after corrosion wear: the average thickness of the samples exposed to vibration in the first series of tests was 0.588 mm, while the average thickness of the samples in the control group was 0.593 mm. For the second series of tests, the corresponding values were 0.556 mm and 0.569 mm.

This conclusion can be explained by the fact that vibration creates more favorable conditions for the destruction of the passivating layer in the electrochemical corrosion process.

Thus, the influence of vibration on the process of corrosion wear of steel samples in an aqueous medium has been established, with vibration contributing to faster destruction of the protective passivating layer formed during corrosion, thereby promoting accelerated corrosion.

The discovered effect is of high theoretical significance to the study of corrosion as a complex electrochemical process under the influence of vibration, and of practical significance as well. The effect must be taken into account in the design and operation of metal structures that experience substantial vibration loads, such as fan cooling towers, vehicles, pipelines, and others.

3.2. Influence of Temperature on Corrosion Wear

The effect of temperature on the corrosion process is of particular scientific interest, although studies on this topic are rare. An increase in corrosion wear at 70˚C was discovered at a coal-fired power plant during a study of boiler walls, where viscous deposits were observed on the walls due to acid condensation

[19]. An increase in susceptibility to stress corrosion cracking for some grades of stainless steel in *KCl* solution under the influence of temperature was noted in [20].

An experimental study of the influence of water temperature on the corrosion wear of thin-walled St3 steel samples has been conducted.

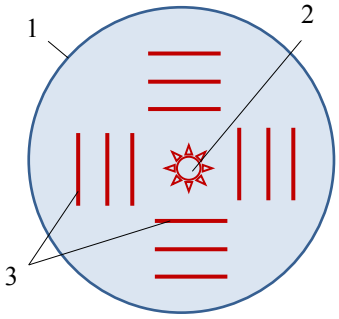

Figure 8. Installation scheme:
1 — cylindrical container; *2* — heating element; *3* — sample holders
S o u r c e: compiled by N.M. Yakupov.

Experimental procedure. A setup has been developed (Figure 8) consisting of a cylindrical container (1) for filling with aggressive liquid.

A heating element (2) is located in the center of the container. Sample holders (3) are installed around the perimeter of the container at equal distances from the center. Temperature sensors are installed near the samples to monitor the temperature of the medium.

In the experiment, three installations located next to each other were used to implement three temperature modes. Samples fixed in a holder are placed in appropriate containers with a particular medium and kept there for a particular period of time. Before and after the experiment, the thickness of the samples under study is inspected and measured.

To evaluate the influence of temperature on the corrosion of circular thin-walled specimens, the combined experimental-theoretical method mentioned above is used.

*St*3 steel samples with a thickness of 0.6 mm were exposed to corrosion wear over 107 days in the following temperature modes: $T_1 = 70^\circ$C, $T_2 = 40^\circ$C, $T_3 = 18^\circ$C. The thicknesses of the samples subjected to corrosion under the influence of the temperature field were as follows: $t_1 = 0.528$ mm, $t_2 = 0.576$ mm, $t_3 = 0.581$ mm, respectively. The "pressure p — deflection H" curves for the considered samples are presented in Figure 9.

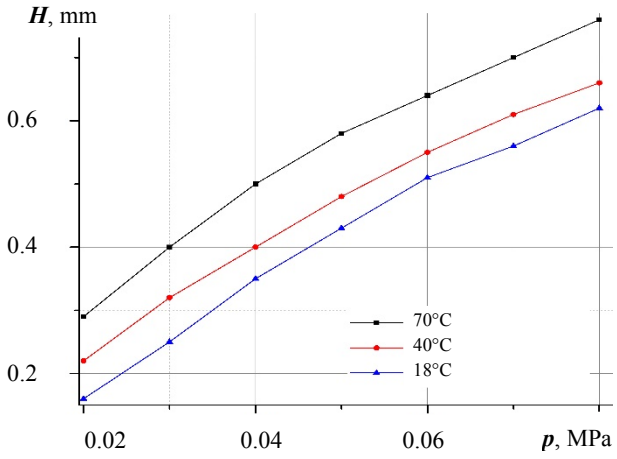

Figure 9. Pressure ***p*** — deflection ***H*** curves
S o u r c e: compiled by R.R. Giniyatullin.

As seen in Figure 9, as the temperature of the medium increases, the deflection of the samples increases, i.e., corrosion wear increases. The resulting elasticity moduli of the corroded samples, calculated according to (2) at $p = 0.02$ MPa, were: $E_1 = 1.778\times10^6$ MPa, $E_2 = 1.946\times10^6$ MPa, $E_3 = 2.051\times10^6$ MPa, respectively.

Figure 10 shows images of the surface of corroded samples at 4x, 10x, and 400x magnification.

As can be seen, corrosion causes the surface of the samples to loosen to a certain depth, and as the temperature rises, cavities form, which merge into large regions at 70°C.

Thus, it has been established that the temperature of the environment significantly affects the corrosion wear of thin-walled steel samples. An increase in the temperature of the environment contributes to a more rapid destruction of the protective passivating layer formed during the corrosion process, thereby leading to an increase in the degree of corrosion wear.

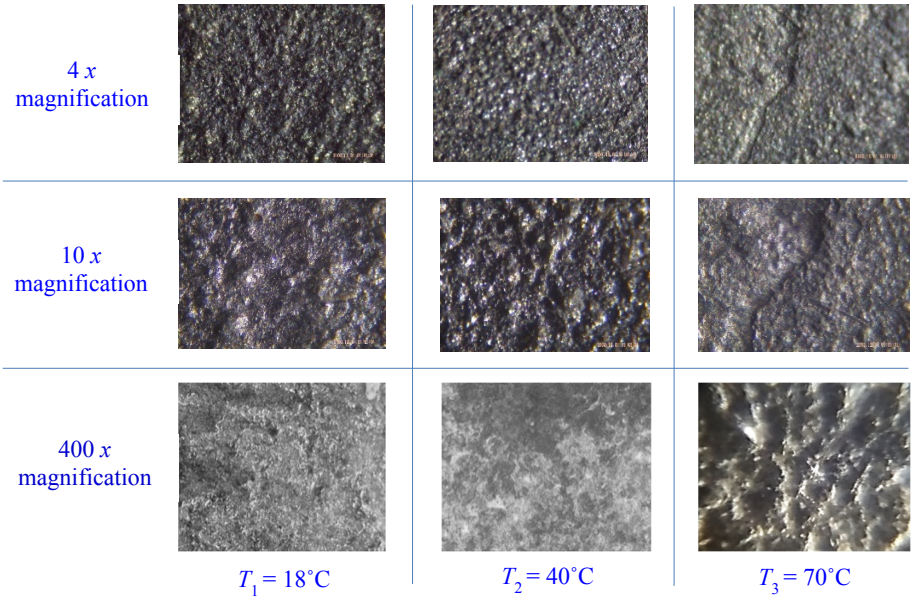

Figure 10. Images of the surface of corroded samples

S o u r c e: compiled by R.R. Giniyatullin.

The established effect is of high theoretical significance in studying the complex electrochemical process of corrosion, taking into account the temperature of the environment. The effect is also of high practical significance, especially for thin-walled structural elements, and must be taken into account in the design and operation of metal structures that interact with high-temperature environments during service, such as fan cooling towers, pipelines, and others.

3.3. Structural Condition of Cooling Tower with Corrosion Defects

As noted above, cooling tower structures operate in severe conditions. Wind, vacuum, and weight loads, as well as vibration from operating fans, high temperatures of the cooled medium, and solar radiation contribute to significant corrosion wear of the structural elements. This results in the formation of various local depressions and holes, and changes in the stiffness properties of the thin-walled elements. All this contributes to an increase in internal stress, appearance of additional stress concentrators, and a reduction in the load-bearing capacity of the entire structure.

In the region of the corrosion defect, the structure of the surface layer material changes. This fact is practically ignored, although it can be critical for thin-walled structural elements. Changes in the structure of the surface layer can lead to significant changes in the integral mechanical properties of thin-walled structural elements. In this regard, to perform the stress analysis of the metal part of the cooling tower structure (Figure 1), the current integral stiffness characteristics of thin-walled elements cut out from the structures during repair were preliminarily determined using the combined experimental-theoretical method. That is, the calculations took into account the actual stiffness properties of the structural elements, which were subjected, in particular, to the influence of vibration and temperature loads during the operational period.

To perform the stress analysis of the metal part of the fan cooling tower, a spline version of the finite element method (*SV FEM*-2) [11] was used, developed for the case of plastic deformation. The method was

developed by the authors. The method is based on a synthesis of the idea of preliminary parameterization of the mid-surface of the shell in a cylindrical coordinate system and the finite element method. The method allows one to determine the stress-strain state of thin-walled structures under static loads. The effects of vibration and temperature are taken into account by specifying relevant integral stiffness characteristics for structural elements. The key points of the spline version of the finite element method (SV FEM-2) are presented below.

Parameterization of the middle surface of the cooling tower shell. The parametric equation in the cylindrical coordinate system used in the cooling tower analysis is as follows:

$$r(t^1,t^2)=x(t^1,t^2)i+\rho(t^1,t^2)e(t^1,t^2)e(t^1,t^2)=\sin\psi(t^1,t^2)\,j+\cos\psi(t^1,t^2)k\,, \tag{3}$$

where $x(t^1,t^2)$ — the linear coordinates; $\psi\left(t^1,t^2\right)$ — the angular coordinates; $\rho(t^1,t^2)$ — the shortest distance from axis *OX* to the middle surface of the shell; t^1, t^2 — the parameters of the unit square; *i, j, k* — the unit vectors of orthogonal axes *OX*, *OY*, *OZ*.

By differentiating position vector r , coordinate vectors r_1 and r_2, the components of the first a_{jk} and second b_{ik} metric tensors and Christoffel symbols Γ^i_{jk} are determined.

Geometrical and physical relationships. The case of moderate bending of a thin shell is considered. In this case, the tangential and bending strains of the mid-surface according to the Kirchhoff — Love model are determined by the formulas [20]

$$2\varepsilon_{ik}=e_{ik}+e_{ki}+\omega_i\omega_k,\quad \kappa_{ik}=-\nabla_i\omega_k-b_i^s e_{ks}\,, \tag{4}$$

where i, k, s = 1, 2; ε_{ik} are the covariant components of the tangential strain tensor; κ_{ik} are the covariant components of the bending and torsional strains; $\omega_i=\nabla_i w+b_i^k u_k$ are the components of the normal line rotation vector m ; $e_{ik}=\nabla_i u_k-b_{ik}w$ are the components of the rotation tensor; ∇_i is the symbol of covariant differentiation with respect to a_{ik} ; u_k, w are the covariant components of the displacement vector $(u_1=u, u_2=v)$, b_i^s are the mixed components of the second metric tensor.

The relationship between stress intensity σ_i and strain intensity ε_i is taken in the form

$$\sigma_i=g(\varepsilon_i)\varepsilon_i. \tag{5}$$

Here $g(\varepsilon_i)$ is a positive function, characteristic for the considered material.

Resolving equations. To derive the resolving equations, Lagrange variational equation is used [11]

$$\delta W-\delta A=0\,, \tag{6}$$

where δW — the variation of the strain potential energy of the shell, δA — the work of the external forces applied to the shell.

In each rectangle Ω_{ij} of the unit square area the solution is expressed in the form of interpolational Hermite cubic spline of two variables

$$u=\varphi(s^1)F_u\varphi(s^2),\ v=\varphi(s^1)F_v\varphi(s^2),\ w=\varphi(s^1)F_w\varphi(s^2)\,, \tag{7}$$

where $\varphi(s^1)$, $\varphi(s^2)$ — the vectors of coordinate functions; F_u, F_v, F_w — the matrices of nodal values of the displacement components, the first and the second mixed derivatives.

The use of preliminary parameterization and the representation of the solution in each rectangle Ω_{ij} in the form of a cubic spline ensure geometric continuity, as well as the continuity of the displacement function

and its first derivatives throughout the entire considered domain Ω, which is an important condition for convergence to the exact solution as the size of rectangles Ω_{ij} decreases. Thus, it is possible to obtain consistent elements based on the Kirchhoff — Love hypothesis for shells of complex geometry.

By substituting variations of displacements and strains into the Lagrange variational equations and taking into account the independence of nodal displacements and their derivatives, after a series of transformations, a system of algebraic equations is obtained

$$[A]\{U\} = \{R\}_p + \{R\}_n. \tag{8}$$

Here $[A]$ is the symmetric stiffness matrix of the system of band structure, $\{U\}$ is the vector of unknowns, $\{R\}_p$ is the load vector, $\{R\}_n$ is the vector of nonlinear components. The solution to the resulting system of nonlinear algebraic equations is determined using the general iteration method.

The algorithm of the above-mentioned spline version of the finite element method for calculating the stress-strain state of shell structures of complex geometry in a cylindrical coordinate system is implemented by the SV FEM-2 software package.

Stress analysis of the metal part of a fan cooling tower, taking into account physical nonlinearity. Based on the spline version of the finite element method (*SV FEM*-2) [11], developed to calculate the stresses and strains of shell structures with complex geometry in a cylindrical coordinate system, taking into account physical nonlinearity, the stress analysis of the metal part of a fan cooling tower is performed (Figure 11).

Information about the ribs is specified at each calculation point in the following format: area, static moment, and moment of inertia of the rib section. Due to the presence of a plane of symmetry, half of the structure is considered, which is divided into 10 elements along the circumferential coordinate (angle θ°) and 23 — along the generatrix. The horizontal sections (Figure 11) are numbered from bottom to top. The zero angle corresponds to the wind direction plane. The distribution of pressure from wind load, both along the height and the circumferential coordinate, is taken in accordance with the building code in force in the Russian Federation, SP 20.13330.2016[1].

The current mechanical characteristics of the thin-walled structural elements were determined using the combined experimental-theoretical method described above. Samples were cut from a cooling tower structure that had been shut down for major repairs. Changes in shell thickness t along the generatrix and the degree of wear of horizontal ribs W for the current version (for some of the most worn sections according to Figure 11) are shown in the Table.

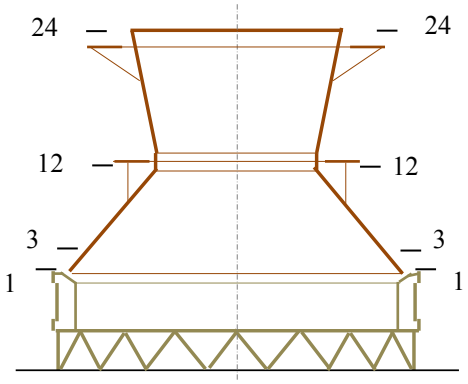

Figure 11. Design diagram of a fan cooling tower

S o u r c e: compiled by N.M. Yakupov.

Change in shell thickness and degree of wear of horizontal ribs

Section	1–1	2–2	3–3	4–4	8–8	9–9	10–10	11–11	12–12	13–13	14–14
t*, *mm	0,35	0,30	0,10	0,00	0,05	0,30	0,35	0,30	0,10	0,05	0,10
***W*, %**	40	30	10	0	5	30	40	30	10	5	10

S o u r c e: compiled by N.M. Yakupov.

[1] SP 20.13330.2016. Set of rules “Loads and actions”. JSC “Reseach center “Construction” — V.A. Kucherenko Central Scientific Research Institute for Building Structures, 2017.

The displacement and stress distributions for the initial and current cooling tower designs were analyzed. Significant stress concentrations were identified in defective areas of the structures, formed as a result of corrosion wear under the influence of vibration from operating fans, high temperatures from the cooled medium, solar radiation, as well as wind, vacuum, and weight loads. The maximum values of stress intensity σ_i along circumferential coordinate θ° at maximum load in a linear setting for the first two horizontal calculated sections (according to Figure 11) are shown in Figure 12 (section 1–1) and Figure 13 (section 2–2).

As seen in Figure 12, stress concentrations in the first section (the area where the reducer is supported by the reinforced concrete part of the cooling tower) are observed in the region of $\theta = 36^0$ and $\theta = 160^0$. In the second section (Figure 13), a stress peak is observed in the zone of $\theta = 63^0$. For the current version, the linear stress exceeds the yield strength for this material (σ_m = 200 MPa).

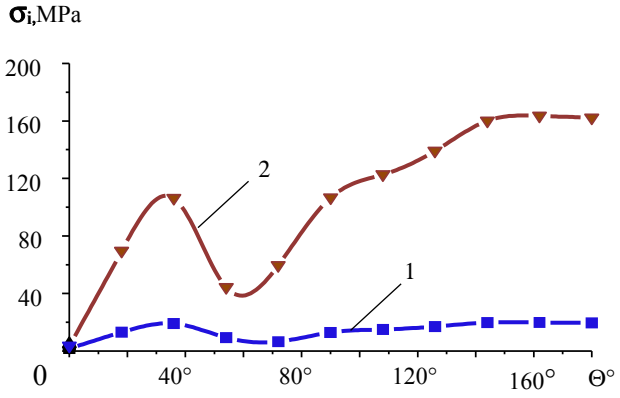

Figure 12. σi–θ° relationship for section 1–1:
1 — initial; *2* — actual
S o u r c e: compiled by N.M. Yakupov.

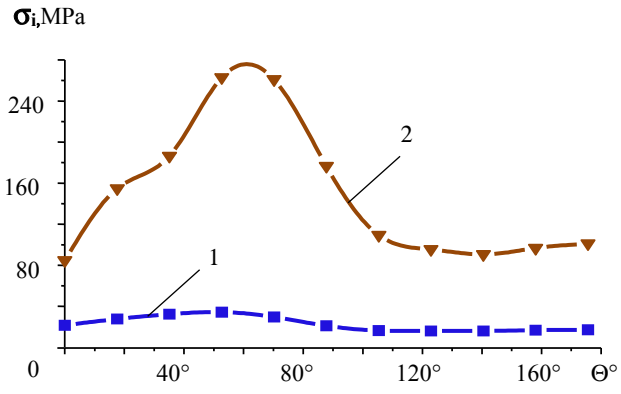

Figure 13. σi–θ° relationship for section 2–2:
1 — initial; *2* — actual
S o u r c e: compiled by N.M. Yakupov.

Figure 14 shows the changes in stress intensity depending on the load value for points *D* and *C* located in section 1–1; point *D* is at some distance from point *C*, where maximum stresses occur.

Line *F* corresponds to σ_m = 200 MPa. As seen from Figure 14 at 82% of the maximum load at point *C*, the stress reaches σ_m and effectively does not increase further.

At point *D*, starting at 82% load, as expected, a more intense increase in stress is observed. That is, load redistribution occurs.

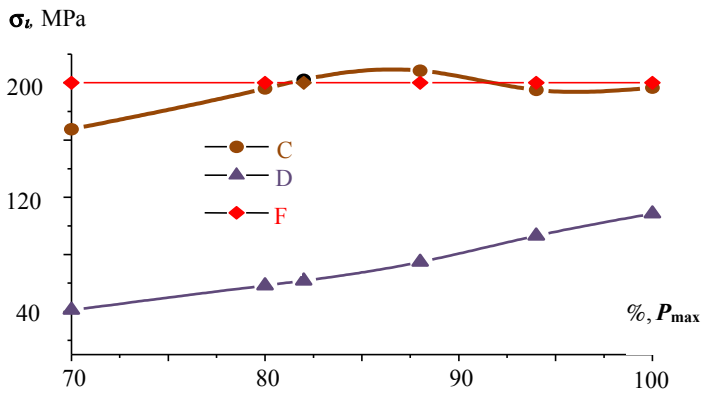

Figure 14. Dependence σ_i–P for points D and C located in section 1–1
S o u r c e: compiled by N.M. Yakupov.

Thus, a spline version of the finite element method in a cylindrical coordinate system has been developed, taking into account plastic deformations. Stress analysis for the initial and current condition of the metal part of the fan cooling tower has been performed. The current mechanical properties of thin-walled structural elements were determined using a combined experimental-theoretical method. In particular, it was established that corrosion wear leads to a significant increase in stress, which may exceed the yield strength of the material. At the same time, the resulting plastic deformations lead to a redistribution of stresses.

4. Conclusion

According to the results of the conducted research, the following should be noted:

1. An approach for diagnostics of metal structures is described using the example of a large-scale fan cooling tower, which is exposed to the combined effects of vibration and elevated temperatures.

2. The corrosion wear of thin-walled steel structural elements exposed to vibration and temperature was investigated using a combined experimental-theoretical method.

3. It has been established that vibration and elevated ambient temperatures contribute to the accelerated destruction of the protective passivating layer of the thin-walled steel elements and thus contribute to accelerated corrosion. At the same time, the effect intensifies with increasing temperature and duration of exposure to vibration.

4. A spline version of the finite element method was developed in a cylindrical coordinate system, and stress analysis was performed for the metal part of the fan cooling tower, taking into account plastic deformations for the initial and current condition of the metal part. When analyzing the current condition, corrosion defects and changes in the stiffness properties of the thin-walled elements caused during operation as a result of the combined effects of vibration and high temperatures were taken into account.

5. It has been established that corrosion wear leads to a significant stress increase in the structural elements, which may exceed the yield strength of the material, while the resulting plastic deformations lead to stress redistribution.

The obtained results are of high theoretical and practical importance and need to be taken into account in the design and operation of metal structures that are exposed to significant vibration loads and operate at high temperatures and under the influence of various types of radiation.

To address the issue of safe operation of thin-walled structures exposed to corrosion wear, when diagnosing their condition, in addition to considering changes in the geometric parameters, it is necessary to consider changes in the mechanical characteristics due to the influence of external factors, in particular vibration, ambient temperature, and physical fields.

References

1. Yakupov N.M., Nurgaliev A.R., Giniyatullin R.R., Yakupov S.N. Operation of structures with corrosive wear. *Russ. Engin. Res.* 2013;33:69–73. https://doi.org/10.3103/S1068798X13020202 EDN: RFESWX

2. Frumkin A. Bemerkung zur Theorie der Wasserstoffüberspannung. *Zeitschrift für Physikalische Chemie*. 1932. Vol. 160. No. 1. P. 116–118.

3. Yang Y., Luo Ya., Sun M., Wang Ju. Effect of magnetic field on corrosion behavior of X52 pipeline steel in simulated soil solution. *International Journal of Electrochemical Science*. 2021;16(10):211010. https://doi.org/10.20964/2021.10.33 EDN: JEJBAE

4. Rocabert U., Parnicki-K.M.A., Maccari F., Tankov N., Ener S. Comprehensive study of τ-phase Mn–Al–C magnets: corrosion resistance, structural integrity, and magnetic properties. *ACS Omega*. 2024;10(1). Available from: https://pubs.acs.org/doi/10.1021/acsomega.4c07540 (accessed: 12.05.2025).

5. Ye X., Yang J., Yang W., Chen T., Li W., Liu Y. Theoretical and experimental study on the effect of magnetic field on the amount of steel bars corrosion. *Corrosion Science*. 2025;255:113082. https://doi.org/10.1016/j.corsci.2025.113082

6. Tang Y.Ch., Davenport A.J. Magnetic field effects on the corrosion of artificial pit electrodes and pits in thin films. *J. Electrochem. Soc.* 2007;154(7):362–370. https://doi.org/10.1149/1.2736662

7. Alimi F., Tlili M., Ben Amor M., Maurin G., Gabrielli C. Influence of magnetic field on calcium carbonate precipitation in the presence of foreign ions. *Surface Engineering and Applied Electrochemistry*. 2009;45(1):56–62. https://doi.org/10.3103/S1068375509010104 EDN: LWGKSH

8. Mushnikov A.N., Povolotskaya A.M., Zadvorkin S.M., Kryucheva K.D. The influence of biaxial symmetric tension on the magnetic properties of a composite specimen made of two steel plates with different mechanical and magnetic properties. *Russian Journal of Nondestructive Testing*. 2024;60(9):1015–1027. https://doi.org/10.1134/S1061830924700773 EDN: ETUOCC

9. Zhao S., Zhang H., Piao H.-G., Wang Y., Sun X., Zhang Y., Huang Y., Zhao Y. The effect of magnetic field pretreatment on the corrosion behavior of carbon steel in static seawater. *RSC Adv*. 2020;10:2060–2066. https://doi.org/10.1039/C9RA09079G EDN: UZVBIB

10. Dugargaramjav T., Pashka B., Munkhbaatar B. Study of the Influence of Electromagnetic Fields on the Corrosion of District Heating Pipelines: Corrosion of District Heating Pipelines. *Journal of Energy Transition.* 2024;2(1):15–21. https://doi.org/10.59264/jet.v2i1.54 EDN: MRVGYL

11. Yakupov S.N., Kiyamov H.G., Yakupov N.M., Mukhamedova I.Z. A new variant of the fem for evaluation the strenght of structures of complex geometry with heterogeneous material structure. *Case Studies in Construction Materials*. 2023;19:e02360. https://doi.org/10.1016/j.cscm.2023.e02360

12. Galimov N.K., Yakupov N.M., Yakupov S.N. Experimental-theoretical method for determining mechanical characteristics of spherical films and membranes of complex structure. *Mechanics of Solids*. 2011;46:380–386. https://doi.org/10.3103/S0025654411030058 EDN: OHZMWJ

13. Staszak N., Gajewski T., Garbowski T. Effective stiffness of thin-walled beams with local imperfections. *Materials (Basel).* 2022;15(21):7665. https://doi.org/10.3390/ma15217665 EDN: WGJHOE

14. Zawada-Michałowska M., Pieśko P. Post-machining deformations of thin-walled elements made of EN AW-2024 T351 aluminum alloy as regards the mechanical properties of the applied, rolled semi-finished products. *Materials (Basel).* 2021;24:7591. https://doi.org/10.3390/ma14247591

15. Zhang K., X. Liu X., L. Zhu L. Prediction reliability improvement on long-term creep life for P91 steel using a hybrid method of artificial neural network and CDM model. *Engineering Fracture Mechanics*. 2025;323:111172. https://doi.org/10.1016/j.engfracmech.2025.111172 DN: EBNVVP

16. Yu Z.Y., Wang X.M., Cao G.W. Environmental effects on the creep response of thin-walled Ni-based single crystal superalloys. *Journal of Materials Engineering and Performance*. 2022;31(9):7263–7276. https://doi.org/10.1007/s11665-022-06791-8 EDN: UJXNVZ

17. Haider Hadi J. Effect of vibration on the corrosion rate of Mg, Al, and Zn cathodes protection in freshwater and the Arab Gulf Seawater. *EHEI Journal of Science and Technology.* 2024;4(2):56–161. https://doi.org/10.34874/PRSM.ehei-jst-vol4iss2.55474

18. Shao R., Wang H., Lu K., Song Ju. Effect of excitation vibration on mechanical property and stress corrosion resistance of cast steel. *Journal of Vibroengineering*. 2023;25(7):1230–1242. https://doi.org/10.21595/jve.2023.23125 EDN: VUMQWY

19. Chen H., Pan P., Wang Yu., Zhao Q. Field study on the corrosion and ash deposition of low-temperature heating surface in a large-scale coal-fired power plant. *Fuel.* 2017;208:149–159. https://doi.org/10.1016/j.fuel.2017.06.120

20. Serafim F.M.F., Alabi W.O., Oguocha I.N.A., Odeshi A.G., Evitts R., Gerspacher R.J., Ohaeri E.G. Stress corrosion cracking behavior of selected stainless steels in saturated potash brine solution at different temperatures. *Corrosion Science.* 2021;178:109025. https://doi.org/10.1016/j.corsci.2020.109025 EDN: HENEBY

СТРОИТЕЛЬНАЯ МЕХАНИКА ИНЖЕНЕРНЫХ КОНСТРУКЦИЙ И СООРУЖЕНИЙ
STRUCTURAL MECHANICS OF ENGINEERING CONSTRUCTIONS AND BUILDINGS

2025. 21(6). 565–584

ISSN 1815-5235 (Print), 2587-8700 (Online)
HTTP://JOURNALS.RUDN.RU/STRUCTURAL-MECHANICS

РАСЧЕТ ТОНКИХ УПРУГИХ ОБОЛОЧЕК
ANALYSIS OF THIN ELASTIC SHELLS

DOI: 10.22363/1815-5235-2025-21-6-565-584
EDN: FQCZQA

Research article / Научная статья

Strength, Stability and Dynamics of Rigid Shells: Analysis of Recent Research

Sergey N. Krivoshapko[1], **Paschal Ch. Chiadighikaobi**[2]✉

[1] RUDN University, *Moscow, Russian Federation*
[2] Afe Babalola University, *Ado-Ekiti, Ekiti State, Nigeria*
✉ chiadighikaobi.paschalc@abuad.edu.ng

Received: May 12, 2025
Revised: September 18, 2025
Accepted: October 2, 2025

Abstract. Many numerical methods of analysis of rigid shells, such as the displacement-based finite element method (FEM), finite difference energy method, method of separation of variables, kinematic method of the theory of limit equilibrium, and so on, were proposed and tested until 2000. Most problems of static and dynamic analysis of canonical shells were successfully solved at the same time. All these methods were used actively after the 2000, too. However, new problems began to appear before structural engineers, architects, and builders. These problems are associated with multi-layer shell walls, with the emergence of new composite construction materials, and therefore, with the solution of physically nonlinear problems. Geometricians presented several hundred new forms of middle surfaces of shells, and that is why the need to select optimal forms from several alternatives using criteria of optimality came into existence. The selection of necessary computing software from many of their types began to be a problem. New problems demanded new methods of approach for their solution. In this paper, a critical evaluation of proposed solutions on strength, stability, and vibration analysis of shells was conducted in connection with new problems that appeared after the year 2000. Rigid shells in the form of analytical surfaces, designed using the canon of parametric architecture, were taken as an example. Analytical middle surfaces of shells, which attracted the attention of architects after 2000, are pointed out, and suitable methods of analysis of these shells are noted for the first time. The review was compiled based on 112 fundamental scientific works published after 2000. Other scientific reviews devoted to the investigation of joint problems of geometry, application, and calculation of assembled rigid thin-walled shells with analytical middle surfaces were not found.

Keywords: shell strength, shell stability, free and forced vibrations of shell, finite difference energy method, method of separation of variables, analytical surface, classification of surfaces

Conflicts of interest. The authors declare that there is no conflict of interest.

Authors' contribution: *Krivoshapko S.N.* — conceptualization of the research, collection and scientific analysis of materials, drafting the text, and synthesis of the results; *Chiadighikaobi P.Ch.* — was responsible for the scientific processing of sources.

For citation: Krivoshapko S.N., Chiadighikaobi P.Ch. Strength, stability and dynamics of rigid shells: analysis of recent research. *Structural Mechanics of Engineering Constructions and Buildings.* 2025;21(6):565–584. http://doi.org/10.22363/1815-5235-2025-21-6-565-584 EDN: FQCZQA

Sergey N. Krivoshapko, Doctor of Technical Sciences, Consulting Professor of the Department of Construction Technology and Structural Materials, Academy of Engineering, RUDN University, 6 Miklukho-Maklaya St, Moscow, 117198, Russian Federation; eLIBRARY SPIN-code: 2021-6966, ORCID: 0000-0002-9385-3699; e-mail: sn_krivoshapko@mail.ru

Paschal Ch. Chiadighikaobi, Ph.D., M.Sc., Senior Lecturer in the Department of Civil engineering, Afe Babalola University, Ado-Ekiti, Ekiti State, Nigeria; ORCID: 0000-0002-4699-8166; e-mail: chiadighikaobi.paschalc@abuad.edu.ng

Прочность, устойчивость и динамика жестких оболочек: анализ современных исследований

С.Н. Кривошапко[1], П.Ч. Чиадигикаоби[2]✉

[1] Российский университет дружбы народов, *Москва, Российская Федерация*
[2] Университет Афе Бабалола, *Адо-Экити, штат Экити, Нигерия*
✉ chiadighikaobi.paschalc@abuad.edu.ng

Поступила в редакцию: 12 мая 2025 г.
Доработана: 18 сентября 2025 г.
Принята к публикации: 2 октября 2025 г.

Аннотация. Многие численные методы анализа жестких оболочек, такие как метод конечных элементов (МКЭ) в перемещениях, метод конечных разностей энергий, метод разделения переменных, кинематический метод теории предельного равновесия и т.д., предложены и апробированы до 2000 г. Большинство задач статического и динамического анализа канонических оболочек были успешно решены одновременно. Все эти методы активно использовались и после 2000-х гг. Однако перед инженерами-конструкторами, архитекторами и строителями стали возникать новые проблемы, связанные с многослойными стенками оболочек, с появлением новых конструктивных композиционных материалов, а следовательно, и с решением физически нелинейных задач. Геометры представили несколько сотен новых форм средних поверхностей оболочек, и поэтому возникла необходимость выбора оптимальных форм из нескольких аналогов с использованием критериев оптимальности. Выбор необходимых вычислительных комплексов из множества их типов стал проблемой. Новые проблемы требовали новых подходов к их решению. Проведен критический анализ предлагаемых решений по выполнению анализа оболочки на прочность, устойчивость и вибрацию в связи с новыми проблемами, появившимися после 2000-го года. В качестве примера взяты жесткие оболочки в виде аналитических поверхностей, спроектированные с использованием канона параметрической архитектуры. Выделены аналитические средние поверхности оболочек, которые привлекли внимание архитекторов после 2000 года, и впервые отмечены подходящие методы анализа этих оболочек. Обзор составлен на основе 112 фундаментальных научных работ, опубликованных после 2000-х годов. Других научных обзоров, посвященных исследованию совместных задач геометрии, применению и расчету сборных жестких тонкостенных оболочек с аналитическими средними поверхностями, авторами найдено не было.

Ключевые слова: прочность оболочки, устойчивость оболочки, свободные и вынужденные колебания оболочки, конечно-разностный энергетический метод, метод разделения переменных, аналитическая поверхность, классификация поверхностей

Заявление о конфликте интересов. Авторы заявляют об отсутствии конфликта интересов.

Вклад авторов: *Кривошапко С.Н.* — концепция исследования, сбор и научный анализ материалов, написание текста, обобщение результатов; *Чиадигикаоби П.Х.* — научная обработка источников.

Для цитирования: *Krivoshapko S.N., Chiadighikaobi P.Ch.* Strength, stability and dynamics of rigid shells: analysis of recent research // Строительная механика инженерных конструкций и сооружений. 2025. Т. 21. № 6. С. 565–584. http://doi.org/10.22363/1815-5235-2025-21-6-565-584 EDN: FQCZQA

1. Introduction

The interest in designing and building shell structures, rigid shells, and facilities of curvilinear forms has increased considerably over the last 25 years. Some experts associate it with the emergence of convenient computer software for accurate analyses of these structures, others prove the advantages of human perception of curvilinear forms [1], and the others foretell the rebirth of the “golden age” of shells [2]. Broad information about research on the structural mechanics of thin shells performed until the middle of the 1960s is presented in the book by Prof. V.G. Rekach [3], who himself took an active part in working out methods of analysis of thin-walled shells of complex geometry using linear shell theory. More and more structural engineers are drawn into the investigation of the structural mechanics of thin shells in

Кривошапко Сергей Николаевич, доктор технических наук, профессор-консультант кафедры технологий строительства и конструкционных материалов, инженерная академия, Российский университет дружбы народов, Российская Федерация, 117198, г. Москва, ул. Миклухо-Маклая, д. 6; eLIBRARY SPIN-код: 2021-6966; ORCID: 0000-0002-9385-3699; e-mail: sn_krivoshapko@mail.ru

Чиадигикаоби Паскал Чимеремезе, доктор философии, магистр наук, старший преподаватель кафедры гражданского строительства, Университет Афе Бабалола, Адо-Экити, штат Экити, Нигерия; ORCID: 0000-0002-4699-8166; e-mail: chiadighikaobi.paschalc@abuad.edu.ng

geometrically and physically linear and nonlinear formulations of the problem. Scientists and structural engineers from different countries made valuable contributions to the development of the shell theory, mentioned in study [4]. The interest in the study of theories of analysis and strength characteristics of construction materials for spatial structures appeared at that time [5]. Plywood, corrugated steel, multi-layer wooden panels, and reinforced plastics were used as construction material of thin rigid shells besides reinforced concrete. Study [6] contains information about increasing interest in the development of new methods of shell analysis in connection with the emergence of numerical methods of calculation and the growing use of computers.

During the "golden age" of shells between the 1920s and 1960s, thin shells were built and designed in great numbers in practically every country. But the majority of shells, used in real structures and designed based on analysis from the geometrical point of view, concerned a limited number of surfaces that are cylindrical, conical, spherical, and torus surfaces, right translational surfaces, paraboloids of revolution, hypars, ellipsoids of revolution, and some others [7]. Shells having more complex forms, generally, were implemented on the basis of experiments or intuition of architects and engineers with the application of the simplest calculation methods.

The list of geometrical shapes for the design of thin shells considerably increased because of the computerization of calculating processes, accurate definition of taken hypotheses for the shell analyses, and the emergence of new construction materials closer to the 21st century [2].

This paper aims to highlight geometrical shapes of thin rigid shells for which methods of strength analysis were obtained. The objectives of this study are:

i. To investigate methods of calculating critical forces that cause local or general buckling.

ii. To explore methods of resistance of shells to dynamic actions.

iii. To highlight analytical, semi-analytical, and numerical methods of shell analysis from the sets of methods proposed in the 20th century, which structural engineers continue to use.

iv. To expose new approaches to strength analysis of thin rigid shells in the 21st century.

2. Methodology

This study used a qualitative approach to achieve the aim and objectives. The study examined the strength, stability, and dynamic of rigid shells after 2000.

3. Shells with Ruled Middle Surfaces

Ruled shells can have only zero or negative Gaussian curvature. There are no ruled shells of positive Gaussian curvature.

3.1. Shells with Ruled Middle Surfaces of Zero Gaussian Curvature

3.1.1. Cylindrical Shells

Cylindrical shells have been known since ancient times. They have not lost their relevance at present. A voluminous review of investigations on cylindrical shells has been conducted in study [8], where the author considers, in general, the works before 2000.

At the present time, cylindrical shells with horizontal and vertical axes are investigated with the help of typical computer software. For example, the derivation of the governing equations for analysis of three-layered vertical cylindrical shells under axisymmetric loading with creep taken into account and with the fixed lower edge was given in study [9]. The solution is performed with the help of the finite element method (FEM) together with Euler's method. It was proved that the creep of the middle layer has a positive influence on the strength of the examined shell. Another approach was taken in the study [10], where the presented analytical method allows for solving two types of engineering problems, which are the

determination of deviation of dimensions of a shell under known parameters of thermal and pressure loading or the determination of ultimate load when limiting deviations are given. Examination of the publications of the last 20 years shows that, at the present time, analysis of cylindrical shells is connected with taking into account multi-layer walls, geometric and physical nonlinearity, new types of external static and dynamic [11] loading, and assumption of accurate hypotheses [12].

Thus, the newest research shows that structural engineers can calculate any cylindrical shell subjected to various loads without difficulty.

Parabolic cylindrical shells. Parabolic cylindrical shells are the most popular after circular cylindrical shells, especially as roofs of warehouses, industrial workshops, and exhibition pavilions. At the present time, additional investigations of these shells are needed. The dynamic behavior of a thin concrete shell resisting jointly with support columns with the application of FEM has been studied [13]. FEM has been used [14] for the evaluation of the influence of cracks on static and dynamic behavior of reinforced concrete roofs. The account of settlement of one of four corner supports under columns is one more direction in the investigation of parabolic cylindrical shells [15].

3.1.2. Conical Shells

Conical shells and cylindrical shells are some of the first spatial structures that humans learned to build. Conical thin shells always attracted the attention of architects (Figure 1).

Figure 1. Conical pavilions of Austria at “EXPO-2020” exhibition

S o u r c e: compiled by Available from: https://www.constructionweekonline.com/cloud/2021/07/07/SwgTuR50-wam-expo-2020-dubai-Austria-Pavilion-1200x801.png (accessed: 04.03.2025).

The investigation of conical shells is realized involving more complex mathematical technique, which allows solving more complex problems as close as possible to present-day reality. Study [16] addresses the issue of thermal stresses and strains in a thin-walled conical shell subjected to uniform heat flow along its side surfaces and at both ends of the thermal insulation shell. The governing equations were derived using a semi-coupled static thermoelastic equation and an energy equation. The Galerkin finite element method was employed. Dissertation [17] deals with a right circular conical shell of variable thickness. A system of three partial differential equations in terms of displacements that was reduced to a system of ordinary differential equations, which was solved by a finite difference method, was derived in this work [17]. The mathematical model of the refined theory depends on three-dimensional equations of the theory of elasticity using approximation of the stress state components by polynomials for the normal coordinate of the middle surface by two exponents higher relative to the classic Kirchhoff — Love theory. It shows that the components of the stress state calculated based on the presented model near the zone of distortion of the stress-strain state differ from alternatives of the classic theory.

The vibrational behavior of shells in the form of truncated cones containing ideal compressible fluid is studied in [18]. The dynamic behavior of the elastic structure is investigated based on the classical shell theory, the constitutive relations of which represent a system of ordinary differential equations written for new unknowns. Small fluid vibrations are described in terms of acoustic approximation using the wave equation for hydrodynamic pressure written in spherical coordinates. Its transformation into the system of ordinary differential equations is carried out by applying the generalized differential quadrature method. The formulated boundary value problem is solved by Godunov's orthogonal sweep method. The natural frequencies of shell vibrations are calculated using the stepwise procedure and the Muller method. The accuracy and reliability of the obtained results are estimated by making a comparison with the known numerical and analytical solutions. For conical, straight, and inverted shells, a numerical analysis has been performed to estimate the possibility of finding configurations, at which the lowest natural frequencies exceed the corresponding values of the equivalent cylindrical shell.

Hence, the calculation of thin conical shells of general type subjected to the action of different factors can be fulfilled, but it is carried out with some difficulties.

Besides the right circular conical shell, the right elliptical conical shell finds application in practice. S.N. Krivoshapko obtained analytical formulae for the calculation of tangential forces using the momentless shell theory.

3.1.3. Developable Shells

Over 400 scientific papers of 280 authors are devoted to the study of the geometry of developable surfaces. The least scientific papers are devoted to the investigation of problems of strength, stability, and dynamics of developable shells. A vast majority of them appeared after 2000. The opening period of the study of developable shells was described in study [19], where it was noted that the main difficulty in the determination of the stress-strain state of developable shells involved the necessity of using a system of 20 governing equations of thin shells given in non-orthogonal conjugate curvilinear coordinates. It allowed to use analytical methods of calculation of the moment shell theory.

The situation improved after the emergence of computer software using numerical methods of analysis of shells with middle surfaces given in arbitrary curvilinear coordinates. Now, a vast majority of studies is devoted to strength analysis of developable shells of equal slope and in the form of evolvent helicoids.

Equal Slope Developable Surfaces with Directrix Ellipse at Base. The problem is solved most simply for equal slope developable shells because their middle surfaces can be defined in principle curvature lines. Firstly, an analysis for the determination of uniformly distributed critical load for an equal slope developable shell with a directrix ellipse at the base has been made in the study [20]. The study calculated a steel shell subjected to vertical load in the form of its weight with the help of the LIRA 9.4 computer software which uses displacement-based FEM. The cases when the low edge is fixed or simply supported were solved in the study. The first two buckling modes for the first case of supports and three modes for the simply supported shell were found. It was shown that the buckling of the shell takes place before exhausting its strength [20].

Static analysis of a developable shell of equal slope with a directrix ellipse at the base was presented first in studies [21; 22]. This analysis was made with the help of two numerical methods. Displacement-based FEM and finite difference energy method of calculation of the action of static external load were used.

Evolvent helicoidal shells. Evolvent helicoid (developable helicoid, Archimedes' screw) is the most known developable surface with a helical edge of regression [23] (Figure 2).

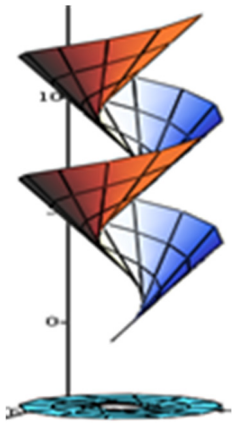

Figure 2. Developable helicoid
S o u r c e: compiled by V.N. Ivanov.

All results on the investigation of the strength parameters of the shell in the form of developable helicoid appeared effectively at the end of the 1990s

and after the 2000. The approximate method of small parameter was used for the calculation of a long developable helicoid with fixed helical edges due to the given displacement of the inner contour [24] and due to the action of its weight [25].

Firstly, study [26] carried out a FEM investigation of the influence of restraining rectilinear edges of a shell in the form of a developable helicoid on the stress-strain state in its middle zone. It was shown that a very small near-support zone reacts on the restraining method of the straight edges of the helicoid. So, the study confirmed that for a long evolvent helicoidal shell, the reduction of the governing system of equations in partial derivatives to three ordinary differential equations with one independent parameter makes sense if the length of the helical edge is greater than its rectilinear edge.

3.1.4. Parabolic Bending of Elastic Thin Plates into Developable Shells

The main theoretical investigations on parabolic bending of plane metal sheets into developable structures are conducted at the Academy of Engineering of the Peoples Friendship University of Russia (RUDN University), Moscow. The main results of the investigation are outlined in study [27], while several works from other organizations can be examined [28; 29]. Seemingly, the results of investigations on this problem are not interesting for engineers. However, neglect of inner normal stresses appearing in the process of bending the sheet can have great consequences. Bending of real plane sheets from plywood, aluminum, or steel into accurate developable shells with the preservation of rectilinear generatrices is impossible because of the presence of the Poisson's ratio of sheet material according to study [30], which was the first to point this out.

The researchers of [31] realized a series of experiments devoted to the bending of copper plates 5 millimeters thick into cylindrical shells. They constructed experimental curves using the results of the experiments. However, the process of bending is why it is necessary to compare experimental results with theoretical results with a certain portion of skepticism.

Metal sheet bending is realized by different methods, and every one of them has specific advantages. One may obtain conical or pipe hardware of different forms with the help of cold bending. This method would be suitable to receive a bend of a big radius in any case.

3.2. Shells with Ruled Middle Surfaces of Negative Gaussian Curvature

Ruled surfaces of negative Gaussian curvature may also be called oblique ruled surfaces or ruled saddle surfaces. Conoids, hyperbolic paraboloids, and one-sheet hyperboloids are twice-ruled surfaces. Hyperbolic paraboloids and one sheet hyperboloids are considered as a part of the "second order surfaces".

3.2.1. Conoids and Cylindroids

Shells in the form of conoids and cylindroids are seldom used in comparison with conical, spherical, umbrella shells or parabolic shells of revolution (Figure 3) or the form of one-sheet hyperboloids of revolution. The general information about conoids and cylindroids is given [32]. The visualization of new conoidal surfaces has been presented in [33]. Here, only papers published recently on the analysis of thin shells in the form of conoids and cylindroids are mentioned, but we shall not repeat known information published before 2000, which is contained in study [32]. It is noted in study [34] that composite conoidal shells are very important for the aerospace field, and that is why it is necessary to investigate the natural vibration of such structures. The investigation of the conoidal shell resting only upon columns is presented [35]. Computer software are used for the design of cylindroids [36].

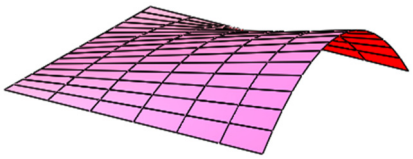

Figure 3. Right parabolic conoid
S o u r c e: compiled by V.N. Ivanov.

Almost all scientific papers devoted to the analysis of conoidal shells were published by scientists from India.

3.2.2. Right Helicoidal Shells

The right helicoid is the only ruled surface from a family of minimal surfaces. This helical shell of negative Gaussian curvature found a wide application after the beginning of the 20th century, especially in mechanical engineering. In buildings, they are used, primarily, as ramps for car parking lots. The growing application of right helicoids calls for the elaboration of reliable methods of analysis. In the first period, these were approximate analytical methods but later, reliable numerical methods appeared on the basis of FEM [23].

Now, analytical methods with the application of equations of the linear theory of shells are used only for static analysis of long right helicoidal shells, when the system of governing equations is reduced to ordinary differential equations [37]. In 1957, V.G. Rekach, using two partial differential equations of E. Reissner, obtained one partial differential equation of the eighth order, which he proposed to solve with the help of Fourier series. But only in 2008, M.I. Rynkovskaya [38] composed a computer program with the help of the MathCad computer language and derived numerical results after the correction of equations obtained by Rekach.

The kinematic method of the theory of limit equilibrium was used for the evaluation of the bearing capacity of a right helicoidal shell in study [39]. Examples of calculation of the upper limit of ultimate load are presented in it. The influence of methods of restraint on the bearing capacity of the shell is discussed. One can continue quoting modern works, for example [40–42], but the review of the investigations shows that these ruled shells continue to be used. Study [41] is devoted to the shape optimization of right and developable helicoids in Comsol Multiphysics. Engineers expect more accurate methods of analysis using the principles of the theory of elasticity and shell theory, but one can consider that now problems on strength, stability, and dynamics of right helicoids are solved quite enough.

Having taken the importance of accurate results for mechanical engineering, study [43] proposes to use the results obtained experimentally.

3.2.3. Oblique Helicoidal Shells

The oblique helicoid found application in mechanical engineering, but it is known much less than the right helicoid [23]. Several works on static analysis, published after 2000, are available; for example, one can read paper [44].

4. Shells of Revolution

Shells of revolution enjoy the greatest popularity among architects and mechanical engineers due to their attractiveness, varieties of geometrical forms [45], and due to satisfaction of the majority of technological, economic, ergonomic, and other desires in the design of large-span buildings and to structures of small size. For example, a selection of shells of revolution using 23 criteria of optimality is proposed in the paper [46]. Research paper [47] proposes to extend geometrical investigations of surfaces of revolution. It will be conducive to the introduction of shells of revolution into different fields of engineering and construction.

All known surfaces of revolution, described in the scientific literature on the geometry of surfaces, are presented in study [45] in graphical form. Part of them found application or were recommended for application in engineering and construction, and that is why the necessity appeared for their subsequent investigation on strength, stability, nature, and forced vibrations.

It is easier to obtain results using the momentless shell theory. Simple formulae for the calculation of longitudinal (meridional) and circular stresses in cylindrical, conical, spherical, ellipsoidal, and toroidal shells loaded by inner pressure are given in [48].

The emergence of numerical methods of analysis allows the calculation of layered shells of revolution [49], shells of revolution with pre-defined geometric characteristics [50], shells with the creep of shell material [9], and shells strengthened by frames.

4.1. Spherical Shells

Sphere is one of the canonical forms used in all branches of manufacturing industry, engineering, and construction. Several hundreds of scientific works are devoted to the investigation of geometry, strength, stability, vibration, and application of thin-walled and thick-walled structures in the form of spherical surfaces. Those who are interested in the achievements of scientists in the field of strength, stability, and dynamics of structures in the form of spherical surfaces can begin investigating these problems by studying the following literature [3, 6, 51, 52]. Practical interest in rigid spherical shells does not go out [17; 53–55]. Almost all new construction materials were used in spherical shells. Spherical structures are present in seven of nine types of spatial curvilinear structures and shells, but rigid spherical shells are among the group "rigid shells." The information presented above shows that designers will not have any problems with designing spherical shells.

4.2. Paraboloids of Revolution

Domes in the form of paraboloids of revolution are not new. These shells are a particular case of elliptic paraboloids. The paraboloid of revolution is also considered to be among surfaces of the class "surfaces of right translation". The results of the investigation of shells in the form of a paraboloid of revolution can be divided into the following groups: momentless theory of shell analysis, moment theory of shell analysis, natural and forced vibrations, stability of shells, experimental research, temperature actions, problems of elasticity theory, and application of paraboloids of revolution in analytical geometry, architecture, building, using optical properties of paraboloids of revolution. The solution to the indicated problems has been the aim of many investigations in the last 30 years. For instance, FEM and Vlasov's shallow shell theory have shown good agreement in terms of stresses [56]. A paraboloid-shaped resonator with characteristics of high-overload resistance is proposed in the study [57]. A model of a paraboloid-shaped shell was established by using the energy method. The characteristics of natural frequency and vibration modes were analyzed, and the effects of structure parameters on the natural frequency were obtained by using the finite element method. Finally, experiments on actual resonators proved that this method is reasonably practicable.

Study [58] established that a significant contribution to the overall stress state of the paraboloid of revolution shell with radial waves is made by normal and tangential stresses. The influence of bending stresses acting in the circumferential direction is also great. The minimum load parameter when the shell buckles is more than three times the margin.

4.3. One-Sheet Hyperboloids of Revolution

One sheet hyperboloid of revolution is the only ruled surface of revolution of negative Gaussian curvature. This form can be seen in hundreds of built cooling towers [59; 60]. The majority of investigations of structures in the form of a one sheet hyperboloid of revolution are devoted to lattice shells. However, interesting results can be obtained if one analyzes rigid shells using the physically non-linear theory. The calculation of a shell subjected to wind load and its weight gives excessive values of displacements in comparison with displacements obtained with the help of the physically linear theory [61].

4.4. Pseudospherical Shells

Pseudospherical surfaces (Figure 4) are regarded by geometricians, physicists, and landscape designers. However, there are proposals for their applications in building shells of negative Gaussian curvature. These gave rise to the elaboration of methods of their analysis. In the 21st century, study [62] shows the results of theoretical investigations on the strength and stability of pseudospherical shells subjected to the action of an

external distributed load. Both geometrical problems of the middle surfaces of the considered shells and the momentless theory of shell analysis were investigated. Later, the momentless shell theory proved useful for the determination of critical load. The results of analytical and numerical calculations by using FEM are presented in tabular form. Numerical analyses have been performed with the help of the ANSYS computer software. The authors showed that the buckling behavior of thin shells is untypical for the majority of shell structures [62].

Detailed study of numerical methods of calculations and the emergence of standard computer programs of strength analysis allowed using geometrically nonlinear shell theory [63; 64].

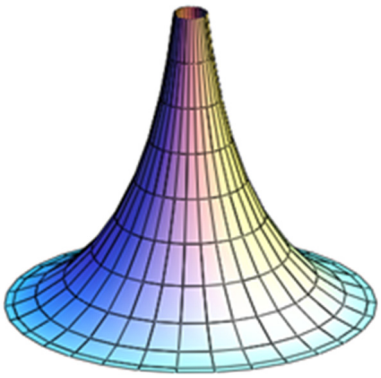

Figure 4. Pseudospherical surface
S o u r c e: compiled by V.N. Ivanov.

4.5. Circular Toroidal Shells

Circular toroidal shells can be seen in aerospace engineering, in objects of nuclear power engineering [65], and in other branches of mechanical engineering [66]. In study [65], an analysis of a smooth toroidal shell is presented. Godunov's method of orthogonal sweep was used for the numerical solution of the system of differential equations (a boundary element method) at the finished stage. A method of designing a solution of composite pressure vessels of high pressure of toroidal form subjected to inner pressure is proposed in study [66]. The asymptotic method was evaluated in the process of studying the vibration of the toroidal shell. This form is rarely used in construction fields. Seemingly, only roofs from toroidal fragments are used in construction and architecture.

4.6. Catenoidal Shells

A catenoid is formed by the rotation of a catenary curve around the axis of the surface of the revolution (Figure 5). Soap film pulled over two wire circles, the planes of which are perpendicular to the axis of rotation, which passes through the centers of the circles, takes the shape of a catenoid. Several buildings in the form of catenoids are available, but their extended application is put off for the future. At the present time, theoretical investigations of the strength of these smooth [67] and ribbed [68] shells are in progress. The catenoid is the only minimal surface of revolution.

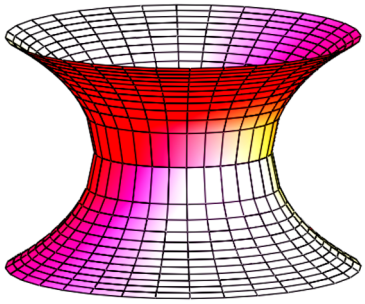

Figure 5. Catenoid
S o u r c e: compiledby by
S.N. Krivoshapko, V.N. Ivanov [67].

Orthographic representations of displacements, internal normal forces, and bending moments have been compared [67]. A conclusion was made that the catenoid shell, based on these parameters, possesses some advantages over four other shells of revolution loaded by the same linear vertical load applied to the upper shell edge.

4.7. Untypical Shells of Revolution

It was pointed out earlier that all known shells of revolution are listed in study [45]. One can design an infinitely large number of new surfaces of revolution in addition to the list presented in study [45]. Some authors created shells of revolution unknown before. They affirm that these shells are necessary for some branches of science, engineering, and construction. For example, the supercritical behavior of any untypical shells of revolution was investigated [69]. A momentless analysis of the hyperbolic-parabolic shell of revolution is proposed and a parabolic-logarithmic shell of revolution is introduced into practice [70]. Generally, the study of these untypical shells of revolution finished after the first published paper.

4.7.1. Egg-shaped Shells

There is no such name in the classic theory of surfaces. However, some authors use this name for a surface. For example, buckling of the egg-shaped shell of revolution was studied in [71].

4.7.2. Shells of Barreled Shapes

The situation is similar for barreled surfaces that are surfaces of rotation of a plane curve around the axis of rotation, but the axis of symmetry of the generatrix curve, that is a meridian, is perpendicular to the axis of rotation. A so-called barreled reservoir has been considered in study [72].

5. Shells With Cyclic Middle Surfaces

A cyclic surface is a surface formed by the motion of a circle of variable (Figure 6) or constant radius in space in some pattern. Prominent geometricians A.P. Norden, V.F. Kagan, V.I. Shulikovskiy, A.M. Yakubovskiy, and others have studied cyclic surfaces.

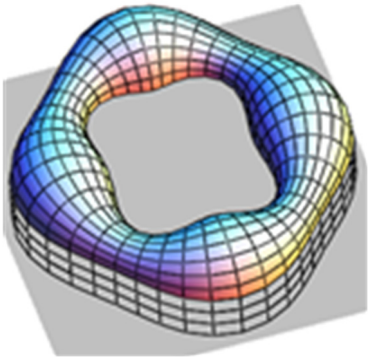

Figure 6. Catenoid
S o u r c e: compiled by V.N. Ivanov [73].

A valuable contribution to the study of the strength of shells with cyclic middle surfaces was made by Prof. V.N. Ivanov [73] and other researchers [74–76]. Prof. V.N. Ivanov paid attention to these shells in 1971 [77] and compiled a complete classification of cyclic surfaces, specified the names of some surfaces, formed many groups and subgroups of cyclic surfaces, and developed computer software for their analysis using the finite difference energy method. The researchers considered the finite difference energy method more convenient for the calculation of cyclic shells.

Method of curvilinear nets, momentless shell theory [77], finite difference method, the equations of linear shell theory in complex form, and the method of complex limitations for the determination of natural frequencies have been used for the analysis of cyclic shells. More than 150 monographs, dissertations, scientific papers, and conference proceedings contain information on geometry (80%), analysis of strength (15%), and vibrations of thin shells with cyclic middle surfaces.

Pipe shells with a bent axis. Study [78] is the first work on the analysis of pipe shells. Several early works devoted to the calculation of cyclic shells are listed in bibliography [3]. Several alternatives of the arrangement of pipe shells with curvilinear center lines are presented in study [79]. Many studies are devoted to static analysis and dynamic behavior of pipes with curvilinear axis. They are not considered in this study because general attention is given to the calculation of rigid, large-span shells.

6. Helical and Helical-Type Shells

The most complete information on helical ruled and cyclic shells is given in study [23] with 181 sources. Results of scientific works published in the 20th century are analyzed in the study.

Investigation of helical and helical-type shells did not stop after the year 2000. Performed investigations showed that engineers and designers, in general, engage with ruled helical surfaces and with helical pipe surfaces, but geometricians have some more classes and groups of surfaces with helical or spiral directrix curves in their toolbox.

Ruled helical shells were considered earlier in the “Evolvent Helicoidal Shells”, “Right Helicoidal Shells”, and “Oblique Helicoidal Shells” sections.

6.1. Helical Pipe Shells

Helical pipe shells find extensive use besides helicoidal ruled shells. Before the year 2000, structural engineers used the method of model equations [52], the method of separation of variables, and the method of the curvilinear net, which is a generalization of the method of finite differences. After the year 2000, in study [80], an analysis of a pipe shell with a bent axis was presented. V.S. Lyukshin distinguished five types of circular helical surfaces, one of which is shown in Figure 7.

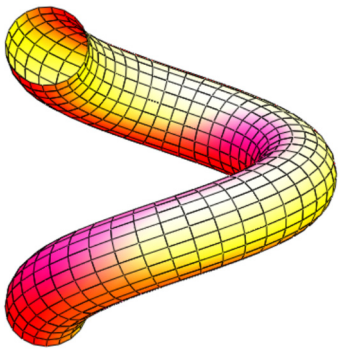

Figure 7. Helical pipe surface with the generatrix circle perpendicular to the axis of the directrix helix
S o u r c e: compiled by S.N. Krivoshapko.

7. Shells with Kinematic Middle Surfaces

The total classification of kinematic surfaces with congruent generatrix curves is given in study [81], containing 38 sources.

7.1. Shells of Right Translation

Fundamental surfaces of right translation that found application in architecture and construction are listed in study [45]. In study [82], examples of using surfaces of right translation in the construction of compound shells were shown. In general, all problems of the design of translation shells were solved after the emergence of design computer programs. Some problems associated with the emergence of new construction materials, taking into account the orthotropy of wooden roofs [83], and with strengthening of the bearing capacity, are solved as new ideas arise [84].

7.2. Velaroidal Shells

Velaroidal surfaces are formed by plane curves of variable curvature, but surfaces of right translation are formed by a plane rigid curve. Formed velaroidal surfaces are supported by straight lines of plane rectangular contour (Figure 8). About ten velaroidal surfaces are presented and studied in scientific and technical literature. In study [85], velaroidal shells are considered from a standpoint of their architectural potential. Scientific paperdevoted to the strength analysis of velaroidal shells began to appear, too [86].

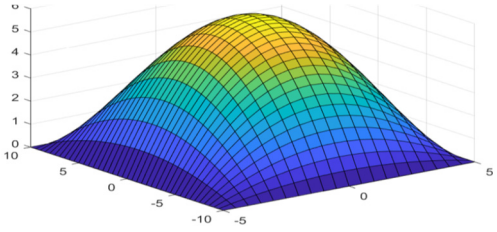

Figure 8. Velaroidal shell
S o u r c e: compiled by E. Tupikova, M. Berdiev [86].

7.3. Shells of Diagonal Translation with Generatrix Curve of Variable Curvature

Interesting surfaces of diagonal translation with generatrix curves of constant and variable curvature of velaroidal type on a rhombic plane were proposed for introduction in building shells in study [87].

8. Second-Order Algebraic Surface Shells

The second-order surfaces (quadrics) form a class of surfaces consisting of 17 names. Five non-degenerate non-disintegrate surfaces will be considered in this section. Four degenerate non-disintegrate surfaces that are elliptical, hyperbolical, parabolic cylinders, and elliptical cones were considered in section "Shells with Ruled Middle Surfaces of Zero Gaussian Curvature". The remaining three imaginary surfaces and five degenerate disintegrated surfaces do not find application in the form of rigid shells.

8.1. Ellipsoids

A more detailed description of the results of investigations on the analysis of thin shells in the form of triaxial ellipsoid, published before 2000, is presented in study [88].

In the second ten years of the 21st century, a group of scientists from Volgograd State Agrarian University [89] worked actively for the improvement of a method of analysis of ellipsoidal shells with the help of FEM. They proposed formulae of representation of the radius-vector of triaxial ellipsoids allowing to perform continuous parametrization of surfaces, but two parameters, used in the formulae, have clear geometrical interpretation. It is very important for the analysis of shell structures in the form of ellipsoids, elliptical cylinders, elliptical cones, and similar to them. In study [90], they derived physical equations without a hypothesis about the separation of deformations into elastic and plastic parts. The condition of proportionality of the components of deviators of stress increments was used for their determination. The application of the equations was performed by using a hybrid prismatic finite element with a triangular base. The method was tried out on a truncated ellipsoid. The study also used a quadrangular curvilinear finite-element with nine degrees of freedom in the node as a discretization element of thin-walled structures of concatenated shells with different properties of materials.

8.2. Elliptical Paraboloids

The application of thin shells in the form of elliptic paraboloids took place both in the 20th century and at the beginning of the 21st century [91], and that is why great attention is paid to investigations on static analysis, buckling, and vibration of elliptical-paraboloid shells. After 2012, studies were devoted to the determination of critical forces [92], the strength analysis [93], the determination of free and forced vibrations [94], and the study of reinforced concrete shells in the form of an elliptic paraboloid with openings [95]. It was determined in study [95] that an opening at the top of a paraboloid reduces shell strength by 14%.

8.3. Hyperbolic Paraboloids

This shell form is very well known. Hyperbolic paraboloids have enjoyed popularity for many years (Figure 9), and their popularity is not going out at present. Hundreds of monographs and scientific manuscripts are devoted to them, examples are [7, 96, 97].

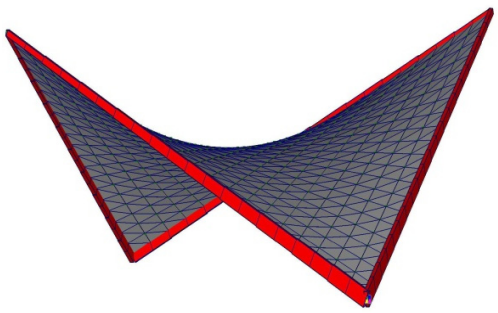

Figure 9. Hyperbolic paraboloid
S o u r c e: compiled by O.O. Aleshina [98].

9. Higher-Order Algebraic Surface Shells

A great number of algebraic surfaces of the higher orders were presented and studied by geometricians. However, a small part of them found application in rigid building shells.

Shells in the Form of Algebraic Surfaces with a Main Frame from Three Superellipses

Taking the main frame of surface in the form of three superellipses placed in three coordinate planes, one can construct three analytical surfaces by the motion of every superellipse with a simultaneous change of its curvature along another superellipse. A surface formed by the motion of the superellipse of variable curvature in the planes parallel to the horizontal coordinate plane is shown in Figure 10, *a*. If one of the superellipses is taken in the form of a rhombus, then one of the obtained surfaces will be a cylindroid [98] (Figure 10, *b*).

In the 2020s, studies were published where the results of static analyses of shells loaded by their weight and which have main frames from three ellipses (Figure 10, *a*) [98]. A thin ruled shell with elliptical base where two of three superellipses of the main frame degenerate into rhombuses (Figure 10, *b*) is considered in study [99]. In study [100], a shell with the middle algebraic surface on a rhombic base is studied.

Superellipsoidal surface is defined by implicit equation

$$(x/a)^{2n} + (y/b)^{2n} + (z/c)^{2n} = 1,$$

which describes a sphere ($n = 1$, $a = b = c$), ellipsoid ($n = 1$), or cuboid ($n = \infty$). Buckling of the shell with a pointed middle surface subjected to external pressure is studied [101].

Unfortunately, all researchers calculating shells in the form of algebraic surfaces with main frames from three superellipses did not mention the order of decomposition of the vectors of inner forces and moments along the local non-orthogonal or orthogonal axes of the shells. This problem appears because the authors use non-orthogonal curvilinear coordinates. That is why it cannot be determined what internal forces or "pseudo-forces" and moments or "pseudo-moments" were derived.

The same questions can be put before the authors of papers on velaroidal shells (Section 6.2), developable shells (Section 2.1.3), and oblique helicoidal shells (Section 2.2.3).

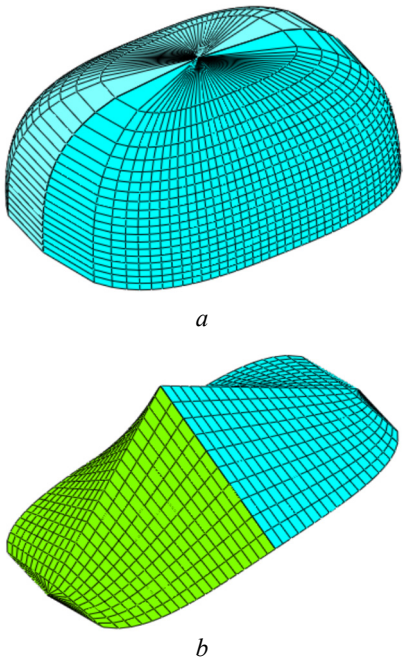

Figures 10. Algebraic surfaces with the frames from three superellipses
S o u r c e: compiled by V.N. Ivanov.

10. Umbrella Shells and Umbrella-Type Shells

V.A. Lebedev was the first to pay serious attention to the advantages of umbrella shells in 1954. In 1958, he published a monography [102] in which the information on methods of formation of these shells was generalized, a method of static analysis was proposed, and recommendations on the application of umbrella domes in buildings were presented. Umbrella shells (Figure 11) enjoy popularity as in former times [103]. Structural engineers defined more exact methods of their analysis and optimization of their form [104].

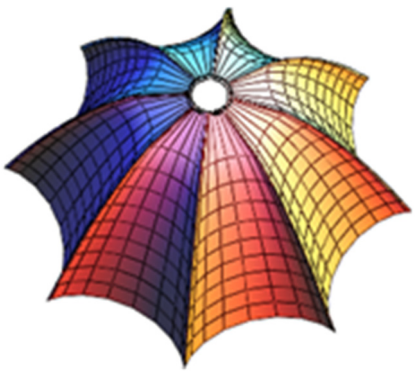

Figure 11. Umbrella surface
S o u r c e: compiled by V.N. Ivanov.

Umbrella-type surfaces are cyclically symmetrical surfaces containing several identical fragments. Complete umbrella-type surfaces and all identical surfaces compiling a complete surface are defined by the same analytical equation. Practically, there are no examples of strength analysis of umbrella-type shells. Only two works on the calculation of these shells were found. In [105], a finite difference energy method was used, and in study [106], FEM was applied. In study [106], a comparative analysis of three shells was made. A shell in the form of a paraboloid of revolution and two umbrella-type shells with radial waves formed by cubic parabolas and sinusoidal curves were studied. The static calculation has been performed for the action of self-weight.

11. New Analytical Forms of Thin Structural Shells, Proposed for Architects

There are many scientific studies devoted to applying new forms of thin shells for public and industrial buildings. The authors of some works adduced the methods of calculation of thin shells with the help of displacement-based FEM, finite difference energy method, method of separation of variables, membrane theory, and so on.

Study [74] elaborated the algorithm of analysis of thin-walled shells in the form of Joachimsthal's canal surfaces with the help of the finite difference energy method. Static calculation of the shell in the form of the considered analytical surface for the action of self-weight and with one fixed lower edge (Figure 12) has been carried out [74]. Joachimsthal's canal surface is a cyclic surface with a plane directrix line of the centers of generatrix circles of changing radius lying in the planes of the pencil [107]. Three scale models of gypsum shells in the form of canal surfaces of Joachimsthal were made [74].

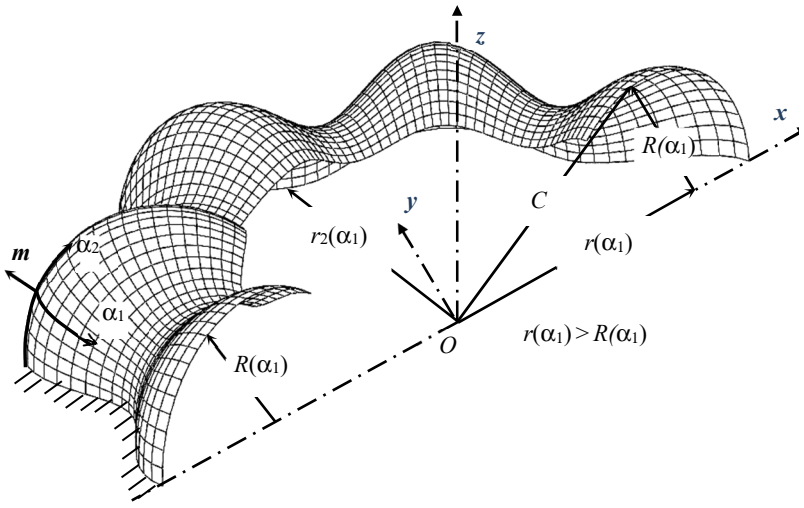

Figure 12. The first type of Joachimsthal's canal surfaces
S o u r c e: compiled by V.N. Ivanov.

Figure 13. Reinforced concrete roof of a house, Nepal
S o u r c e: compiled by G.P. Lamichhane [76].

The author of [76] verified the finite difference energy method and method of global elements on the example of consecutively joined compartments of thin shells in the form of carved parabolic and sinusoidal surfaces of positive and negative Gaussian curvature. The theoretical elaborations of study [76] were implemented in the real reinforced concrete roof of a house (Figure 13). Carved parabolic and sinusoidal surfaces are formed by the movement of a sinusoidal curve at the normal plane of a quadratic parabola [107].

Carved surfaces of general type are formed by a plane fixed generatrix curve, one point of which moves along any directrix curve, and all the time, the generatrix curve must be in the normal plane of the directrix curve. Static analysis of thin shells in the form of carved surfaces of general type was presented by [75], but the author did not show the real application of these shells in practice.

12. Results

Architects determined that 47 of 600 analytical surfaces, most of which are described in encyclopedia [107], were implemented in architectural projects. Architects and engineers proposed additional analytical surfaces for introduction, which did not find architectural implementation, but study [108] considered that they must be reserved for future application.

Practically all analytical surfaces used before 2000 were implemented in the forms of real building structures at the beginning of the 21st century. Besides the analytical surfaces pointed out above, inclined cylindrical, developable, truncated conical (the new Astronomy Centre of the Royal Observatory, Greenwich, 2007), ordinary helical box-shaped, umbrella, drop-shaped, rotational (roof of the Water Sports Complex, Rostov-on-Don, Russia), velaroidal, wave-shaped ("The Wave" residential complex, Vejle, Denmark, 2006–2015), and wavy (Irina Viner-Usmanova Gymnastics Palace in Luzhniki, Moscow) surfaces, spiral (wedding chapel in the form of two spiral staircases, Onomichi, Japan, 2013) and spiral-shaped surfaces, cylindrical helical strip (fence of helical car parking lot), conoids and cylindroids, nodoids, "The Egg" surface of revolution, circular torus, helix-shaped surfaces, triaxial ellipsoids (the observation site of "Zhivopisny Bridge", Moscow, 2007), elliptical paraboloids (lattice roof of the "Shachtar Stadium", Donetsk, DNR, 2009), and one-sided ruled surface (340 m long "Mobius Strip" landscape attraction, VDNKh, Moscow, 2023) were used after the year 2000. But all thin shells with the mentioned analytical middle surfaces do not belong to the "rigid shells" group. They form the remaining eight structural types of shells. The additional information on the classification of curvilinear structures can be acquired in paper [2].

Having summarized the written above, one can say, that many earlier review papers with narrow focus of investigations of rigid thin-walled shells were published in the beginning of the 21st century, for example, on strength analysis of cylindrical shells [8], on geometrical modelling of shell shapes [45, 81], on architectural styles as applied to shells, on the application of shells in architecture [7], on distinguished structural scientists [4], on the reserve of shells for the future [106], and so on. In the presented manuscript, the researchers have tried, for the first time, to join all solved problems devoted to shell design in the last 25 years in one review. Some problems unsettled today were noted too.

In this review, for the first time, thin shells, formed by analytical surfaces, and for which methods of strength analysis under static external load were developed and verified, are presented. The critical buckling parameters and buckling modes are given. The papers where one may explore the methods of determination of natural frequencies, are presented. The subject-matter of review [109] is the closest one to the topic of the presented study. The authors of that paper reviewed research on the compound thin-walled shell structures composed of regular shell elements joined together along their common boundaries. They considered shell junctions of simple forms.

Methods and instructions, pointed out in this review, are contained in the 112 given sources. These works show the main directions in investigations of the last 25 years in structural mechanics of thin rigid shells with analytical middle surfaces. The sources, used in the review, show a high potential of rigid shell structures that are claimed at the beginning of the 21st century [2]. For example, additional information on the structural mechanics of thin shells is given in works [4] with 96 references and in [110] with 1163 references. Review paper [4] mentions the researchers who improved the theory, calculation methods in aspects of strength, stability, and vibrations of thin elastic shell structures. In this review, the results of contemporary research of thin shell theory are presented. The combined stress state exists widely in nature and engineering. Hence, strength of materials and shell structures under the combined stress state is a general problem. Strength theory is of great significance in theoretical research and engineering application. Review paper [110] presents a survey of the advances in strength theory (yield criteria, failure criterion, etc.) of materials, including concrete, iron, polymers, and wood, under combined stress and gives a method of selecting reasonable failure criterion for application in research and engineering.

Design of shell structures begins with the process of "form finding," when architects and designers explore geometric shapes that naturally distribute loads and stresses. This process involves finding a form

that minimizes material usage while maintaining structural integrity. The second stage is the selection of construction materials for the shell. The third stage contains the structural analysis of shell structures that involves complex mathematical modelling to understand how stresses and strains are distributed throughout the shell. So, architectural principles such as form finding, curvature, and attention to visual appearance converge with engineering principles like structural analysis, material selection, and construction techniques to bring these shell structures to life [111]. Architects, designers, and structural engineers can use the materials of this review at every stage of the design process of buildings. It is important to recognize that concrete thin shells have only had a lifespan of less than a century, quite a short time in comparison to other systems [112], but due to construction economy and the inherent beauty of these shapes, they can be widely used in recent years.

13. Conclusion

Nine structural types of shells are known. Researchers limit themselves to the scientific analysis of existing methods of analysis on strength, stability, and dynamics of only rigid building shells. Some types of designs can be implemented only in large-span curvilinear structures. These are exhibition pavilions, planetariums, trade centers, warehouses, cultural facilities, and many others. Having united the experience and knowledge of geometricians, architects, structural engineers, and IT specialists, one can realize virtually any idea in construction and mechanical engineering fields. Curvilinear structures built in the last 25 years, the reliability of which is secured by correct static and dynamic analyses, confirm this assumption. The safety of buildings depends on structural engineers, on rightly defined problems for engineers, on the information related to the design objective. Presented materials show that, today, there are many problems as applied to rigid shells that must be solved in the future or already solved.

It was established that the greatest number of rigid building shells was constructed in the form of cylindrical and conical surfaces, surfaces of revolution and hypars. Accordingly, the greatest number of analytical and numerical methods of analysis on the action of static, thermal and dynamic external loading is devoted to these single or multilayered shells from new construction materials in linear or non-linear definition of the problem.

Using the materials of this study, researchers can independently make a list of unused surfaces for the design of shell forms in architecture and engineering and can propose methods of analysis of shells of unusual form.

This scientific review can help researchers to select future exploration directions and can help clients to define design objectives more accurately.

References

1. Marchenko L.A., Negay G.A. Curvilinear analysis in architecture. *New Ideas of the New Century: Proceedings of the International Scientific Conference of Faculty of Architecture and Design of Pacific National University*. 2013;1:191–197. (In Russ.) EDN: PZAIAB

2. Alborova L.A., Mamieva I.A. Curvilinear forms in architecture of buildings and structures up to the XXI Century. *Academia. Architecture and Construction*. 2023;(3):154–164. https://doi.org/10.22337/2077-9038-2023-3-154-164 EDN: JEOEOY

3. Rekach V.G. The Basic Bibliography on Structural Mechanics. Moscow: UDN; 1968. (In Russ.)

4. Karpov V.V., Bakusov P.A., Maslennikov A.M., Semenov A.A. Simulation models and research algorithms of thin shell structures deformation part I. Shell deformation models. *Izvestiya of Saratov University. Mathematics. Mechanics. Informatics.* 2023;23(3):370–410, https://doi.org/10.18500/1816-9791-2023-23-3-370-410 EDN: YSOXDU

5. Yu M.H. Advances in strength theories for materials under complex stress state in the 20th Century. *Applied Mechanics Reviews*. 2002;55(3):169–218. https://doi.org/10.1115/1.1472455 EDN: XOASEP

6. Noor A.K. Bibliography of books and surveys on shells. *Applied Mechanics Reviews*. 1990;43(9):223–234. https://doi.org/10.1115/1.3119170 EDN: OKFSTG

7. Bradshaw R., Campbell D., Gargari M., Mirmiran A., and Tripeny P. Special structures. Past, present, and future. *Journal of Structural Engineering.* 2002;128:691–701. https://doi.org/10.1061/(ASCE)0733-9445(2002)128:6(691)

8. Lee Y.S. Review on cylindrical shell research. *Transactions of the Korean Society of Mechanical Engineers — A*. 2009;33(1):1–26. https://doi.org/10.3795/KSME-A.2009.33.1.1

9. Chepurnenko A.S., Yazyev B.M., Lapina A.P. Calculation of a three-layer cylindrical shell taking the creep into account. *Construction and Architecture*. 2018;6(4):14–18. https://doi.org/10.29039/article_5c35ed650acfc0.48169070 EDN: YULYWL

10. Hudoley A.L., Baran O.A., Goman A.M. Determination of radial displacements of cylindrical shell under thermo-forced loading. *Vestnik of Brest State Technical University. Series: Mechanical Engineering*. 2006;(4):9–13. (In Russ.) Available from: https://rep.bstu.by/handle/data/12497 (accessed: 02.05.2024).

11. Montes R.O.P., Silva F.M.A., Pedroso L.J. Free vibration analysis of a claim cylindrical shell with internal and external fluid interaction. *Journal of Fluids and Structures*. 2024;125:104079. https://doi.org/10.1016/j.jfluidstructs.2024.104079

12. Firsanov V.V., Vo A.H. Investigation of strengthened cylindrical shells under action of local load on refined theory. *Trudy MAI*. 2018;102. Available from: http://trudymai.ru/published.php?ID=9866 (accessed: 03.03.2025).

13. Sahu R., Kumar B., Shrotriya D. Dynamic study of parabolic cylindrical shell: a parametric study. *International Journal of Trend in Scientific Research and Development*. May-June 2021;5(4):1545–1548. Available from: www.ijtsrd.com e-ISSN: 2456-6470 (accessed: 03.03.2025).

14. Robles S.I., Ortega N.F. Damage evaluation in shells from changes in its static parameters. *Open Construction and Building Technology Journal*. 2011;5:182–189. https://doi.org/10.2174/1874836801105010182

15. Yadav P., Patil K. Studies on parabolic cylindrical shell roof subjected to support settlement. *International Journal of Engineering Science Invention Research & Development*. 2017;3(11):1–6. Available from: https://www.ijesird.com/wp-content/uploads/2023/10/1_amay_10_17.pdf (accessed: 03.03.2025).

16. Mohammadlou V., Khoddami Maraghi Z., Ghorbanpour Arani A. Thermoelastic analysis of axisymmetric conical shells: Investigating stress–strain response under uniform heat flow with semi-coupled approach. *Numerical Heat Transfer, Part A: Applications*. 2024;86(15):5100–5121. https://doi.org/10.1080/10407782.2024.2326943

17. Pham V.T. *Stress-Strain State of Spherical and Conical Shells Based on More Accurate Theory*. Dis. PhD. Moscow: NIU MAI; 2021.

18. Bochkarev S.A., Lekomtsev S.V. Analysis of natural vibration of truncated conical shells partially filled with fluid. *International Journal of Mechanical System Dynamics*. 2024;4(2):142–152. https://doi.org/10.1002/msd2.12105 EDN: QWVIXK

19. Krivoshapko S.N. Static analysis of shells with developable middle surfaces. *Applied Mechanics Reviews*. 1998; 5(12):731–746. https://doi.org/10.1115/1.3098985EID EDN: LEVKML

20. Timoshin M.A. Numerical methods of statical analysis for strength and stability of three shells of zero Gaussian curvature with a directrix ellipse. *Proc. of All-Russian Scientific-and-Practical Conference "Engineering Systems — 2008." Moscow, April 7–11. 2008*. Moscow: RUDN Publ.; 2008. p. 209–212. ISBN 978-5-209-03294-6

21. Aleshina O.O., Ivanov V.N., Grinko E.A. Investigation of the equal slope shell stress state by analytical and two numerical methods. *Structural Mechanics and Analysis of Constructions*. 2020;(6):2–13. (In Russ.) https://doi.org/10.37538/0039-2383.2020.6.2.13 EDN: YXWWNT

22. Aleshina O.O. Studies of geometry and calculation of torso shells of an equal slope. *Structural Mechanics and Analysis of Constructions*. 2019;(3):63–70. (In Russ.) EDN: MGZGMR

23. Krivoshapko S.N. Geometry and strength of general helicoidal shells. *Applied Mechanics Reviews*. 1999;52(5): 161–175. https://doi.org/10.1115/1.3098932 EDN: XOOZHE

24. Duheisat S.A. *Solution of problems of stress analysis of thin elastic shells in the form of right and evolvent helicoids by analytical and numerical methods*: Diss. PhD. Moscow: UDN; 1989.

25. Rynkovskaya M.I. Support draft calculation for a ramp in the form of developable helicoid. *IOP Conference Series Materials Science and Engineering*. 2018;371(1):012041. https://doi.org/10.1088/1757-899X/371/1/012041

26. Aleksandrov A.V., Kosizin S.B., Kosizin A.S. *Nontraditional models of finite elements of high orders. Theoretical Bases of Construction*. Warszawa 2.07.96-5.07.96. Moscow: ASV Publ.; 1996. p. 26–30.

27. Krivoshapko S.N. About parabolic bending of a flat metal sheet into a torso structure. *Mechanical Engineering Technology*. 2020;11(221):14–24 (In Russ.) EDN: QMSSJF

28. Williams O.G., Skaggs R.L. *Method of forming a parabolic trough*. United States Patent US4236399A, 1978.

29. Shrinkin V.N. Moment at elastic-plastic bending of steel sheet. Part 1. Parabolic approximation of steel's hardening zone. *Ferrous Metals*. 2021;(3). https://doi.org/10.17580/chm.2021.03.04

30. Hollister S.M. *Plate development and expansion*. 2002. Available from: http://www.pilot3Dcom//Plate%20Development.htm (accessed: 17.04.2025)

31. Kokhan L.S., Morozov Yu.A. Investigation of deformation in the process of bending of sheet materials. *State, Problems and Prospects of Metal Industry Development and Pressure Metal Treatment*. Moscow: MGVMI; 2003;3:90–91. (In Russ.)

32. Krivoshapko S.N. The application of conoid and cylindroid in forming of buildings and structures of shell type. *Building and Reconstruction*. 2017;5(73):34–44. (In Russ.) EDN: ZUCUTX

33. Ivanov V.N., Aleshina O.O. Geometry of right conoids with orthogonal system of coordinates. *Structural Mechanics and Analysis of Constructions*. 2023;(2):53–62. (In Russ.) http://doi.org/10.37538/0039-2383.2023.2.53.62 EDN: EYGQEO

34. Sahoo S. Dynamic characters of stiffened composite conoidal shell roofs with cutouts: design aids and selection guidelines. *Journal of Engineering*. 2013;(5):230120. http://doi.org/10.1155/2013/230120

35. Watts G., Pradyumna S., Singha M.K. Large deformation analysis of point supported conoidal shells using element free Galerkin method. *Sixth International Congress on Computational Mechanics and Simulation.* India, June 2016. 4 p.

36. Ivaschenko A.B., Stepura A.V. Modeling the surface of a cylindroid using CAD systems. *Science Prospects.* 2023; 1(160):121–124. (In Russ.) EDN: MHRRUD

37. Rynkovskaya M., Ivanov V. Analytical method to analyze right helicoid stress-strain. *Advanced Structured Materials.* 2019;92:157–171. https://doi.org/10.1007/978-3-319-79005-3_11

38. Rynkovskaya M. Analytical methods of analysis of right and open helicoids. *Conference: 2009 American Society for Engineering Education. North-East Section*. Univ. of Bridgeport; 2009.

39. Dekhtyar A.S. Bearing capacity of helicoidal shell. *Structural Mechanics and Analysis of Constructions*. 2013; (6):2–5.

40. Gil-oulbe Mathieu, Markovitch A.S., Tupikova E.M., Zhurbin Yu.V. Numerical modelling of stability of ruled helicoidal shells. *RUDN Journal of Engineering Research*. 2018.19(2):203–213. https://doi.org/10.22363/2312-8143-2018-19-2-203-213

41. Rynkovskaya M., Ermakova E. Modern software capabilities for shape optimization of shells. *Vietnam Journal of Science and Technology*. 2024;62(1):184–194. https://doi.org/10.15625/2525-2518/18788

42. Savićević S., Janjić M. Analysis of the helicoidal shell bending on cylindrical shell. *10th International Research/ Expert Conference "Trends in the Development of Machinery and Associated Technology*." *TMT 2006, Barcelona-Lloret de Mar, Spain, 11–15 Sept. 2006*. p. 1431–1434.

43. Savićević S., Janjić M., Vukčević M., Šibalić N. Stress research of helicoidal shell shape elements. *Scientific Proceedings X International Congress "Machines, Technologies, Materials."* 2013;2:92–94. ISSN 1310-3946.

44. Tupikova E.M. Investigation of V.G. Rekach's method of stress-strain analysis of the shell of long shallow oblique helicoid form. *Structural Mechanics and Analysis of Constructions*. 2016;(1):14–19.

45. Strashnov S.V., Rynkovskaya M.I. On question about classification of analytical surfaces. *Geometry & Graphics.* 2022;10(1):36–43. https://doi.org/10.12737/2308-4898-2022-10-1-36-43

46. Krivoshapko S.N. Optimal shells of revolution and main optimizations. *Structural Mechanics of Engineering Constructions and Buildings.* 2019;15(3):201–209. http://doi.org/ 10.22363/1815-5235-2019-15-3-201-209

47. Gbaguidi Aisse G.L. Influence of the geometrical research of surfaces of revolution and translation surfaces on design of unique structures. *Structural Mechanics of Engineering Constructions and Buildings*. 2019;15(4):308–314. http:// doi.org/10.22363/1815-5235-2019-15-4-308-314

48. Frolova O.A. *Analysis of Shells under Action of Inner Pressure*. Orenburg: OGU; 2018. (In Russ.) Available from: https://elib.osu.ru/bitstream/123456789/13068/1/%D0%A4%D1%80%D0%BE%D0%BB%D0%BE%D0%B2%D0%B0.pdf (accessed: 17.04.2025)

49. Kiselyov A.P., Kiselyova R.Z. On account of stratified shells of revolution by a finite element method. *Engineering Systems — 2008, Proceedings All-Russian Scientific and Practical Conference. Moscow, April 7–11, 2008*. Moscow: RUDN; 2008. p. 223–226. ISBN 978-5-209-03294-6

50. Krikanov A.A. Equally equilibrium form of meridian of shell formed by winding of several families of ribbons. *Mekh. Kompozitz. Mater. i Konstruktziy*. 2001;7(4):413–426. (In Russ.) EDN: JWPWCT

51. Jawad M.H.. *Design of Plate & Shell Structures*. NY: ASME PRESS; 2004. 476 p. ISBN: 0-7918-0199-3

52. Novozhilov V.V., Chernikh K.F., Mikhailovskiy E.I. *Linear Theory of Thin Shells*. Leningrad: Politechnika Publ.; 1991. ISBN 5-7325-0127-4

53. Sibgatullin E.S., Islamov K.F. Determination of bearing capacity of cermet spherical shell. *Fundamental Research*. 2015;(9-3):512–516. Available from: https://fundamental-research.ru/ru/article/view?id=39215 (accessed: 11.05.2025).

54. Ilgamov M.A. Stability of spherical form of shells and space. *Works of the Institute of Mechanics of Ufa Federal Research Centre of the Russian Academy of Sciences*. Ufa: Gilem; 2007;5(1):38–59. https://doi.org/10.21662/uim2007.1.001 (accessed: 11.05.2025)

55. Lychev S.A., Saifutdinov Yu.N. Motion equations of a 3-layered spherical viscoelastic shell. *Vestnik SamGU. Naturally Scientific Series.* 2005;6(40):70–88. Available from: https://vestniksamgu.ssau.ru/est/2005web6/mech/200560102.pdf (accessed: 12.05.2025).

56. Tamboli N., Kulkarni A.B. Bending analysis of paraboloid of revolution shell. *International Journal of Civil Engineering Research* (India). 2014;5(4):307–314. Available from: http://www.ripublication.com/ijcer.htm, ISSN 2278-3652 (accessed: 12.05.2025).

57. Ma X., ZSu Z., Liu H., Liu L. Research on paraboloid-shaped resonator of novel solid vibratory gyroscope. *Journal of Vibroengineering.* 2015;17(1):82–91.

58. Gil-oulbé M., Markovich A.S., Ngandu P., Anosova S.V. Geometric nonlinear analysis of thin elastic paraboloid of revolution shaped shells with radial waves. *RUDN Journal of Engineering Research*. 2020;21(3):208–214. http://doi.org/ 10.22363/2312-8143-2020-21-3-208-214

59. Cao M.L., Qiu X.J. Stress and stability analysis of a cooling tower by ANSYS. *Advanced Materials Research*. 2014;919-921:222–225. https://doi.org/10.4028/www.scientific.net/AMR.919-921.222

60. Zhao L., Ge Y., Chen X., Ke S., Zhang J. Review on wind‐induced stability and vibration effect of large cooling towers. *Zhendong Ceshi Yu Zhenduan.* 2022;42(1):1–10.

61. Gil-oulbe M., Jazzan M., Qbaily J. Geometric modelling and materially nonlinear numerical analysis of shells in the shape of one-sheet hyperboloid of revolution. *Structural Mechanics of Engineering Constructions and Buildings*. 2019;15(3):210–218. https://doi.org/10.22363/1815-5235-2019-15-3-210-218

62. Jasion P., Magnucki K. Theoretical investigation of the strength and stability of special pseudospherical shells under external pressure. *Thin-Walled Structures.* 2015;93:88–93. https://doi.org/10.1016/j.tws.2015.03.012

63. Krawczyk J. Infinitesimal isometric deformations of a pseudospherical shell. *Journal of Mathematical Sciences*. March 2002;109(1):1312–1320. https://doi.org/10.1023/A:1013769300256

64. Gil-oulbé Mathieu, Ndomilep I.J., Ngandu Prosper. Pseudospheric shells in the construction. *RUDN Journal of Engineering Research.* 2021;22(1):84–99. http://doi.org/10.22363/2312-8143-2021-22-1-84-99

65. Kadymov V.A., Maksyutov M.S., Kostikov Yu.A., Pavlov V.Yu., Romanenkov A.M., Ternovskov V.B. Modeling of safe state of toroidal shells in nuclear energy. *Innovations and Investments*. 2018;(5):202–206. EDN: GWILFN

66. Sarbayev B.S., Muravyev V.V., X. Zhang. Design of the toroidal composite pressure vessel made by meridional winding of fibers. *Technology of Textile Industry*. 2021;(6):256–263. https://doi.org/10.47367/0021-3497-2021-6-256

67. Krivoshapko S.N., Ivanov V.N. Catenoidal shells. *Industrial and Civil Engineering.* 2018;(12):7–13. (In Russ.) EDN: YTVZYD

68. Aseev A.V., Makarov A.A. On visualization of some thin shells and their stress-strain state. *Vestnik of Saint Petersburg University. Applied Mathematics. Computer Science. Control Processes*. 2016;(3):18–31. https://doi.org/10.21638/11701/spbu10.2016.302

69. Jasion P., Magnucki K. Buckling and post-buckling analysis of an untypical shells of revolution. In book: *Insights and Innovations in Structural Engineering, Mechanics and Computation*. 2016. p. 766–771. https://doi.org/10.1201/9781315641645

70. Nazarov G.I., Puchkov A.A. Momentless equilibrium of hyperbolic-and-parabolic shell of revolution with changing sign of Gaussian curvature. *Bulletin of Universities.* Construction. 1992;(5, 6):54–60. (In Russ.)

71. Zhang J., Wang M., Wang W., Tang W. Buckling of egg-shaped shells subjected to external pressure. *Thin-Walled Structures*. 2017;113:122–128. https://doi.org/10.1016/j.tws.2017.01.017

72. Jasion P., Magnucki K. A pressure vessel with a special barreled shape. *Ocean Engineering*. 2022;263(1):112414. https://doi.org/10.1016/j.oceaneng.2022.112414

73. Ivanov V.N. *Cyclic surfaces: geometry, classification, shell construction. Architecture of Shells and Strength Analysis of Thin-Walled Civil and Mechanical Engineering Structures of Complex Form*. Moscow: RUDN Publ.; 2001. p. 126–134.

74. Nasr Y., Abbushi A. *Geometry, Design, and Investigation of Stress-Strain State of Shells in the Form of Joachimsthal' Chanal Surfaces*: Dis. PhD. Moscow: RUDN, 2002.

75. Muhammad R. *Geometry, Design, and Investigation of Stress-Strain State of Shells in the Form of Monge's surfaces of General Type*. Dis. PhD. Moscow: RUDN Publ.; 2004.

76. Lamichhane G.P. *Investigation of Stress-Strain State of Intersecting Fragments of Thin Shells with the Help of a Method of Global Elements*. Dis. PhD. Moscow: RUDN Publ.; 2007.

77. Ivanov V.N. *Analysis of Shells in the Form of Cyclical Surfaces*. Diss. k.t.n., Moscow: UDN; 1974.

78. Bantlin A. Formanderung und Beauspruchung Ausgleichsrohren. *Z. Ver. Deut. Ing*. 1910;(54):43–49.

79. Ivanov V.N. Geometry and construction of the tube shells. *RUDN Journal of Engineering Researches*. 2005; 1(11):109–114. (In Russ.)

80. Zubov L.M. On large deformation of bending and torsion of elastic shells having form of helical surface. *Problems of Mechanics of Deformable Solid Body. Interuniversity collection dedicated to the 70th anniversary of Academician N.F. Morozov.* St. Petersburg: St. Petersburg State University Publ.; 2002. p. 130–136. (In Russ.)

81. Krivoshapko S.N. Kinematic surfaces with congruent generatrix curves. *RUDN Journal of Engineering Research.* 2023;24(2);166–176. https://doi.org/10.22363/2312-8143-2023-24-2-166-176

82. Feng R-q., Ge J-m. Shape optimization method of free-form cable-braced grid shells based on the translational surfaces technique. *International Journal of Steel Structures.* 2013;13(3):435–444. https://doi.org/10.1007/s13296-013-3004-3

83. Kolesnikov A.G. Nonlinear methods of mechanics of shallow wooden shells on rectangular plane. *Building and Reconstruction.* 2021;3(95):6–14. (In Russ.) https://doi.org/10.33979/2073-7416-2021-3-6-14

84. Zhikharev F.K. Calculation for assembly reinforced concrete shells with positive Gaussian curvature. *Vestnik MGSU [Monthly Journal on Construction and Architecture]*. 2011;(2):98–104. (In Russ.) EDN: OUVYPF

85. Alborova L.A. Opportunities of velaroidal shells. Engineering Systems. *Proceedings of Applied Science Conference with International Participation, Devoted to 60 Years of Peoples' Friendship University of Russia.* 2020;1:59–65. (In Russ.) ISBN 978-5-209-10101-7

86. Tupikova E., Berdiev M. The comparison of velaroidal shell structures of square plane load bearing properties. *IOP Conference Series: Materials Science and Engineering. "International Scientific Conference Construction Mechanics, Hydraulics and Water Resources Engineering, CONMECHYDRO 2020."* 2020. https://doi.org/10.1088/1757-899X/883/1/012218 EDN: AVDLJI

87. Krivoshapko S.N. Surfaces of diagonal translation of the velaroidal type on a rhomb plan. *Building and Reconstruction.* 2023;2(106):59–69. https://doi.org/10.33979/2073-7416-2023-106-2-59-69

88. Krivoshapko S.N. Research on general and axisymmetric ellipsoidal shells used as domes, pressure vessels, and tanks. *Applied Mechanics Reviews*. 2007;60(6):336–355. https://doi.org/10.1115/1.2806278

89. Klochkov Yu.V., Nikolaev A.P., Kiseleva T.A. To the question on continuous parameterization of spatial figures having an ellipse in a section. Bulletin of Universities. Mathematics. 2017;61(9):27–31. https://doi.org/10.3103/S1066369X17090031

90. Kiseleva R.Z., Kirsanova N.A., Nikolaev A.P., Klochkov Yu.V., Ryabukha V.V. Mixed FEM for shells of revolution based on flow theory and its modifications. *Structural Mechanics of Engineering Constructions and Buildings.* 2024;20(1): 27–39. http://doi.org/10.22363/1815-5235-2024-20-1-27-39

91. Krivoshapko S.N., Gbaguidi Aïssè G.L. Geometry, static, vibration and buckling analysis and applications to thin elliptic paraboloid shells. *The Open Construction and Building Technology Journal*. 2016;10(1):576–602. https://doi.org/10.2174/1874836801610010576

92. Zingoni A., Mudenda K., French V., Mokhothu B. Buckling strength of thin-shell concrete arch dams. *Thin-Walled Structures.* 2013;64:94–102. https://doi.org/10.1016/j.tws.2012.12.001

93. Rao A.B., Suresh Y.R. ANN model for predicting the significance of parameters in the structural behaviour of an elliptical paraboloid shell roof. *Materials Today: Proceedings*. 2022;66:1938–1944. https://doi.org/10.1016/j.matpr.2022.05.427 EDN: TNSEXN

94. Sahoo S. Relative performance of laminated composite doubly curved shell roof with cutout. *International Journal of Materials Chemistry and Physics*. 2016;2(1):15–21.

95. Meleka N.N., Safan M.A., Bashandy A.A., Abd-Elrazek A.S. Repairing and strengthening of elliptical paraboloid concrete shells with openings. *Archives of Civil Engineering.* 2013;59(3):401–420. https://doi.org/10.2478/ace-2013-0022

96. Vekariya M.S., Makwana A.H. A review on thin-shell structures: Advances and trends. *International Journal of Research Publication and Reviews.* 2021;2(12):1593–1609. Available from: https://ijrpr.com/uploads/V2ISSUE12/IJRPR2224.pdf (accessed: 12.05.2025)

97. Su Ch., Fan M.Yu., Zhu L., Hu N. Parametric design and modular construction of a large additive-manufactured hypar shell. *Architectural Intelligence*. 2023;2(1):1–14. https://doi.org/10.1007/s44223-023-00041-0

98. Aleshina O.O. Geometry and static analysis of thin shells in the form of a diagonal translation surface of velaroidal type. *Structural Mechanics of Engineering Constructions and Buildings.* 2023;19(1):84–93. http://doi.org/10.22363/1815-5235-2023-19-1-84-93

99. Mamieva I.A., Karnevich V.V. Geometry and static analysis of thin shells with ruled middle surfaces of three superellipses as main frame. *Building and Reconstruction.* 2023;1(105):16–27. https://doi.org/10.33979/2073-7416-2023-105-1-16-27

100. Tupikova E.M. Shells in the form of algebraic ruled surfaces on a rhombic base. *Structural Mechanics of Engineering Constructions and Buildings*. 2023;19(5): 510–519. (In Russ.) http://doi.org/10.22363/1815-5235-2023-19-5-510-519

101. Ma Y.Q., Wang C.M., Ang K.K. Buckling of super ellipsoidal shells under uniform pressure. *Thin-Walled Structures.* 2008;46(6):584–591. https://doi.org/10.1016/j.tws.2008.01.013

102. Lebedev V.A. *Thin-Walled Umbrella Shells*. Leningrad: Gosstroyizdat Publ.; 1958. 172 p. (In Russ.)

103. Kozyreva A.A., Rynkovskaya M.I., Tupikova E.M. Umbrella shells for covering of sport center. *RUDN Journal of Engineering Research.* 2017;18(1):70–78. https://doi.org/10.22363/2312-8143-2017-18-1-70-78

104. Imam M.H. Shape optimization of umbrella-shaped concrete shells subjected to self-weight as the dominant load. *Computers & Structures.* 1998;69(4):513–524. EDN: ABJJDH

105. Ivanov V.N. Stress-strain state analysis of trade center in the form of umbrella-type shell by variation-difference energy method. *Structural Mechanics of Engineering Constructions and Buildings*. 2008;(4):86–89. (In Russ.) EDN: JWQFGV

106. Tupikova E.M., Ershov M.E. Trial design of umbrella type shell structures. *Structural Mechanics of Engineering Constructions and Buildings.* 2021;17(4):414–424. http://doi.org/10.22363/1815-5235-2021-17-4-414-42 4

107. Krivoshapko S.N., Ivanov V.N. *Encyclopedia of Analytical Surfaces.* Switzerland: Springer International Publ.; 2015. https://doi.org/10.1007/978-3-319-11773-7

108. Gil-oulbe Mathieu. Reserve of analytical surfaces for architecture and construction. *Building and Reconstruction.* 2021;6(98):63–72. https://doi.org/10.33979/2073-7416-2021-98-6-63-72

109. Pietraszkiewicz W., Konopińska V. Junctions in shell structures: A review. *Thin-Walled Structures*. July 2015; 95(2):310–334. https://doi.org/10.1016/j.tws.2015.07.010

110. Mao-Hong Yu. Advances in strength theories for materials under complex stress state in the 20th Century. *Applied Mechanics Reviews*. May 2002;55(3):169–218. https://doi.org/10.1115/1.1472455

111. Vidya Vijay K.P, Pooja S.M., Shivakumar G.S. Exploring the design, analysis, and applications of shell structures. *International Journal of Engineering Research & Technology (IJERT).* 2023;12(11):4. Available from: http://www.ijert.org (accessed: 17.04.2025)

112. Mayur S. Vekariya Er. Ashish H. Makwana. A review on thin-shell structures: advances and trends. *International Journal of Research Publication and Reviews*. 2021;2(12):1593–1609. Available from: www.ijrpr.com ISSN 2582-7421 (accessed: 17.04.2025)

СТРОИТЕЛЬНАЯ МЕХАНИКА ИНЖЕНЕРНЫХ КОНСТРУКЦИЙ И СООРУЖЕНИЙ
STRUCTURAL MECHANICS OF ENGINEERING CONSTRUCTIONS AND BUILDINGS

2025. 21(6). 585–604

ISSN 1815-5235 (Print), 2587-8700 (Online)

HTTP://JOURNALS.RUDN.RU/STRUCTURAL-MECHANICS

СТРОИТЕЛЬНЫЕ МАТЕРИАЛЫ И ИЗДЕЛИЯ
CONSTRUCTION MATERIALS AND PRODUCTS

DOI: 10.22363/1815-5235-2025-21-6-585-604
EDN: FQPAPB

Review article / Обзорная статья

Self-Healing Mechanisms in Nano-Modified Concrete: A Comprehensive Review of Synergy Between Microbial Biomineralization and Nano-Additives

Armin Ehsani✉, Shahin Nasimi, Svetlana L. Shambina, Serdar B. Yazyev, Oleg L. Kireev

RUDN University, *Moscow, Russian Federation*

✉ arminehsani97@gmail.com

Received: June 22, 2025
Revised: September 13, 2025
Accepted: September 30, 2025

Abstract. The environmental impact of using different building materials to make sustainable concrete is important. The use of nanotechnology in industry has become increasingly important since sustainable development was established as a necessity to protect the environment and the interests of future generations. However, cracking is still a big problem, causing structural deterioration and shorter service life. Novel approaches to self-healing concrete have been made possible by recent developments in nanotechnology and biotechnology, which have improved the material's endurance and mechanical qualities. This study investigates the use of microbial agents, namely alkali-resistant bacteria like Bacillus, and nanomaterials, including carbon nanotubes and nano-silica, to create self-repairing concrete. While microorganisms incorporated in porous expanded clay (LECA) create calcium carbonate to seal cracks on their own, nanomaterials enhance the strength, impermeability, and resistance of concrete to external conditions. In addition, technologies like as shape-memory alloys, hollow fibers, and microencapsulation are being researched for crack repair. Additionally, by comprehending self-healing nano-concrete's remarkable mechanical qualities and durability performance, environmental effects and retrofitting expenses related to structures can be reduced. According to experimental findings, bacterial self-healing concrete closes all cracks in two months, but conventional concrete only closes 33% of them. These technologies promise a fundamental change toward sustainable, long-lasting, and intelligent infrastructure, despite obstacles including high costs, nanoparticle dispersion, and long-term viability. Future studies seek to refine these techniques for widespread use while maintaining environmental safety and economic viability.

Keywords: self-healing concrete, nanotechnology, biological concrete, smart concrete

Conflicts of interest. The authors declare that there is no conflict of interest.

Armin Ehsani, postgraduate student, Department of Construction Technologies and Structural Materials, Academy of Engineering, RUDN University, 6 Miklukho-Maklaya St, Moscow, 117198, Russian Federation; ORCID: 0000-0002-4590-8552; e-mail: arminehsani97@gmail.com

Shahin Nasimi, postgraduate student, Department of Construction Technologies and Structural Materials, Academy of Engineering, RUDN University, 6 Miklukho-Maklaya St, Moscow, 117198, Russian Federation; ORCID: 0000-0001-5939-3257; e-mail: shahin.nasimi@yahoo.com

Svetlana L. Shambina, Candidate of Technical Science, Associate Professor in Department of Construction Technologies and Structural Materials, Academy of Engineering, RUDN University, 6 Miklukho-Maklaya St, Moscow, 117198, Russian Federation; Scopus Author ID: 57060572700; eLIBRARY SPIN-code: 5568-0834; ORCID: 0000-0002-9923-176X; e-mail: shambina_sl@mail.ru

Serdar B. Yazyev, Doctor of Technical Sciences, Head of the Department Construction Technologies and Structural Materials, Academy of Engineering, RUDN University, 6 Miklukho-Maklaya St, Moscow, 117198, Russian Federation; eLIBRARY SPIN-code: 6065-1733, ORCID: 0000-0002-7839-7381; e-mail: yazyev_sb@pfur.ru

Oleg L. Kireev, Senior Lecturer of the Department of Construction Technology and Structural Materials, Academy of Engineering, RUDN University, 6 Miklukho-Maklaya St, Moscow, 117198, Russian Federation; ORCID: 0009-0002-1523-9439; e-mail: kireev_ol@pfur.ru

Authors' contribution: *Ehsani A., Nasimi Sh.* — conceptualization, collection of materials, processing of results, conclusions; *Shambina S.L., Yazyev S.B.* — editing, processing of references, general review; *Kireev O.L.* — working with English-language sources. All of the authors read and approved the final version of the article.

For citation: Ehsani A., Nasimi Sh., Shambina S. L., Yazyev S.B., Kireev O.L. Self-healing mechanisms in nano-modified concrete: a comprehensive review of synergy between microbial biomineralization and nano-additives. *Structural Mechanics of Engineering Constructions and Buildings.* 2025;21(6):585–604. http://doi.org/10.22363/1815-5235-2025-21-6-585-604 EDN: FQPAPB

Механизмы самовосстановления в наномодифицированном бетоне: комплексный обзор взаимодействия биоминерализации и нанодобавок

А. Эхсани✉, Ш. Насими, С.Л. Шамбина, С.Б. Язьев, О.Л. Киреев

Российский университет дружбы народов, *Москва, Российская Федерация*

✉ arminehsani97@gmail.com

Поступила в редакцию: 22 июня 2025 г.
Доработана: 13 сентября 2025 г.
Принята к публикации: 30 сентября 2025 г.

Аннотация. Влияние использования различных строительных материалов на окружающую среду при производстве экологически безопасного бетона имеет большое значение. Использование нанотехнологий в промышленности становится все более актуальным с тех пор, как устойчивое развитие стало необходимостью для защиты окружающей среды и интересов будущих поколений. Однако растрескивание по-прежнему остается большой проблемой, вызывающей ухудшение структуры и сокращение срока службы. Новые подходы к самовосстановлению бетона стали возможны благодаря последним разработкам в области нанотехнологий и биотехнологий, которые повысили выносливость и механические качества материала. Авторами изучено использование микробных агентов, а именно щелочеустойчивых бактерий типа Bacillus, и наноматериалов, включая углеродные нанотрубки и нанокремнезем, для создания самовосстанавливающегося бетона. В то время как микроорганизмы, внедренные в пористый керамзит, создают карбонат кальция для самостоятельной заделки трещин, наноматериалы повышают прочность, непроницаемость и устойчивость бетона к внешним условиям. Кроме того, для ремонта трещин исследуются такие технологии, как сплавы с памятью формы, полые волокна и микрокапсулы. Также осознание замечательных механических свойств и долговечности самовосстанавливающегося нанобетона позволяет сократить воздействие на окружающую среду и расходы на модернизацию конструкций. Согласно экспериментальным данным, бактериальный самовосстанавливающийся бетон закрывает все трещины за два месяца, в то время как обычный бетон закрывает только 33 % из них. Эти технологии обещают фундаментальные изменения в сторону устойчивой, долговечной и интеллектуальной инфраструктуры, несмотря на такие препятствия, как высокая стоимость, дисперсность наночастиц и долгосрочная жизнеспособность. Будущие исследования направлены на совершенствование этих технологий для широкого применения при сохранении экологической безопасности и экономической жизнеспособности.

Ключевые слова: Самовосстанавливающийся бетон, нанотехнологии, биобетон, «умный» бетон

Заявление о конфликте интересов. Авторы заявляют об отсутствии конфликта интересов.

Вклад авторов: *Эхсани А., Насими Ш.* — концепция исследования, сбор материалов, обработка результатов исследования, выводы; *Шамбина С.Л, Язьев С.Б.* — редактирование текста, обработка списка литературы, общее рецензирование; *Киреев О.Л.* — работа с англоязычными источниками. Авторы ознакомлены с окончательной версией статьи и одобрили ее.

Для цитирования: *Ehsani A., Nasimi Sh., Shambina S.L., Yazyev S.B., Kireev O.L.* Self-healing mechanisms in nano-modified concrete: a comprehensive review of synergy between microbial biomineralization and nano-additives // Строительная механика инженерных конструкций и сооружений. 2025. Т. 21. № 6. С. 585–604. http://doi.org/10.22363/1815-5235-2025-21-6-585-604 EDN: FQPAPB

Эхсани Армин, аспирант кафедры технологий строительства и конструкционных материалов, инженерная академия, Российский университет дружбы народов; Российская Федерация, 117198, г. Москва, ул. Миклухо-Маклая, д. 6; ORCID: 0000-0002-4590-8552; e-mail: arminehsani97@gmail.com
Насими Шахин, аспирант кафедры технологий строительства и конструкционных материалов, инженерная академия, Российский университет дружбы народов; Российская Федерация, 117198, г. Москва, ул. Миклухо-Маклая, д. 6; ORCID: 0000-0001-5939-3257; e-mail: shahin.nasimi@yahoo.com
Шамбина Светлана Львовна, кандидат технических наук, доцент аспирант кафедры технологий строительства и конструкционных материалов, инженерная академия, Российский университет дружбы народов, Российская Федерация, 117198, г. Москва, ул. Миклухо-Маклая, д. 6; Scopus Author ID: 57060572700; eLIBRARY SPIN-код: 5568-0834; ORCID: 0000-0002-9923-176X; e-mail: shambina_sl@mail.ru
Язьев Сердар Батырович, доктор технических наук, заведующий кафедрой технологий строительства и конструкционных материалов, инженерная академия, Российский университет дружбы народов, Российская Федерация, 117198, г. Москва, ул. Миклухо-Маклая, д. 6; eLIBRARY SPIN-код 6065-1733, ORCID: 0000-0002-7839-7381; e-mail: yazyev_sb@pfur.ru
Киреев Олег Леонидович, старший преподаватель кафедры технологий строительства и конструкционных материалов, инженерная академия, Российский университет дружбы народов, Российская Федерация, 117198, г. Москва, ул. Миклухо-Маклая, д. 6; ORCID: 0009-0002-1523-9439; e-mail: e-mail: kireev_ol@pfur.ruu

1. Introduction

Concrete, in a broad sense, refers to any material or compound that is composed of a cementitious adhesive. This adhesive is generally the result of the interaction of hydraulic cements and water. Concrete is one of the most widely used building materials. The main feature of concrete is its cheapness and availability of raw materials. The use of concrete can be seen in all construction works such as buildings, reservoirs and power plants, offshore structures such as piers, roads and paths, dams, etc. So far, many studies have been conducted to improve the quality of concrete, most of which have examined changes in the composition of concrete (called the concrete mixing plan), However, the use of additives as well as the replacement of conventional materials used in concrete with new materials has always been considered. Nanomaterials are one of the new materials that have been able to improve the mechanical and physical properties of concrete. Nanomaterials can completely transform the concrete world due to their properties on very small surfaces.

Currently, the importance of the application of nanotechnology in industry, with the introduction of sustainable development as a necessity to protect the environment and the interests of future generations, has become more apparent. Nanotechnology has entered the construction industry in various fields such as metals, concrete, soil, glass, energy and air conditioning, water treatment, sensors, coatings, paints and insulators [1]. Extensive research has been conducted in the last decade on the application of nanotechnology in concrete technology. Concrete as a macro material is strongly influenced by the properties of nano-technology. Understanding the behavior of concrete and the performance of structures at the micro and nano scale improves and enhances the properties of concrete and thus contributes the construction and production of concrete with performance commensurate with today's needs [2]. So far, nanotechnology in the concrete industry has proven the possibility of improving the basic characteristics such as strength, lightness, durability, flexibility, impermeability, construction of smart aggregates and cements, thermal insulation, self-cleaning and self-healing. And ongoing research continues to unravel the mystery of the industry.

One of the problems in the subject of concrete and reinforced concrete structures is the issue of cracks. Cracks are now recognized as one of the problems of reinforced concrete structures. Improvement or repair of cracks with a width of less than 0.2 mm is mainly due to the large range of small particles of non-hydrated cement on the surface of the cracks. Therefore, we need side mechanisms and mechanisms of high self-healing. In such a way that in addition to preventing cracking, cracked sections with self-healing ability are not vulnerable.

A mechanism based on the use of mineral bacteria in crack repair has been studied and developed in several laboratories. Cracks are effectively closed by the deposition of minerals while the bacteria in the mixture are sprayed on the damaged surface and injected manually into the cracks [3]. Here, the bacterial eggs and the organic compounds present enter the porous expanded clay particles (LECA) before being added to the mixing scheme. It is hypothesized that the protection and maintenance of bacterial cells within porous aggregates will increase their viability period as well as increase the efficiency of self-healing concrete when placed in the microstructure. Ever since cement was discovered in its present form, the subsequent combination of cement with stone and water has produced a cohesive body called concrete [4]. To date, much research has been done on cement and other adhesives in concrete, which has increased human knowledge about the various properties and applications of concrete. Concrete is increasingly used in the construction of various structures due to its good performance and lack of destructive environmental effects, as the current production of more than one ton of concrete per person per year in the world indicates this. Self-compacting concrete is one of the new generation concretes that has been considered by engineers due to its many capabilities such as proper flow and efficiency, strength and penetration. Self-compacting concrete does not need compactors [5]. Nanoscience and nanoengineering, sometimes referred to as nano-improvement in concrete, are names used to describe two pathways in nanotechnology research in concrete. Nanoscience is concerned with measuring and describing the structure of nano- and micro-scale cementitious base materials for a better understanding of large-scale (macro) behavior and its performance through the use of advanced atomic or molecular surface description and modeling techniques [6].

Nanotechnology is a branch of science that studies the comprehension and manipulation of materials at the nanoscale with the goal of enhancing their qualities in products [7]. The idea of nanotechnology has been used more and more in a variety of industries in recent years, including construction, chemistry, electronics, biomechanics, pharmaceuticals, textiles, and medicine [7–8]. Numerous studies on the different uses of nanotechnology in the building materials industry, particularly in cement-based materials, have been conducted in recent years [9]. Numerous national initiatives have been started in the European Union or in nations like America, Canada, Japan, Russia, and China to aid in the development of nanomaterials and nanotechnology. Numerous worldwide professional organizations have formed commissions, groupings, and working committees. One such committee is the TC 197 NCM, which was established by RILEM [10].

Like other scientific and engineering fields, the construction sector keeps a close eye on nanotechnology advancements and looks for possible new application areas. The usage of nanoparticles in construction materials is becoming more and more popular. In addition to improving material qualities like strength and durability, nanoparticles may be used to provide novel functionalities like pressure sensing and photocatalysis [11–13]. These nuclei are responsible for the crystal development process that forms cement hydration products. As hydration products begin to develop between the cement grains, the presence of nanoparticles speeds up the production of a highly void-free interior structure as compared to a reference mixture without nanoparticles. This might lead to the production of cement base materials with high compressive strength and increased voids at an early age [14–16].

Nano engineering includes nanometer-scale structure manipulation techniques to create a new and suitable generation of cementitious composites with ideal mechanical behavior. And it is even possible to create concrete with new properties such as low electrical resistance, intelligence, self-cleaning, self-repairing, high ductility, etc. Recent research activities in the field of nanotechnology in concrete include the inherent study of hydration in cement, the effect of adding nano silica to concrete, the addition of nanoparticles to cement, concrete and cementitious coatings, and the observation of their effects on behavior and properties [17].

Experimental research has shown that nanoscale clay particles enhance concrete's mechanical qualities while lowering shrinkage and chloride permeability [18]. The surface area or size of these particles is significant in terms of cement hydration kinetics as the hydration rate is linked to the reactions that take place on the reactive surfaces of nanoparticles [19]. Cement hydration is also accelerated by nanoparticles like CSH artificial grains. Although nucleation processes, which are required for crystal formation under normal circumstances, are not required with this approach, time is lost and the dead period of cement hydration is reduced [20–23].

Nanotechnology, like all new technologies, needs an economic justification. Currently, the high cost of nanoparticles sometimes prevents the increasing development of these products and their use in industry. For this reason, the use of nanotechnology in the concrete industry on a commercial scale is still limited to a few products available in the market[1] [24–26].

Another problem in using nanomaterials is their uniform distribution in the concrete matrix. These materials usually accumulate as lumps when added to concrete and are not well distributed in the mix, obviously, powerful mixers can be used to solve this problem. Another drawback is the very high water absorption of nanoparticles. These particles absorb large amounts of water due to their very large specific surface area and may affect the performance of concrete [26–28]. So, there are challenges that must be addressed before expanding the use of nanotechnology in the concrete industry, such as uniform distribution of nanomaterials, compatibility of nanomaterials with cement, processing, production, safety, transportation issues, mass production and costs [29].

In addition to introducing these new materials to society through social infrastructure requires more understanding of their impact on the environment and human health [30]. However, now, 50 years after Feynman's (Feynman. R) famous article, it is clear that nanotechnology is changing the views of scientists

[1] Nanotechnology in Construction Market Outlook. Available from: https://researchintelo.com/report/nanotechnology-in-construction-market (accessed: 22.06.2025)

and engineers on one of the oldest man-made materials, concrete [31; 32]. Concrete is the most popular building material, and we have been trying to make it more sustainable since the Romans built the Temples of the Gods about 2,000 years ago. No matter how carefully we combine or harden it, all concrete will one day crack, and in some cases, these cracks will lead to the collapse of the building [33; 34].

Professor Henk Jonkers of Delft University of Technology in the Netherlands explains that the problem with concrete cracks is that they leak. If there are cracks, water will seep into the basement or parking lot. Second, if this water reaches the reinforced steel part of the concrete — all the concrete has these rebars, and if they rust, the building will collapse [35]. But Jonkers has come up with a whole new way to extend the life of concrete. So called "bio concrete" has been invented, that can repair itself with bacteria [36].

Bio concrete has exactly the same composition as ordinary concrete, but with an additional element, a restorative agent. This agent remains intact during mixing and only dissolves and activates when concrete cracks and water enters [37; 38]. Jonkers, a microbiologist, has been working on it since 2006, when concrete technologists asked him if it was possible to use a bacterium to make self-healing concrete. It took him three years to solve the problem, but he faced many complex challenges [39; 40]. You need bacteria that can survive in harsh concrete environments, Jonkers said [41]. He went on to say that the material was similar to rock or stone and was very dry. Concrete is highly alkaline, and the repairing bacteria must be dormant for years before being able to be activated by water [42].

Jonkers chose the bacillus bacterium for this, because they grow in an alkaline environment and produce pollen that can survive for years without food and oxygen. Jonkers explained that the next challenge was that in addition to keeping bacteria in the concrete active, we had to force it to produce concrete repair agents [43; 44], which are limestone.

Basil is needed as a food source to produce limestone. Sugar is one of the solutions, but adding sugar to the mixture weakens and softens the concrete. In the end, Jonkers chose calcium lactate. He placed the bacteria and calcium lactate in a biodegradable rubber capsule and mixed it with wet cement. When the cracks finally start to form in the concrete, water enters and opens the capsules. The bacteria then grow and begin to multiply by eating lactate. By doing so, they combine calcium with carbon ions to produce calcite or limestone, which closes the gaps.

Now Jonkers hopes that his concrete can create a new era of biological buildings as this is "a combination of building materials and nature". Nature has provided us with many free capabilities, such as limestone-producing bacteria. If we can use it in our materials, we can make the most of it. This was a good example of nature and the environment coming together to come up with a new concept [45; 46].

Sewage sludge has been considered for these destructive effects due to the environmental problems it can cause in its landfill. On the other hand, today in countries with the construction of more wastewater treatment plants, the production of these wastes has increased. Therefore, the possibility of creating a suitable cycle for the use and consumption of these materials is a very good way to reduce the environmental hazards caused by its burial [47–49]. Although it does not take long for nanoparticles to be used as advanced materials in concrete, extensive research has demonstrated the tremendous effectiveness of these materials in concrete [50]. The use of sewage sludge or mosses as a biological ash in concrete has led to the creation of concrete, which is welcomed today [51]. A group of civil researchers at the Malaysian University of Technology have succeeded in producing a type of concrete that can repair cracks with the help of specific microorganisms [52]. This ability to repair has resulted in higher strength and durability than conventional concrete [53]. Structures made of this type of concrete are able to withstand harsher environmental conditions and are more resistant to damage caused by acid rain, etc. [54].

At first various researchers have conducted research on the production of self-healing concrete and have succeeded in presenting such concretes, but the vast majority of them have chosen chemical methods in this field.

Recent studies that have led to the production of self-healing concretes have used biological methods [55]. So, despite the high level of technology required to produce them, it has provided the possibility of producing cheap self-healing concretes. Researchers have named these concretes biologically self-healing concrete [56–58].

The future of design and architecture requires innovative thinking about the application of current construction techniques to be able to expand their capabilities [59]. Sustainability is inferred from something beyond a trend and has become a constant part of the design process. Sustainability solutions have always pushed the current state of design. Scientists created the type of concrete that holds and nurtures many biological organisms on its surface [60].

There are facades of buildings with vegetation, but what sets biological concrete apart from other systems is that vegetations are an integral part of the structure [61]. This system consists of three layers on structural elements that together bring environmental, thermal and aesthetic benefits to the building. In this case, the acceptable amount needs to be reduced. This was not the ideal situation that researchers at UPC were looking for. Instead, they created a biological layer using magnesium phosphate cement, which is slightly more acidic and does not need to lower the pH. [62; 63]. Mosses can grow at pH less than 5. To the extent that most other plants do not prefer. Restricting competition by lowering the pH is likely to expand moss colonization. The researchers' strategy led to the development of different types of cement with variable pH distributions that help grow certain types of organisms such as mosses, microalgae or lichens. The installation of this living concrete consists of three layers on a structural surface. The first layer is a waterproof shell that protects structural elements from water penetration. A new biological layer of concrete is applied to this layer. This layer absorbs rainwater and acts like a microscopic structure that stores rainwater. The last layer is a discontinuous cover that allows rainwater to enter and traps it between this cover and the waterproof cover. This optimizes the amount of water that gets trapped inside the biological coating without compromising the structure [64; 65]. There are many benefits of this system. Plants absorb CO_2 from the air and release oxygen. This layer also acts as thermal insulation and helps regulate the heat inside the building by absorbing heat and preventing it from entering the building in hot weather or escaping from the building in cold weather. This material has been registered but is still in the testing phase [66]. Researchers are experimenting with different cements that can be used to grow certain species of plants. These changes in the facade, both in terms of decoration and environment, give variety and color to any facade and turn it into a new or renovated building [67].

2. Materials and Methods

The study used a multi-phase method to create and test self-compacting smart nano-concrete that has better self-healing abilities. The main binding agent was Ordinary Portland Cement (OPC, Grade 43), which met ASTM C150 standards. It was mixed with Class F fly ash (20% replacement) and nano-silica (2% of the cement's weight) to improve particle packing density and pozzolanic reactivity. The reinforcement system included multi-walled carbon nanotubes (MWCNTs, 0.5 wt.%) that were evenly spread using ultrasonic homogenization in a polycarboxylate-based superplasticizer to avoid clumping.

To obtain biological self-healing concrete, alkali-resistant Bacillus pseudofirmus spores (10^6 CFU/g cement) were trapped inside pre-saturated porous expanded clay aggregates (LECA, 2–4 mm size), along with calcium lactate (5% by weight of LECA) as an organic mineral precursor to promote microbially induced calcium carbonate precipitation (MICP). The concrete mixtures had a water-to-binder ratio (w/b) of 0.35 and achieved self-compacting properties through a specific blend of polycarboxylate ether (PCE) superplasticizer (1.2% by cement weight) and viscosity-modifying admixture (VMA, 0.05%) to ensure flow ability (> 650 mm slump flow) while reducing segregation. For comparison, control mixtures without bacterial or nano additives were made alongside three experimental groups: (1) nano-modified concrete (NMC) with MWCNTs/nano-silica, (2) bio-concrete (BC) with bacteria-encapsulated LECA, and (3) hybrid smart concrete (HSC) combining both nanomaterials and bacterial agents. Mechanical and durability tests were conducted following ASTM C39 for compressive strength, ASTM C496 for splitting tensile strength, and ASTM C1202 for rapid chloride permeability. Self-healing efficiency was measured by pre-cracking specimens to create a 0.3 mm crack width using three-point bending, followed by immersing them in water for 56 days. Also, crack closure was evaluated using optical microscopy and X-ray computed tomography

(X-CT), while thermo-gravimetric analysis (TGA) and Fourier-transform infrared spectroscopy (FTIR) confirmed the formation of $CaCO_3$. To create smart features, shape-memory alloy (SMA, Ni-Ti) fibers were added at a volume of 1.5% to test how well they could recover from cracks when heated to 70°C. Also, we made microvascular networks that imitate biological systems using 3D-printed templates. These networks help deliver healing agents, which include methyl methacrylate monomer and an initiator, directly to the cracks. We looked at the environmental impact by conducting a life cycle assessment (LCA) to compare the embodied carbon between traditional and smart concrete systems. To confirm our results statistically, we used ANOVA ($p < 0.05$) along with Tukey's post-hoc test to check for significant differences among the mixtures. The findings showed that the hybrid smart concrete group healed 92% of its cracks compared to just 35% in the control group and had a compressive strength that was 28% higher after 90 days at 68 MPa than regular OPC concrete. This supports the combined benefits of nanotechnology and bio mineralization.

In this study, nanotechnology and its application in the construction industry were investigated. The main characteristics and basic applications of nanomaterials, especially in the civil engineering industry, were the main and important areas of this research at the initial stage. Then, this research studied the effect of nanomaterials, including the use and effect of bacteria for self-healing concrete to close concrete cracks with the bond strength and cohesion of the concrete microstructure and the use of filled microcapsules that are injected into the concrete as a repair agent by taking inspiration from red blood cells in blood clotting and repair. Also, the thermal selector method, which is the most efficient and intelligent method, was used to repair concrete with two methods: self-diagnostic composites and plasticity organic film tube. The next method is the use of cement composites inspired by the healing of injuries to living organisms, which allows hairline cracks to spread and prevents the formation of deep cracks. Another important method was the use of low quantities of CNT in concrete to improve the mechanical properties of concrete. The use of hollow fibers was a method inspired by the mechanism of bruising of living organisms. Another method investigated in this study was the use of shape memory alloys, which have the ability to recover their original shape in shape changes due to temperature and stress. In the following sections, a further examination of these methods, including the efficiency, advantages and disadvantages of the methods, are presented.

3. Results

3.1. Using Bacteria to Make Self-Healing Concrete

Bacteria used in concrete should be suitable as a repair agent. For example, these bacteria should be able to close cracks effectively during the useful life of the structure. The main mechanism for closing cracks is that the bacteria themselves act as a catalyst and convert the organic compounds into a suitable filler for cracks [68]. Therefore, for effective self-healing, both bacteria and microstructure compounds must be mixed. However, the presence of bacteria and organic compounds in the microstructure should not have negative impact on other properties of concrete. There are some bacteria in nature that promote bonding and cohesion of concrete microstructure. And these bacteria belong to a specific group of alkali-resistant bacteria formed. An interesting feature of this type of bacteria is that they are able to form eggs that have spherical cells with a thick wall similar to plant seeds (Figure 1). These eggs are viable but inactive and can withstand mechanical and chemical stresses and can survive in the dry state for more than 50 years. In fact, in this process, Bacillus bacteria are used as one of the self-healing agents of self-compacting concrete.

Active bacteria can be seen in Figure 1, and the spores have a diameter of one micrometer. When bacterial eggs are added directly (unprotected) to the concrete mixing plan, their lifespan is limited to one or two months. Continuous cement hydration may be the cause of the bacterial eggs' reduced lifespan from several decades in the dry state to one or two months in the unprotected state at the time of microstructure, which results in holes that are smaller in diameter than bacterial eggs, which have a micrometer diameter [70]. A further concern is whether additional undesired qualities of concrete may be lost as a result of the direct addition of top organic bio-mineral compounds. Leading biomineral substances like calcium acetate, peptone, and yeast juice have been shown in subsequent research to dramatically lower compressive strength.

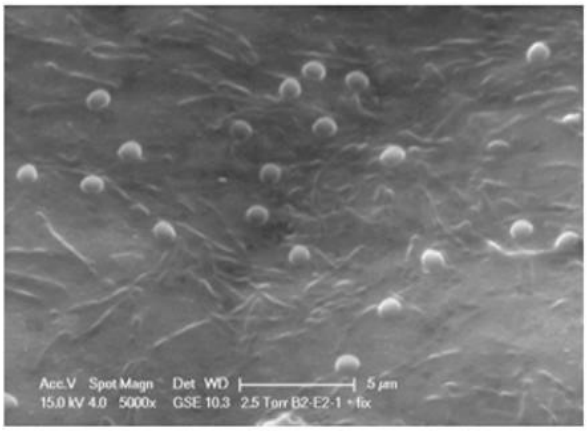

Figure 1. Active bacteria and alkali resistant spores (Electron microscope image)
S o u r c e: compiled by H.M. Jonkers [42].

The only exception is calcium lactate, which increases compressive strength by 10% compared to other control samples [68].

Currently, biodegradability tests show that no viability deficiency has been observed for more than 6 months after setting and it is recommended to pay attention to the long-term viability seen in the dry state (when it does not fit in the concrete) [71]. In subsequent experiments, expanded clay particles (LECA) containing two representatives of biochemical compounds were used as additives in the concrete micro-structure to test the repair capacity of concrete-containing concrete [72]. Jonkers [42] investigated the immobilization of these components on porous expanded clay particles in order to extend the shelf life, the related functionality of the bacteria in the concrete, the impact of bacterial spores, and the concurrently needed biomineral organic compound precursor (calcium lactate). The results showed a significant increase in shelf life.

Its good long-term condition, as observed in the dry state, was maintained when fitted to the concrete, as evidenced by the fact that no loss of spore efficacy was seen after six months of integration [69]. This method is used to make self-healing concrete with the help of a special type of bacteria in nature that are able to live in alkaline environments above concrete. This bacterium is called Bacillus, which has been able to live long in alkaline lakes in Russia and Egypt. These bacteria, along with their power supply, are embedded in small ceramic pellets and placed in suspension in concrete water to prevent premature activation in the wet concrete mix (Figure 2). The bacteria remain proactive or so-called dormant in the concrete until the crack is formed, and then they are activated by the expansion of the crack and the infiltration of water into the cross section [68; 73].

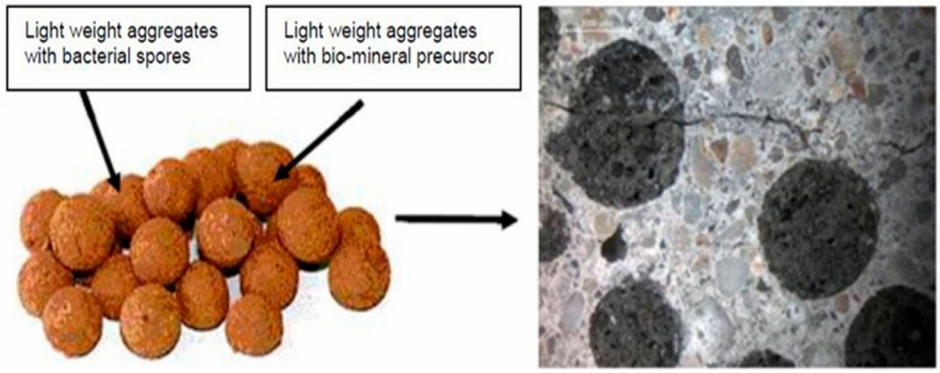

a *b*

Figure 2. Self-healing additives consisting of expanded clay particles:
a — filled with spore bacteria; *b* — in organic mineral composition (calcium lactate).
S o u r c e: compiled by H.M. Jonkers [42].

Figure 3 shows how to perform the self-healing mechanism using bacteria. According to the figure, after cracking in the concrete section, water penetrates into the section and activates the bacteria. At this point, the bacteria go from dormant to active and block the cracks by producing calcium carbonate deposits. It should be mentioned that prior to the discovery of the bacterium; concrete cracks were repaired using mineral bacterial products. However, because manpower was required to manually install these bacteria in

the damaged area along with considering that the bacteria's reaction with concrete compounds produced ammonia toxin, the process did not last long or develop much. In this method, concrete test specimens are made where a portion of the aggregate material, for example 2 to 4 mm in size, is replaced with clay particles, which contain self-healing biochemical bacteria. Before carrying out the work, the load-bearing clay particles inside it (for a week at 40°C) are dried so that no more weight loss is observed due to water evaporation [71].

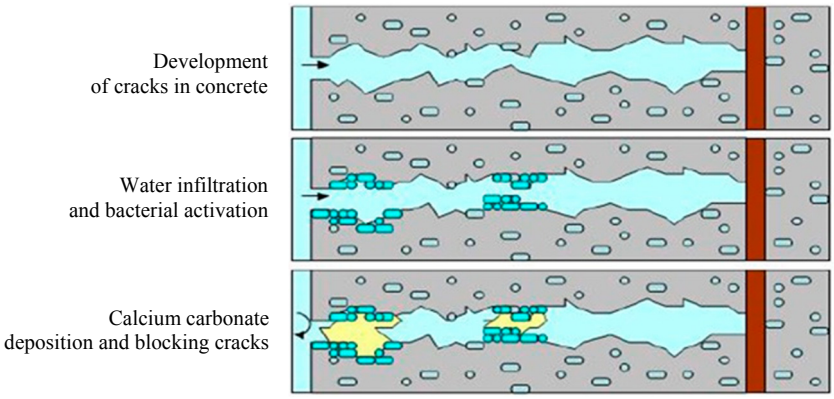

Figure 3. The process of repairing cracks in smart concrete by bacteria
S o u r c e: compiled by K. Van Breugel [74].

The concept of the bacterial-based crack repair mechanism (Figure 3) is expected in this question. It states that after the concrete breaks, the bacteria in the cracks start to grow with water by precipitating minerals like calcium carbonate to seal the fissures and shield the steel from chemical attacks from the outside world. The aggregates used in this case make up about 50% of the total grain size. Replacing high-fracture sand and gravel with expanded clay particles will have consequences for the strength properties of the derived concrete. In this particular case we will have a 50% reduction in compressive strength after 28 days of processing compared to samples with similar compositions but without replacement of crushed sand with LECA. [68]. Although samples containing expanded clay (LECA) show a substantial decrease in strength, the repair capacity of cracks in the samples increases dramatically where expanded clay particles containing bacteria and the leading organic mineral compounds (calcium lactate) are used.

In concrete test specimens, identically sized expanded clay particles loaded with the biochemical self-healing agent (bacterial spores 1.7×105 g^{-1} expanded clay particles, corresponding to 5×10^7 spores dm^{-3} concrete, plus 5% w/w fraction calcium lactate, corresponding to 15 g dm^{-3} concrete) were used to replace a portion of the aggregate material, or the 2–4 mm size class. Loaded expanded clay particles were oven-dried for one week at 40ºC prior to application, or until no more weight loss from water evaporation was noticeable. Although the aggregate composition of the control specimens was comparable, the biochemical agent was not present in these enlarged clay particles. Expanded clay particles of both kinds loaded for bacterial specimensand empty for control specimens were checked. Table displays the composition of the concrete sample. The self-healing capacity of precracked concrete specimens is determined from cylindrical specimens treated with water for 50 days using very fine microscopic images before and after permeability [73]. Before that, the precracked concrete specimens are glued in an aluminum ring and permeability testing is performed on them. Cracks in concrete specimens (1.5 cm thick and 10 cm in diameter) are formed in a controlled manner using compressive and tensile stresses (Figure 4, *a*).

Compositions of concrete samples

Compositions	Volume, cm^3	Mass, g
LWA, 2–4 mm LECA	196	167
LWA, 1–2 mm LECA	147	125
Sand, 0.5–1 mm	147	397
Sand, 0.25–0.5 mm	128	346
Sand, 0.125–0.25 mm	69	186
Cement	122	384
Water	192	192
Total	1001	1796

S o u r c e: compiled by A.M. Neville [73].

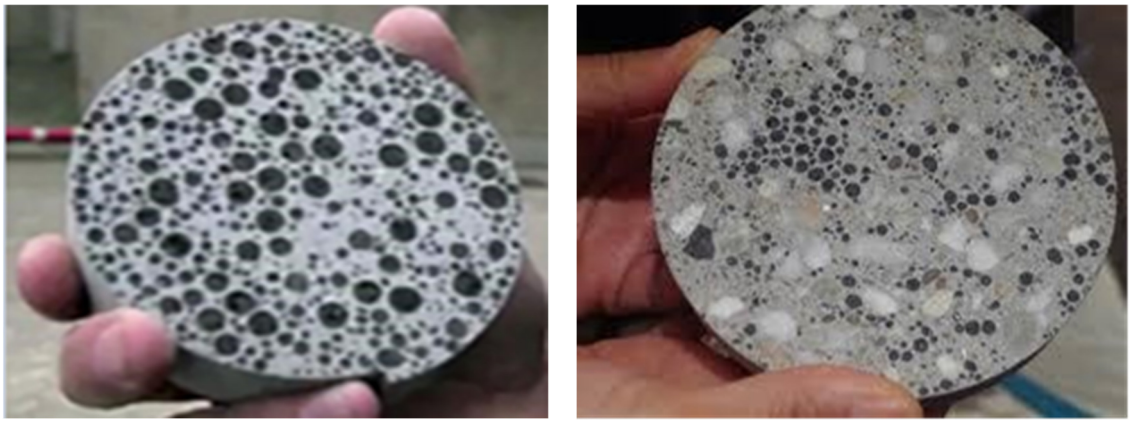

a *b*

Figure 4. Concrete with special additives:
a — with microcapsules containing crack fillers; *b* — self-healing concrete
S o u r c e: Bio-Concrete: The Walls are Alive. Available from:
https://sigearth.com/bio-concrete-the-walls-are-alive (accessed: 22.04.2025).

The resulting cracks are cracks 8 cm long that occur at a depth of 0.15 mm and a thickness of 1.5 cm along the sample. After the formation of cracks, both control samples containing expanded clay particles (LECA), without bacterial eggs and organic compounds, and samples containing bacteria to which expanded clay particles containing bacterial eggs and organic compounds were added, were submerged for 2 weeks. They are placed at room temperature. The permeability of all cracked samples is then automatically determined by the computer by recording the amount of water penetration within 24 hours. Comparison between control concrete specimens and specimens containing bacteria (Figure 4, *b*) shows major differences in permeability and, of course, in repair capacity or ability. The cracks of the 6 samples containing the bacteria are completely closed, meaning that we no longer have any permeability (0 ml/h), but only 2 of the 6 control samples almost recover; the other 4 samples will have water permeability 0 ml/h to 2 ml/h [69]. Microscopic testing of the cracks (shown next to the concrete specimen in the water column) indicates that calcium carbonate deposition occurs on the basis of mineral sediments in both control and bacterial specimens. Calcium carbonate deposition in concrete specimens occurs significantly near the edges of the cracks, which prevents the main parts of the cracks from being repaired, while in samples containing bacteria, we have complete and effective repair of cracks, in which case mineral deposition often occurs inside the cracks.

3.2. Use of Filled Microcapsules to Repair Concrete (Micro Encapsulated Heating)

In this method, inspired by red blood cells in blood clotting and repair, very small capsules are injected into the concrete as a repair agent. The microcapsules carrying the repair agent are usually made of polymer particles embedded inside the capsule and with a catalyst coating in the body. The microcapsules are broken during impact with the crack and in the vicinity of the catalyst, they perform the polymerization action and by forming construction materials, they repair the cracks in the concrete [75]. In fact, spherical microcapsules act like red blood cells and catalysts act like platelets in the process of blood clotting when repairing an incision in the skin (Figure 5).

In this method, by increasing the number of microcapsules, the homogeneity and uniformity of concrete may be affected and may reduce the strength and toughness of the concrete piece. Therefore, in order to improve performance, there is a need to inject repair fluid through an intelligent system. Recent research indicates the possibility of micro vascular network in the form of transfer of the repair agent, relying on the capillary property from the source to the site of failure and polymerization in the vicinity of the catalyst,

resulting in the formation of hard material and crack repair. Future research will seek to develop a capillary network in the concrete carrying the restorative agent, as intelligently as the biological system. This method is based on intelligent methods that self-repair to close the cracks created in the concrete section. The capacity of microvascular networks to facilitate the repeated repair of damage in both synthetic and biological systems is particularly intriguing. For instance, damage to human skin may be repaired repeatedly in one place (Figure 6).

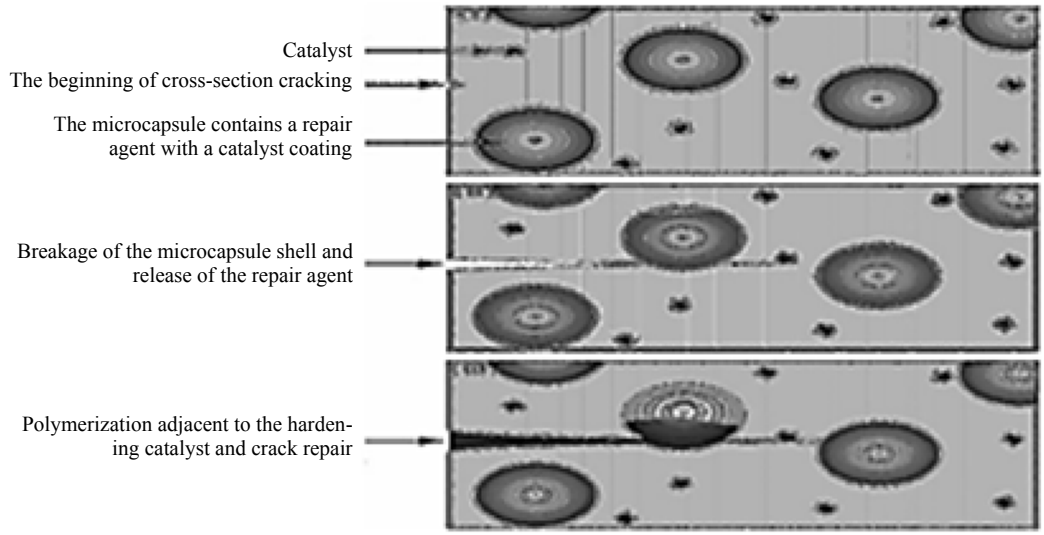

Figure 5. Mechanism of action of microcapsules in crack repair in self-compacting concrete

S o u r c e: compiled by M. Nejati [76].

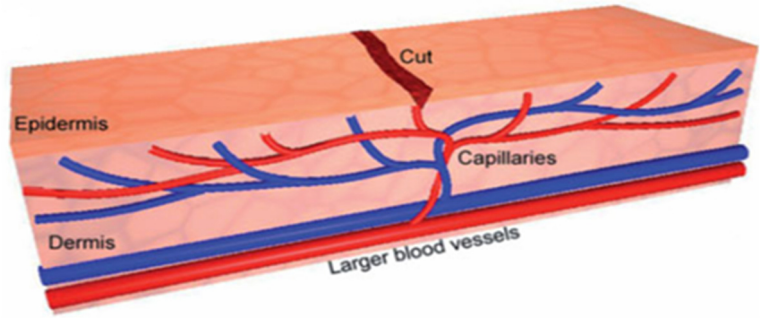

Figure 6. Concrete healing by a capillary network for the development and installation of microcapsules inspired by a biological system

S o u r c e: compiled by M. Nejati [76].

3.3. Heat Zone Selector Method (Selective Heating)

Formerly, one of the most efficient and intelligent self-healing systems is the heating zone selector system. This system consists of two main parts:

1. Self-diagnostic composites made of fibers and conductors of electricity that also have the capability of a strain gauge and as an efficient material have the ability to record the time history of failure in the structure.

2. The repair part (Heat-Plasticity Organic Film Pipe), which consists of pipes made of materials with plasticity and ductility against heat and the content of the repair agent, in such a way that they prevent the repair agent from leaving before spreading any cracks. When a crack occurs in the part, the first part detects

a slight strain at the crack site as a sensor and by sending a message to the repairing part (like the function of neurons in the body of living things), the repairing agent is released and repairs the crack [75]. Of course, the design of this system, which uses thermal energy to repair the release of the repair agent trapped in the coating, is associated with many sensitivities. So that the increase in temperature in concrete should not lead to evaporation of internal water and disintegration of the internal structure or any other harmful process for the strength and functional properties of concrete. This system, when completed, can provide external human control to the demolition process outside the structure by monitoring information and pathology and displaying defects, which will lead to a huge change in the concrete improvement and repair industry in sensitive structures.

3.4. Use of Cement Composites for Automatic Repair of Concrete (Engineered Cementitious Composite-ECC)

The performance of concretes that are made using only engineered cementitious composites (ECCs) is inspired by the healing of injuries to living organisms.

This system does not allow cracks to spread and to create deep cracks as it is continuously repairing the resulting small cracks (injuries), even if the damaged concrete piece is repeatedly loaded. In fact, the most important characteristic of ECC is that only hair-wide cracks with a maximum width of 60 micrometers will be possible to repair, instead of deep cracks in concrete. In other words, new concretes (ECC) have a considerable flexibility compared to conventional concretes [68]. Research shows that the use of fly ash pozzolans in ECC greatly improves the performance and repair of concrete. Air ash reacts with calcium hydroxide from the hydration process of cement to produce a white gel that is capable of suturing hair-wide cracks and self-healing (Figure 7).

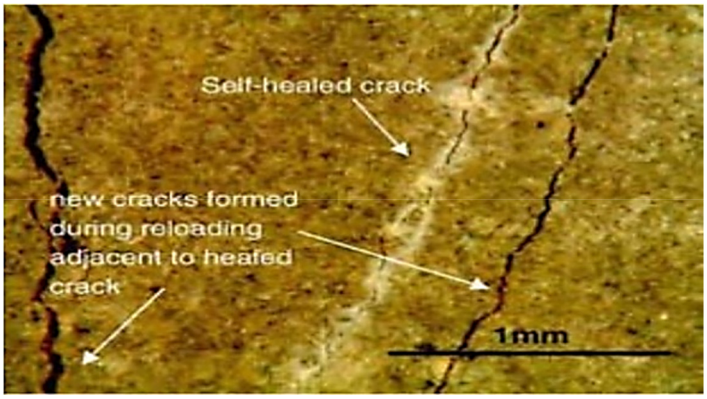

Figure 7. Self-repair of cracks in ECC concrete and expansion of cracks after reloading
S o u r c e: compiled by M. Nejati [76].

This type of self-repairing concrete is very important for protection of reinforced concrete in corrosive environments such as chlorinated environments where the possibility of chlorine ions dissolved in water can penetrate through micro cracks and start corrosion of reinforcements and as a result to reduce the overall strength of reinforced concrete.

3.5. Carbon Nanotubes

Carbon nanotubes (CNTs) are an allotropic form of carbon that was first discovered in Russia in 1952 but forgotten. It again found a special place in the nanotechnology circle in 1990. Nanotubes are produced in cylindrical forms of Single Walled Nano Tubes (SWNT) and Multi Walled Nano Tubes (MWNT) with length up to several millimeters (Figure 8).

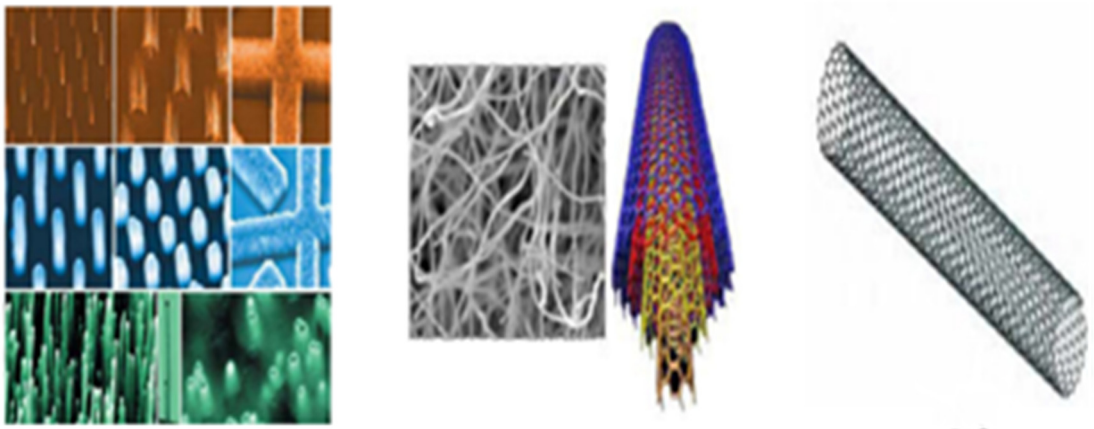

a *b* *c*

Figure 8. Different types of carbon nanotubes:
a — Single-walled carbon nanotubes; *b* — multi-walled carbon nanotubes, *c* — CNT pipes are magnified
S o u r c e: compiled by M. Nejati [76].

The mechanical properties of the concrete can be improved by adding small amounts of CNT (about 1 wt.%) to the cement mixture. These nanomaterials are also used in self-healing concrete processes. Of course, the main problem of using CNT in concrete is the connection of nanotubes to each other as strings and lack of sufficient adhesion between them in concrete [71]. Research is still ongoing to investigate how these materials are used in the self-healing process.

3.6. Use Hollow Fibers

In the method of using fluorescent dyes in the current repair agent in these fibers, the phenomenon of bruising in living organisms is simulated, which itself plays an important role in identifying the site of injury. The repair agent is released from a thin hollow fiber to fill the cracks, and as a result the crack is repaired [71]. The mechanism of repairing by hollow fiber method is shown in Figure 9.

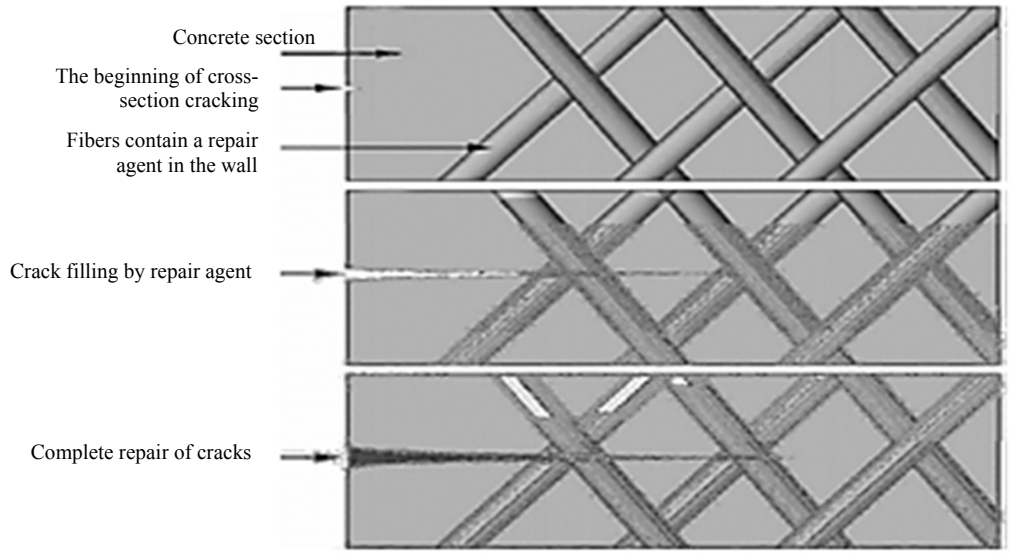

Figure 9. Mechanism of crack repair by hollow fiber method
S o u r c e: compiled by M. Nejati [76].

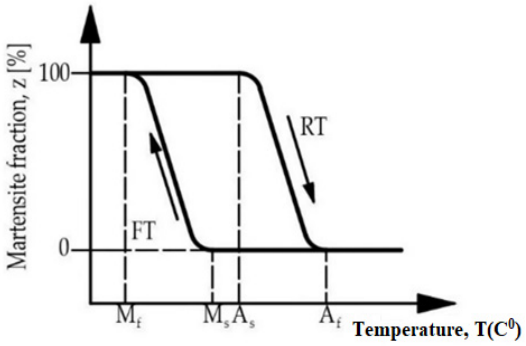

Figure 10. Behavior of shape-memory alloys in stress-free state and under the influence of temperature changes

S o u r c e: compiled by A. Cladera [82].

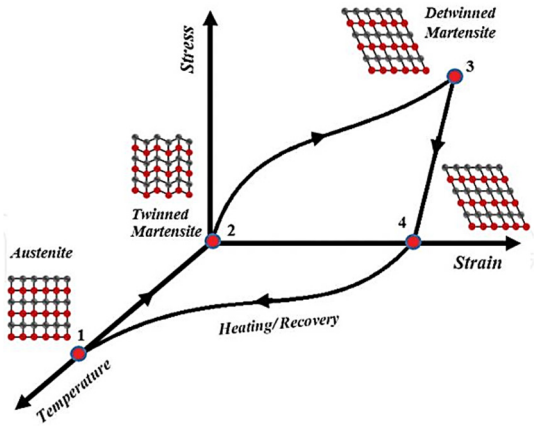

Figure 11. Stress-strain curve of super-elastic Property

S o u r c e: compiled by D.C. Lagoudas [83].

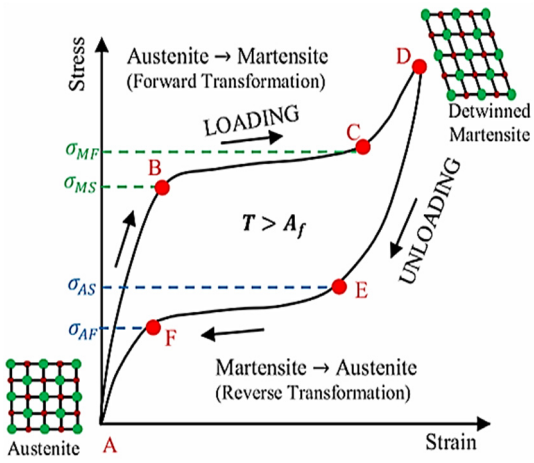

Figure 12. Stress-strain curve of shape memory property

S o u r c e: compiled by D.C. Lagoudas [83].

3.7. Using of Memory Alloys in Intelligent Self-Compacting Concrete

Shaped memory alloys are alloys with special ability to recover their original shape after deformation due to temperature and stress. In 1932, the Swedish scientist Lander first discovered super-elastic behavior in cation gold (Au-Cd) [79]. In 1951, Cheng and Reed discovered a reversible phase conversion in the same alloy, which is also the first recorded phase conversion. In 1963, Boiler and colleagues at the US Naval Weapons Laboratory discovered a shape memory effect on a nickel-titanium (Ni–Ti) alloy and named it Nitinol [26]. About 30 types of memory alloys have been reported so far [80].

The reason for the unique behavioral properties of shape-memory alloys should be sought in their multiphase or multi-structural nature. In other words, the arrangement of the atoms of shape-memory alloys within their crystal lattice gives rise to two states of behavior, martensite and austenite. The austenitic state is stable at high temperatures and low stresses and is responsible for super-elastic behavior. Martensite is stable at low temperatures and is responsible for developing shape memory behavior. When the material is cooled (without stresses), the first phase transition, known as a martensitic (or forward) transformation (FT), takes place. At the temperature Ms (martensite start), the martensite starts to form, and at the temperature Mf (martensite completion), the process is complete. Heating the material (without any stresses) causes the reverse transformation (RT), which starts at the austenite start temperature (As) and ends at the austenite finish temperature (Af). Figure 10 illustrates these procedures. Different forms of martensite phase can also be converted to each other at low temperatures and form the process of reorientation or pairing and non-pairing. Figures 11 and 12 show the strain stress curves for super-elastic behavior and memory property [81].

3.8. Performance of Self-Healing Concrete

Self-healing concrete works in such a way that when a crack is created in it and a very thin white layer of calcium carbonate acts and prevents the spread of cracks and it actually repairs cracks. Calcium carbonate is a very resistant compound that is found in nature in abundance in strong fortifications such as turtles and snails. Wetting and drying the concrete to repair the joint may take between 4 and 5 times [85]. Today, builders reinforce concrete with steel bars to keep them as small as possible. But still these cracks are not small enough to be repaired because of the salts that sometimes penetrate the concrete through the cracks for

defrosting. They cause corrosion in reinforcements and reduce the overall strength of reinforced concrete. Self-repairing concrete is completely safe from corrosion as it does not need to be reinforced and reinforced to keep cracks small. By reversing the process of concrete deterioration and significantly reducing costs and environmental effects in creating new buildings, using this self-healing concrete, the building can be restored for a longer period and self-healing concrete can be used optimally. Regarding the new scientific achievement of self-healing concrete, which has attracted the attention of the civil engineering scientific community, there are a few notable points that we will address:

- More comprehensive information explaining how this project works and detailed test results will soon be available to the public in future issues of several prestigious scientific journals as well as the University of Michigan Science Database. Professor Victor Lee, the original inventor of this material in 2009 at the International Conference on Self-Repairing Materials in Chicago, presented all the results and performance of this material in the article entitled "Automatic repair process of cementitious compounds in wet cycles" and offered multiple drying.
- According to the project's researchers, they are currently studying how to enter the construction industry. Imagine buildings that do not use reinforced concrete or the volume of use of steel materials in it is significantly reduced, this equates to a significant resistance deduction from their manufacturing costs or even imagine that there is no need for long-term retrofitting and restoration of structures as before. All these ideas create only one result in the minds of engineers and specialists, that self-repairing concrete made a revolution in the construction industry.
- Another point to note is how the researchers from the University of Michigan have achieved these astonishing results in recent scientific achievement. Previously an article was presented about a new bracing system for tall structures reinforced with concrete with steel fibers, which was also one of the recent scientific achievements of the University of Michigan.

The key results of the study on advanced self-healing and smart concrete technologies yielded significant findings in terms of material performance, durability and sustainability are summarized below:

1. **Self-Healing Efficiency**

Bacterial Self-Healing Concrete:

- Achieved 100% crack closure within two months, compared to only 33% in conventional concrete.
- Bacillus bacteria, embedded in porous expanded clay (LECA), produced calcium carbonate ($CaCO_3$) to autonomously seal cracks.
- Bacterial viability increased from 2 months (unprotected) to 6 months (protected in LECA), enhancing long-term self-repair capability.

Microencapsulation & Hollow Fibers:

- Microcapsules filled with healing agents (e.g., polymers) ruptured upon cracking, releasing repair material.
- Hollow fibers demonstrated self-repair efficiency by mimicking biological bruising, enabling crack detection and sealing.

2. **Mechanical & Durability Enhancements**

Nanotechnology in Concrete:

- Nano-silica and carbon nanotubes (CNTs) improved compressive strength, impermeability, and resistance to chloride penetration.
- Challenges included uniform nanoparticle dispersion and high-water absorption, requiring optimized mixing techniques.

Shape Memory Alloys (SMAs):

- Nickel-Titanium (Ni-Ti) alloys enabled crack recovery through super-elasticity and shape memory effects, reducing structural deformation.

3. **Biological Concrete for Sustainable Facades.** Three-layer biological concrete system (waterproofing, biological, and discontinuous cover layers) supported moss and microalgae growth.

Benefits included:

- CO_2 absorption & O_2 production (improving air quality).
- Thermal regulation (reducing building energy consumption).
- Self-sustaining vegetation without external irrigation.

4. **Smart Concrete & AI Integration**
   - Self-sensing concrete with embedded sensors allowed real-time crack detection and dynamic load analysis.
   - AI-controlled neural networks optimized self-healing responses, improving structural longevity.
5. **Challenges & Limitations**
   - High production costs of nanomaterials and bacterial additives to concrete.
   - Short-term viability of bacteria in harsh concrete environments.
   - Scalability issues for large-scale construction applications.

4. Conclusion

In recent years, the technology of making concrete to compensate for the disadvantages in concrete has made a lot of progress. The use of complex approach to concrete or the use of special cements leads to some special features of concrete. According to the above, it can be said that in fact concrete is intelligent and lively material that is able to be changed including through nanotechnology.

The concrete industry is one of the most widely used industries today, and in recent years, the amazing achievements of nanotechnologies to improve its behavior and performance, has evoked a unique way in this industry for researchers. Meanwhile, the process of self-healing, by imitating what happens in the body of living organisms to deal with damage, is being developed with extensive research. Obviously, the development of these methods and their application in the construction industry will have a great impact on increasing the safety of structures in line with the goals of sustainable development. Also, the current high costs of nanotechnology products, with mass production and consideration of long-term return on investment due to increased useful life of the structure and reduced repair costs, will be economically justified. On the other hand, inactive bacteria embedded in LECA can significantly self-repair and close cracks created in concrete sections. Based on what has been stated by different recearchers, it was observed that Bacillus was suitable for use as a repair agent for self-compacting concrete cracks, because there was 100% crack recovery in 2 months in concrete samples containing bacteria, while in the control samples there was 33% crack recovery.

The viability of bacterial eggs increases from 2 to 6 months when added to LECA in a protected form compared to direct (unprotected) addition. From this study it can be concluded that active bacteria due to mineral deposition, can cause effective closure of cracks and at the same time reduce the permeability of concrete. The future of construction lies in the development of smart, self-sustaining materials that enhance durability, reduce maintenance costs, and minimize environmental impact. This study explored the integration of nanotechnology, biotechnology, and artificial intelligence in concrete production, leading to groundbreaking advancements such as self-healing concrete, biological concrete, and intelligent self-compacting concrete. The main findings show that:

1. Nanomaterials (nano-silica, carbon nanotubes) significantly improve concrete's mechanical properties, impermeability and resistance to environmental degradation.

2. Microbial self-healing concrete (using Bacillus bacteria) achieves 100% crack closure within two months, compared to only 33% in conventional concrete, through bio-mineralization (calcium carbonate precipitation).

3. Biological concrete integrates vegetation into structural elements, offering thermal regulation, CO_2 absorption, and aesthetic benefits, while self-healing mechanisms eliminate the need for manual repairs.

4. Smart concrete leverages shape-memory alloys, microcapsules, and hollow fibers to autonomously detect and repair damage, extending structural lifespan.

Despite challenges such as high production costs, nanoparticle dispersion, and long-term bacterial viability, these innovations represent a paradigm shift toward sustainable, resilient, and intelligent infrastructure. Future research should focus on scaling production, optimizing cost-efficiency, and ensuring environmental safety to facilitate widespread adoption. By embracing these advancements, the construction industry can move toward self-repairing, energy-efficient, and eco-friendly structures, revolutionizing how we build for generations to come.

References

1. Alam M.S., Youssef M.A., Nehdi M.L. Exploratory investigation on mechanical anchors for connecting SMA bars to steel or FRP bars. *Materials and Structure.* 2010;43(1):91–107. https://doi.org/10.1617/s11527-010-9601-0

2. Edvardsen C. Water permeability and autogenous healing of cracks in concrete. *ACI Materials Journal*. 1999; 96(4):448–454. https://doi.org/10.1680/iicsdac.28241.0047

3. Jonker H.M. Self healing concrete: A Biological Approach. In: van der Zwaag S., editor. *Self Healing Materials. Springer Series in Materials Science.* Dordrecht: Springer; 2007;100:195–204. https://doi.org/10.1007/978-1-4020-6250-6_9

4. Wang J., Van Tittelboom K., De Belie N., Verstraete W. Use of silica gel or polyurethane immobilized bacteria for self-healing concrete. *Construction and Building Materials*. 2012;26(1):532–540. https://doi.org/10.1016/j.conbuildmat. 2011.06.054

5. Monteiro P., Miller S., Horvath A. Towards sustainable concrete. *Nature Materials*. 2017;16(7):698–699. https:// doi.org/10.1038/nmat4930

6. Polonina E.N., Leonovich S.N, Zhdanok S.A. Nanogranular Nature of CSH: Experimental Confirmation by Nanoindentation. *J Eng Phys Thermophy*. 2024;97:617–624. https://doi.org/10.1007/s10891-024-02930-1

7. Birgisson B., Mukhopadhyay A.K., Geary G., Khan M., & Sobolev K. *Nanotechnology in concrete materials: A synopsis*. Washington, USA: Transportation Research Board; 2012. https://doi.org/10.17226/22672

8. Balaguru P.N., Chong K. *Nanotechnology and concrete: research opportunities. SP-254: Nanotechnology of concrete: Recent Developments and Future Perspectives*. 2008. https://doi.org/10.14359/20208

9. Kawashima S., Pengkun H., David J. Corr D.J., Surendra P., Shah S.P. Modification of Cement-Based Materials with Nanoparticles. *Cement & Concrete Composites*. 2013;6:8–15. https://doi.org/10.1016/j.cemconcomp.2012.06.012

10. Falikman V.R., Petushkov A.V. Development of Russian Market of Nanotechnology Construction Products till 2020, *4th International Symposium on Nanotechnology in Construction*. 2012. https://sciup.org/14265685

11. Lackhoff M., Prieto X., Nestle N., Dehn F., Niessner R. Photocatalytic activity of semiconductor-modified cement influence of semiconductor type and cement ageing. *Applied Catalysis B Environmental.* 2003;43(3):205–216. https://doi.org/ 10.1016/S0926-3373(02)00303-X.

12. Li H., Xiao H.G., Ou J.P. A Study on Mechanical and pressure-sensitive properties of cement mortar with nanophase materials. *Cement and Concrete Research.* 2004;34(3):435–438. https://doi.org/10.1016/j.cemconres.2003.08.025

13. Jayapalan A.R., Lee B.Y. Kurtis K.E. Can nanotechnology be 'green'? Comparing efficacy of nano and microparticles in cementitious materials. *Cement & Concrete Composites.* 2013;36(1):6–24. https://doi.org/10.1016/j.cemconcomp. 2012.11.002

14. Porro A., Dolado J.S., Campillo I., Erkizia E., De Miguel Y., De Ibarra Y., Ayuela A. Effects of nanosilica additions on cement pastes. *Applications of Nanotechnology in Concrete Design*: *Proceedings of the International Conference, University of Dundee, Scotland, UK, 2005.* p. 87–96. https://doi.org/10.1680/aonicd.34082.0009

15. Qing Y., Zenan Z., Deyu K., Rongshen C. Influence of Nano-SiO2 Addition on Properties of Hardened Cement Paste as Compared with Silica Fume. *Construction and Building Materials.* 2007;21(3):539–545. https://doi.org/10.1016/ j.conbuildmat.2005.09.001

16. Björnström J., Martinelli A., Matic A., Börjesson L., Panas I. accelerating effects of colloidal Na. *Chemical Physics Letters*. 2004;392(1-3):242–248. https://doi.org/10.1016/j.cplett.2004.05.071

17. Zhang P., Han S., Golewski G.L., Wang X. Nanoparticle-reinforced building materials with applications in civil engineering. *Advances in Mechanical Engineering.* 2014;12(10). https://doi.org/10.1177/1687814020965438

18. Sanchez F., Sobolev K. Nanotechnology in Concrete — A Review. *Construction and Building Materials*. 2010; 24(11):2060–2071. https://doi.org/10.1016/j.conbuildmat.2010.03.014

19. Land G., Stephan D. The Influence of nano-silica on the hydration of ordinary Portland cement. *J Mater Sci*. 2012;47(2):1011–1017. https://doi.org/10.1007/s10853-011-5881-1

20. Thomas J.J., Jennings H.M., Chen J.J. Influence of nucleation seeding on the hydration mechanisms of tricalcium silicate and cement. *J. Phys. Chem. C.* 2009;113(11):4327–4334. https://doi.org/10.1021/jp809811w

21. Alizadeh R., Beaudoin J., Raki L., Rakar J., Moudrakovski I. C-S-H seeding: an approach for the nanostructural tailoring of cement-based materials. *13th International Congress on the Chemistry of Cement.* Madrid, Spain, 2011. Record identifier: 0fa8151f-e642-4870-bfc3-b74202623ff4

22. Nicoleau L. New Calcium silicate hydrate network. *Journal of the Transportation Research Board*. 2010; 2142(2142):42–51. https://doi.org/10.3141/2142-07

23. Nicoleau L. Accelerated growth of calcium silicate hydrates: Experiments and simulations. *Cement and Concrete Research*. 2011;41:1339–1348. https://doi.org/10.1016/j.cemconres.2011.04.012

24. De Belie N., Gruyaert E., Al-Tabbaa A., et al. A Review of Self-Healing Concrete for Damage Management of Structures. *Advanced Materials Interfaces*. 2018;5(17):1800074. https://doi.org/10.1002/admi.201800074

25. Ashraf W., Olek J., and Jain J. Microscopic features of non-hydraulic calcium silicate cement paste and mortar. Cem. Concr. Res. 2017;100:361–372. https://doi.org/10.1016/j.cemconres.2017.07.001

26. Konsta M., Metaxa Z., Shan S.P. Highly dispersed carbon nanotube reinforced cement based materials. *Cement and Concrete Composites*. 2020;40(7):1052–1059. https://doi.org/10.1016/j.cemconres.2010.02.015

27. Liew K., Kai M., Zhang L. Carbon nanotube reinforced cementitious composites: an overview. *Compos. A Appl. Sci. Manuf.* 2016;91(1):301–323. https://doi.org/10.1016/j.compositesa.2016.10.020

28. Sanchez F., Sobolev K. Nanotechnology in concrete — A review. *Construction and Building Materials*. 2010; 24(11):2060–2071. https://doi.org/10.1016/j.conbuildmat.2010.03.014

29. Pietroiusti A. Stockmann-Juvala H., Lucaroni F., Savolainen K. Nanomaterial exposure, toxicity, and impact on human health. *WIREs Nanomedicine and Nanobiotechnology*. 2018;10(5):e1513. https://doi.org/10.1002/wnan.1513

30. Saleem H., Zaidi S.J., Alnuaimi N.A. Recent advancements in the nanomaterial application in concrete and its ecological impact. *Materials.* 2021;14(21):6387. https://doi.org/10.3390/ma14216387

31. Feynman R. There's plenty of room at the bottom. *Caltech Engineering and Science.* 1960;23(5):22–36. Available from: https://calteches.library.caltech.edu/47/2/1960Bottom.pdf (accessed: 12.03.2025)

32. Constantinides G., Ulm F.-J. The nanogranular nature of C-S-H. *Journal of the Mechanics and Physics of Solids*. 2007;55(1):64–90. https://doi.org/10.1016/j.jmps.2006.06.003

33. Jackson M.D., Chae S.R., Mulcahy S.R., Meral C, Taylor R., Li P., Emwas A.H., Moon J., Yoon S., et al. 2013, Unlocking the secrets of Al-tobermorite in Roman seawater concrete. *American Mineralogist.* 2013;98(10):1661–1677. https://doi.org/10.2138/am.2013.4484

34. Mehta P.K., Monteiro P.J.M. *Concrete: microstructure, properties, and materials*. 4th ed. New York: McGraw-Hill Education; 2014. ISBN 9780071797870

35. Jonkers H.M. Self-healing concrete: A biological approach. In: van der Zwaag S., editor. *Self-Healing Materials: An Alternative Approach to 20 Centuries of Material Science.* Springer, Inc., The Netherlands. 2007. p. 195–204. https://doi.org/10.1007/978-1-4020-6250-6_9

36. Jonkers H.M., Schlangen E. Crack repair by concrete-immobilized bacteria. *Proceedings of the first international conference on self-healing materials*. Springer; 2007. P. 1–7. Available from: https://scispace.com/pdf/crack-repair-by-concrete-immobilized-bacteria-3e9mtjsxsm.pdf (accessed: 12.03.2025)

37. Jonkers H.M., Thijssen A., Muyzer G., Copuroglu O., Schlangen E. Application of bacteria as self-healing agent for the development of sustainable concrete. *Ecol Eng*. 2010;36(2):230–235. https://doi.org/10.1016/j.ecoleng.2008.12.036

38. Radhakumar L., Murugan S., Comparative study on the strength behavior of self-healing concrete using silica gel and bacteria as healing agents. *Journal of Materials in Civil Engineering*. 2023;35(12):15986. https://doi.org/10.1061/JMCEE7.MTENG-15986

39. Lucas S.S., Moxhama C., Tziviloglou E., Jonkers H. Study of self-healing properties in concrete with bacteria encapsulated in expanded clay. *Science and Technology of Materials.* 2018;30:93–98.

40. Jonkers H.M. Bacteria-based self-healing concrete. *Heron Journal.* 2011;56(1):49–79. Available from: https://heronjournal.nl/56-12/1.pdf (accessed: 12.03.2025)

41. Mors R., Jonkers H. Bacteria-based self-healing concrete: evaluation of full scale demonstrator projects. *RILEM Technical Letters*. 2020;4:138–144. https://doi.org/10.21809/rilemtechlett.2019.93

42. Jonkers H.M., Influence of self-healing induced by polylactic-acid and alkanoates-derivates precursors on transport properties and chloride penetration resistance of sound and cracked mortar specimens. *Construction and Building Materials.* 2022;319(8):26081. https://doi.org/10.1016/j.conbuildmat.2021.126081

43. Wiktor V., Jonkers H.M. Quantification of crack-healing in novel bacteria-based self-healing concrete. *Cem Concr Compos*. 2011;33(7):763–770. https://doi.org/10.1016/j.cemconcomp.2011.03.012

44. Erşan Y.Ç., Gruyaert E., Louis G., Lors C., De Belie N., Boon N. Self-protected nitrate reducing culture for intrinsic repair of concrete cracks. *Front Microbiol*. 2015;6:1228. https://doi.org/10.3389/fmicb.2015.01228

45. Jonkers H.M., Schlanger E. *Development of a bacteria-based self-healing concrete*. Tailor Made Concrete Structures — Walraven & Stoelhorst (eds). London: Taylor & Francis Group, 2008. ISBN 978-0-415-47535-8 https://doi.org/10.1201/9781439828410.ch72

46. Tziviloglou E., Virginie W., Jonkers H.M, Schlangen E. selection of nutrient used in biogenic healing agent for cementitious materials. *Frontiers in Materials.* 2017;4:15. https://doi.org/10.3389/fmats.2017.00015

47. Fytili D., Zabaniotou A. Utilization of sewage sludge in EU application of old and new methods — A review. *Renew Sustain Energy Rev*. 2008;12(1):116–140. https://doi.org/10.1016/j.rser.2006.05.014

48. Kacprzak M., Neczaj E., Fijałkowski K., Grobelak A., Grosser A., Worwag M., Rorat A., Brattebo H., Åsgeir Almås A., Singh B.R. Sewage sludge disposal strategies for sustainable development. *Environ Res*. 2017;156:39–46. https://doi.org/10.1016/j.envres.2017.03.010

49. Cyr M., Coutand M., Clastres P. Technological and environmental behavior of sewage sludge ash (SSA) in cement-based materials. *Cem Concr Res*. 2007;37(8):1278–1289. https://doi.org/10.1016/j.cemconres.2007.04.003

50. Sanchez F., Sobolev K. Nanotechnology in concrete — A review. *Constr Build Mater*. 2010;24(11):2060–2071. *https://doi.org/10.1016/j.conbuildmat.2010.03.014*

51. Vashistha P., Kumar V., Singh S.K., Dutt D., Tomar G. Sustainable utilization of deinking paper mill sludge for the manufacture of building bricks. *J Clean Prod*. 2018;204:321–333. https://doi.org/10.1016/j.jclepro.2018.09.028

52. Khaliq W., Ehsan M.B. Crack healing in concrete using bio-mineralization techniques. *Constr Build Mater*. 2016;102(1):349–357. https://doi.org/10.1016/j.conbuildmat.2015.11.006

53. Jonkers H.M., Schlangen E. Development of bacteria-based self-healing concrete. *Tailor Made Concr Struct*. 2008. p. 425–430. https://doi.org/10.1201/9781439828410.ch72

54. Wiktor V., Jonkers H.M. Bacteria-based concrete: from concept to market. *Smart Materials and Structures* 2016;25(8):084006. https://doi.org/10.1088/0964-1726/25/8/084006

55. White S.R., Sottos, N., Geubelle, P., Moore J.S., Kessler M.R., Sriram S.R., Brown E.N. & Viswanathan S. Autonomic healing of polymer composites. *Nature*. 2001;409:794–797. https://doi.org/10.1038/35057232

56. Elgendy I.M., Elkaliny N.E., Saleh H.M., Darwish G.O., et. al. Bacteria-powered self-healing concrete: Break-throughs, challenges, and future prospects. *Journal of Industrial Microbiology and Biotechnology*. 2025;52:kuae051. https://doi.org/10.1093/jimb/kuae051

57. Seifan M., Samani A.K. & Berenjian A. Bioconcrete: next generation of self-healing concrete. *Appl Microbiol Biotechnol.* 2016;100:2591–2602 https://doi.org/10.1007/s00253-016-7316-z

58. De Belie N., Gruaert E., Al-TabbaaA., Antonaci P., Baera C., et al. A review of self-healing concrete for damage management of structures. *Advanced Materials Interfaces*. 2018;5(17):1800074. https://doi.org/10.1002/admi.201800074

59. Hensel M.U. Performance-oriented architecture — towards a biological paradigm for architectural design and the built environment. *Form Academisk*. 2010;3(1):36–56. https://doi.org/10.7577/formakademisk.138

60. Patel S. Bio-receptive concrete for building façade application. 2021.

61. De Muynck W., Debrouwer D., Nele de Belie, Verstraete W. Bacterial carbonate precipitation improves the durability of cementitious materials. *Cement and Concrete Research*. 2008;38(7):1005–1014. https://doi.org/10.1016/j.cemconres.2008.03.005

62. Morakinyo T.E., Lai A.K., Lau K.K., Ng E. Thermal benefits of vertical greening in a high-density city: Case study of Hong Kong. *Urban Forestry & Urban Greening*. 2017;37:42–55. https://doi.org/10.1016/j.ufug.2017.11.010

63. Xu Q., Zhang W., Dong C., Sreeprasad T.S., Xia Z. 2016 Biomimetic selfcleaning surfaces: synthesis, mechanism and applications. *J.R. Soc. Interface*. 2016;13:20160300. http://dx.doi.org/10.1098/rsif.2016.0300

64. Uygunogly T., Topcu I.B. Effect of Water Proofing Materials on Self-Healing Concrete. *European Journal of Formal Sciences and Engineering.* 2020;3(1):35. https://doi.org/10.26417/190vto47v

65. Frantová M., Štemberk P., Wudi V., Husarčíková M. Aplicability of magnesium phosphate cement for bioreceptive concrete tilesaplicability of magnesium phosphate cement for bioreceptive concrete tiles. *Civil Engineering Journal*. 2024;33(4):499–512. https://doi.org/10.14311/cej.2024.04.0034

66. Manso S., Castro-Gomes J. Green wall systems: A review of their characteristics. *Renewable and Sustainable Energy Reviews*. 2015;41:863–871. https://doi.org/10.1016/j.rser.2014.07.203

67. Jaubovskis R. Biophilic façades: The potentiality of bioreceptive concrete. *Buildings*. 2025;15(20):3646; https://doi.org/10.3390/buildings15203646

68. Li V.C., Yang E.H. Self healing in concrete materials. In: van der Zwaag S., editor. Self healing materials. Springer series in materials science. Dordrecht: Springer; 2007;100:161–193. https://doi.org/10.1007/978-1-4020-6250-6_8

69. Muller W., Pacheco V., Carvalho C.M., Fernandes F., Valiati V.H., Modolo R.C.E., Ehrenbring H.Z., Tutikian B.F. Analysis of cementitious matrices self-healing with bacillus bacteria. *Revista IBRACON de Estruturas e Materiais.* 2022; 15(4):e15404. https://doi.org/10.1590/s1983-41952022000400004

70. Roig-Flores M., Formagini S., Serna P. Self-healing concrete for sustainable infrastructure: From lab to field. *Materials*. 2021;14(15):4208. https://doi.org/10.3989/mc.2021.07320

71. Jody W.C. A Hollow Fiber Reinforced Polymer Composite Encompassing self-healing and Enhances Damage Visibility. *Composites Science and Technology*. 2005;65(11–12):1791–1799. https://doi.org/10.1016/j.compscitech.2005.03.008

72. Jonkers H.M., Schlangen E. Development of a bacteria-based self-healing concrete. In: Walraven JC & Stoelhorst D., editors. *Tailor made concrete structures — new solution our society. Proc. Int. FIB symposium.* 2008. P. 425–430. https://doi.org/10.1201/9781439828410.ch72

73. Neville A.M. Autogenous healing — A concrete miracle? *Concrete int.* 2002;24(11):76–82. Available from: https://trid.trb.org/View/728174 (accessed: 12.02.2025)

74. Van Breugel K. Self-healing material concepts as solution for aging infrastructure. In: *Proceedings of the 37th Conference on Our World in Concrete & Structures*. 2012;29:89–103.

75. Nishiwaki T., Mihashi H. Development of self-healing system for concrete with selective heating around crack. *Journal of Advanced concrete tec.* 2006;4(2):267–275. https://doi.org/10.3151/jact.4.267

76. Nejati M., Abbasnejad B. Increasing durability of concrete by nanotechnology and biotechnology materials for sustainable developments. *Conference: Creative Construction Conference.* Budapest, Hungary, 2013. p. 546–554.

77. Toohey K.S., Sottos N.R., Lewis J., Moore J.S., White S.R. Self-healing materials with microvascular networks. *Nature Materials.* 2007;6(8):581–585. https://doi.org/10.1038/nmat1934

78. Ayobami A.B., Williams K.K., Tolulope R.L., Rotimi E.S., Snyman J., Julius N. Use of sustainable materials in self-healing concrete. In book: *Strength of Materials [Working Title]*. 2020. https://doi.org/10.5772/intechopen.86768

79. De Muynck W., De Belie N., Verstraete W. Microbial carbonate precipitation in construction material: A review. *Ecological Engineering.* 2010;36(2):118–136. https://doi.org/10.1016/j.ecoleng.2009.02.006

80. Jonker H.M., Thijssen A., Muyzer G., Copuroglu O., Schlangen E. Application of bacteria as self-healing agent for the development of sustainable concrete. *Ecological Engineering.* 2010;36(2):230–235. https://doi.org/10.1016/j.ecoleng.2008.12.036

81. Lahmann D., Edvardsen C., Kessler S. Autogenous self-healing of concrete: Experimental design and test methods — A review. *Engineering Reports*. 2023;5(1):e12565. https://doi.org/10.1002/eng2.12565

82. Cladera A., Weber B., Leinenbach C., Czaderski C., Shahverdi M., Motavalli M. Iron-based shape memory alloys for civil engineering structures: An overview. *Construction and Building Materials.* 2014(63):281–293. https://doi.org/10.1016/j.conbuildmat.2014.04.032

83. Lagoudas D.C. *Shape memory alloys: Modeling and engineering applications.* Springer Science+Business Media. 2008. https://doi.org/10.1007/978-0-387-47685-8

84. Gołaszewski J., Klemczak B., Smolana A., Gołaszewska M., Cygan G., Mankel C., Peralta I., Röser F., Koenders E.A.B. Effect of foaming agent, binder and density on the compressive strength and thermal conductivity of ultra-light foam concrete. *Buildings*. 2022;12:1176. https://doi.org/10.3390/ buildings12081176

85. De Belie N., Gruyaert E., Al-Tabbaa A., Antonaci P., Baera C., Bajare D., Snoeck D.A Review of self-healing concrete for damage management of structures. *Advanced Materials Interface.* 2018;5(17):1800074. https://doi.org/10.1002/ admi.201800074

СТРОИТЕЛЬНАЯ МЕХАНИКА ИНЖЕНЕРНЫХ КОНСТРУКЦИЙ И СООРУЖЕНИЙ
STRUCTURAL MECHANICS OF ENGINEERING CONSTRUCTIONS AND BUILDINGS

2025. 21(6). 605–622

ISSN 1815-5235 (Print), 2587-8700 (Online)
HTTP://JOURNALS.RUDN.RU/STRUCTURAL-MECHANICS

ЭКСПЕРИМЕНТАЛЬНЫЕ ИССЛЕДОВАНИЯ
EXPERIMENTAL RESEARCH

DOI: 10.22363/1815-5235-2025-21-6-605-622
EDN: FWXOUY

Научная статья / Research article

Интегральный критерий выбора алюминиевого сплава для строительства резервуаров в условиях Арктики

О.А. Корнев[1], А.Н. Шувалов[1], А.В. Корнилова[1,2], В.А. Ермаков[1]✉

[1] Московский государственный строительный университет (национальный исследовательский университет), *Москва, Российская Федерация*
[2] Российский университет дружбы народов, *Москва, Российская Федерация*
✉ ermakov@mgsu.ru

Поступила в редакцию: 17 сентября 2025 г.
Доработана: 24 ноября 2025 г.
Принята к публикации: 30 ноября 2025 г.

Аннотация. Цель исследования — разработка интегрального критерия выбора алюминиевого сплава для резервуаростроения в условиях пониженных температур. В ходе работы были проведены экспериментальные исследования четырех алюминиевых сплавов 1915Т, 6082-Т6, АД35Т1, 1565ч согласно российским нормативам. Для обработки результатов испытаний применялись стандартные алгоритмы математической статистики: расчет выборочных характеристик, проверка выборок на нормальность распределения и исключение грубых погрешностей измерений. Выделены группы характеристик, влияющие на эффективность применения сплава: стандартные механические свойства, ударная вязкость, характеристики трещиностойкости, усталостные характеристики, сопротивление коррозии, стоимостно-весовые характеристики. Проведенные в процессе исследования экспертные опросы позволили определить весовые коэффициенты как внутри групп, так и самих групп при формировании интегрального критерия. Показано, что наибольший вес имеют усталостные характеристики и характеристики трещиностойкости, что указывает на необходимость включения расчета параметров усталости и трещиностойкости в нормативные документы по проектированию резервуаров из алюминиевых сплавов. Важность повышения усталостных характеристик и трещиностойкости алюминиевых сплавов для применения в арктических условиях должна быть учтена и при проектировании новых сплавов, и термических обработках существующих. Из рассмотренных в исследовании сплавов наилучший интегральный показатель у сплава 1915Т. Этот сплав обладает существенно более высокими усталостными характеристиками и ударной вязкостью по сравнению с остальными исследован-

Корнев Олег Александрович, заместитель директора Научно-исследовательского института экспериментальной механики, Национальный исследовательский Московский государственный строительный университет (НИУ МГСУ), Российская Федерация, 129337, г. Москва, Ярославское шоссе, д. 26; eLIBRARY SPIN-код: 4890-2128, ORCID: 0009-0009-5545-5284; e-mail: KornevOA@mgsu.ru

Шувалов Александр Николаевич, кандидат технических наук, доцент кафедры испытаний сооружений, Национальный исследовательский Московский государственный строительный университет (НИУ МГСУ), Российская Федерация, 129337, г. Москва, Ярославское шоссе, д. 26; eLIBRARY SPIN-код: 8488-4644, ORCID: 0009-0007-0289-7412; e-mail: AShuvalov@mgsu.ru

Корнилова Анна Владимировна, доктор технических наук, старший научный сотрудник Научно-исследовательского института экспериментальной механики, Национальный исследовательский Московский государственный строительный университет (НИУ МГСУ), Российская Федерация, 129337, г. Москва, Ярославское шоссе, д. 26; профессор кафедры строительных технологий и конструкционных материалов, инженерная академия, Российский университет дружбы народов, Российская Федерация, 117198, г. Москва, ул. Миклухо-Маклая, д. 6; eLIBRARY SPIN-код: 6569-6240, ORCID: 0000-0001-5569-9320; e-mail: KornilovaAV@mgsu.ru

Ермаков Валентин Алексеевич, кандидат технических наук, старший научный сотрудник Научно-исследовательского института экспериментальной механики, Национальный исследовательский Московский государственный строительный университет (НИУ МГСУ), Российская Федерация, 129337, г. Москва, Ярославское шоссе, д. 26; eLIBRARY SPIN-код: 3227-6815, ORCID: 0000-0002-8862-8139; e-mail: Ermakov@mgsu.ru

ными сплавами. Наихудший интегральный показатель у сплава АД35Т1, что косвенно подтверждает преимущества естественного старения алюминиевых сплавов. Лучшими стоимостно-весовыми характеристиками обладает сплав 1565ч. Дальнейшее исследование предполагает расширение показателей, входящих в предложенный интегральный критерий за счет введения показателей свариваемости.

Ключевые слова: алюминиевый сплав, пониженные температуры, ударная вязкость, усталостные характеристики, трещиностойкость, коррозионная стойкость, вес, стоимость

Заявление о конфликте интересов. Авторы заявляют об отсутствии конфликта интересов.

Вклад авторов: *Корнев О.А.* — общее руководство и проведение экспериментальных исследований; *Шувалов А.Н.* — разработка идеологии исследования; *Корнилова А.В.* — проведение опросов, экспериментальных данных, написание текста статьи; *Ермаков В.А.* — создание графического материала, написание теста статьи. Все авторы ознакомлены с окончательной версией статьи и одобрили ее.

Благодарности. Авторы благодарят профессора Андрея Валентиновича Коргина, коллектив лаборатории ЛИСМиК НИИ ЭМ, начальника научно-технического управления НИУ МГСУ доцента Павла Дмитриевича Капырина, руководство компании АО «Русал», Алюминиевую ассоциацию за предоставление материала для экспериментальных испытаний.

Для цитирования: *Корнев О.А., Шувалов А.Н., Корнилова А.В., Ермаков В.А.* Интегральный критерий выбора алюминиевого сплава для строительства резервуаров в условиях Арктики // Строительная механика инженерных конструкций и сооружений. 2025. Т. 21. № 6. С. 605–622. http://doi.org/10.22363/1815-5235-2025-21-6-605-622 EDN: FWXOUY

Integral Criterion for the Selection of Aluminum Alloy for the Construction of Reservoirs in the Arctic

Oleg A. Kornev[1], Aleksandr N. Shuvalov[1], Anna V. Kornilova[1,2], Valentin A. Ermakov[1]✉

[1] Moscow State University of Civil Engineering (National Research University), *Moscow, Russian Federation*
[2] RUDN University, *Moscow, Russian Federation*

✉ ermakov@mgsu.ru

Received: September 17, 2025
Revised: November 24, 2025
Accepted: November 30, 2025

Abstract. The purpose of the study is to develop an integral criterion for choosing an aluminum alloy for tank construction at low temperatures. In the course of the work, experimental studies of four aluminum alloys 1915T, 6082-T6, AD35T1, 1565ch were carried out in accordance with Russian standards. Standard mathematical statistics algorithms were used to process the test results: calculating sample characteristics, checking samples for the normality of the distribution, and eliminating gross measurement errors. Groups of characteristics that affect the effectiveness of the alloy are identified: standard mechanical properties, impact strength, crack resistance characteristics, fatigue characteristics, corrosion resistance, cost and weight characteristics. The expert surveys conducted during the study allowed to determine the weighting coefficients both within the groups and when forming the integral criterion. It is shown that fatigue characteristics and crack resistance characteristics have the greatest weight, which indicates the need to include the calculation of fatigue and crack resistance parameters in regulatory documents for the design of aluminum alloy tanks. The importance of increasing the fatigue characteristics and crack resistance of aluminum alloys for use in Arctic conditions should be taken into account when designing new alloys and thermal treatments of existing ones. Of the alloys considered in the study, alloy 1915T has the best integral index. This alloy has significantly higher fatigue characteristics and impact strength compared to the other alloys studied. The AD35T1 alloy has the worst integral index, which indirectly confirms the advantages of natural aging of aluminum alloys. Alloy 1565ch has the best cost and weight characteristics. Further research suggests expanding the indicators included in the proposed integral criterion by introducing weldability indicators.

***Oleg A. Kornev*,** Deputy Director, Scientific Research Institute of Experimental Mechanics, Moscow State University of Civil Engineering (National Research University), 26 Yaroslavskoye Shosse, Moscow, 129337, Russian Federation; eLIBRARY SPIN-code: 4890-2128, ORCID: 0009-0009-5545-5284; e-mail: KornevOA@mgsu.ru

Alexandr N. Shuvalov, Candidate of Technical Sciences, Associate Professor of the Department of Testing of Structures, Moscow State University of Civil Engineering (National Research University), 26 Yaroslavskoye Shosse, Moscow, 129337, Russian Federation; eLIBRARY SPIN-code: 8488-4644, ORCID: 0009-0007-0289-7412; e-mail: AShuvalov@mgsu.ru

Anna V. Kornilova, Doctor of Technical Sciences, Senior Researcher at the Scientific Research Institute of Experimental Mechanics, Moscow State University of Civil Engineering. University (National Research University); Professor of the Department of Construction Technology and Structural Materials, Academy of Engineering, RUDN University, 6 Miklukho-Maklaya St, Moscow, 117198, Russian Federation; eLIBRARY SPIN-code: 6569-6240, ORCID: 0000-0001-5569-9320; e-mail: KornilovaAV@mgsu.ru

Valentin A. Ermakov, Candidate of Technical Sciences, Senior Researcher at the Scientific Research Institute of Experimental Mechanics, Moscow State University of Civil Engineering (National Research University), 26 Yaroslavskoye Shosse, Moscow, 129337, Russian Federation; eLIBRARY SPIN-code: 3227-6815, ORCID: 0000-0002-8862-8139; e-mail: Ermakov@mgsu.ru

Keywords: aluminum alloy, low temperatures, impact strength, fatigue characteristics, crack resistance, corrosion resistance, weight, cost

Conflicts of interest. The authors declare that there is no conflict of interest.

Authors' contribution: *Kornev O.A.* — general guidance and conduct of experimental research; *Shuvalov A.N.* — development of research ideology; *Kornilova A.V.* — conducting surveys, experimental data, text writing; *Ermakov V.A.* — graphic material, text writing. All of the authors read and approved the final version of the article.

Acknowledgements. The authors would like to thank Professor Andrey Valentinovich Korgin, the staff of the LISMiK Laboratory of the EM Research Institute, the Head of the Scientific and Technical Department of the MGSU, Associate Professor Pavel Dmitrievich Kapyrin, the management of JSC Rusal, and the Aluminum Association for providing material for experimental testing.

For citation: Kornev O.A., Shuvalov A.N., Kornilova A.V., Ermakov V.A. Integral criterion for the selection of aluminum alloy for the construction of reservoirs in the Arctic. *Structural Mechanics of Engineering Constructions and Buildings.* 2025;21(6): 605–622. (In Russ.) http://doi.org/10.22363/1815-5235-2025-21-6-605-622 EDN: FWXOUY

1. Введение

В мире уделяется большое внимание ускорению развития Арктического пространства. Программы по освоению ресурсов Арктической зоны активно разрабатываются в США, Канаде, Дании, Исландии, Норвегии, Финляндии и Швеции. В Российской Федерации Указом Президента РФ[1] утверждена собственная Стратегия развития Арктической зоны и обеспечения национальной безопасности на период до 2035 г. Основным направлением стратегии является проведение фундаментальных и прикладных научных исследований в интересах освоения Арктики, создание функциональных и конструкционных материалов, необходимых для осуществления хозяйственной деятельности в арктических условиях.

Одним из путей реализации этого направления из вышеуказанной Стратегии является использование алюминиевых сплавов, которые обладают рядом известных преимуществ перед другими конструкционными и функциональными материалами. В [1] доказывается, что эти сплавы обладают высокой коррозионной стойкостью. В [2] доказана низкая степень влияния температуры окружающей среды на коррозионную стойкость алюминиевых сплавов и показаны перспективы применения сплавов алюминия в регионах с повышенной влажностью и в агрессивных средах. В [3] отражено влияние параметров термообработки на свойства широко применяемого алюминиевого сплава 6082. В [4] показано, что сплавы алюминия имеют малый удельный вес, при этом обеспечивают увеличение срока службы листовых конструкций по сравнению со стальным прокатом. В экспериментальном исследовании [5] выявлено, что при понижении температуры испытаний механические свойства алюминиевых сплав повышаются, что, в свою очередь, является положительным фактором для применения этих сплавов северных условиях. Кроме того, стальные вертикальные цилиндрические резервуары (ВЦР) уязвимы для испарений нефти и нефтепродуктов. При контакте паров сернистой нефти и нефтепродуктов со сплавами железа образуется сернистое железо, которое разъедает стенки и днища резервуара и увеличивает риск воспламенения.

Использование алюминиевых сплавов позволяет снизить транспортные расходы, уменьшить стоимость эксплуатационных расходов во время жизненного цикла объекта и его капитальных ремонтов. Кроме того, коррозионная стойкость позволяет существенно увеличивать срок службы объектов [4; 6]. В [6] проведено сравнение технико-экономических показателей резервуаров из стали и алюминиевого сплава АМг-6М одинаковой конструкции. Преимущество конструкции из алюминиевых сплавов проявилось в уменьшении удельной металлоемкости (на 32 % от сметной стоимости армирования фундаментной плиты), стоимости транспортировки (на 8 % при расчете тонны на километр), а также в уменьшении эксплуатационных расходов и сокращении числа капитальных

[1] Указ Президента РФ от 26 октября 2020 г. № 645 «О Стратегии развития Арктической зоны Российской Федерации и обеспечения национальной безопасности на период до 2035 года» (с изменениями и дополнениями).

ремонтов (на 5 % на первые 15 лет эксплуатации). Первые в Японии алюминиевые резервуары для хранения сжиженного кислорода, построенные в 1960 г., до сих пор находятся в эксплуатации. Резервуар емкостью 80000 м^3 имеет внутренний диаметр 50 м, толщина стенки в максимальной зоне достигает 69 мм. В качестве конструкционного материала использован алюминиевый сплав 5063-0. Вся цилиндрическая оболочка и 80 % кровельных конструкций выполнены автоматической сваркой (рис. 1).

В период с 2010 г. по настоящее время во всем мире растет интерес к применению алюминиевых сплавов при лабораторных, низких, сверхнизких и повышенных температурах [7–17]. В [7] изучалось влияние низкой температуры на механические свойства и микроструктуру алюминиевого сплава 6061-T6 (AA6061-T6), подвергнутого динамическому нагружению. В [8] исследовались свойства алюминиевого двутавра при низких температурах. Работа [9] посвящена влиянию температуры на коррозионные свойства сплавов. В [10] доказана эффективность криогенной обработки алюминиевых сплавов. В [11–15] представлены исследования различных аспектов усталости алюминиевых сплавов (величина предела выносливости при различных температурах и коэффициентах асимметрии цикла, угол наклона ветви многоцикловой усталости кривой Веллера). Кроме того, в [11–13] сделаны попытки прогнозирования срока службы конструкций из алюминиевых сплавов, в том числе с привлечением нейронных сетей [13]. В [14; 15] изучено влияние упрочняющих лазерных технологий на усталостную долговечность алюминиевых сплавов посредством введения твердых частиц и лазерным ударом, в [16] упрочнения предлагается проводить легированием редкоземельными элементами, в [17] сделана попытка прогнозировать свойства алюминиевого проката по дюраметрии.

Рис. 1. Вертикальные цилиндрические резервуары из алюминиевого сплава, построенные в Японии в 1960 г. (фото сделано в 2025 г.)

И с т о ч н и к: https://en.wikipedia.org/wiki/Liquefied_natural_gas_terminal

Figure 1. Vertical cylindrical aluminum alloy tanks, built in Japan in 1960 (photo taken in 2025)

S o u r c e: https://en.wikipedia.org/wiki/Liquefied_natural_gas_terminal

Наиболее эффективно применение алюминиевых сплавов для строительства резервуаров в условиях Крайнего Севера и приближенных к нему регионов. Однако для строительства таких резервуаров используют в основном стали[2], что увеличивает материальные затраты при монтаже и эксплуатации и повышает вероятность разрушения из-за охрупчивания в условиях пониженных температур. Так в феврале 1970 г. в Якутске Российской Федерации при температуре окружающего воздуха минус 57 °С полностью разрушился стальной ВЦР объемом 700 м^3 [18]. Хрупкая трещина возникла в нижнем уторном узле. Аналогичные аварии со стальными конструкциями ВЦР произошли в зимнее время в г. Воскресенске Челябинской обл. Российской Федерации (резервуар объемом 5000 м^3), в г. Пучеж Ивановской обл. Российской Федерации (резервуар объемом 2000 м^3) [19]. При составле-

[2] ГОСТ 31385-2023. Резервуары вертикальные цилиндрические стальные для нефти и нефтепродуктов. Общие технические условия. Москва : ФГБУ «РСТ», 2023. 122 с.

нии настоящего обзора аварий ВЦР не выявлено ни одного случая хрупкого разрушения конструкций из алюминиевых сплавов.

Однако случаи усталостного разрушения алюминиевых листовых конструкций отмечены в [20; 21], в связи с этим возникает необходимость исследовать закономерности образования усталостных трещин при отрицательных температурах эксплуатации. Но действующие нормативные документы проектирования металлических конструкций[3] предусматривают расчет листовых конструкций, в частности стальных резервуаров, только на воздействие статических нагрузок.

В 2016 г. был актуализирован свод правил[4], касающихся алюминиевых строительных конструкций, в том числе резервуаров для хранения нефти, нефтепродуктов и сжиженного газа, в котором также указывается, что Правила не распространяются на проектирование алюминиевых конструкций и сооружений, подвергающихся многократному воздействию нагрузок (т.е. не учитывается усталостная прочность). В связи с таким подходом мало исследованы усталостные характеристики ряда алюминиевых сплавов для строительства ВЦР в условиях Крайнего Севера, что затрудняет выбор сплавов для резервуаров, обеспечивающий оптимальные условия монтажа и эксплуатации конструкции.

При составлении обзора в наукометрических базах данных (РИНЦ, Scopus, Web Of Science) не обнаружено ни одного источника, в котором бы были сформулированы и статистически доказаны комплексные требования к характеристикам алюминиевых сплавов для конструкций, эксплуатируемых в условиях Крайнего Севера. В связи с этим была сформулирована *цель настоящего исследования* — разработка интегрального критерия, учитывающего комплекс характеристик алюминиевых сплавов, и на его основе алгоритма оптимизации выбора сплавов для ВЦР при отрицательных температурах эксплуатации. Объектом исследования являются алюминиевые сплавы для строительства резервуаров.

2. Методы, оборудование и материалы

В работе исследовались четыре наиболее применяемых для резервуаростроения алюминиевых сплава 1915Т, 6082-Т6, АД35Т1, 1565ч. Химический состав определялся оптико-эмиссионным спектрометром ARL easySpark. Экспериментальные исследования свойств проводились на образцах с рекомендованной нормативной документацией[5] для данных сплавов обработкой:

АД35. Сплав системы Al-Mg-Si — охлаждение с температуры горячего процесса изготовления и искусственное старение на максимальную прочность (Т1);

1915. Сплав системы Al-Zn-Mg — закалка и естественное старение (Т);

6082. Сплав системы Al-Mg-Si — закалка и искусственное старение (Т6);

1565ч. Сплав системы Al-Mg — упрочнение только в процессе наклепа при прокатке листа (сплав термонеупрочняемый).

В качестве критериев оценки сплавов выбраны:

- стандартные механические характеристики: предел прочности, предел текучести, относительное сужение, относительное удлинение, модуль упругости;

[3] См.: ГОСТ 31385-2016. Резервуары вертикальные цилиндрические стальные для нефти и нефтепродуктов. Общие технические условия. Москва : Стандартинформ, 2016. 96 с.; РД 16.01-60.30.00-КТН-026-1-04. Нормы проектирования стальных вертикальных резервуаров для хранения нефти объемом 1000–50000 м^3. Москва : ОАО «АК «Транснефть», 2004. 60 с.; СТО-СА-03-002-2009. Правила проектирования, изготовления и монтажа вертикальных цилиндрических стальных резервуаров для нефти и нефтепродуктов. Москва : Ростехэкспертиза, 2009. 216 с.; РД 16.01-60.30.00-КТН-026-1-04. Нормы проектирования стальных вертикальных резервуаров для хранения нефти объемом 1000–50000 м^3. Москва : ОАО «АК «Транснефть», 2004. 60 с.; СТО-СА-03-002-2009. Правила проектирования, изготовления и монтажа вертикальных цилиндрических стальных резервуаров для нефти и нефтепродуктов. Москва : Ростехэкспертиза, 2009. 216 с.

[4] СП 128.13330.2016. Алюминиевые конструкции. Актуализированная редакция СНиП 2.03.06-85. Москва : АО «НИЦ «Строительство» ЦНИИСК им. В.А. Кучеренко, институт ЦНИИПСК им. Мельникова, ЗАО «МЕТАКОН ЦЕНТР», 2016. 80 с.

[5] ГОСТ 21631–2019. Листы из алюминия и алюминиевых сплавов. Технические условия. Москва : Стандартинформ, 2020. 35 с.

- характеристики трещиностойкости: значение коэффициента интенсивности напряжений для максимального значения нагрузки, временное значение вязкости разрушения при плоской деформации, критический J-интеграл, раскрытие в вершине трещины при максимальной нагрузке;
- ударная вязкость.

Все испытания проводились при температурах +20 °С, –20 °С, –40 °С, –70 °С и –104 °С.

Нагружение образцов производилось с использованием универсального силового испытательного оборудования: Instron 8802, Instron 3382, LabTest 6.500H.5.0, SATEC тип 1000HDX, Instron MPX-450 для определения ударной вязкости. Перемещения определялись с помощью преобразователя перемещений серии 2600, тип 2630-106. Охлаждение образцов до требуемой температуры проводилось в термокамерах Instron 3119-407 и LaborTech TK3-80. Измерение деформаций выполнялось тензорезисторами с базой 1,0–3,0 мм. На всех уровнях нагрузки при проведении экспериментов каждой группы испытывалось 8 образцов всех марок сплавов.

Для статистической обработки результатов испытаний применялись стандартные алгоритмы математической статистики: расчет выборочных характеристик[6], проверка выборок на нормальность распределения[7] и исключение грубых погрешностей измерений.

В ходе исследования было проведено три экспертных опроса, в которых участвовало 10 экспертов со стажем не менее 15 лет (4 инженера-эксплуатационщика ВЦР, 4 ученых-металловеда, 2 аттестованных РОСТЕХНАДЗОРом эксперта по промышленной безопасности).

При обработке опросов экспертов рассчитывался коэффициент конкордации W Кендела [22]:

$$W = \frac{12S}{m^2\left(n^3 - n\right)}, \tag{1}$$

где m — количество экспертов, принявших участие в опросе; n — количество параметров, оцениваемых экспертами; S — сумма квадратов отклонений сумм рангов каждого фактора от средней суммы рангов.

$$S = \sum\nolimits_{i=1}^{n}\left[\sum\nolimits_{k=1}^{m} r_{ik} - 0{,}5m\left(n+1\right)\right]^2.$$

Значимость коэффициента конкордации оценивалась по критерию χ^2 Пирсона [23]. Нормированное кодирование натуральных факторов осуществлялось по известному алгоритму, например [24].

В процессе обработки экспериментальных данных формировались критерии оптимизации. Нормированное кодирование применялось в связи с тем, что натуральные характеристики имеют разную размерность.

Проведенные исследования имеют ограничения: изучался только листовой материал конструкций ВЦР, не рассматривались сварные соединения и работа концентраторов напряжений в условиях циклически изменяющихся напряжений, температурный интервал ограничивался значениями от +20 до –104 °С.

3. Результаты и обсуждение

Все характеристики, влияющие на эффективность применения алюминиевых сплавов в арктических условиях, разделены на шесть групп: стоимостно-весовые (определяют экономическую эффективность на стадии изготовления ВЦР), стандартные механические характеристики, ударная вязкость, характеристики трещиностойкости, усталостные характеристики, коррозионная стойкость.

[6] ГОСТ Р 8.736–2011. Государственная система обеспечения единства измерений. Измерения прямые многократные. Методы обработки результатов измерений. Основные положения. Москва : Стандартинформ, 2019. 26 с.

[7] ГОСТ Р ИСО 5479-2002. Проверка отклонения распределения вероятностей от нормального распределения. Москва : Госстандарт России, 2002. 27 с.

В работе приняты следующие обозначения:

- $Y_{kgt°C}$ — $k_{2ijt°C}$ — локальные обобщенные критерии по каждой из 6 групп характеристик ($g = 1$ стоимостно-весовые характеристики, $g = 2$ — стандартные механические характеристики, $g = 3$ — ударная вязкость, $g = 4$ – характеристики трещиностойкости, $g = 5$ – характеристики сопротивления усталости; $g = 6$ – коррозионная стойкость) при каждой температуре испытаний t °C;
- $k_{1ijt°C}$ ...$k_{6ijt°C}$ — нормированное кодированное значение характеристики i внутри группы для сплава j ($j = 1$ – АД35Т1, $j = 2$ – 1915Т, $j = 3$ – 6082-Т6, $j = 4$ – 1565 ч) при каждой температуре испытаний t °C;
- α_i, β_i и γ_i — внутригрупповые весовые коэффициенты для стандартных механических характеристик, трещиностойкости и коррозионной стойкости соответственно;
- δ_g — весовые коэффициенты групп характеристик, входящих в интегральный критерий $Y_{t°C}$.

Все весовые характеристик определены с помощью статистической обработки экспертных опросов.

3.1. Стоимостно-весовые характеристики

Удельный вес сплавов рассчитывался исходя из массовых процентов, входящих в сплав элементов и их удельного веса, который определялся по справочным данным[8]. Химический состав исследованных сплавов, определенный спектрометром ARL easySpark, приведен в табл. 1.

С учетом удельного веса для каждого сплава определялся вес стандартного листа 10×1200×3000, данные по стоимости листового материала получены из прайс-листов металлообрабатывающих компаний и сети интернет (табл. 2).

Таблица 1. **Химический состав сплавов, % /** *Table 1.* **Chemical composition of alloys, %**

Марка сплава / Alloy grade	**Fe**	**Si**	**Mn**	**Cr**	**Ti**	**Al**	**Cu**	**Mg**	**Zn**	**Zr**
АД35Т1 / AD35T1	0,50	1,00	0,70	0,25	0,10	96,25	0,10	0,90	0,20	
1915Т	0,40	0,35	0,45	0,13	0,04	92,49	0,10	1,40	4,50	0,14
6082-Т6	0,30	1,00	0,70	0,25	0,10	96,45	0,10	0,90	0,20	
1565ч / 1565ch	0,30	0,20	0,80	0,35	0,03	91,55	0,10	5,65	0,83	0,20

И с т о ч н и к: выполнено О.А. Корневым / S o u r c e: made by O.A. Kornev.

Таблица 2. **Стоимостно-весовые характеристики сплавов /** *Table 2.* **Cost and weight characteristics of alloys**

Марка сплава j / Alloy grade j	**Удельный вес сплава, г/см^3 / Specific gravity of the alloy, g/cm^3**	**Вес листа, кг / Sheet weight, kg**	**Стоимость листа, тыс. р. / The cost of the sheet, thousand rubles**	**Отношение стоимости листа к весу 10×1200×3000, руб/кг / The ratio of the cost of the sheet to the weight 10×1200×3000, RUB / kg**	**Нормированные кодированные значения выборки отношения стоимости листа к его весу k_{1j} / Normalized coded sample values of the ratio of the cost of a sheet to its weight k_{1j}**
АД35Т1 / AD35T1	277,48	100	69,25	69250	0,20
1915Т	301,10	108	74,79	74790	1
6082-Т6	280,74	101	63,67	63660	–0,61
1565ч / 1565ch	265,38	96	60,95	60951	–1

И с т о ч н и к: выполнено О.А. Корневым / S o u r c e: made by O.A. Kornev.

[8] Таблица удельного веса металлов. URL: https://pkf-uralmet.ru/uploadedFiles/files/Tablitsa_udelnogo_vesa_metallov.pdf (дата обращения: 20.08.2025).

Локальный обобщенный критерий Y_1 по стоимостно-весовым характеристикам не зависит от температуры испытаний и равен k_{1j} для каждого сплава. Минимальными стоимостно-весовыми характеристиками (оптимальными по данной группе характеристик) обладает сплав 1565ч.

3.2. Стандартные механические характеристики

Стандартные механические характеристики определялись экспериментально при лабораторной температуре +20 °С и отрицательных температурах (от –20 до –104 °С) согласно ГОСТ 1497[9]. Данные сведены в табл. 3. В качестве примера приведены диаграммы деформирования сплавов АД35Т1 и 1915Т при температуре +20 °С (рис. 2).

Таблица 3. **Механические характеристики сплавов при различных температурах испытаний**
Table 3. **Mechanical characteristics of alloys at various test temperatures**

t, °C	Механическая характеристика i / Mechanical characteristics i	Натуральные значения / Natural values				Нормированные кодированные значения $k_{2ijt°C}$ / Normalized coded values $k_{2ijt°C}$			
		Марка сплава / Alloy grade j							
		АД35Т1 / AD35T1	1915Т	6082Т6	1565ч / 1565ch	АД35Т1 / AD35T1	1915Т	6082-Т6	1565ч / 1565ch
+20	Предел прочности, МПа / Ultimate strength, MPa	302	360	330	390	–1	0,32	–0,36	1
	Предел текучести, МПа / Yield strength, MPa	293	255	315	285	0,27	–1	1	0
	Относительное сужение, % / Relative narrowing, %	36	28	23	15	1	0,24	–0,24	–1
	Относительное удлинение, % / Relative elongation, %	12,2	10,9	13	12	0,24	–1	1	0,05
	Модуль упругости, МПа / Modulus of elasticity, MPa	72000	71000	72000	71000	1	–1	1	–1
–20	Предел прочности, МПа / Ultimate strength, MPa	345	365	330	390	–0,5	0,17	–1	1
	Предел текучести, МПа / Yield strength, MPa	320	265	332	285	0,64	–1	1	–0,4
	Относительное сужение, % / Relative narrowing, %	38	27,6	23	16	1	0,05	–0,36	–1
	Относительное удлинение, % / Relative elongation, %	13	11,2	14	12,5	0,29	–1	1	–0,07
	Модуль упругости, МПа / Modulus of elasticity, MPa	74000	73000	74000	71000	1	0,33	1	–1
–40	Предел прочности, МПа / Ultimate strength, MPa	350	370	345	400	–0,82	–0,09	–1	1
	Предел текучести, МПа / Yield strength, MPa	325	270	335	290	0,69	–1	1	–0,38
	Относительное сужение, % / Relative narrowing, %	37,5	27,5	22	17,5	1	0	–0,55	–1
	Относительное удлинение, % / Relative elongation, %	13,1	13	14,8	13	–0,89	–1	1	–1
	Модуль упругости, МПа / Modulus of elasticity, MPa	74200	73500	74500	71500	0,8	0,33	1	–1

[9] ГОСТ 1497-2023. Металлы. Методы испытаний на растяжение. Москва : ФГБУ «РСТ», 2024. 62 с.

Окончание табл. 3 / Ending of the Table 3

t, °C	Механическая характеристика *i* / Mechanical characteristics *i*	Натуральные значения / Natural values				Нормированные кодированные значения $k_{2ijt°C}$ / Normalized coded values $k_{2ijt°C}$			
		Марка сплава / Alloy grade *j*							
		АД35Т1 / AD35T1	1915Т	6082Т6	1565ч / 1565ch	АД35Т1 / AD35T1	1915Т	6082-Т6	1565ч / 1565ch
–70	Предел прочности, МПа / Ultimate strength, MPa	360	395	350	405	–0,64	0,64	–1	1
	Предел текучести, МПа / Yield strength, MPa	337	275	350	290	0,65	–1	1	–0,6
	Относительное сужение, % / Relative narrowing, %	36	26,5	21,5	19	1	–0,12	–0,71	–1
	Относительное удлинение, % / Relative elongation, %	14	13,5	15,5	14,5	–0,5	–1	1	0
	Модуль упругости, МПа / Modulus of elasticity, MPa	76500	75000	77000	74000	0,67	–0,33	1	–1
–104	Предел прочности, МПа / Ultimate strength, MPa	390	415	375	420	–0,33	0,78	–1	1
	Предел текучести, МПа / Yield strength, MPa	356	280	360	295	0,9	–1	1	–0,63
	Относительное сужение, % / Relative narrowing, %	37,2	26	21	20	1	–0,3	–0,88	–1
	Относительное удлинение, % / Relative elongation, %	14,6	13,5	16	16,5	–0,27	–1	0,67	1
	Модуль упругости, МПа / Modulus of elasticity, MPa	81000	77000	78500	77000	1	–1	-0,25	–1

И с т о ч н и к: выполнено О.А. Корневым / S o u r c e: made by O.A. Kornev.

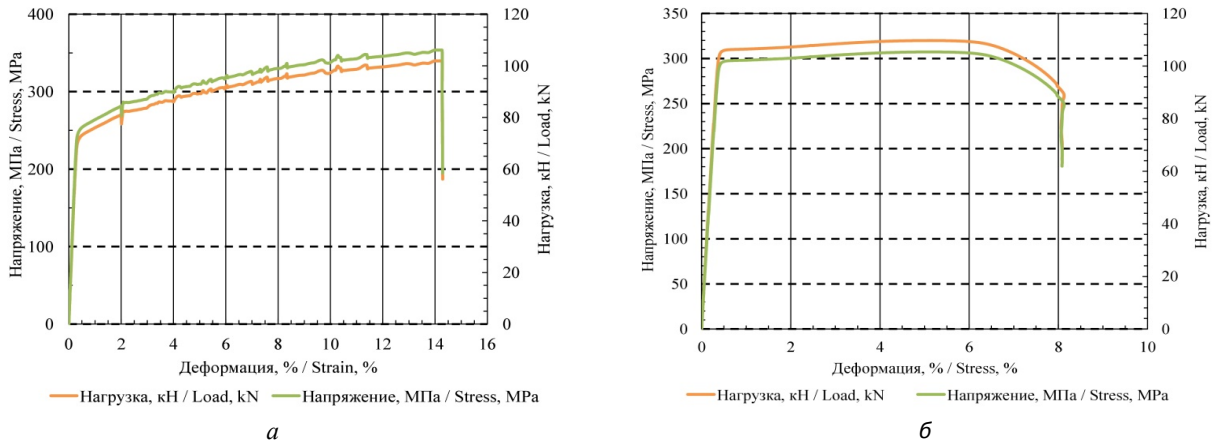

а *б*

Рис. 2. Диаграмма «Напряжение/Нагрузка-деформация» при температуре +20 °С:
а — для сплава 1915Т; *б* — АД35Т1
И с т о ч н и к: выполнено О.А. Корневым.

Figure 2. “Stress/Load-strain” diagram at a temperature of +20 °C:
а — for alloy 1915T; *б* — AD35T1
S o u r c e: made by O.A. Kornev.

С целью определения весовых коэффициентов значимости каждой из стандартных механических характеристик алюминиевых сплавов для ВЦР в арктических условиях был проведен экспертный опрос. Коэффициент конкордации опроса W составил 0,67 по (1), уровень значимости (вероятность ошибки первого рода), определенный по Пирсону, составил 0,01. Весовые коэффициенты (α_i), полученные в результате статистической обработки опросной таблицы, составили для характери-

стик этой группы: предел прочности $\alpha_1 = 0,27$; предел текучести $\alpha_2 = 0,33$; относительное сужение $\alpha_3 = 0,20$; относительное удлинение $\alpha_4 = 0,13$; модуль упругости $\alpha_5 = 0,07$, т.е. наиболее значимой характеристикой этой группы факторов, по мнению опрашиваемой группы экспертов, принят предел текучести материала, наименее значимой — модуль упругости. С учетом весовых коэффициентов были рассчитаны значения локального обобщенного критерия $Y_{2t°C}$ для характеристик этой группы:

$$Y_{2t°C} = \sum_{i=1}^{5} k_{2ijt°C}\alpha_i, \quad (2)$$

где $k_{2ijt°C}$ — нормированное кодированное значение характеристики (*i*) для сплава (*j*) при температуре испытаний (*t* °C) из табл. 3 (табл. 4).

Таблица 4. **Локальный обобщенный критерий $Y_{2t°C}$ для стандартных механических характеристик по (2)**
Table 4. **Local generalized criterion $Y_{2t°C}$ for standard mechanical characteristics according to (2)**

***t*, °C**	**АД35Т1 / AD35T1**	**1915Т**	**6082-Т6**	**1565ч / 1565ch**
+20	0,12	–0,4	0,38	0,01
–20	0,38	–0,38	0,19	–0,14
–40	0,15	–0,46	0,15	–0,26
–70	0,22	–0,33	0,12	–0,2
–104	0,44	–0,38	–0,05	–0,08

И с т о ч н и к: выполнено О.А. Корневым / S o u r c e: made by O.A. Kornev.

Максимальными характеристиками (оптимальными по данной группе характеристик) при температуре +20 °C обладает сплав 6082-Т6, при температурах –20 °C, –70 °C, –104 °C — сплав АД35Т1, при температуре –20 °C — сплавы 6082-Т6 и АД35Т1 показывают равное между собой, но существенно большее, чем остальные изучаемые сплавы, значение обобщенного локального критерия $Y_{2t°C}$.

3.3. Ударная вязкость

Испытания по определению ударной вязкости сплавов проводились по ГОСТ 9454[10]. Экспериментальные данные приведены в табл. 5 и на рис. 3.

Таблица 5. **Ударная вязкость *KCV* при различных температурах испытаний**
Table 5. **Impact toughness *KCV* at various test temperatures**

***t*, °C**	**Натуральные значения, Дж/см² / Natural values, *J*/cm²**				**Нормированные кодированные значения $k_{3ijt°C}$ / Normalized coded values $k_{3ijt°C}$**			
	Марка сплава / Alloy grade *j*							
	АД35Т1 / AD35T1	1915Т	6082Т6	1565ч / 1565ch	АД35Т1 / AD35T1	1915Т	6082-Т6	1565ч / 1565ch
+20	8,1	38,1	11,8	25,1	–1	1	–0,75	0,13
–20	9,2	42,3	12,2	21,9	–1	1	–0,82	–0,23
–40	9,4	42,1	11,9	21,1	–1	1	–0,85	–0,28
–70	9,6	41,1	11,1	20,8	–1	1	–0,9	–0,29
–104	9,8	41,8	12,3	20,1	–1	1	–0,84	–0,36

И с т о ч н и к: выполнено О.А. Корневым / S o u r c e: made by O.A. Kornev.

[10] ГОСТ 9454-78. Металлы. Метод испытания на ударный изгиб при пониженных, комнатной и повышенных температурах.

Все изломы хрупко-вязкие с преобладанием вязкой составляющей. Изломы состоят из плоской центральной части, губ среза и области сжатия в месте удара маятника копра. С понижением температуры испытаний у сплава 1565ч шероховатость центральной части увеличивается, уменьшаются губы среза, эта фрактографическая особенность может свидетельствовать об увеличении доли хрупкой составляющей в изломе, что и подтверждено уменьшением ударной вязкости при понижении температуры испытаний. Изменений в характере изломов остальных сплавов не произошло. На рис. 4 показан характер изломов образцов сплава 1915Т при температуре испытаний +20 и –104 °С.

По ударной вязкости локальный обобщенный критерий Y_3 равен $k_{3ijt°C}$. Максимальная величина $k_{3ijt°C}$ (оптимум для данной группы характеристик) соответствует сплаву 1915Т при всех температурах испытаний.

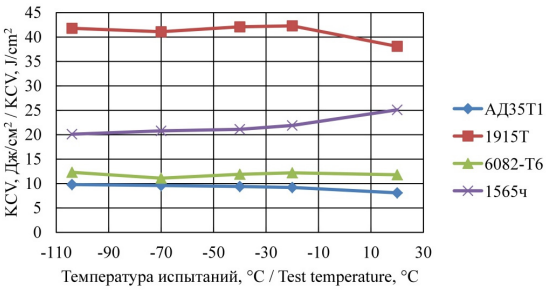

Рис. 3. Экспериментальные значения *KCV* сплавов при различных температурах испытаний
И с т о ч н и к: выполнено В.А. Ермаковым.

Figure 3. Experimental KCV values of alloys at different test temperatures
S o u r c e: made by V.A. Ermakov.

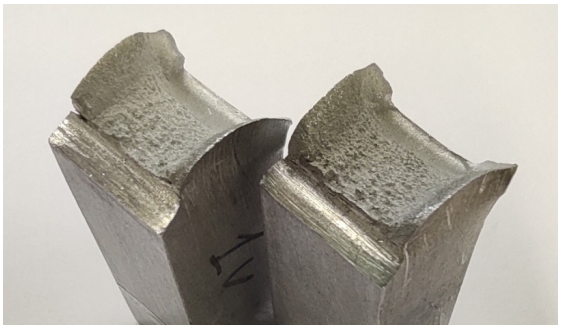

а *б*

Рис. 4. Излом образца сплава 1915Т:
а — при температуре испытаний +20 °С;
б — при температуре испытаний –104 °С
И с т о ч н и к: выполнено О.А. Корневым

Figure 4. Fracture of the 1915T alloy sample:
а — at a test temperature of +20 °C;
б — at a test temperature of –104 °C
S o u r c e: made by O.A. Kornev.

3.4. Характеристики трещиностойкости

Характеристики трещиностойкости определялись в соответствии с требованиями ГОСТ 25.506[11]: условный коэффициент интенсивности напряжений K_C* — это значение коэффициента интенсивности напряжений для максимального значения нагрузки и исходной длины трещины l, K_Q — временное значение вязкости разрушения при плоской деформации, J_c — критический J-интеграл, δ_c — раскрытие в вершине трещины при максимальной нагрузке.

С целью определения весовых коэффициентов значимости каждой из характеристик трещиностойкости алюминиевых сплавов для ВЦР в арктических условиях был проведен экспертный опрос. Коэффициент конкордации опроса W составил 0,58, уровень значимости (вероятность ошибки первого рода), определенный по Пирсону, составил 0,02. Весовые коэффициенты β_i, полученные в результате статистической обработки: коэффициент интенсивности напряжений для максимального значения нагрузки и исходной длины трещины $\beta_1 = 0,4$; временное значение вязкости разрушения при плоской деформации $\beta_2 = 0,3$; критический J-интеграл $\beta_2 = 0,1$; раскрытие в вершине трещины при максимальной нагрузке $\beta_4 = 0,2$.

С учетом весовых коэффициентов были рассчитаны значения локального обобщенного критерия $Y_{4t°C}$ для характеристик рассматриваемой группы:

$$Y_{4t°C} = \sum_{i=1}^{3} k_{4ijt°C}\beta_i - \beta_4 k_{44jt°C}, \quad (3)$$

где $k_{4ijt°C}$ — нормированное кодированное значение характеристики (i) для сплава (j) при температуре испытаний (t, °С) из табл. 5. Данные сведены в табл. 6, 7.

[11] ГОСТ 25.506-85. Расчеты и испытания на прочность. Методы механических испытаний металлов. Определение характеристик трещиностойкости (вязкости разрушения) при статическом нагружении.

Таблица 6. **Характеристики трещиностойкости**
Table 6. **Crack resistance characteristics**

***t*, °C**	**Характеристика трещиностойкости *i* / Crack resistance characteristics *i***	**Натуральные значения / Natural values**				**Нормированные кодированные значения $k_{4ijt°C}$ / Normalized coded values $k_{4ijt°C}$**			
		Марка сплава / Alloy grade *j*							
		АД35Т1 / AD35T1	1915Т	6082Т6	1565ч / 1565ch	АД35Т1 / AD35T1	1915Т	6082-Т6	1565ч / 1565ch
+20	K_C*, МПа·м$^{1/2}$ / MPa·m$^{1/2}$	42,0	43,0	44,1	52,0	–1	–0,8	–0,58	1
	K_Q, МПа·м$^{1/2}$ / MPa·m$^{1/2}$	29,5	34,0	32,0	37,0	–1	0,2	–0,33	1
	J_c, МДж/м^2 / MJ/m^2	0,044	0,075	0,041	0,096	–0,89	0,24	–1	1
	δ_c, мм / mm	0,138	0,279	0,136	0,289	–0,97	0,87	–1	1
–20	K_C*, МПа·м$^{1/2}$ / MPa·m$^{1/2}$	40,5	41,0	43,9	48,0	–1	–0,87	–0,09	1
	K_Q, МПа·м$^{1/2}$ / MPa·m$^{1/2}$	31,0	35,0	31,3	38,5	–1	0,07	–0,92	1
	J_c, МДж/м^2 / MJ/m^2	0,048	0,079	0,044	0,083	–0,79	0,79	–1	1
	δ_c, мм / mm	0,137	0,285	0,13	0,25	–0,91	1	–1	0,55
–40	K_C*, МПа·м$^{1/2}$ / MPa·m$^{1/2}$	45,0	43,0	46,9	48,0	–0,2	–1	0,56	1
	K_Q, МПа·м$^{1/2}$ / MPa·m$^{1/2}$	30	35	29,6	37,5	–0,9	0,37	–1	1
	J_c, МДж/м^2 / MJ/m^2	0,046	0,083	0,043	0,08	–0,2	0,24	–0,24	0,2
	δ_c, мм / mm	0,146	0,291	0,14	0,24	–0,92	1	–1	0,32
–70	K_C*, МПа·м$^{1/2}$ / MPa·m$^{1/2}$	43	43	44,4	51	–1	–1	–0,65	1
	K_Q, МПа·м$^{1/2}$ / MPa·m$^{1/2}$	30,5	33,5	30,9	29,0	–0,33	1	–0,16	–1
	J_c, МДж/м^2 / MJ/m^2	0,051	0,074	0,045	0,067	–0,59	1	–1	0,52
	δ_c, мм / mm	0,136	0,261	0,13	0,204	–0,23	0,25	–0,25	0,03
–104	K_C*, МПа·м$^{1/2}$ / MPa·m$^{1/2}$	42,0	44,0	43,5	51,0	–1	–0,56	–0,67	1
	K_Q, МПа·м$^{1/2}$ / MPa·m$^{1/2}$	29,0	33,5	30,7	34,0	–1	0,8	–0,32	1
	J_c, МДж/м^2 / MJ/m^2	0,053	0,061	0,047	0,049	–0,14	1	–1	–0,71
	δ_c, мм / mm	0,135	0,215	0,14	0,161	–1	1	–0,88	–0,35

И с т о ч н и к: выполнено О.А. Корневым / S o u r c e: made by O.A. Kornev.

Таблица 7. **Локальный обобщенный критерий $Y_{4t°C}$ для характеристик трещиностойкости по (3)**
Table 7. **Local generalized criterion $Y_{4t°C}$ for crack resistance characteristics according to (3)**

***t*, °C**	**АД35Т1 / AD35T1**	**1915Т**	**6082-Т6**	**1565ч / 1565ch**
+20	–0,595	–0,41	–0,231	0,60
–20	–0,597	–0,448	–0,212	0,69
–40	–0,186	–0,465	0,1	0,656
–70	–0,512	–0,05	–0,358	0,146
–104	–0,514	–0,084	–0,288	0,699

И с т о ч н и к: выполнено О.А. Корневым / S o u r c e: made by O.A. Kornev.

Очевидно, что оптимальные характеристики по локальному критерию $Y_{4t°C}$ показал сплав 1915Т.

3.5. Усталостные характеристики

Предел выносливости определялся согласно Межгосударственному стандарту ГОСТ 25.502[12]. Частота нагружения 10 Гц, циклы пульсирующие (коэффициент асимметрии цикла 0) (табл. 8). Разрушенные в результате испытаний на усталость образцы показаны на рис. 5. У излома сплава 1915Т больше зона, включающая в себя очаг разрушения и стабильного роста трещины до начала долома, по сравнению с остальными исследуемыми сплавами.

Таблица 8. **Предел выносливости сплавов при пульсирующем нагружении на базе $2 \cdot 10^6$ циклов**
Table 8. **Fatigue limit of alloys under fluctuating loading based on $2 \cdot 10^6$ cycles**

t, °C	Натуральные значения, МПа / Natural values, MPa *i*				Нормированные кодированные значения $k_{5iit°C}$ / Normalized coded values $k_{5iit°C}$			
	Марка сплава / Alloy grade *j*							
	АД35Т1 / AD35T1	1915Т	6082Т6	1565ч / 1565ch	АД35Т1 / AD35T1	1915Т	6082-Т6	1565ч / 1565ch
+20	70	110	105	80	–1	1	0,75	–0,50
–20	72	112	110	82	–1	1	0,90	–0,50
–40	76	116	116	86	–1	1	1	–0,50
–70	82	120	122	89	–1	0,90	1	–0,65
–104	89	124	129	92	–1	0,75	1	–0,85

И с т о ч н и к: выполнено О.А. Корневым / S o u r c e: made by O.A. Kornev.

По пределу выносливости локальный обобщенный критерий Y_5 равен $k_{5ijt°C}$. Очевидно, что максимальная величина $k_{5ijt°C}$ (оптимум для данной группы характеристик) соответствует сплаву 1915Т при всех температурах испытаний.

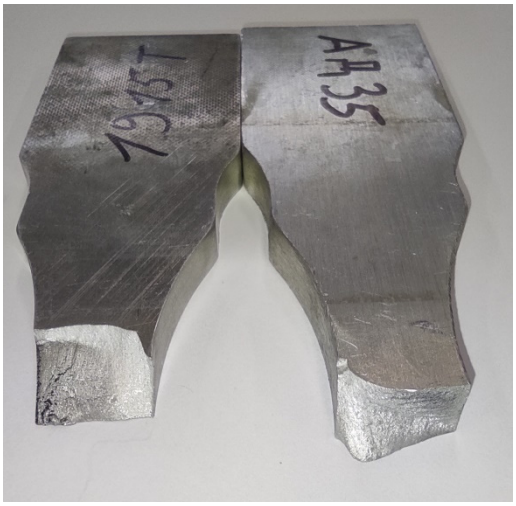

Рис. 5. Разрушенные в результате испытаний на усталость образцы
И с т о ч н и к: выполнено О.А. Корневым.

Figure 5. Samples destroyed as a result of fatigue tests
S o u r c e: made by O.A. Kornev.

[12] ГОСТ 25.502-79. Расчеты и испытания на прочность в машиностроении. Методы механических испытаний металлов. Методы испытаний на усталость. Москва, 1985. 50 с.

3.6. Характеристики коррозионной стойкости

Собственные испытания сплавов на коррозионную стойкость не проводились. Данные, полученные от производителей алюминиевых сплавов для температуры эксплуатации +20 °С, сведены в табл. 9.

Таблица 9. **Характеристики коррозионной стойкости сплавов**
Table 9. **Corrosion resistance characteristics of alloys**

Вид коррозии / Type of corrosion	**Натуральные значения *i* / Natural values *i***				**Нормированные кодированные значения k_{6icj} / Normalized coded values k_{6icj}**			
	Марка сплава *j* / Alloy grade *j*							
	АД35Т1 / AD35T1	1915Т	6082Т6	1565ч / 1565ch	АД35Т1 / AD35T1	1915Т	6082-Т6	1565ч / 1565ch
МКК, мм / IGC, mm	0	0	0,1	0,08	–1	–1	1	0,6
РСК, балл / LC, points	1	3	1	2	–1	1	–1	0

Примечание: МКК — межкристаллитная коррозия (мм/год), РСК — расслаивающиеся коррозия (балл). Чем меньше балл, тем более коррозионностойкий сплав, 1 — отсутствие коррозионных повреждений.

Note: IGC — intergranular corrosion (mm/year), LC — layer corrosion (points). Lower point score indicates greater corrosion resistance of the alloy, 1 — no corrosion damage.

И с т о ч н и к: выполнено О.А. Корневым / S o u r c e: made by O.A. Kornev.

Было принято, что оба вида коррозии равноопасны при эксплуатации ВЦР и их весовые коэффициенты равны $\gamma_{c1} = \gamma_{c2} = 0,5$. Следовательно, обобщенный локальный критерий Y_6 определяется следующим образом:

$$Y_6 = \sum_{c=1}^{2} k_{6icj}\ \gamma_c. \tag{4}$$

Соответственно по (4) значения обобщенного локального критерия этой группы составляют: для сплава АД35Т1 — $Y_6 = -1$; для сплава 1915Т — $Y_6 = 0$; для сплава 6082-Т6 — $Y_6 = 0$; для сплава 1565ч — $Y_6 = 0,3$.

3.7. Интегральный критерий

Для формирования интегрального критерия был проведен опрос для определения весовых коэффициентов групп характеристик. Коэффициент конкордации опроса *W* составил 0,63, уровень значимости (вероятность ошибки первого рода), определенный по Пирсону, составил 0,01. Весовые коэффициенты (δ_i), полученные в результате статистической обработки: стоимостно-весовые характеристики $\delta_1 = 0,04$; стандартные механические характеристики $\delta_2 = 0,19$; ударная вязкость $\delta_3 = 0,14$; характеристики трещиностойкости $\delta_4 = 0,24$; усталостные характеристик $\delta_5 = 0,29$; коррозионная стойкость $\delta_6 = 0,1$.

Интегральный критерий в соответствии с вышеизложенным:

$$Y_{t°C} = -Y_1\delta_1 + Y_{2t°C}\delta_2 + Y_{3t°C}\delta_3 + Y_{4t°C}\delta_4 + Y_{5t°C}\delta_5 - Y_6\delta_6, \tag{5}$$

Или с учетом локальных обобщенных критериев:

$$Y_{t°C} = -k_{1j}\delta_1 + \left(\sum_{i=1}^{5} k_{2ijt°C}\,\alpha_i\right)\delta_2 + k_{3ijt°C}\delta_3 + \\ + \left(\sum_{i=1}^{3} k_{4ijt°C}\,\beta_i - \beta_4 k_{44\,jt°C}\right)\delta_4 + k_{5ijt°C}\delta_5 - \left(\sum_{c=1}^{2} k_{6icj}\gamma_c\right)\delta_6. \tag{6}$$

Минус в выражении (6) стоит перед слагаемым, соответствующим тем группам характеристик, у которых оптимальными являются минимальные значения. Приняв интегральный критерий как целевую функцию оптимизации, можно утверждать, что оптимальным будет сплав, удовлетворяющий условию

$$Y_{t^\circ\mathrm{C}} \to \max. \qquad (7)$$

Результаты определения интегрального критерия сведены в табл. 10.

Таблица 10. **Значения интегрального критерия $Y_{t^\circ C}$ при различных температурах испытаний**
Table 10. **Values of the integral criterion $Y_{t^\circ C}$ at different test temperatures**

***t*, °C**	**АД35Т1 / AD35T1**	**1915Т**	**6082-Т6**	**1565ч / 1565ch**
+20	–0,46	0,22	0,15	0,03
–20	–0,41	0,21	0,16	–0,03
–40	–0,35	0,19	0,25	–0,07
–70	–0,42	0,29	0,13	–0,22
–104	–0,42	0,28	0,15	–0,10

И с т о ч н и к: выполнено О.А. Корневым / S o u r c e: made by O.A. Kornev.

Максимальная величина интегрального критерия при всех температурах эксплуатации, кроме –40°С, соответствует сплаву 1915Т, при температуре –40°С максимальное значение интегрального критерия у сплава 6082-Т6.

В работе впервые предложен оригинальный подход к выбору алюминиевых сплавов для строительства ВЦР в условиях Крайнего Севера и приближенных к ним регионов. Предложенный подход позволил сформулировать интегральный критерий, принятый в качестве целевой функции оптимизации свойств сплавов. В процессе работы были проведены экспертные опросы, позволившие выявить весовые коэффициенты характеристик сплавов, которые вошли в окончательную формулировку критерия. Альтернативами предлагаемого подхода к решению задачи мог бы быть метод TOPSIS, который сводится к измерению сходства с идеальным решением. В рассматриваемой инженерной задаче не предусмотрено идеального решения, выбор осуществляется из имеющегося набора экспериментально определенных характеристик. Другой альтернативой мог бы быть метод AHP, который предусматривает сравнение альтернатив по шкале Саати, но он в задачах такого типа дает грубую оценку функции полезности. Применение нечетких методов вносит субъективную составляющую в решение. Другие методы многокритериальной оптимизации, например метод Парето, адекватно работают при наличии конкурирующих альтернатив. В поставленной задаче такого однозначного разделения нет. Применение функции желательности Харрингона основано на произвольной калибровке шкал откликов, что не позволяет получить точного решения в переходных областях. Поэтому авторы считают, что реализованный в данной работе подход дает наиболее адекватные результаты при поиске оптимального решения и, более того, подобный подход можно распространить на другие задачи подобного типа.

Практическая ценность проведенного исследования заключается в определении комплекса характеристик наиболее распространенных алюминиевых сплавов, которые могут быть использованы проектировщиками ВЦР, эксплуатируемых при различных отрицательных температурах.

В дальнейшем предполагается проведение экспериментальных исследований сварных швов в алюминиевых конструкциях, полученных различными технологиями сварки, и расширение номенклатуры исследуемых сплавов.

4. Заключение

Статистическая обработка проведенных в процессе исследования экспертных опросов определила весовые коэффициенты внутри каждой группы характеристик и весовые коэффициенты групп характеристик, входящих в интегральный критерий выбора алюминиевого сплава для строительства резервуаров в условиях Арктики.

Весовые коэффициенты α_i составили внутри группы стандартных механических характеристик: для предела прочности $\alpha_1 = 0,27$; предела текучести $\alpha_2 = 0,33$; относительного сужения $\alpha_3 = 0,20$; относительного удлинения $\alpha_4 = 0,13$; модуля упругости $\alpha_5 = 0,07$.

Весовые коэффициенты внутри группы характеристик трещиностойкости β_i: для коэффициента интенсивности напряжений для максимального значения нагрузки и исходной длины трещины $\beta_1 = 0,4$; временного значения вязкости разрушения при плоской деформации $\beta_2 = 0,3$; критического *J*-интеграл $\beta_2 = 0,1$; раскрытия в вершине трещины при максимальной нагрузке $\beta_4 = 0,2$. Весовые коэффициенты внутри группы характеристик сопротивления коррозии $\gamma_{c1} = \gamma_{c2} = 0,5$. Весовые коэффициенты δ_i групп характеристик следующие: для стоимостно-весовых характеристик $\delta_1 = 0,04$; стандартных механических характеристик $\delta_2 = 0,19$; ударной вязкости $\delta_3 = 0,14$; характеристик трещиностойкости $\delta_4 = 0,24$; усталостных характеристик $\delta_5 = 0,29$; коррозионной стойкости $\delta_6 = 0,1$. Наибольший вес, согласно экспертным опросам, имеют усталостные характеристики и характеристики трещиностойкости, что указывает на необходимость включения расчета параметров усталости и трещиностойкости в нормативные документы по проектированию ВЦР из алюминиевых сплавов. Важность усталостных характеристик и трещиностойкости алюминиевых сплавов для применения в арктических условиях должна быть учтена и при проектировании новых сплавов, и при термических обработках существующих.

1. На основании проведенных экспериментальных исследований и экспертных опросов получен интегральный критерий, который предлагается использовать как целевую функцию выбора алюминиевого сплава для строительства резервуаров в арктических условиях.

2. Из рассмотренных в исследовании сплавов наилучший интегральный показатель у сплава 1915Т, наихудший у АД35Т1, что косвенно подтверждает преимущества естественного старения алюминиевых сплавов. Лучшими стоимостно-весовыми характеристиками обладает сплав 1565ч, лучшими стандартными механическими характеристиками при температуре +20 °С обладает сплав 6082-Т6, при температурах –20 °С, –70 °С, –104 °С — сплав АД35Т1, при температуре –20 °С — сплавы 6082-Т6 и АД35Т1 показывают равное между собой, но существенно большее, чем остальные изучаемые сплавы, значение обобщенного локального критерия. Сплав 1915Т обладает существенно более высокими усталостными характеристиками и ударной вязкостью по сравнению с остальными исследованными сплавами.

Список литературы

1. *Альтман М.Б.* Применение алюминиевых сплавов. Москва : Металлургия, 1973. 408 с.

2. *Reza Kashyzadeh K., Ghorbani S., Averyanov A.S.* Influence of Environmental Temperature on the Corrosion Resistance of Various Aluminum Alloys: an Experimental Study // RUDN Journal of Engineering Research. 2025. Vol. 26. No. 1. P. 94–106. https://doi.org/10.22363/2312-8143-2025-26-1-94-106 EDN LACBPD

3. *Sovetbayev R., Nugman Ye., Shayakhmetov Ye., Kawalek A.* Preparation of AlMgSi1 (6082) aluminum alloy for the study of mechanical and physico-chemical properties in the rolling process // Bulletin of the L.N. Gumilyov Eurasian National University. Technical Science and Technology Series. 2024. No. 147. P. 231–244. https://doi.org/10.32523/2616-7263-2024-147-2-231-244 EDN: IVEQDU

4. *Лессиг Е.Н., Лилеев А.Ф., Соколов А.Г.* Листовые металлические конструкции. Москва : Изд-во Литературы по строительству, 1970. 244 с.

5. *Шувалов А.Н., Корнев О.А., Ермаков В.А.* Исследование физико-механических характеристик алюминиевых сплавов 1915Т, 1565ч и 6082-Т6 при низких температурах // Строительство: наука и образование. 2024. Т. 14. № 1. С. 73–94. https://doi.org/10.22227/2305-5502.2024.1.5 EDN: HACFND

6. *Горицкий В.М., Гусева И.А., Кулемин А.М.* Особенности трещинообразования в вертикальных монтажных стыках резервуара объемом 50 000 м^3, изготовленного из высокопрочной стали 16Г2АФ // Промышленное и гражданское строительство. 2008. № 5. С. 14–16. EDN: IULFTV

7. *Kopec M., Liu X., Gorniewicz D., Modrzejewski P., Zasada D., Jóźwiak S., Janiszewski Ja., Kowalewski Z.L.* Mechanical response of 6061-T6 aluminium alloy subjected to dynamic testing at low temperature: Experiment and modeling //

International Journal of Impact Engineering. 2024. Vol. 185. Article no. 104843. https://doi.org/10.1016/j.ijimpeng.2023.104843 EDN: SSQTOL

8. *Yan J.B., Kong G., Wang Zh., Zhang L., Wang X.* Compression behaviours of aluminium alloy I-column at low temperatures // Structures. 2022. Vol. 44. P. 418–435. https://doi.org/10.1016/j.istruc.2022.08.009 EDN: GPKMMX

9. *Chikhalikar A., Roy I., Abouelella H., Umretiya R., Hoffman A., Larsen M., Rebak R.B.* Effect of aluminum on the FeCr(Al) alloy oxidation resistance in steam environment at low temperature (400°C) and high temperature (1200°C) // Corrosion Science. 2022. Vol. 209. Article no. 110765. https://doi.org/10.1016/j.corsci.2022.110765 EDN: BICKUB

10. *Fernandes R.F., Jesus J.S., Branco R., Borrego L.P., Costa J.D., Ferreira J.A.M.* Effect of low-temperature stress relieving heat treatments on fatigue behaviour and failure mechanisms of L-PBF AlSi10Mg aluminium alloy // Engineering Failure Analysis. 2025. Vol. 169. Article no. 109210. https://doi.org/10.1016/j.engfailanal.2024.109210 EDN: OMKGIA

11. *Yang H., Cui Y., Qin F., Lin T., Zheng Y.* Fatigue failure analysis and life prediction of forged 6061 aluminum alloy wheel hubs based on precipitate size effects and multiaxial stress modeling // Engineering Failure Analysis. 2025. Vol. 182. Part C. Article no. 110181. https://doi.org/10.1016/j.engfailanal.2025.110181

12. *Cong J., Liu Z., Zhou S., Zhu X., Gao S.* Fatigue life prediction of ultrasonic impact treatment aluminum alloy weld joint based on the continuous damage model and artificial neural network // Engineering Fracture Mechanics. 2025. Vol. 327. Article no. 111503. https://doi.org/10.1016/j.engfracmech.2025.111503

13. *Liu Z., Li J., Zhang L.* Fatigue characteristics of high-strength aluminum alloy with and without surface mechanical rolling treatment in the transition regime between high cycle and very-high cycle fatigue // Engineering Fracture Mechanics. 2025. Vol. 328. Article no. 111585. https://doi.org/10.1016/j.engfracmech.2025.111585

14. *Wang H., Zhang Z.J., Zhu S.Z., Li X.T., Zhu Y.K., Liu R., Hou J.P., Gong B.S., Liu H.Z., Wang D., Ma Z.Y., Zhang Z.F.* Enhancing the high-cycle fatigue property of aluminum alloy by adding fine-sized hard particles // Composites Part A: Applied Science and Manufacturing. 2026. Vol. 200. Article no. 109344. https://doi.org/10.1016/j.compositesa.2025.109344

15. *Song S., Wu Z., Zhao J., Zhou L., Guo S., Kan Q., Chen X., Zhang X.* Crystal plasticity modeling of uniaxial tensile and fatigue failure behaviors of laser shock peened aluminum alloy // International Journal of Fatigue. 2025. Vol. 201. Article no. 109145. https://doi.org/10.1016/j.ijfatigue.2025.109145

16. *Konstantinov I.L., Baykovskiy Yu.V., Yuryev P.O., Bezrukikh A.I., Sidelnikov S.B., Saparova A.S., Mansurov Yu.N., Partyko E.G., Bozhko D.N.* Study of deformability during the rolling of aluminum alloy 1580 doped with small additions of erbium and ytterbium // Metallurgist. 2025. https://doi.org/10.1007/s11015-024-01833-z EDN IPZBXD

17. *Шаталов Р.Л., Хоанг Ф.В., Куанг Ч.В.* Определение механических свойств полос из алюминиевого сплава АД33 по различным показателям твердости при холодной прокатке // Технология металлов. 2021. № 9. С. 31–37. https://doi.org/10.31044/1684-2499-2021-0-9-31-37 EDN XYBVMJ

18. *Лукиенко М.И.* Исследование прочности и технологичности листовых резервуарных конструкций из алюминиевых сплавов: дис. ... канд. техн. наук: 05.23.01. Москва, 1980. 199 с.: ил.

19. *Купреишвили С.М.* Механика разрушения вертикальных цилиндрических резервуаров // Промышленное и гражданское строительство. 2004. № 5. С. 40–42. EDN PLFWJH

20. *Vuherer T., Kramberger J., Milčić D., Glodež S.* Fatigue behaviour of friction stir welded AA-2024 aluminium alloy sheet // IOP Conference Series: Materials Science and Engineering. 2019. Vol. 659. Article no. 012032. https://doi.org/10.1088/1757-899X/659/1/012032

21. *Wang M.Z., Kassner M.E.* Tensile and fatigue properties of aluminum alloy sheet 6022 // Journal of Materials Engineering and Performance. 2002. Vol. 11. P. 166–168. https://doi.org/10.1361/105994902770344222

22. *Kendall M.G.*, *Gibbons J.D.* Rank correlation methods. 5th ed. London: Edward Arnold, 1990. 260 p.

23. *Pearson K.* On the criterion that a given system of deviations from the probable in the case of a correlated system of variables is such that it can be reasonably supposed to have arisen from random sampling // Philosophical Magazine Series. 2009. Series 5. Vol. 50. Issue 302. P. 157–175. https://doi.org/10.1080/14786440009463897

24. *Милова Ю.А., Дикарев А.В.* Нормированный натуральный ряд. Полипараметрическое кодирование // European Journal of Technical and Natural Sciences. 2020. № 3. С. 19–23. https://doi.org/10.29013/EJTNS-20-3-19-23 EDN SWBNAA

References

1. Al'tman M.B. *Application of aluminum alloys.* Moscow: Metallurgy Publ.; 1973. (In Russ.)

2. Reza Kashyzadeh K., Ghorbani S., Averyanov A.S. Influence of Environmental Temperature on the Corrosion Resistance of Various Aluminum Alloys: an Experimental Study. *RUDN Journal of Engineering Research*. 2025;26(1):94–106. https://doi.org/10.22363/2312-8143-2025-26-1-94-106 EDN: LACBPD

3. Sovetbayev R., Nugman Ye., Shayakhmetov Ye., Kawalek A. Preparation of AlMgSi1 (6082) aluminum alloy for the study of mechanical and physico-chemical properties in the rolling process. *Bulletin of the L.N. Gumilyov Eurasian National University. Technical Science and Technology Series*. 2024;(147):231–244. https://doi.org/10.32523/2616-7263-2024-147-2-231-244 EDN: IVEQDU

4. Lessig E.N., Lileev A.F., Sokolov A.G. *Sheet metal structures.* Moscow: Literature on Construction Publ.; 1970. (In Russ.)

5. Shuvalov A.N., Kornev O.A., Ermakov V.A. Investigation of physical and mechanical characteristics of aluminium alloys 1915T, 1565ch and 6082-T6 at low temperatures. *Construction: science and Education*. 2024;14(1):73–94. (In Russ.) https://doi.org/10.22227/2305-5502.2024.1.5 EDN: HACFND

6. Gorickij V.M., Guseva I.A., Kulemin A.M. Peculiarities of cracking in vertical erection joints of a tank of 50 000 m^3 made of high-strength steel 16G2AF. *Industrial and Civil Engineering*. 2008;(5):14–16. (In Russ.) EDN: IULFTV

7. Kopec M., Liu X., Gorniewicz D., Modrzejewski P., Zasada D., Jóźwiak S., Janiszewski Ja., Kowalewski Z.L. Mechanical response of 6061-T6 aluminium alloy subjected to dynamic testing at low temperature: Experiment and modeling. *International Journal of Impact Engineering.* 2024;185:104843. https://doi.org/10.1016/j.ijimpeng.2023.104843 EDN: SSQTOL

8. Yan J.B., Kong G., Wang Zh., Zhang L., Wang X. Compression behaviours of aluminium alloy I-column at low temperatures. *Structures*. 2022;44:418–435. https://doi.org/10.1016/j.istruc.2022.08.009 EDN: GPKMMX

9. Chikhalikar A., Roy I., Abouelella H., Umretiya R., Hoffman A., Larsen M., Rebak R.B. Effect of aluminum on the FeCr(Al) alloy oxidation resistance in steam environment at low temperature (400°C) and high temperature (1200°C). *Corrosion Science*. 2022;209:110765. https://doi.org/10.1016/j.corsci.2022.110765 EDN: BICKUB

10. Fernandes R.F., Jesus J.S., Branco R., Borrego L.P., Costa J.D., Ferreira J.A.M. Effect of low-temperature stress relieving heat treatments on fatigue behaviour and failure mechanisms of L-PBF AlSi10Mg aluminium alloy. *Engineering Failure Analysis*. 2025;169:109210. https://doi.org/10.1016/j.engfailanal.2024.109210 EDN: OMKGIA

11. Yang H., Cui Y., Qin F., Lin T., Zheng Y. Fatigue failure analysis and life prediction of forged 6061 aluminum alloy wheel hubs based on precipitate size effects and multiaxial stress modeling. *Engineering Failure Analysis*. 2025;182: 110181. https://doi.org/10.1016/j.engfailanal.2025.110181

12. Cong J., Liu Z., Zhou S., Zhu X., Gao S. Fatigue life prediction of ultrasonic impact treatment aluminum alloy weld joint based on the continuous damage model and artificial neural network. *Engineering Fracture Mechanics.* 2025;327:111503. https://doi.org/10.1016/j.engfracmech.2025.111503

13. Liu Z., Li J., Zhang L. Fatigue characteristics of high-strength aluminum alloy with and without surface mechanical rolling treatment in the transition regime between high cycle and very-high cycle fatigue. *Engineering Fracture Mechanics*. 2025;328:111585. https://doi.org/10.1016/j.engfracmech.2025.111585

14. Wang H., Zhang Z.J., Zhu S.Z., Li X.T., Zhu Y.K., Liu R., Hou J.P., Gong B.S., Liu H.Z., Wang D., Ma Z.Y., Zhang Z.F. Enhancing the high-cycle fatigue property of aluminum alloy by adding fine-sized hard particles. *Composites Part A: Applied Science and Manufacturing*. 2026;200:109344. https://doi.org/10.1016/j.compositesa.2025.109344

15. Song S., Wu Z., Zhao J., Zhou L., Guo S., Kan Q., Chen X., Zhang X. Crystal plasticity modeling of uniaxial tensile and fatigue failure behaviors of laser shock peened aluminum alloy. *International Journal of Fatigue*. 2025;201: 109145. https://doi.org/10.1016/j.ijfatigue.2025.109145

16. Konstantinov I.L., Baykovskiy Yu.V., Yuryev P.O., Bezrukikh A.I., Sidelnikov S.B., Saparova A.S., Mansurov Yu.N., Partyko E.G., Bozhko D.N. Study of deformability during the rolling of aluminum alloy 1580 doped with small additions of erbium and ytterbium. *Metallurgist*. 2025. https://doi.org/10.1007/s11015-024-01833-z EDN IPZBXD

17. Shatalov R.L., Hoang F.V., Kuang Ch.V. Determination of mechanical properties of aluminum alloy strips AD33 according to various hardness parameters during cold rolling. *Metal technology*. 2021;(9):31–37. (In Russ.) https://doi.org/10.31044/1684-2499-2021-0-9-31-37 EDN: XYBVMJ

18. Lukienko M.I. *Investigation of the strength and manufacturability of aluminum alloy sheet tank structures:* [dissertation]. Moscow, 1980. (In Russ.)

19. Kupreishvili S.M. Mechanics of destruction of vertical cylindrical tanks. *Industrial and civil engineering.* 2004; (5):40–42. (In Russ.) EDN: PLFWJH

20. Vuherer T., Kramberger J., Milčić D., Glodež S. Fatigue behaviour of friction stir welded AA-2024 aluminium alloy sheet. *IOP Conference Series: Materials Science and Engineering.* 2019;659:012032. https://doi.org/10.1088/1757-899X/659/1/012032

21. Wang M.Z., Kassner M.E. Tensile and fatigue properties of aluminum alloy sheet 6022. *Journal of Materials Engineering and Performance*. 2002;11:166–168. https://doi.org/10.1361/105994902770344222

22. Kendall M.G., Gibbons J.D. *Rank correlation methods.* 5th ed. London: Edward Arnold Publ.; 1990.

23. Pearson K. On the criterion that a given system of deviations from the probable in the case of a correlated system of variables is such that it can be reasonably supposed to have arisen from random sampling. *Philosophical Magazine Series*. 2009;5(50):157–175. https://doi.org/10.1080/14786440009463897

24. Milova Yu.A., Dikarev A.V. Rationed natural row. Polyparametric coding. *European Journal of Technical and Natural Sciences*. 2020;(3):19–23. (In Russ.) https://doi.org/10.29013/EJTNS-20-3-19-23 EDN: SWBNAA